LA-UR-99-895

Title: THERMOACOUSTIC ENGINES AND REFRIGERATORS: A SHORT COURSE

Author(s): G.W. Swift

Submitted to: Joint 137th Meeting of Acoustical Societies of America and Europe

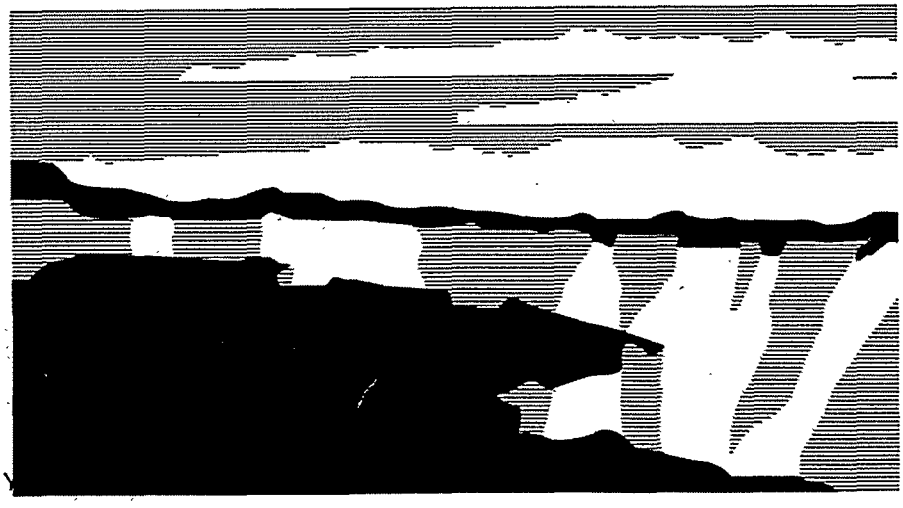

Los Alamos
NATIONAL LABORATORY

Form No. 836 R5
ST 2629 10/91

DISCLAIMER

Thermoacoustic engines and refrigerators

Greg Swift
Condensed Matter and Thermal Physics Group
Los Alamos National Laboratory
Rough draft—Berlin version

Winter 1999

CONTENTS

Preface

I'm excited by the power density and efficiency recently achieved by thermoacoustic engines and refrigerators, and fascinated by new developments in thermoacoustics: deliberate superposition of steady flow, mixture separation via oscillating thermal diffusion. At night I often dream of a future world in which thermoacoustics is widely practiced. One dream had loudspeaker-driven thermoacoustic heat pumps atop the hot-water heaters in half the homes in Phoenix, pumping heat from room air into the hot water—the production of a little cooling in the homes was a nice by-product. Another dream featured a small thermoacoustic system next to the liquid-nitrogen and liquid-oxygen dewars in back of our local hospital; this system had a gas-fired thermoacoustic engine driving several pulse-tube refrigerators, which provided the cooling necessary to liquefy air, distill it to produce purified nitrogen and oxygen, and reliquefy them for storage in the dewars. A third dream had hundreds of enormous combustion-powered thermoacoustic natural-gas liquefiers arrayed on an offshore platform, using the methane itself as the thermoacoustic working gas and filling a vacuum-insulated supertanker with LNG for transport to distant shores. Yet another dream showed an extensive thermoacoustic apparatus on Mars—a thermoacoustic engine driven by a small nuclear reactor produced 100 kW of acoustic power, which was piped to assorted thermoacoustic mixture separators and refrigerators, splitting atmospheric carbon dioxide and mined frozen water into pure H_2 and O_2 and liquefying these for use in fuel cells on each of the many robots scooting around building a colony for eventual human habitation.

The dreams are always different, but they have some features in common. First, they all feature low-tech hardware: big pipes and heat exchangers; welded steel, conventional shell-and-tube heat exchangers, molded plastic, etc. Second, I know that this simplicity is deceptive, because the technical challenge of designing this easy-to-build hardware is extreme. Third, there are no people in these dreams...because I know there are few people who are skilled in thermoacoustic engineering today. So I wake up, afraid that none of this will ever happen, afraid that integrated thermoacoustic process engineering is an opportunity that will never have a chance. So, I get up and I write another few paragraphs of this book, hoping to help newcomers learn basic thermoacoustics quickly, so they can design, build, and debug wonderful thermoacoustic systems of all kinds.

This is an introductory book, not a full review of the current status of the field of thermoacoustics. It is evolving from my March 1999 short course on this subject at the Berlin acoustics meeting. The hardware examples used here to illustrate the elementary principles are thermoacoustics apparatus developed at Los Alamos or with our close collaborators, and the mathematical approach to the gas dynamics and power flows closely follows that pioneered by Nikolaus Rott. (Time pressure induces me to stick with topics most familiar to me! and, indeed, the Los Alamos approach to thermoacoustics has been quite successful.) Many aspects of thermoacoustics will be introduced, in an attempt to help the reader acquire both an intuitive understanding and the ability to design hardware, build it, and diagnose its performance.

At Los Alamos, we have found it most productive to stay focused on experimental and development hardware, while maintaining several abstract points of view including phasor display of acoustic variables, a mental picture of gas motion, and an entropy-generation perspective on the second law of thermodynamics. Intuition is important because it helps us humans organize our thoughts. Mathematics is unavoidable, because it is the common

language with which scientists and engineers communicate, and it allows us to interpolate and extend our knowledge quantitatively. But experiment is the source of all real truth, so the experiments are our most important and time-consuming activity at Los Alamos. Weaving intuition, mathematics, and experimental results together in this book, I will at first put the most emphasis on the mathematics, because without this common vocabulary we can get nowhere. Intuition gets second-highest emphasis, as appropriate for an introductory treatment. Experimental results get the least emphasis in this text. But please remember that the mathematical and intuitive discussions presented here are actually distillations of many experiments spanning many decades in many countries.

Many readers will find that they have only part of the background needed to learn thermoacoustics. Mechanical engineers and chemical engineers may have insufficient acoustics background; they should study an introductory treatment like Chapters 5–10 (and perhaps 14) in *Fundamentals of Acoustics* by Kinsler, Frey, Coppens, and Sanders. Acousticians, on the other hand, may need to study something like the first half of *Fundamentals of Classical Thermodynamics* by Van Wylen and Sonntag. Someone for whom the expression $i = \sqrt{-1}$ is unfamiliar must begin with a review of elementary complex arithmetic in an engineering mathematics text such as *Advanced Engineering Mathematics* by Kreysig.

The present rough draft of this book can be duplicated freely, and is distributed at no cost from the Los Alamos thermoacoustics web site, http://rott.esa.lanl.gov (maintained by Bill Ward). Be sure to get the animations as well as the book—studying this material without the animations would be as frustrating and ineffective as studying an engineering text without looking at the figures. On the website, the book is in pdf format, which can be viewed and printed using Adobe's free Acrobat Reader software. The photographs in Chapters 1 and 6 are color, so you might want to print at least some pages with a color printer.

1. INTRODUCTION

From thermodynamics [1, 2, 3], we know that the heat engine (sometimes known as a prime mover) produces work from high-temperature heat, and the refrigerator (or heat pump) uses work to pump heat. These devices are illustrated in Fig. 1.1, where the central rectangles represent the devices, operating between two thermal reservoirs at different temperatures T. In the heat engine, heat Q_H flows into the device from the reservoir at T_H, while the device produces work and delivers waste heat Q_0 into the reservoir at T_0. In the refrigerator, work flows into the device, which lifts heat Q_C from the reservoir at T_C and rejects waste heat Q_0 into the reservoir at T_0.

The laws of thermodynamics place bounds on the efficiency of such devices. The first law of thermodynamics is simply energy conservation: If the device is in steady state, what goes in must come out. So the sum of the energies going into the device must equal the sum of the energies going out. For the engine, this implies

$$Q_H = W + Q_0, \tag{1.1}$$

while for the refrigerator

$$Q_0 = W + Q_C. \tag{1.2}$$

The second law of thermodynamics, more subtle, says that the entropy of the universe can only increase or stay the same; it can never decrease. Here, the universe consists of three pieces: the two reservoirs and the device itself. If the device is in steady state then its entropy doesn't change with time, and work carries no entropy, so the universe consists of only the two reservoirs. Hence, for the engine the entropy increase Q_0/T_0 of the cold reservoir has to be greater than or equal to the entropy decrease Q_H/T_H of the hot reservoir

$$\frac{Q_0}{T_0} \geq \frac{Q_H}{T_H}, \tag{1.3}$$

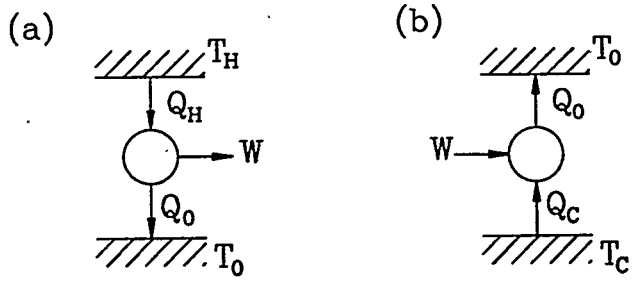

Figure 1.1: A heat engine (a) and a refrigerator (b), showing energy flow directions and thermal reservoirs.

and similarly for the refrigerator

$$\frac{Q_0}{T_0} \geq \frac{Q_C}{T_C}. \tag{1.4}$$

Combining Eq. (1.1) with Eq. (1.3) by eliminating the uninteresting variable, Q_0, yields an inequality for the efficiency. The efficiency is what you want divided by what you have to spend to get it. For the engine, the efficiency η is the work produced by the engine divided by the heat supplied by the hot reservoir:

$$\eta = \frac{W}{Q_H} \leq \frac{T_H - T_0}{T_H}. \tag{1.5}$$

The temperature ratio on the right is called the Carnot efficiency, which bounds the actual efficiency of all engines. Similarly, for the refrigerator the coefficient of performance COP is the heat of refrigeration divided by the work consumed by the device

$$COP = \frac{Q_C}{W} \leq \frac{T_C}{T_0 - T_C}. \tag{1.6}$$

The temperature ratio on the right is called the Carnot COP, which bounds the actual COP of all refrigerators.

In the real world, the device of Fig. 1.1a or Fig. 1.1b typically performs its function by taking an ideal gas or other fluid through a thermodynamic cycle or cycles. The Carnot cycle shown in Fig. 1.2 is one such cycle, which Carnot himself used to derive his well-known ultimate efficiency. This cycle is a favorite of textbooks because it is simple to analyze and has this highest possible efficiency. The Stirling cycle also has the Carnot efficiency, but we will not examine the idealized Stirling cycle or other textbook cycles in detail here, because real Stirling engines and refrigerators [4, 5] are so complex that the Stirling *cycle* itself, like the Carnot cycle, is of only academic interest. Parcels of gas in different parts of real Stirling machines experience totally different thermodynamic cycles, as is shown in Ani. Tashe /a. This animation shows a two-piston Stirling engine, with moving pistons taking the gas through a cycle of compression, rightward displacement, expansion, and leftward displacement. Between the pistons are two heat exchangers, colored to match the pistons, at temperatures $T_H = 600°\text{C}$ and $T_0 = 30°C$. Between these is a regenerator. The ellipses above the pistons are "indicator diagrams," which trace pressure vs volume for each piston; the difference between their purple elliptical areas is the net work W done by the gas in each cycle. The red arrows below each of the two heat exchangers show the heats Q_H and Q_C transfered to or from the gas in each cycle. The three moving vertical blue lines within the regenerator mark slices of the moving gas itself; together with the piston faces, these show clearly that the gas motion is small compared to the length of the engine. A typical slice of gas, such as the one indicated by the central blue line, *never* contacts either heat exchanger, so its cycle can hardly be analyzed by reference to a textbook heat-engine cycle. Furthermore, the smooth time dependences of the motion and pressure in real engines contrasts starkly with the four discrete steps in textbook cycles.

Nevertheless, the presence of four steps in typical thermodynamic cycles suggests the need for proper phasing between two or more phenomena. In the Carnot cycle shown in Fig. 1.2, the relevant phenomena are the pressure changes and the thermal contact to the

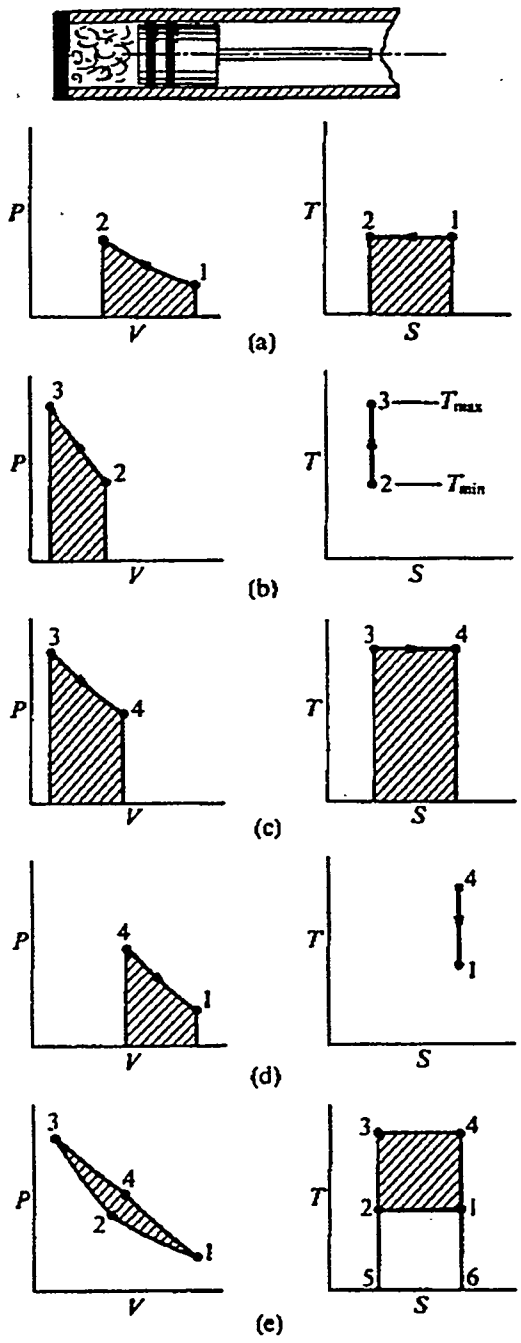

Figure 1.2: The Carnot cycle for an engine. (a)—(d) the four individual steps: isothermal compression, isentropic compression, isothermal expansion, isentropic expansion, respectively. (e) the combination of (a) through (d) produces a complete cycle, with the area enclosed on the PV plane equal to the net work produced by the engine. Reproduced from Walker [4].

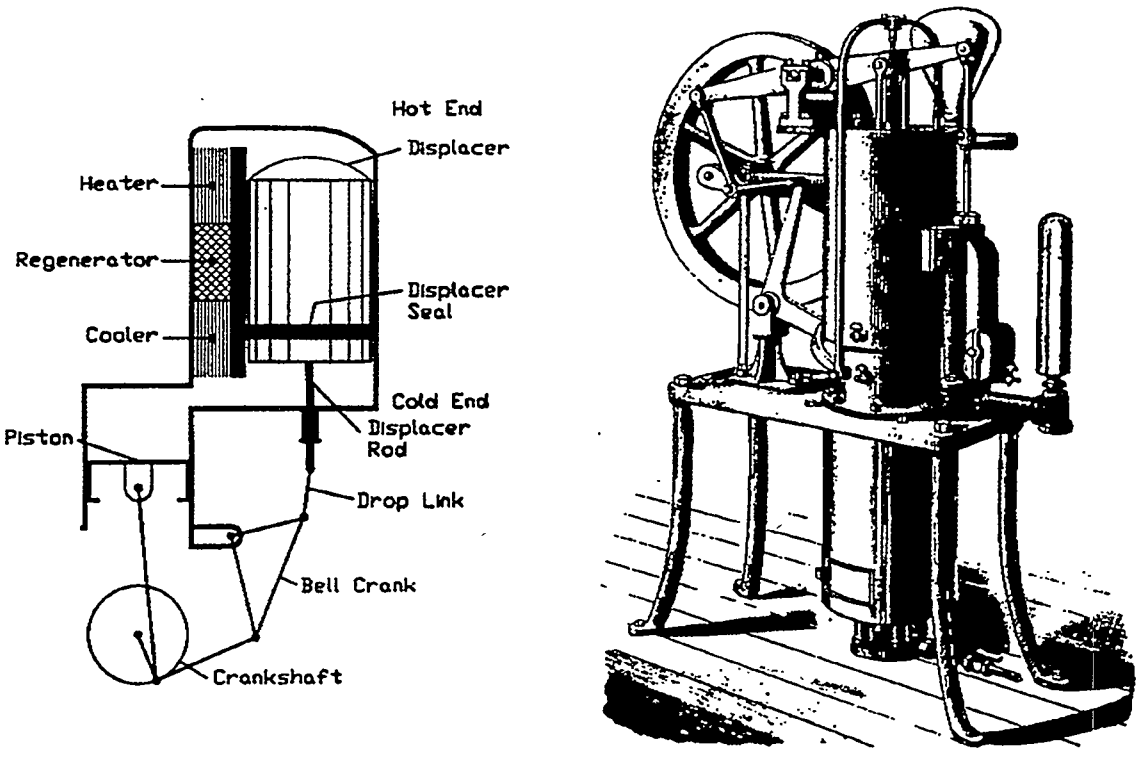

Figure 1.3: Early Stirling engines. Reproduced from Senft [6].

reservoirs; the mechanism by which the thermal contact to the reservoirs is made and broken is left to our imagination. Conventional heat engines and refrigerators (e.g. Stirling) use piston motion both to cause pressure changes and to push the working gas through the heat exchangers, with the phasing between the pressure changes and the resulting thermal contact in the heat exchangers determined by the phasing of the pistons' motions, as shown in Ani. Tashe /a. Thermoacoustic heat engines and refrigerators also use gas motion to control thermal contact in the heat exchangers, with the phasing between motion and pressure determined by acoustics.

Figure 1.3 shows the layout typical of a Stirling engine of a century ago. There are many moving parts: rotating crankshafts, moving connecting rods, reciprocating pistons. The mechanical parts dominated the thermal parts—in volume, weight, and visual impact—in the early Stirling machines. In the intervening century, engineers have sought to simplify such heat engines and refrigerators by elimination of moving parts. In 1969 William Beale was thinking about resonance effects when moving pistons bounced against gas compressibility in Stirling machines, and he realized that under the correct circumstances the forces on the connecting rods were small while the pistons continued to move correctly. This invention has led to what are called free-piston [7, 4] Stirling engines and refrigerators, as illustrated in Fig. 1.4, in which the moving pistons bounce against gas springs in resonance, and other moving parts such as connecting rods and crankshafts are eliminated. Another method to eliminate moving parts is the liquid-piston Stirling engine, also known as the Fluidyne engine [8], as shown in Fig. 1.5. In Fluidyne engines, liquid in two U tubes serves the function of the two

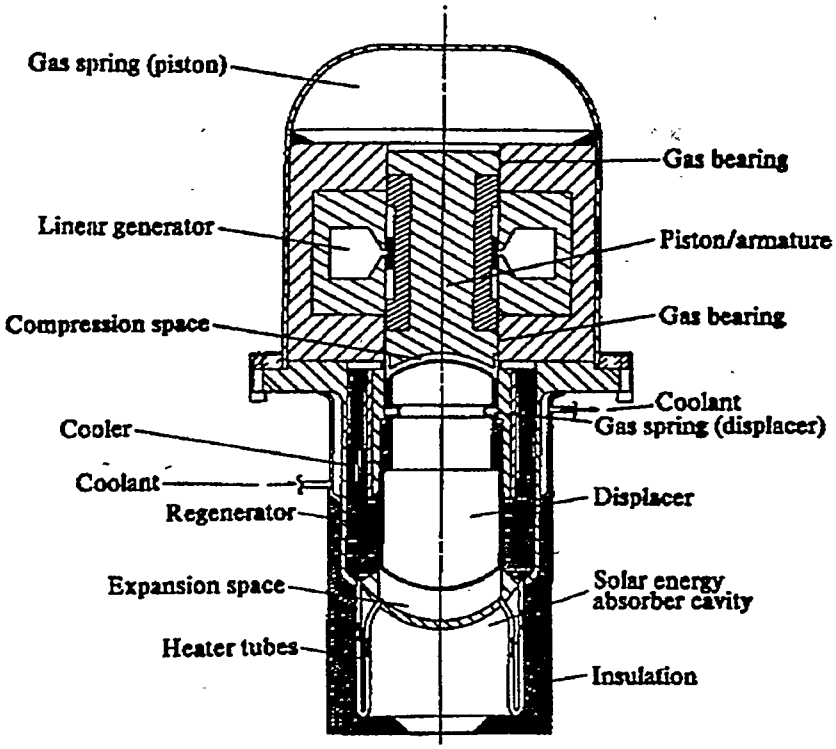

Figure 1.4: A typical free-piston Stirling engine. Reproduced from Walker [4].

pistons of the ordinary Stirling engine, confining and moving the working gas appropriately; the resonance phenomena are similar to those of the free-piston Stirling engines, but with gravity and liquid density contributing to the effective spring constant of the resonance. More recently, Peter Ceperley [9, 10] realized that the phasing between pressure and velocity in the thermodynamic elements of Stirling machines is the same as the phasing between pressure and velocity in a traveling acoustic wave, so he proposed eliminating everything but the working gas itself, using acoustics to control the gas motion and gas pressure. Figure 1.6 shows such a device, with two heat exchangers and a regenerator but no pistons or any other moving parts.

Ceperley's work showed the need to consider sound-wave behavior [12, 13] in the working gas of Stirling devices, with variations in important variables such as pressure p and velocity u depending importantly and continuously on the coordinate x along the direction of gas motion, and with these x dependences due to inertial and compressive effects in the gas in addition to the effects of flow resistance.

Basic sound wave behavior is simple to derive. In acoustics, we often express quantities like pressure having sinusoidal time dependence in complex notation,

$$p = p_m + \mathrm{Re}\left[p_1(x)\, e^{i\omega t}\right], \tag{1.7}$$

with the pressure p expressed as a mean value p_m plus the real part of a complex function of x times $e^{i\omega t}$. We will use this style of notation throughout the book. The simplest acoustics derivation, for sound propagating along the direction x, starts with three simple equations.

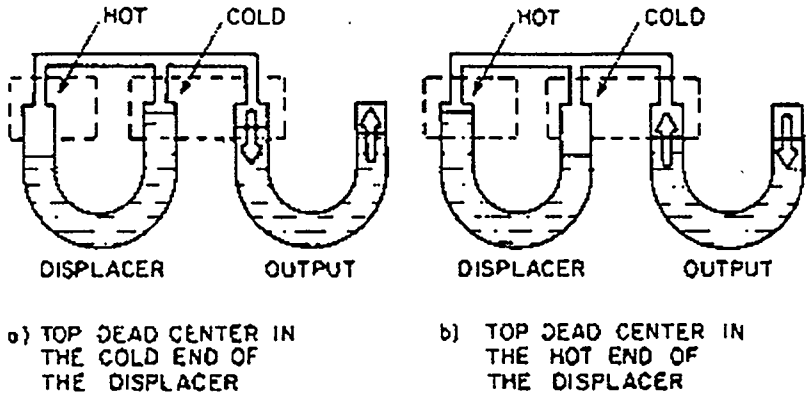

Figure 1.5: The Fluidyne (liquid piston) Stirling engine. Reproduced from West [11].

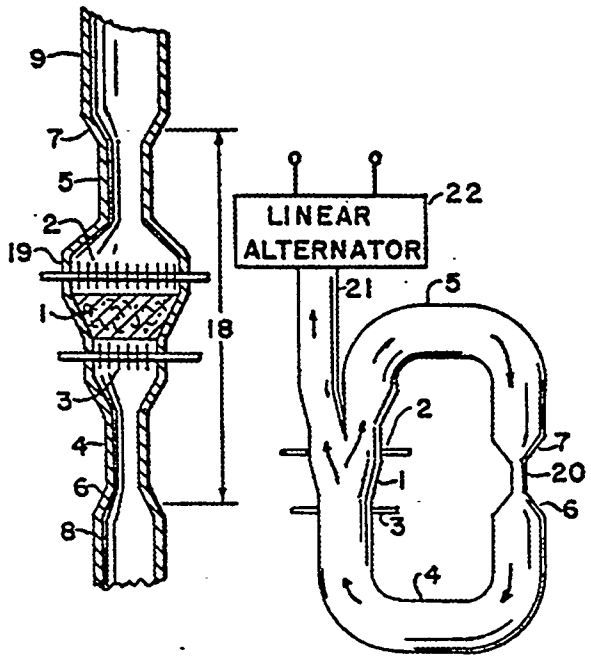

Figure 1.6: The traveling-wave engine concept. Reproduced from one of Ceperley's patents.

The first is this version of the momentum equation:

$$i\omega\rho_m u_1 = -\frac{dp_1}{dx}. \tag{1.8}$$

The force on the gas is the pressure gradient dp_1/dx, which according to Newton's law must equal the mass density ρ_m times the acceleration $i\omega u_1$. The second is this version of the continuity equation:

$$i\omega\rho_1 + \rho_m \frac{du_1}{dx} = 0, \tag{1.9}$$

which expresses mass conservation, with the time derivative of mass density at any point, $i\omega\rho_1$, arising from the gradient of mass flux density $d(\rho_m u_1)/dx$ at that point. The third is a part of the equation of state of the gas

$$\frac{p_1}{\rho_1} = \left(\frac{\partial p}{\partial \rho}\right)_s = a^2, \tag{1.10}$$

which gives the proportionality constant a^2 —the square of the sound speed—linking pressure changes with density changes under adiabatic conditions. Combining these three equations by eliminating u_1 and ρ_1 gives a simple wave equation

$$p_1 + \frac{a^2}{\omega^2}\frac{d^2 p_1}{dx^2} = 0. \tag{1.11}$$

whose solution is sines and cosines of x. (Technically this is a Helmholtz equation, since the time derivatives are written as ω's.)

This simple wave equation is appropriate for plane waves under spatially isothermal, temporally adiabatic conditions—in other words, the gas average temperature is independent of x and the gas exchanges no heat with its surroundings on the time scale of the acoustic oscillations. Amazingly, it was only 20 years ago that anyone was able to derive the correct wave equation for sound waves propagating in a duct with a temperature gradient in the duct along the direction of propagation, and with significant thermal contact between the gas and the side walls of the duct. This equation [14]

$$\left[1 + (\gamma - 1)\, f_\kappa\right] p_1 + \frac{\rho_m a^2}{\omega^2}\frac{d}{dx}\left(\frac{1 - f_\nu}{\rho_m}\frac{dp_1}{dx}\right) - \frac{a^2}{\omega^2}\frac{f_\kappa - f_\nu}{1 - \sigma}\frac{1}{T_m}\frac{dT_m}{dx}\frac{dp_1}{dx} = 0 \tag{1.12}$$

was published by Nikolaus Rott in 1969. You can see pieces of Eq. (1.11) in it. The f_κ and f_ν factors in Rott's equation arise from thermal and viscous contact with the walls of the duct.

In this book, we will try to integrate all of the aforementioned threads together into a coherent picture, with physical, mathematical, and intuitive foundations. We will try to develop a vision of these heat engines and refrigerators, using the kind of mathematics that Rott developed, and with many of the features of the work of Beale, West, and especially Ceperley—the elimination of moving parts whenever possible to achieve simplicity and reliability, while maintaining the highest possible efficiency.

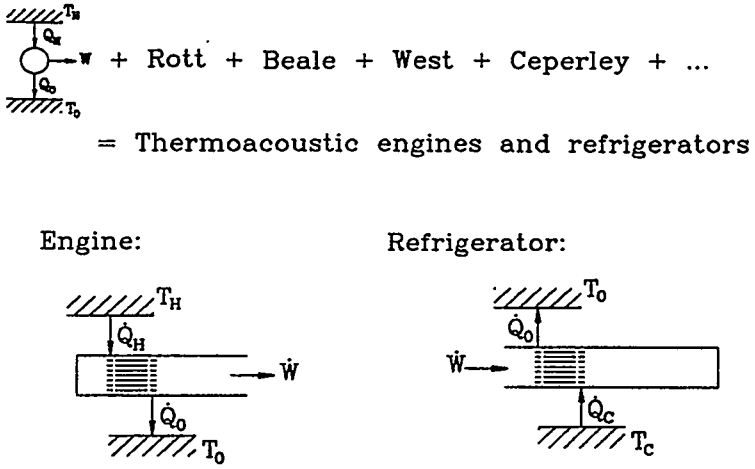

Figure 1.7: The type of devices under consideration in this book.

As illustrated in Fig. 1.7, this integration will generally involve devices in which the gas-enclosing cavity comprises some kind of acoustic resonator that determines the relationship between gas motion and pressure, in which heat exchangers exchange heat with external heat reservoirs, and in which a stack or a regenerator between the heat exchangers make the device function as a thermoacoustic standing-wave device or a Stirling device.

In one respect, thermoacoustic devices are more interesting than crankshaft-based systems, such as that shown in Fig. 1.3, in which hardware motion was determined, by design, and exerted direct control on gas motion. In thermoacoustic systems, including linear-motor, free-piston Stirling systems, oscillating pressure gradients cause the oscillating motion, and the oscillating motion causes the oscillating pressure gradients; analyzing a dynamical system having such interdependent causes and effects is inherently challenging.

1.1. Length scales

The important length scales in thermoacoustic engines and refrigerators are illustrated in Fig. 1.8.

Along the wave-propagation direction x (the direction of motion of the gas), the wavelength of sound $\lambda = a/f$, where f is the oscillation frequency, is an important length scale. When the gas inertia itself provides the resonance behavior, the whole length of the apparatus may typically be a half wavelength or a quarter wavelength; but when massive mechanical components participate meaningfully in the resonance behavior, as in free-piston Stirling systems, the size of the system is typically much smaller than the wavelength. In all cases, the lengths of heat-exchange components are much shorter than the wavelength.

Another important length scale in the x direction is the gas displacement amplitude $|x_1|$, which is the velocity amplitude $|u_1|$ divided by the angular frequency $\omega = 2\pi f$ of the wave. This displacement amplitude is often a very large fraction of the stack length or regenerator length, and may be larger than the lengths of the heat exchangers at either end of the stack or regenerator. The displacement amplitude is always shorter than the wavelength.

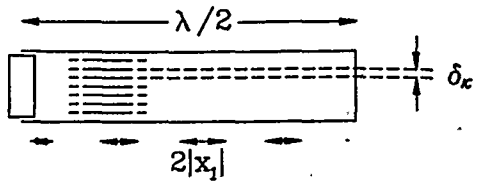

Figure 1.8: Important length scales in a thermoacoustic device.

Perpendicular to the direction of motion of the gas, the characteristic lengths are the thermal penetration depth $\delta_\kappa = \sqrt{2k/\omega\rho c_p} = \sqrt{2\kappa/\omega}$ and the viscous penetration depth $\delta_\nu = \sqrt{2\mu/\omega\rho} = \sqrt{2\nu/\omega}$, where k and κ are the thermal conductivity and diffusivity of the gas, μ and ν are its dynamic and kinematic viscosities, and c_p is its specific heat per unit mass at constant pressure. These characteristic lengths tell us how far heat and momentum can diffuse laterally during a time interval of the order of the period of the acoustic oscillation divided by π. For gas at distances much greater than these penetration depths from the nearest solid boundary, the sound wave feels no thermal contact or viscous contact with the solid boundaries; in parts of the apparatus whose lateral dimensions are of the order of the viscous and thermal penetration depths, the gas does feel both thermal and viscous effects from the boundaries. Clearly the heat exchange components in thermoacoustic systems must have lateral dimensions of the order of δ_κ or smaller, in order to exchange heat with the working gas.

In the ratio of these two penetration depths,

$$\frac{\delta_\nu}{\delta_\kappa} = \sqrt{\frac{\mu c_p}{k}} = \sqrt{\sigma} \lesssim 1, \tag{1.13}$$

the frequency and the density cancel out, leaving the ratio of viscosity times heat capacity to thermal conductivity. This ratio is called the Prandtl number σ of the gas. It's close to unity for typical gases, so viscous and thermal penetration depths are comparable. Hence thermoacoustic engines and refrigerators will always suffer from substantial viscous effects.

In ordinary audio acoustics, the displacement amplitude of gas is much smaller than the thermal and viscous penetration depths, which in turn are much smaller than the wavelength. In thermoacoustic engines and refrigerators typically the gas displacement amplitudes are much larger than the penetration depths, but still much smaller than acoustic wavelengths:

$$\delta_\kappa \ll |x_1| \ll \lambda. \tag{1.14}$$

[Incidentally, the standard expression for *bulk* attenuation of sound, α, can easily be expressed in terms of the viscous and thermal penetration depths. From Eq. 7.36 in Kinsler, Frey, Coppens, and Sanders (3rd ed.) [12]:

$$\alpha = \pi^2 \frac{\omega}{a} \left[\frac{4}{3} \frac{\delta_\nu^2}{\lambda^2} + (\gamma - 1) \frac{\delta_\kappa^2}{\lambda^2} \right]. \tag{1.15}$$

From this viewpoint, viscous bulk sound attenuation is small if the viscous penetration depth is small compared to the wavelength, and thermal attenuation is small if the thermal

penetration depth is small compared to the wavelength. The ratios of penetration depths to wavelength are strongly frequency dependent, because the wavelength is proportional to $1/f$ while the penetration depths are proportional to $\sqrt{1/f}$. So low frequency, long wavelength sound suffers the least bulk attenuation. The presence of solid boundaries in the resonators and heat-exchange components of thermoacoustic engines and refrigerators has thus far caused boundary-based attentuation to far exceed such bulk attenuation.]

1.2. Examples

I will repeat the same four examples of real thermoacoustic hardware in almost every chapter in this book, introducing the examples briefly here and examining various aspects in greater detail at appropriate places in subsequent chapters. Mark these pages (with clips or tape or ...) so you can refer back to them easily. The four examples include two engines and two refrigerators; two standing wave systems and two traveling wave systems; and two research systems and two systems bringing thermoacoustics toward a more practical stage of development. In this chapter, I will just briefly introduce the four examples, discussing their purpose, overall function, and characteristic dimensions.

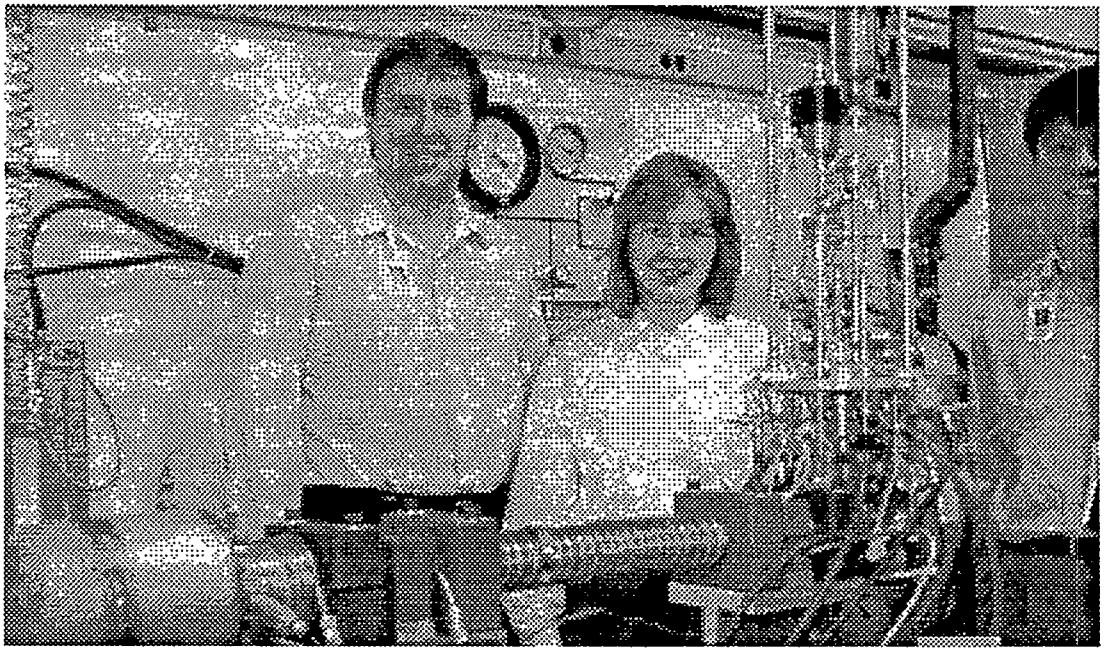

Figure 1.9: Standing-wave engine example: Tektronix researchers with a heat-driven refrigerator, 1995. The resonator, horizontal, has standing-wave engines on each end. The two-stage orifice pulse tube refrigerator stands vertically near the right end. Photo courtesy of Kim Godshalk.

The standing-wave heat engine was part of the heat-driven cryogenic refrigerator [15] assembled at Tektronix in 1994 and shown in Figs. 1.9 and 1.10. This system was under development in order to provide a small amount of cryogenic refrigeration for electronic components, with the system powered by red-hot electric heaters and hence having

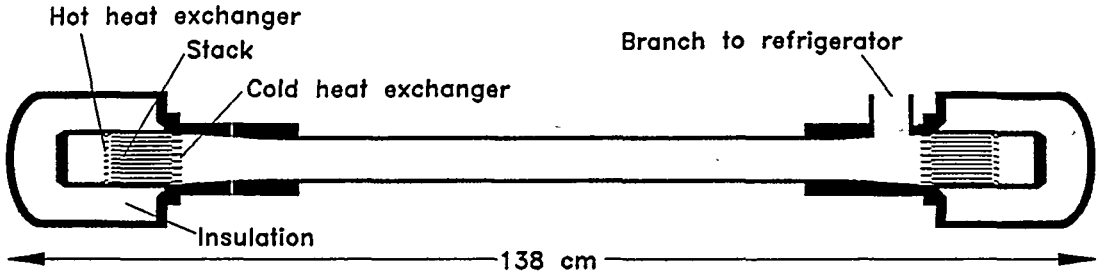

Figure 1.10: Scale drawing of the Tektronix resonator and its standing-wave engines. The annular spaces around each end are thermal insulation. The spacing in stacks and heat exchangers is not to scale. The upward opening near the right end is the connection to the two-stage pulse tube refrigerator.

no moving parts. The resonator lies horizontally in the figures, with standing-wave thermoacoustic engines on each end, and an upward side branch near the right end connecting to the two-stage orifice pulse tube refrigerator. Water cooling lines, seen extending through the tabletop in Fig. 1.9, removed waste heat from the engines and the refrigerator. Our focus in this book will be on the heat-driven engines and the resonator, which delivered up to 1 kW of acoustic power to the pulse tube refrigerator, and delivered 500 W to the pulse tube refrigerator with an efficiency of 23% of the Carnot efficiency. We hoped to make the system as small as possible, and sufficiently efficient that the necessary electrical power could be supplied from an ordinary wall plug. The working gas was helium at a pressure of 30 atmospheres. The sound speed of helium is about 1000 meters per second at room temperature, and the horizontal length of the resonator in Figs. 1.9 and 1.10 is about half a meter, so you would expect that the half-wavelength resonance in this system would be near 500 Hz; and, indeed, the system operated at 350 Hz. At this pressure and frequency, the thermal penetration depth in helium is approximately 0.2 mm; correspondingly, the spacing in the heat exchange components was approximately 1 mm.

The key idea in this and other standing-wave engines is that the gas in the stack must experience thermal expansion when the pressure is high and thermal contraction when the pressure is low. Thus the gas in the stack does work every acoustic cycle, pumping acoustic power into the standing wave. The standing wave in turn provides the oscillating pressure, and the oscillating motion that causes the gas in the stack to experience the oscillating temperature responsible for the thermal expansion and contraction. The velocity of the gas along the stack's temperature gradient is 90° out of phase with the oscillating pressure, so imperfect thermal contact between gas and stack is required to enable the thermal expansion and contraction steps to be in phase with the oscillating pressure. These complex, coupled oscillations appear spontaneously whenever the temperature at the hot ends of the stacks is high enough.

The standing-wave refrigerator shown in Figs. 1.11 and 1.12 was assembled by Bob Reid to investigate the deliberate superposition of steady flow [16] with the oscillating flow of the standing thermoacoustic refrigeration process. The refrigerator was driven by four loudspeakers, enclosed in the obvious aluminum housings shown in Fig. 1.11. The left and

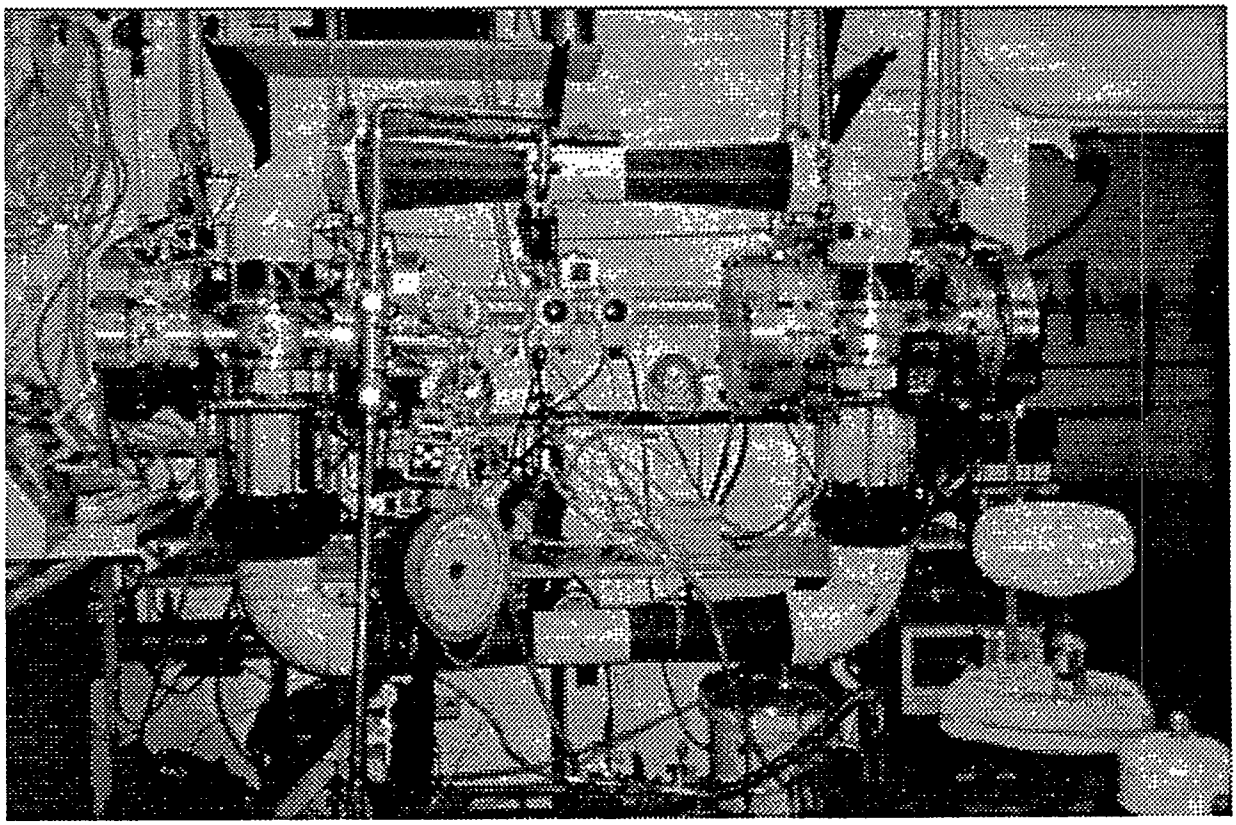

Figure 1.11: Standing-wave refrigerator example: Loudspeaker-driven-research apparatus for investigating the superposition of deliberate steady flow on the oscillatory thermoacoustic flow.

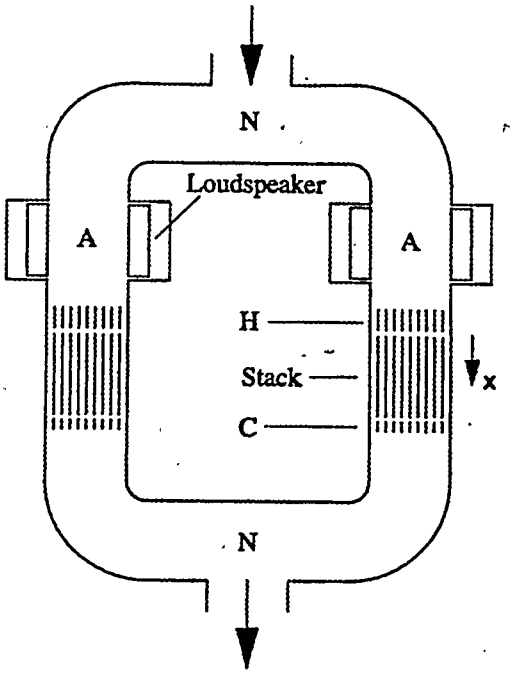

Figure 1.12: Schematic of the standing-wave refrigerator example.

right pairs of loudspeakers were driven 180° out of phase, to produce a standing wave in the toroidal resonator having essentially one full wavelength around the circumference of the torus, with pressure nodes centered in the top and bottom sections of the resonator and pressure anti-nodes near the loudspeakers. With the resonator filled with a mixture of 92% helium and 8% argon at three atmospheres of pressure, this resonance occurred at 94 Hz. Slow steady flow of the gas mixture from top to bottom through the heat exchange components, superimposed on the thermoacoustic oscillating flow, produced cold gas leaving the resonator at the bottom pressure node. The spacing in the heat exchange components was about 1 mm, a few times the thermal penetration depth in this gas.

The key idea in this and other standing-wave refrigerators is that the gas in the stack experiences partly adiabatic temperature oscillations, in phase with the standing-wave pressure oscillations, and oscillating standing-wave displacements in phase with the pressure oscillations and hence in phase with those temperature oscillations. Thus the gas in the stack cools a little as it is displaced downward in Fig. 1.12, and warms a little as it is displaced upwards. Imperfect thermal contact between gas and stack enables the required heat transfer at the extremes of the motion. (The superimposed steady-flow velocity in this particular apparatus was much smaller than the standing-wave oscillatory velocity, as we will discuss in Chapter 5.)

The traveling-wave engine shown in Figs. 1.13 and 1.14 was built by Scott Backhaus to demonstrate Stirling cycle engine thermodynamics with no moving parts, and to investigate the issues affecting its efficiency [17]. Heat was supplied to the engine electrically, and waste heat was removed by a water stream, delivering acoustic power to the resonator. Some of that acoustic power was dissipated in the resonator, but most was delivered to a variable

acoustic load, the small vertical cylinder near the center of Fig. 1.13. This engine has delivered power to the resonator with 40% of the Carnot efficiency. Suppression of steady flow around the small torus containing the heat exchangers is crucial for this high efficiency, as we will discuss in Chapter 5. Thirty-atmosphere helium fills the system, oscillating at 80 Hz. The resonator is essentially half-wavelength, with pressure oscillations 180° degrees out of phase at the right end of the fat portion on the right and in the small torus containing the heat exchangers on the left. The highest velocity occurs in the center of the resonator, at the small end of the long cone.

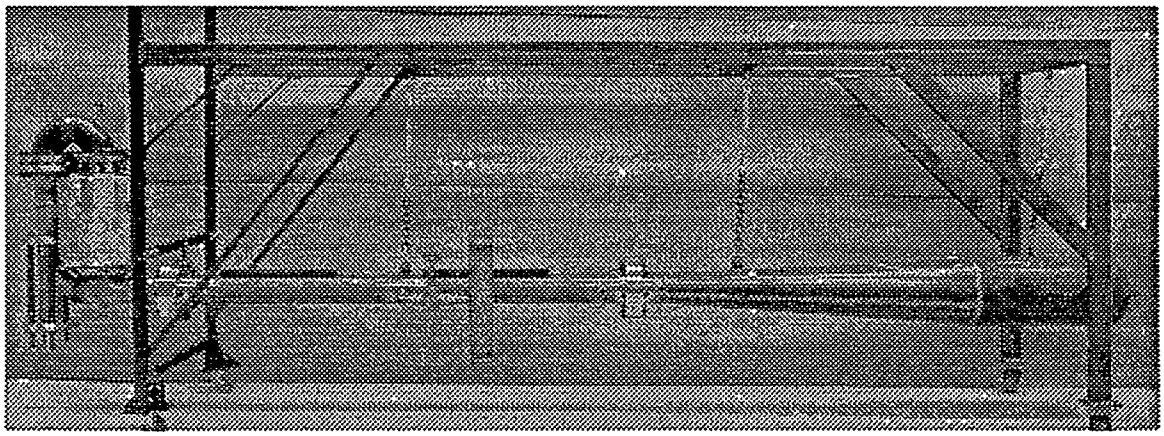

Figure 1.13: Traveling-wave engine example: A research apparatus for initial Los Alamos studies of the performance of a traveling-wave-engine.

The key idea in this and other traveling-wave engines is that the gas in the regenerator experiences thermal expansion when the pressure is high and thermal contraction when the pressure is low. Thus the gas in the regenerator does work every acoustic cycle, pumping acoustic power into the sound wave. The sound wave in turn provides the oscillating pressure, and oscillating motion that causes the gas in the regenerator to experience the oscillating temperature responsible for the thermal expansion and contraction. These complex, coupled oscillations appear spontaneously whenever the temperature at the hot end of the regenerator is high enough. The velocity of the gas along the regenerator's temperature gradient is substantially in phase with the oscillating pressure, so excellent thermal contact between gas and regenerator is required to cause the thermal expansion and contraction steps to be in phase with the oscillating pressure. This thermal contact is achieved by making the channel size in the regenerator much smaller than the thermal penetration depth.

Finally, **the traveling-wave refrigerator—an orifice pulse-tube refrigerator—** shown in Figs. 1.15 and 1.16 was built at Cryenco for liquefaction of natural gas [18, 19]. At about 3 atmospheres, natural gas (methane) liquefies at 120 Kelvin; this refrigerator provided 2 kW of refrigeration at that temperature, with a COP as high as 23% of the Carnot COP. The working gas was helium at a pressure of thirty atmospheres, driven at 40 Hz by a thermoacoustic engine through a resonator, not shown in the figures. The dimensions of the parts shown in the figures are much smaller than the 25 m wavelength of the sound wave, so resonance phenomena are of no concern in this refrigerator.

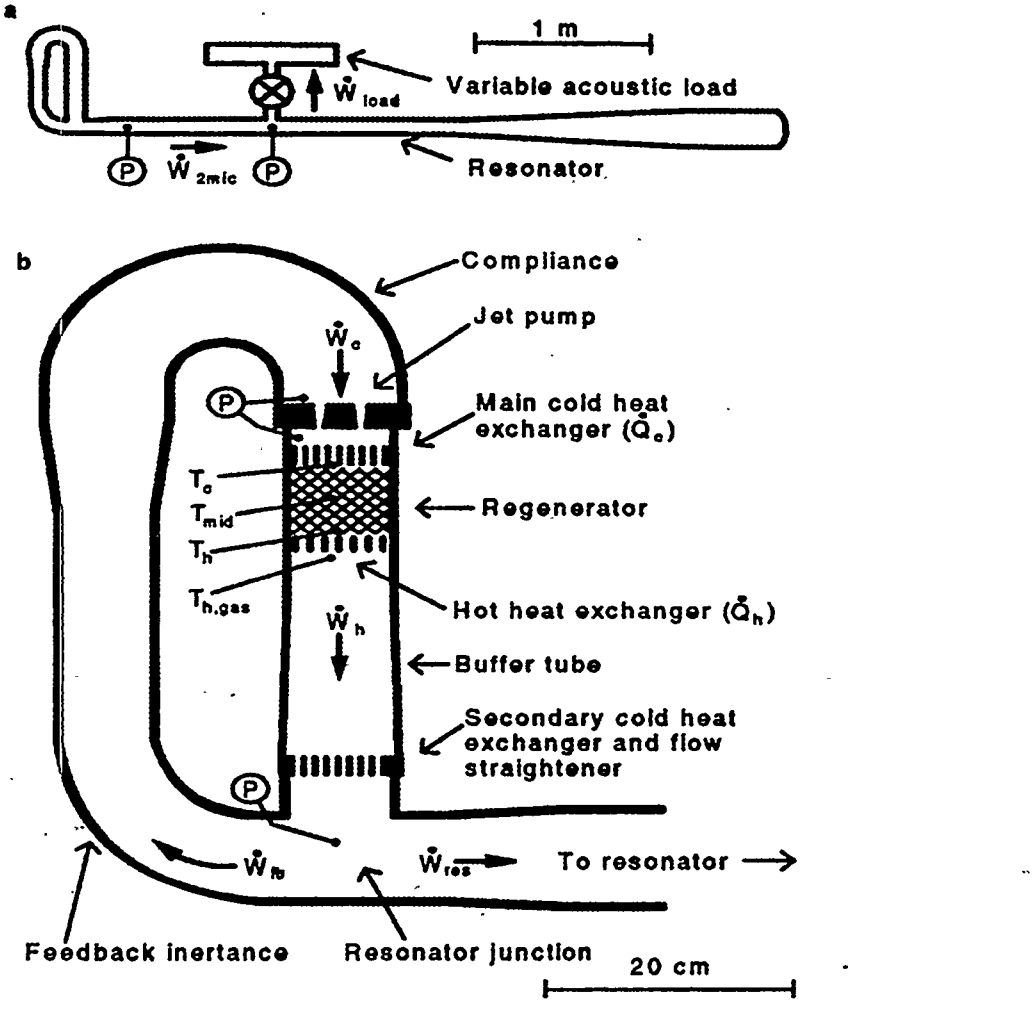

Figure 1.14: The traveling-wave engine. (a) Overview, as in the photo. (b) The heart of the traveling-wave engine.

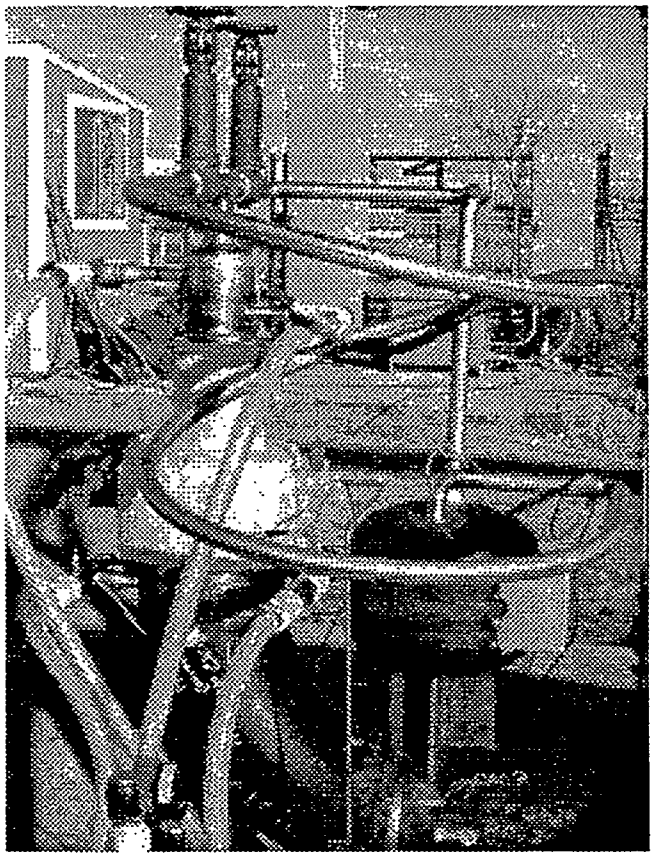

Figure 1.15: Traveling-wave refrigerator example: the Cryenco 2 kW orifice pulse-tube refrigerator.

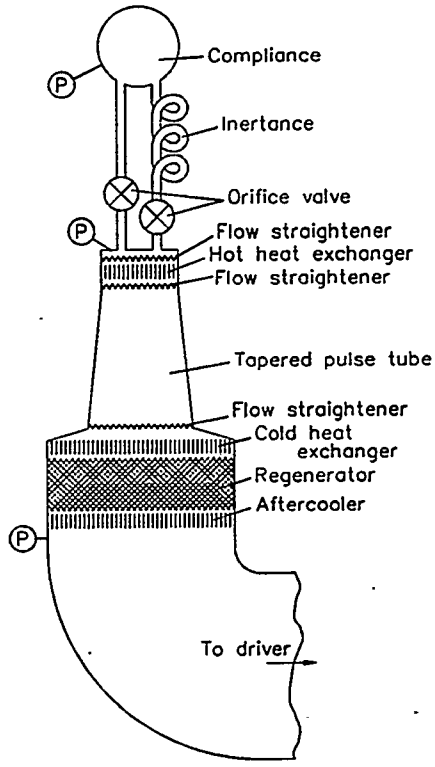

Figure 1.16: Schematic of the Cryenco orifice pulse-tube refrigerator. "P" indicates the location of a pressure sensor.

The key idea in this and other Stirling, pulse-tube, or traveling-wave refrigerators is that gas near the cold heat exchanger must be displaced into the open space of the pulse tube, adiabatically cooled, and displaced back through the cold heat exchanger where it can absorb heat from the load. The sound wave must provide oscillating pressure and oscillating displacement with this required phasing.

1.3. Thermoacoustics and conventional technology

With these four examples of thermoacoustic devices in mind, consider what the advantages and disadvantages of thermoacoustic systems might be in comparison to the energy conversion systems that are in widespread use, such as the internal combustion engine, the steam turbine, the reverse Rankine or vapor compression refrigeration cycle, the gas turbine, etc.

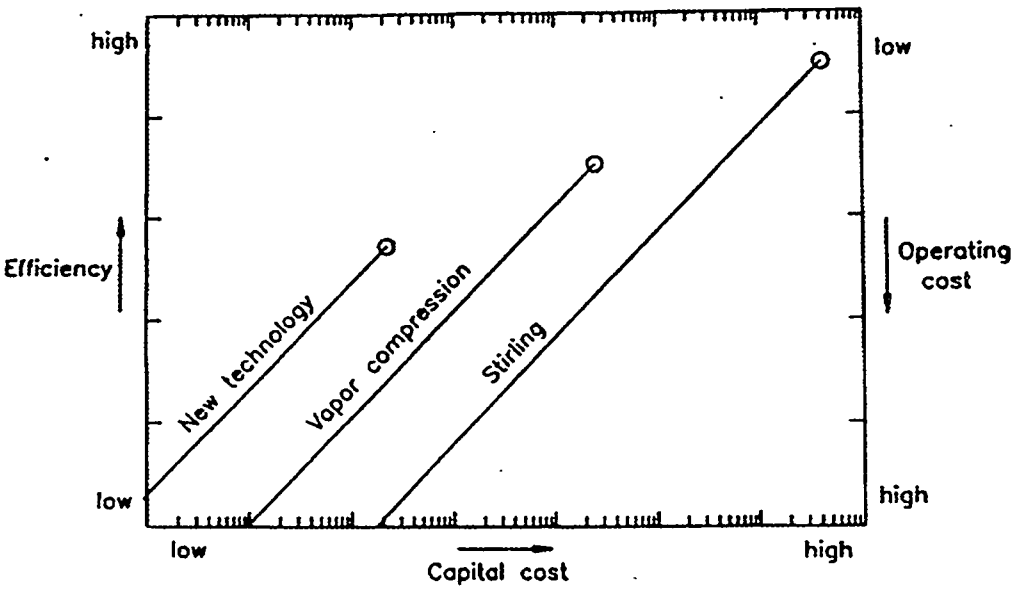

Figure 1.17: Different technologies exhibit different trade-offs between cost and efficiency.

Those conventional systems have moving parts; from that point of view one might think of them as being less reliable and more expensive than thermoacoustic devices. However, decades of investment in engineering development have given these conventional devices high reliability, and decades of manufacturing experience have given them low cost. Thermoacoustic devices seem to have the immediate potential to have comparable high reliability and low cost, because they use no moving parts, no exotic materials, and no close tolerances. Realizing this potential is one of our challenges.

Decades of investment in the engineering development of conventional energy-conversion devices has also given them very high efficiencies. Today's automobile engines convert the heat of combustion to shaft work with over 20% efficiency; the largest diesel engines achieve 40%. Vapor-compression refrigeration systems with COP's above 50% of Carnot's

are common. Thermoacoustic devices haven't yet achieved such high efficiencies; increasing thermoacoustic device efficiency into this range is another of our challenges.

It is important to realize that the efficiency of a new technology need not exceed that of older technologies in order to succeed commercially. This point is illustrated in Fig. 1.17. The Stirling refrigerator is quite old, and in principle it can have Carnot's COP. However, high COP can only be achieved at great expense, as the mass of heat exchange metal, quality of lubricants, etc. is made exceedingly large. For instance, qualitatively, the efficiency vs capital cost of a Stirling refrigerator might resemble the Stirling curve in Fig. 1.17, with very high efficiency possible if you're willing to spend an exponentially large amount of money building the refrigerator. However, in the commercial world, energy costs are currently low enough that no one chooses to invest so much capital to achieve high efficiency. Instead, vapor-compression refrigeration is used for almost all real-world refrigeration systems, because it has lower capital cost than Stirling refrigeration, even though the COP of vapor compression refrigeration can in principle never approach the ultimate COP of the Stirling cycle. Furthermore, each application requires a different compromise between construction costs and efficiency; for example, the vapor-compression air-conditioning system for a large office building in Phoenix might lie higher on the efficiency-cost curve than the vapor-compression chiller in a soft-drink vending machine in Seattle. If thermoacoustics turns out to have an efficiency–cost curve somewhere to the left of existing technologies, it will succeed in some commercial markets. Whether the terminus of the thermoacoustics curve is higher or lower than that of older technologies is not as important as whether the capital costs will be lower at modest efficiencies.

1.4. Notation

We pause now to carefully establish the notation to be used throughout the book for time-dependent variables such as pressure. Except in Chapter 5, we will assume that all time dependence is purely sinusoidal, at frequency f and angular frequency $\omega = 2\pi f$. Then variables such as pressure *could* be written

$$p(x,t) = p_m + C(x)\cos\left[\omega t + \phi(x)\right]. \tag{1.16}$$

Consider this expression carefully. It indicates that we are considering the pressure to be the sum of a mean value p_m, which is independent of both position x and time t, and an oscillating part that oscillates in time at angular frequency ω. Both the amplitude A and phase ϕ of the time oscillation are functions of position x.

It is much more convenient to rewrite Eq. (1.16) as

$$p(x,t) = p_m + \mathrm{Re}\left[p_1(x)e^{i\omega t}\right], \tag{1.17}$$

where $p_1(x)$ is a complex function of x such that

$$|p_1(x)| = C(x), \tag{1.18}$$

$$\mathrm{phase}[p_1(x)] = \phi(x). \tag{1.19}$$

This notation is convenient because a single symbol with subscript 1 stands for both amplitude and phase, and because all the shortcuts of complex arithmetic can be used (with care). In this book, all variables with subscript 1 will be complex.

Sometimes we get lazy or forgetful, and we don't write Re[] explicitly, and we just say that $p_1(x)$ is the oscillating pressure; but of course we really always mean that $\mathrm{Re}[p_1(x)e^{i\omega t}]$ is the oscillating pressure, and $p_m + \mathrm{Re}\,[p_1(x)e^{i\omega t}]$ is *the* pressure. Sometimes we abbreviate further to simply p_1, leaving the fact that is depends on x to memory.

One of the reasons that thermoacoustics is at first confusing is that the acoustic variables are wavelike functions of both position and time. Remember that the time dependence is assumed to be exactly sinusoidal in our acoustic approximation; the spatial dependence need not be sinusoidal but sometimes turns out to be nearly so over portions of an apparatus. When talking about the phase of such a wave, it is occasionally necessary to explicitly say *temporal* phase to identify interest in the phase of the *time* oscillation, not the x dependence.

To be sure this notation is clear, we will revisit the continuity equation, Eq. (1.9) above. Consider a lossless acoustic wave oscillating adiabatically along the x direction in a gas with no overall temperature gradient along x. We can write the pressure p, density ρ, and velocity u as

$$p(x,t) = p_m + \mathrm{Re}\left[p_1(x)e^{i\omega t}\right], \tag{1.20}$$

$$\rho(x,t) = \rho_m + \mathrm{Re}\left[\rho_1(x)e^{i\omega t}\right], \tag{1.21}$$

$$u(x,t) = \mathrm{Re}\left[u_1(x)e^{i\omega t}\right], \tag{1.22}$$

with the absence of u_m in Eq. (1.22) indicating that no steady wind is superimposed on the oscillating flow. Defining a^2 as the proportionality constant linking adiabatic density changes and adiabatic pressure changes,

$$a^2\, d\rho = dp, \tag{1.23}$$

we can simplify the most general continuity equation

$$\frac{\partial \rho}{\partial t} + \nabla \cdot (\rho \mathbf{v}) = 0 \tag{1.24}$$

in one dimension, yielding

$$\frac{\partial p}{\partial t} + a^2 \frac{\partial}{\partial x}(\rho u) = 0. \tag{1.25}$$

Substituting our complex notation expressions Eqs. (1.20)–(1.22) into Eq. (1.25), and neglecting the term involving the product of ρ_1 and u_1, which is smaller than the other surviving terms, yields

$$\mathrm{Re}\left[i\omega p_1(x)e^{i\omega t}\right] + \rho_m a^2 \frac{\partial}{\partial x}\mathrm{Re}\left[u_1(x)e^{i\omega t}\right] = 0. \tag{1.26}$$

Note the freedom we have to interchange the orders of space and time derivatives, and to interchange the order of derivatives and the "real" operator. Hence, we can always write an equation like Eq. (1.26) in an abbreviated form:

$$i\omega p_1 + \rho_m a^2 \frac{du_1}{dx} = 0. \tag{1.27}$$

This expression is mathematically true, but in terms of physically realistic variables it is an abbreviation of Eq. (1.26).

For further clarification of the complex notation, consider some simple waves. A pure traveling wave, traveling in the positive x direction, as shown in Ani. Wave /t, is represented in complex notation as

$$p_1(x) = Ce^{-ikx}, \tag{1.28}$$

where $|C|$ is the amplitude, and the phase of the complex number C defines the overall temporal phasing of the wave relative to our choice of $t = 0$. A pure standing wave, as shown in Ani. Wave /s, is represented in complex notation as

$$p_1(x) = C\cos kx. \tag{1.29}$$

In a graphical representation of this complex notation known as a phasor diagram, the complex variables are plotted on the complex plane with the real axis horizontal and the imaginary axis vertical. Conventionally, arrows from the origin "point" to each such complex variable, and we will follow this convention here, as shown in Fig. 1.18. If you imagine a phasor ξ_1 in a phasor diagram rotating counterclockwise at angular frequency ω, then the time-dependent variable $\xi(t) = \mathrm{Re}\,[\xi_1 e^{i\omega t}]$ represented by the phasor is the projection of the phasor on the real axis.

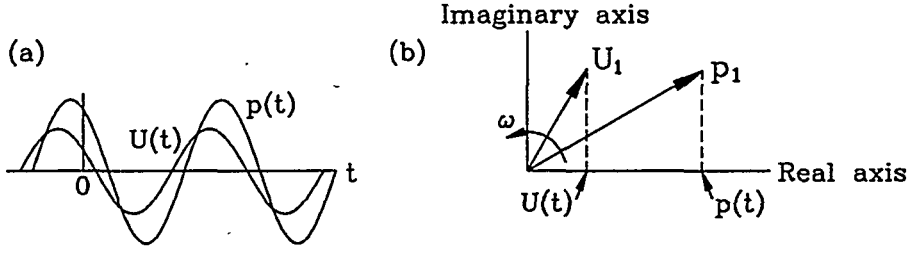

Figure 1.18: Phasors show complex variables in the complex plane. (a) Two sinusoidally time-dependent variables $p(t)$ and $U(t)$, with U leading p by 30°. (b) The phasor representation of these two variables can be imagined as two vectors whose magnitudes are the amplitudes of p and U, rotating counterclockwise at angular frequency ω. The true, time-dependent values of the associated variables are the projections on the real axis of these rotating phasors.

Phasor diagrams are extremely useful for indicating the relationships in magnitude and phase among many variables in complicated thermoacoustic systems, as we shall see later. For example, if a second variable is proportional to i times a first variable, the phasor for the second variable will point 90° counter-clockwise from the direction of the phasor for the first variable, and we say that the second variable "leads" the first variable by 90°. We use phasor diagrams so frequently that we usually neglect to label the axes "Real part" and "Imaginary part." Usually we are only illustrating the relative magnitudes and phases of variables—not their actual magnitudes—so we also neglect to provide quantitative scale. In fact, in such cases we often display variables having different units on the same plot, to

convey phase information without cluttering the figure with scale information, as in Fig. 1.19 where both p_1 and U_1 are shown for the simple lossless waves of Eqs. (1.28) and (1.29).

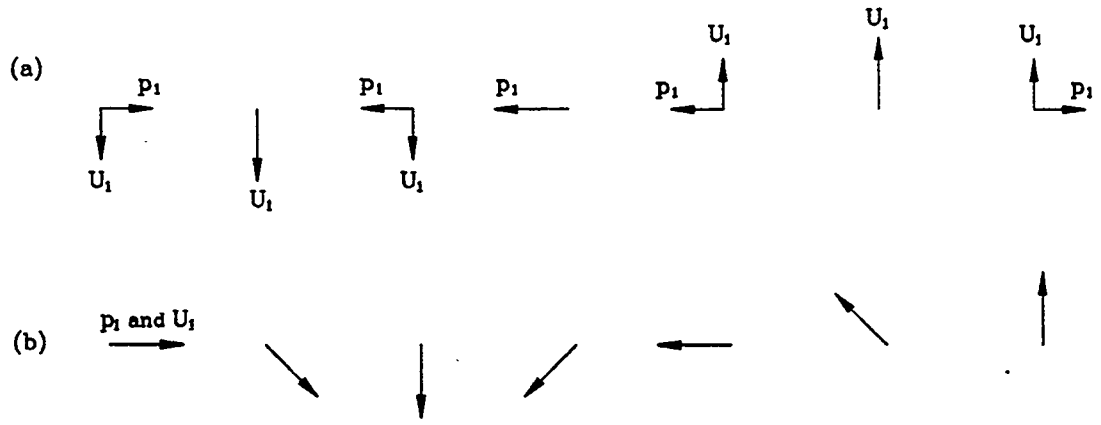

Figure 1.19: Phasors at seven locations in standing and traveling waves. The pressure p_1 and the volumetric velocity U_1 are shown. (a) Phasor diagram for Ani. Wave /s, corresponding to Eq.(1.29). (b) Phasor diagram for Ani. Wave /t, corresponding to Eq. (1.28). The phase of p_1 at the left edge of the animation screen is arbitrarily chosen to be zero in both cases.

1.5. Computations (DeltaE)

Most of the first half of the book emphasizes the development of intuition, lumped-element impedance estimates, and the promotion of a particular point of view. However, in daily practice of thermoacoustics I spend most of my time working with numerical integrations of the thermoacoustic equations, using DeltaE. It is hard to imagine progress in thermoacoustics today without use of such software.

Any one-dimensional acoustic wave equation, such as Eq. (1.11) or (1.12), is derived from a momentum equation such as Eq. (1.8) and a continuity equation such as Eq. (1.9) with appropriate details added as needed. Noting that the momentum and continuity equations can be solved for dp_1/dx and dU_1/dx respectively, an easy method of numerical integration suggests itself: $p_1(x)$ can be obtained by integrating the momentum equation with respect to x, while simultaneously $U_1(x)$ is obtained by integrating the continuity equation with respect to x. We will see in future chapters that the x dependence of mean temperature in stacks is subtle and can be determined by consideration of the conservation of energy flux through the stack, leading to a third fundamental differential equation that can be integrated to obtain $T_m(x)$ simultaneously with the other two equations.

DeltaE [20] integrates these one-dimensional equations, in a geometry given by the user as a sequence of segments, such as ducts, compliances, transducers, and thermoacoustic stacks or regenerators. In each segment, DeltaE uses locally appropriate momentum, continuity, and energy equations, controlled by local parameters (e.g. area or perimeter) and by global parameters (e.g. frequency and mean pressure). Solutions $p_1(x)$, $U_1(x)$, and $T_m(x)$ are

found for each segment and are matched together at the junctions between segments to piece together $p_1(x)$, $U_1(x)$, and $T_m(x)$ for the entire apparatus.

It is clear that this solution $T_m(x)$, $p_1(x)$, $U_1(x)$, is only determined uniquely if one real and two complex boundary conditions are imposed, because the governing equations comprise one real plus two complex coupled first-order equations in one real plus two complex variables. This is true whether considering a single segment or a one-dimensional string of segments with each joined to its neighbor(s) by continuity of T_m, p_1, and U_1. If all boundary conditions are known at the intial segment, then the integration is utterly straightforward. But usually some of the boundary conditions are known elsewhere. Under such conditions, DeltaE uses a shooting method, by guessing and adjusting any unknown boundary conditions at the initial segment to achieve desired boundary conditions elsewhere. The user of DeltaE enjoys considerable freedom in choosing which variables are used as boundary conditions and which are computed as part of the solution. For example, in a simple plane-wave resonator, DeltaE can compute the input impedance as a function of frequency, or the resonance frequency for a given geometry and gas, or the length required to give a desired resonance frequency, or even the concentration in a binary gas mixture required to give a desired resonance frequency in a given geometry.

Hoping that the usefulness of this book will greatly outlive version 4 of DeltaE, I have put typical DeltaE i/o files for each of the four examples that we will re-examine throughout the book in the Appendix. For interested readers, these show how to configure a simple file for DeltaE for each of these examples, and may occasionally be consulted to learn a specific dimension of a piece of apparatus. We find that DeltaE and experiment agree best when considerable detail is included in the DeltaE file; often, we have over 50 segments in a file to account for all the little details in hardware as built. To avoid intimidating the newcomer, the first two files in the Appendix are stripped of such details; they use only the key segments necessary to describe the hardware. The third file, for the traveling-wave engine, is fully encumbered with details, typical of what we actually work with; if you are new to DeltaE or to thermoacoustics, skip it! The fourth file, for the orifice pulse-tube refrigerator, includes only about 25% of the segments actually used to model this refrigerator, in order to hide Cryenco proprietary information.

The user's guide to DeltaE is available at http://rott.esa.lanl.gov, and it might be consulted occasionally while studying this book. A beta version of the code itself can be obtained from Bill Ward at ww@lanl.gov. The use of DeltaE in this book for examples requiring numerical integration is convenient for me, because it's the only thermoacoustics code I routinely use. However, I believe that some other codes, such as Sage by Gedeon [21], Thermoacoustica by Tominaga [22], and Regen3 by Radebaugh's group [23], are also accurate and useful for modeling thermoacoustic devices. Although each code has strengths and weaknesses, the good ones are in agreement on the fundamentals.

1.6. Animations

The computer animation "Ani. Wave" discussed above is the first of many animations to be used in this book. Studying them is vital.

These animations run in Windows 95, Windows 98, in full-screen DOS windows in Windows computers, and in raw DOS. They may run a little jerkily on old 386 computers.

Unless you have a DOS emulator, Macs are not an option.

Remember to use the "filename /option" form of the command line. Example: "wave /t" starts the Wave animation with traveling-wave settings; "wave /s" starts it with standing-wave settings. If you start an animation without typing the option, you may find yourself automatically sequencing through options in the order that I most often use in lectures.

For Windows 95 or 98, keep the same subdirectory structure on your hard disk as you received, so that the shortcuts in folder Win95-98 know where to find the executable files. Open the Win95-98 folder and double-click a shortcut icon to launch the appropriate animation /option. Example: Clicking "Wave_s (Standing)" executes the DOS command line "Wave /s".

For Windows 3.1, execute these the programs from a DOS-box window, or exit windows and run in raw DOS. To run the animations, "cd" to the DOS directory and type the program name with the option character, if any (e.g. /s), as specified here in the text. Either upper or lower case is acceptable.

Warning: If the typed text in the animations looks scrunched or incorrectly located, your DOS window is not using its default font settings or is not sized to the full screen. Edit properties to set font and screen size to defaults, and switch to full-screen DOS window (alt-enter). Better yet, avoid this problem in the first place by never starting an animation from a DOS window that's been modified: If you use Windows 3.1, exit to DOS and change directories to where the animations are; if you use Windows 95 or 98, start a fresh DOS window from "Start...Programs...MS-DOS Prompt" and change directories to where the animations are. These methods apparently cause Windows to open the DOS window in its default state. (This hassle arises because the animations were written in Microsoft Quickbasic, which uses DOS settings and fonts for locating and typing text. Hence the coordinate system where text appears on the screen in the animations depends on the DOS font settings.)

1.7. Outline

This book will not provide a complete description of how these heat engines and refrigerators work—for that, consult publications specific to each type, such as Refs. [7, 5, 4, 24, 25]. Instead, this book promotes one point of view allowing an understanding of all these devices. This point of view is based firmly on acoustics, with thermodynamics added as necessary.

Chapter 2 —Waves—examines the oscillatory pressure and velocity. This includes the relevant fundamentals of ordinary acoustics, resonance phenomena in resonators, and viscous damping and thermal contact to the side walls of the channel in which the wave propagates. One climax of that chapter is Rott's wave equation, Eq. (1.11) above. After studying the Waves chapter, you should be able to visualize and understand the overall wave behavior of a thermoacoustic apparatus, based on a drawing or description. This process involves thinking about all the dimensions of the apparatus in comparison to λ, δ_κ, and δ_ν, locating the nodes and antinodes of p_1 and U_1, identifying which parts of the wave are inertial and which are compliant, identifying which parts are affected by viscous flow resistance or by thermal relaxation effects, and predicting approximately the relative phases of p_1 and U_1 throughout the apparatus. At a coarse, qualitative level this process can be done by eye and by hand; quantitative results can be obtained by numerical integration of the momentum

and continuity equations.

The power—both thermal and acoustic—is of greatest interest in heat engines and refrigerators, so Chapter 3 —Power—adds these concepts to the pressure and velocity discussion. Acoustic power, the time-averaged product of p_1 and U_1, is produced in engines and consumed by refrigerators. Total power, which is the power that is subject to the first law of thermodynamics, is of even greater importance. After studying the Power chapter, you should be able to understand thermoacoustic engines and refrigerators in terms of energy-conservation, power flows, and acoustic-power dissipation and production. Quantitative results can be obtained as desired from products of the dynamical variables of Chapter 2.

This completes the portion of the book based closely on the work of Rott.

The second law of thermodynamics, which puts bounds on the performance of thermoacoustic engines and refrigerators, forms the basis of Chapter 4 —Efficiency. Key concepts are entropy generation, which can be subdivided according to location and mechanism, and exergy, which provides a quantitative figure of merit for thermodynamic devices and their interactions with their environment. Together, these concepts provide a standard, formal accounting method for sources of inefficiency. After studying this chapter, you should have an understanding of thermodynamic efficiency that goes beyond what is taught in standard physics courses and undergraduate engineering courses, and you should be able to visualize and understand the locations and mechanisms of irreversibility in a thermoacoustic apparatus, and account quantitatively for the irreversibilities.

Chapter 5 introduces many important issues that go beyond the low-amplitude, monofrequency approximation implicit in Rott's work. These issues include turbulence, entrance effects, superimposed steady flow, and harmonics. While the first four chapters stand on a firm foundation, these high-amplitude issues are at the frontier of current knowledge. However, they are of great concern in real devices, which usually operate at high amplitude in order to achieve high power per unit volume.

Chapter 6 presents practical construction techniques we've adopted at Los Alamos, Chapter 7 outlines methods of measurement used to diagnose thermoacoustic behavior, and Chapter 8 describes common pitfalls. An appendix gives some DeltaE files; I may drop this from the final version of the book, because I suspect they will become obsolete quickly.

A symbol table and references are included at the end.

(General overview references: fluid dynamics [26, 27], thermodynamics [2, 3, 28, 29, 1], acoustics [12, 13], thermoacoustics [30, 25, 31, 32, 33], Stirling systems [34, 7], pulse-tube refrigeration [24, 35].)

1.8. Exercises

1.1 Review the ideal-gas equation of state and other properties of ideal gases: For your favorite working gas, and your favorite temperature and pressure, look up γ, calculate the sound speed, density, and isobaric specific heat. Look up the viscosity and thermal conductivity. Pick your favorite frequency. Calculate λ, δ_κ, and δ_ν. Compare these lengths to various dimensions in your favorite piece of thermoacoustics hardware. Do you know the order of magnitude of $|x_1|$? Verify that $\delta_\nu/\delta_\kappa = \sqrt{\sigma}$. (If you don't have a personal favorite gas, etc., then use air at 300 K and atmospheric pressure, 440 Hz, and dimensions in your office. Estimate $|x_1|$ using the fact that conversational acoustics has $|p_1| \simeq 10^{-6}$ bar.)

1.2 Can you think of any other length scale in simple-harmonic oscillatory motion and thermodynamics in an ideal gas, besides λ, $|x_1|$, δ_ν, and δ_κ? If you can, when would it be important in thermoacoustics? How can we be sure we haven't forgotten an important length?

1.3 Do you know roughly what a kitchen refrigerator costs, and what is the cost of the electricity it consumes each year? If so, would you expect most people to choose to pay 50% more to buy a refrigerator that uses 50% less electricity?

1.4 A mixture of helium and argon has a sound speed of 500 m/s at 300 Kelvin. What is the concentration of argon in the mixture?

1.5 Thermodynamics review: Show that the ratio of isothermal compressibility to adiabatic compressibility is the same as the ratio γ of isobaric to constant-volume specific heats. Hence, show that $\rho_m a^2 = \gamma p_m$.

1.6 More thermodynamics review: Derive an expression for isothermal sound speed, instead of the usual adiabatic sound speed. Show that the isothermal sound speed is about 18% lower than the true, adiabatic speed in air, for which $\gamma = 7/5$. Can you think of circumstances in which sound propagates isothermally?

1.7 Review of complex notation: Derive Eq. (1.11) from whatever version of the starting equations (momentum, continuity, and state) you are most familiar with. Express all variables as in Eq. (1.7), and justify the neglect of all terms that you have to throw away to get to the desired answer. Review how the time derivatives in the starting equations become $i\omega$ in the complex acoustic approximation.

2. WAVES

The focus of this chapter will be on the dynamic variables, pressure and velocity, for wave propagation in the x direction in a channel or duct. Adopting increasingly sophisticated perspectives on the continuity equation, we will see how oscillations in pressure are coupled to spatial gradients in velocity. Adopting increasingly sophisticated perspectives on the momentum equation, we will see how oscillations in velocity are coupled to spatial gradients in pressure. Coupling these pictures together yields wave propagation. Initially, we will examine the lossless concepts of inertia and compressibility, later adding viscous loss to the momentum equation and thermal hysteresis (and gain) to the continuity equation. We'll alternate between formal mathematics, figures, and computer animations, to integrate quantitative tools with intuition. Throughout, we will assume monofrequency, constant-amplitude, small oscillations—an approximation that we will, for brevity, refer to simply as "the acoustic approximation."

The principle variables are oscillatory pressure p_1 and oscillatory volumetric velocity U_1, which is the integral of the x component of the velocity, u_1, over the cross sectional area A of the channel. At the transition between two channels, U_1 and p_1 are taken to be continuous. For example, at a transition from a first duct to a second duct, U_1 out of the first duct has nowhere to go but into the second duct, so $U_{1f} = U_{1s}$, and hence if the areas of the ducts are A_f and A_s then the velocity (not volumetric velocity!) changes by the factor A_f/A_s. At such a junction between two ducts, p_1 must also be continuous, because any pressure discontinuity represents a shock front, outside the realm of the acoustic approximation and today's thermoacoustics.

2.1. Lossless acoustics; ideal resonators

The simplest lossless version of the acoustic continuity equation, Eq. (1.9) or (1.27), can be rewritten

$$p_1 = -\frac{\gamma p_m}{i\omega A\,\Delta x}\Delta U_1 \tag{2.1}$$

$$= -\frac{1}{i\omega C}\Delta U_1 \tag{2.2}$$

for the short length Δx of channel of cross-sectional area A shown in Fig. 2.1a. To arrive at these equations, we have used Eq. (1.10) to express ρ_1 in terms of p_1, and used the ideal-gas identity $\rho_m a^2 = \gamma p_m$, which is derived in one of the exercises at the end of Chapter 1. In Eq. (2.2),

$$C = \frac{V}{\gamma p_m} \tag{2.3}$$

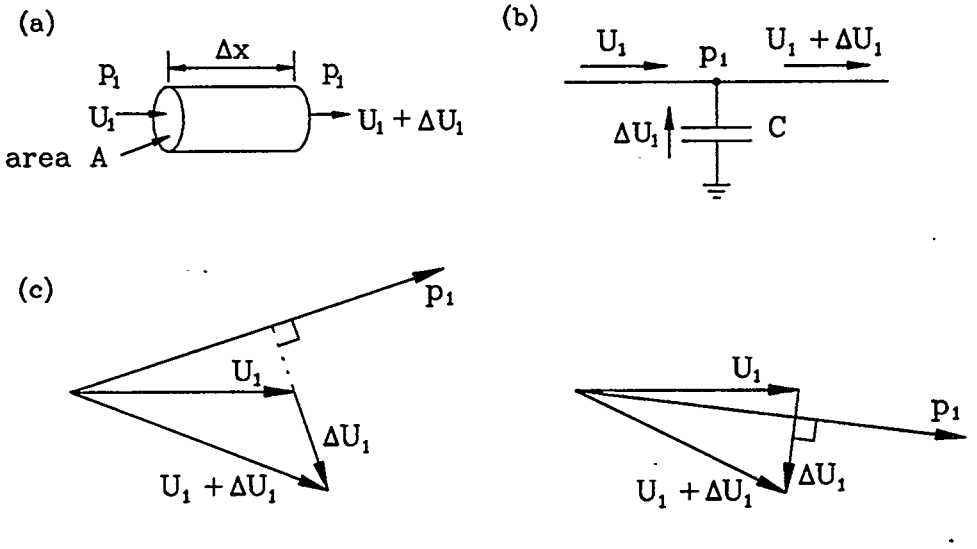

Figure 2.1: (a) A short channel in which the compressibility of the gas is important. (b) Symbolic impedance diagram of the channel. The symbol C indicates compliance. (c) Two possible phasor diagrams for the channel.

is called the compliance of the channel. The compliance is the ratio of the volume $V = A\Delta x$ of the channel to the compressibility γp_m; larger volume or lower ("softer") compressibility means greater compliance. This combination of variables gives us the springy, compressive properties of the gas in the channel.

Similarly, the lossless version of the acoustic momentum equation, Eq. (1.8), can be rewritten

$$\Delta p_1 = -i\omega \frac{\rho_m \Delta x}{A} U_1 \tag{2.4}$$

$$= -i\omega L U_1, \tag{2.5}$$

for the short length of channel shown in Fig. 2.2a. Note that the channel illustrated is the same as in Fig. 2.1a; the figures differ only because we're focusing our attention on different properties of this channel in the two situations. In Eq. (2.5),

$$L = \frac{\rho_m \Delta x}{A} \tag{2.6}$$

is called the inertance of the channel. It is the product of the gas density ρ_m and the length Δx divided by the cross-sectional area A of the channel. This combination of variables describes the inertial properties of the gas in the channel.

Writing the continuity and momentum equations in this way allows an accurate analog between acoustic systems and ac electrical circuits, motivating the symbolic "circuit" diagrams of Figs. 2.1b and 2.2b. The analog of oscillating pressure p_1 is ac voltage; the analog of oscillating volumetric velocity U_1 is ac current. The analog of compliance is capacitance to ground, and the analog of inertance is series inductance. (Note that "inertance" sounds a little like the electrical word "inductance" and a little like the mechanical word "inertia.")

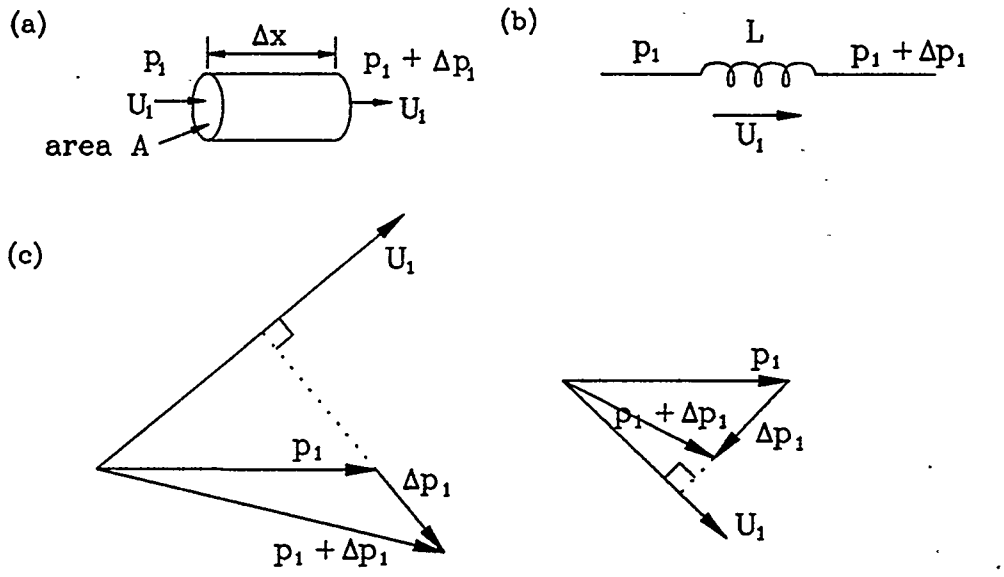

Figure 2.2: (a) A short channel in which the inertia of the gas is important. (b) Symbolic impedance diagram of the channel. The symbol L signifies the inertance. (c) Two possible phasor diagrams for the channel.

We will rely on this point of view extensively, because I suspect that many readers (especially physicists and electrical engineers) have some prior experience with ac electric circuits. However, I've noticed that other engineers and scientists often gain no intuition from what is to them a totally unfamiliar analog. Such readers, unfamiliar with ac electrical circuits, can take the "circuit diagrams" to be no more than abstract representations of the acoustic impedance networks themselves, and I will try to use nothing but acoustic terminology in referring to these diagrams. When you look at the symbol for inertance in Fig. 2.2b, think of a long, coiled tube through which the dense gas must accelerate. When you look at the symbol for resistance in figures later in this chapter, think of a kinked tube through which the gas must overcome viscous resistance. When you look at the symbol for compliance in Fig. 2.1b, think of a spongy cushion between the two parallel lines, whose gap changes in response to pressure.

Figures 2.1c and 2.2c show possible phasor diagrams for a compliance and an inertance, respectively. In Fig. 2.1c, note that $|U_1 + \Delta U_1|$ could be either larger or smaller than $|U_1|$; the only strict requirement imposed by Eq. (2.2) is that ΔU_1 must lag p_1 by 90°. Similarly, in Fig. 2.2c, the only strict requirement imposed by Eq. (2.5) is that Δp_1 must lag U_1 by 90°. Beyond these requirements, anything is possible, depending on the relative magnitudes and phases of p_1 and U_1.

Usually, both the inertance and the compliance of a channel simultaneously contribute to the behavior of the wave propagation in the channel, as illustrated in Fig. 2.3 for a channel of differential length dx. As before, note that dp_1 lags U_1 by 90°, and dU_1 lags p_1 by 90°.

The complex ratio $Z = -p_1/U_1$, which is called the impedance, is of great utility in discussing acoustic systems. Sometimes we refer to the impedance at a location in a wave, but sometimes we refer to the impedance of a component so that $Z = -\Delta p_1/U_1$ is related

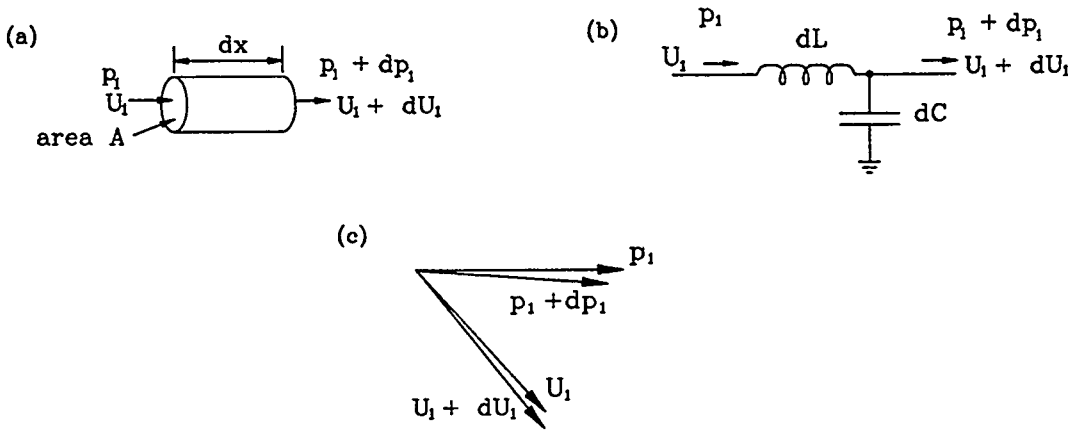

Figure 2.3: (a) A very short channel in which both the compressibility and the inertia of the gas are important. (b) Symbolic impedance diagram of the channel. (c) A possible phasor diagram for the channel.

to the pressure difference across the component or $Z = -p_1/\Delta U_1$ describes the change in volumetric velocity caused by the component. In the latter modes, Eq. (2.5) shows that the impedance of an inertance is $Z = i\omega L$, and Eq. (2.2) shows that the impedance of a compliance is $Z = 1/i\omega C$.

The double Helmholtz resonator, illustrated in Fig. 2.4, is a simple acoustic resonator consisting of two bulbs, each of volume V, connected by a short neck with length Δx and cross-sectional area A. All dimensions are shorter than the acoustic wavelength, so the lumped-impedance models of Figs. 2.1 and 2.2 are directly applicable: Each bulb is a compliance C, and the neck connecting the two bulbs is an inertance L. (In the simple, textbook Helmholtz resonator, the compliance of the neck and inertial effects in the compliances are assumed negligible.) Imagine the inertial mass of gas in the neck bouncing back and forth sinusoidally against forces exerted by the gas springs in the two bulbs. Combining Eqs. (2.2) and (2.5) appropriately (or remembering that series ac electric circuits are resonant when the sum of the impedances is zero), it is easy to show that p_1 and U_1 are nonzero only if

$$i\omega L + 2/i\omega C = 0, \tag{2.7}$$

and hence that the resonance frequency of the Helmholtz resonator is given by

$$(2\pi f)^2 = \omega^2 = \frac{2}{LC} = 2\frac{\gamma p_m}{\rho_m}\frac{A}{V\,\Delta x}. \tag{2.8}$$

At this frequency, either Eq. (2.2) or (2.5) gives the relative magnitudes of p_1 and U_1, and their relative phases. The relative phases are illustrated in the phasor diagram in Fig. 2.4c, where we have arbitrarily picked the phase of U_1 in the inertance to be zero.

In lossless acoustic resonators more complicated than the Helmholtz resonator, the acoustic waves are described by the coupled differential equations (1.8) and (1.9). Hence, to understand lossless acoustic waves in a duct or resonator, we must simultaneously keep

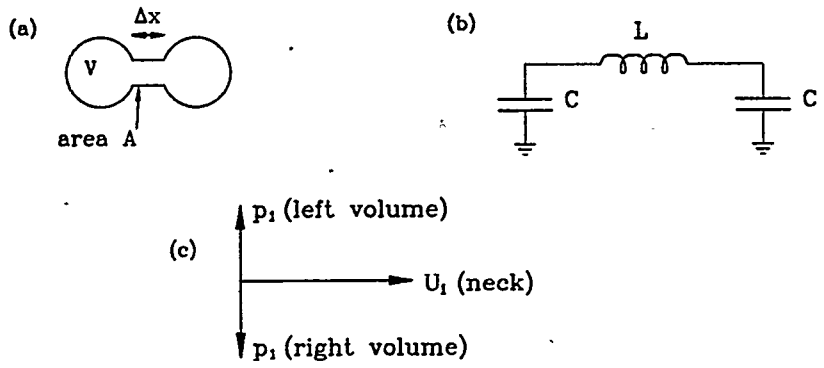

Figure 2.4: The double Helmholtz resonator. (a) Schematic of the resonator, comprising two bulbs connected by a neck. (b) Impedance diagram of the resonator. (c) Phasor diagram.

in mind the concepts of compliance and inertance. First consider the standing wave shown in Ani. Wave /s. This animation illustrates a wave oscillating horizontally in a duct of uniform cross section. The uppermost graph shows the pressure of the gas in the wave as a function of position and time. The middle graph shows the velocity in the gas as a function of position and time (with positive velocity to the right). The lower part of the display shows the motion, or displacement, of the gas in the duct. The moving vertical lines move with the gas; imagine that these lines are massless sheets of cellophane or thin clouds of smoke moving with the gas.

First focus attention on the velocity node, where the gas never moves. This region of the duct is functionally similar to a bulb of the double Helmholtz resonator described above. With zero velocity, Eq. (2.5) indicates that there should be no spatial pressure gradient, and indeed the animation shows that the oscillating pressure has no gradient in the vicinity. Hence, the inertance per unit length in the duct is irrelevant in this vicinity. The nonzero oscillating p_1 in this vicinity, however, indicates that Eqs. (2.1) and (2.2) are important. This region of the duct has compliance per unit length, so that the oscillating pressure can only occur in the presence of a spatial gradient in velocity, which is needed to supply and remove the mass necessary to cause the local density to increase and decrease. The presence of i in Eq. (2.2) indicates a 90° temporal phase shift between the pressure oscillations and the oscillating velocity gradient; this temporal phase relationship is also evident in the animation.

Now focus attention on one of the pressure nodes in Ani. Wave /s. This region of the duct is functionally similar to the neck of the double Helmholtz resonator described above. Here, $p_1 = 0$, so Eq. (2.2) indicates that gradients in velocity must be zero and that the compliance per unit length in this portion of the duct is irrelevant. However, the nonzero oscillating velocity in this region and Eq. (2.5) show that here the oscillating pressure must have nonzero gradients, as seen in the animation; additionally, both Eq. (2.5) and the animation indicate a 90° temporal phase shift between pressure gradient and velocity.

Precisely at the pressure node in the standing wave, the compliance per unit length is irrelevant. Precisely at the velocity node, the inertance per unit length is irrelevant. Everywhere else in the standing wave, where neither p_1 nor U_1 are zero, both inertance and

compliance per unit length contribute to the behavior of the wave. (This is, in fact, what makes it a wave instead of a lumped-impedance oscillator such as the double Helmholtz resonator.) Near the pressure antinodes, the compliance per unit length is more important than the inertance per unit length; near the velocity antinodes, the inertance per unit length is more important than the compliance per unit length.

While separate regions of predominantly compliance and predominantly inertance are apparent in the standing wave, in the traveling wave illustrated in Ani. Wave /t each location is a time-shifted replica of any other location, with inertance and compliance temporally alternating in importance at each location. If you focus your attention on one location in the animation, you should be able to "see" this alternation. In wave propagation, the thermophysical properties responsible for compliance, γp_m, and for inertance, ρ_m, are combined to form the sound speed $a = \sqrt{\gamma p_m / \rho_m}$.

Phasor diagrams for both wave animations are shown in Fig. 1.19.

Example: standing-wave engine. The resonator of the standing wave engine illustrated in Figs. 1.9 and 1.10 is particularly simple. It is essentially a half-wavelength-long resonator, closed at both ends so that the velocity nodes are at the ends and the pressure node is in the center. This overall wave shape is illustrated roughly in Ani. Standing /k. However, note in Fig. 1.10 that the diameter of the central portion of the resonator is slightly smaller than the diameter of the two ends. This diameter variation serves several functions, most of which we will discuss in Chapter 5. One of those functions is to lower the resonance frequency slightly below $f = a/2\Delta x$, where Δx is the overall length of the resonator. This frequency reduction is considered quantitatively in one of the exercises at the end of this chapter. However, using the concepts of inertance and compliance, it is easy to see qualitatively how this diameter variation leads to a lower resonance frequency: The half-wavelength resonator can be thought of crudely as consisting of two compliances on the two ends with an inertance the middle, so that the resonance crudely resembles that of the double Helmholtz resonator shown in Fig. 2.4. If the diameter of the inertance is reduced, L goes up according to Eq. (2.6), and hence the resonance frequency of the CLC resonator goes down as suggested by Eq. (2.8). From an alternative point of view, if the diameter of the compliances is increased, the value of C goes up according to Eq. (2.3), and again the resonance frequency of the CLC circuit goes down according to Eq. (2.8). In the example drawn to scale in Fig. 1.10, but with the branch to the refrigerators sealed off, the resonance frequency was 10% lower than the frequency for which the half wavelength equals the length of the apparatus. (Nevertheless, we will continue to speak loosely of such a resonator as a half wavelength resonator, because this phrase captures the essential nature of the standing wave: pressure maxima at the two ends and a velocity maximum in the center.)

Example: standing-wave refrigerator. The standing-wave refrigerator resonator, shown in Figs. 1.11 and 1.12, also employs variations in diameter (visible in Fig. 1.11) to reduce the resonance frequency below that for which a full wavelength would equal the total path length around the resonator. The apparatus has left-to-right symmetry, so that driving the loudspeaker pairs 180° out of phase ensures that pressure nodes appear at the top center and bottom center of the resonator. Hence, these are the locations of high

velocity, where inertance is important. The parts of the resonator near the loudspeakers have high pressure amplitude and hence are the regions where compliance is important. These compliance portions are enlarged in diameter relative to the inertance portions, so the resonance frequency is reduced.

Example: lumped approximation to half-wavelength resonator. For the uniform-diameter half-wavelength resonator shown in Fig. 2.5a, the most accurate impedance diagram would have an infinite number of inertances dL and compliances dC, as suggested by the large number of them in Fig. 2.5a, which would yield the sinusoidal x dependences of p_1 and U_1 shown. Numerical integrations for accurate results might have 10 or 20 such segments, with each being integrated by a Runge-Kutta method so that each is effectively subdivided even further. However, the essence of the resonance is simply what is shown in the phasor diagram of Fig. 2.5b, with pressure oscillations at the two ends having equal magnitudes and opposite phases, and the velocity in the center phased 90° from the pressures. Hence, if numerically accurate results are not needed, the essence can be captured with the simpler impedance diagram shown in Fig. 2.5c, in which the central third of the resonator is modeled as an inertance and the two ends as compliances. The accuracy of this crude approximation is suggested by the close resemblance of the trapezoidal distributions for p_1 and U_1, as compared to the sinusoids of Fig. 2.5a. (For further consideration of the accuracy of this crude approximation, see one of the exercises at the end of the chapter.)

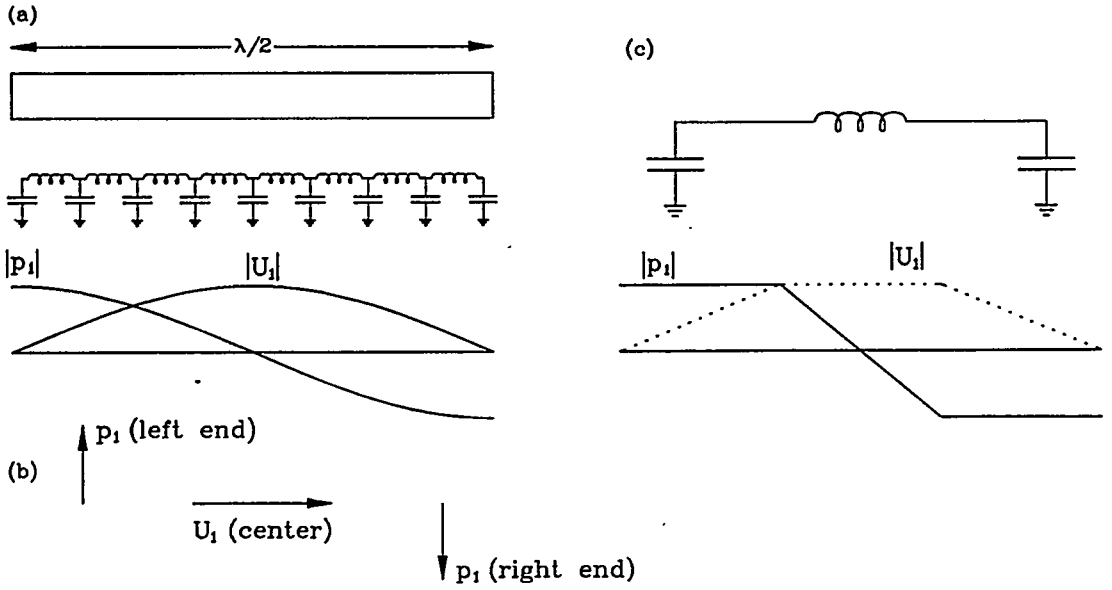

Figure 2.5: (a) The half-wavelength resonator, with sinusoidal $p_1(x)$ and $U_1(x)$, is properly regarded as an infinite series of infinitely small inertances and compliances. (b) The phasors at the ends and center are particularly simple. (c) Two compliances and one inertance capture these simple end behaviors, with reduced accuracy in values of p_1 and U_1 at intermediate x.

2.2. Viscous and thermal effects in large channels

To introduce the key concepts of dissipation and gain into the lossless acoustics picture developed so far, we'll start with a simple "complete" thermoacoustics problem: the ordinary viscous and thermal attenuation of sound propagating in a large channel due to the sound wave's interaction with the solid channel wall.

We consider sound propagating in the x direction in an ideal gas within a channel with constant cross-sectional area A and perimeter Π. The hydraulic radius

$$R_h = A/\Pi \tag{2.9}$$

is conventionally defined as the ratio of cross-sectional area to perimeter. (The hydraulic radius can also be thought of as the ratio of gas volume to gas-solid contact area, or as the distance from a typical parcel of gas to the nearest solid surface. Note that the hydraulic radius of a circular channel is *half* the circle's actual radius!) In this section, we will consider only channels for which $R_h \gg \delta_\nu$ and $R_h \gg \delta_\kappa$: the boundary-layer approximation. We use our usual complex notation for time-oscillatory quantities (pressure p, temperature T, velocity component u in the x direction, density ρ, entropy per unit mass s) :

$$p = p_m + \mathrm{Re}\left[p_1(x)e^{i\omega t}\right] + \ldots , \tag{2.10}$$

$$u = \mathrm{Re}\left[u_1(x,y)e^{i\omega t}\right] + \ldots , \tag{2.11}$$

$$T = T_m + \mathrm{Re}\left[T_1(x,y)e^{i\omega t}\right] + \ldots , \tag{2.12}$$

$$\rho,\ s,\ \text{etc.} = \text{similar to } T, \tag{2.13}$$

with μ, k, etc. constant. In this section, the channel is assumed to be spatially isothermal, so T_m is independent of x in Eq. (2.12). The coordinate y measures the distance from the wall of the channel, with $y = 0$ at the wall, as shown in Fig. 2.6.

2.2.1. Viscous resistance

To develop quantitative understanding of viscous effects, we consider the situation illustrated in Fig. 2.6 to find the y dependence of the gas velocity, using the x-component of the momentum equation, for which the acoustic approximation is

$$i\omega\rho_m u_1(x,y) = -\frac{dp_1(x)}{dx} + \mu\frac{\partial^2 u_1(x,y)}{\partial y^2} . \tag{2.14}$$

The x derivatives of u_1 have been neglected because they are of order $1/\lambda$, and hence are much smaller than the y derivatives, of order $1/\delta_\nu$. This equation is the appropriate approximation to Newton's law, $F = ma$, for a differential volume of gas: The left hand side is mass times acceleration, and the right hand side is the sum of the forces—the pressure force and the viscous force.

Equation (2.14) is an ordinary differential equation for $u_1(x,y)$ as a function of y. With two boundary conditions, $u_1(y=0) = 0$ at the solid surface and u_1 finite as $y \longrightarrow \infty$, its solution is

$$u_1 = \frac{i}{\omega\rho_m}\left[1 - e^{-(1+i)y/\delta_\nu}\right]\frac{dp_1}{dx}. \tag{2.15}$$

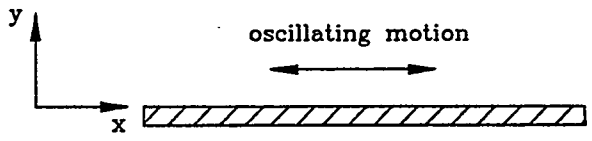

Figure 2.6: The coordinate system used in this section. In the boundary-layer approximation, the opposite wall of the channel is at such large y that it doesn't appear in this figure.

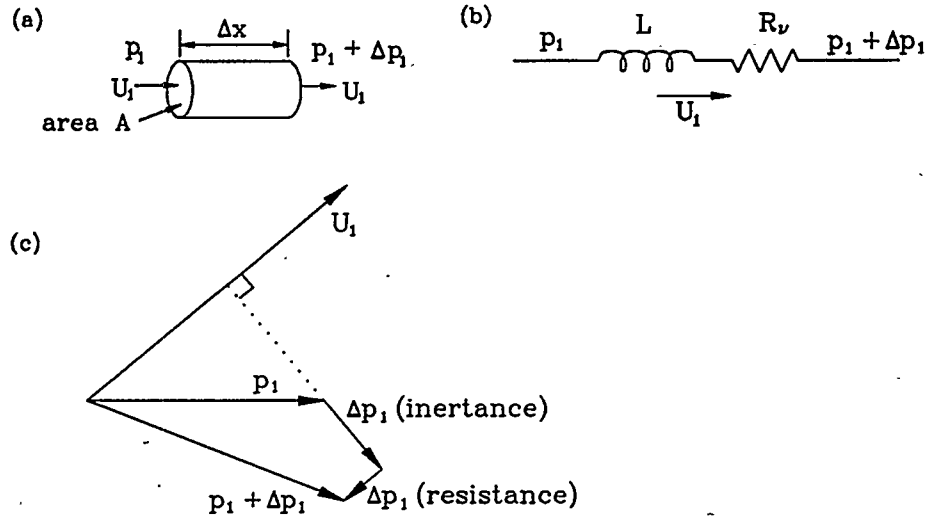

Figure 2.7: The momentum equation describes inertial and resistive effects in a channel. (a) A short channel, of length Δx and cross-sectional area A. (b) Impedance diagram showing inertance L and resistance R_ν. (c) A typical phasor diagrams for this situation, showing that the pressure difference Δp_1 is the sum of inertial and resistive components.

This function shows how viscosity reduces the magnitude of the oscillatory velocity and shifts its phase.

The complex notation is compact and easy to manipulate, but difficult to interpret intuitively. To gain a visual appreciation for the boundary-layer velocity expression, Eq. (2.15), study Ani. Viscous /m, which displays the particle displacement $x(y,t) = \mathrm{Re}\left[u_1(y)e^{i\omega t}/i\omega\right] \propto \mathrm{Re}\left[\left(1 - e^{-(1+i)y/\delta_\nu}\right)e^{i\omega t}\right]$ with y vertical and the acoustic oscillation direction x horizontal. The moving line can be imagined to be a very thin cloud of smoke moving with the oscillating gas. The tic mark spacing on the vertical axis is the viscous penetration depth δ_ν. Gas that is much closer than δ_ν to the solid boundary is nearly at rest. Gas that is much farther than δ_ν from the solid boundary experiences essentially no viscous shear; it moves with a velocity and displacement that are independent of y. This inviscid motion is purely inertial; the acceleration is in phase with the force, which is $-dp_1/dx$, so the displacement is in phase with $+dp_1/dx$. Gas that is roughly δ_ν from the nearest solid surface moves with a modified, y-dependent velocity and a significant, y-dependent phase shift.

In boundary-layer approximation, we often need the spatial average, over the cross-

sectional area A, of a boundary-layer function $F(y)$ such as Eq. (2.15). Using Eq. (2.9) defining the hydraulic radius, we can write such an average as

$$\langle F \rangle = \frac{1}{A} \int F \, dA = \frac{1}{\Pi R_h} \int_0^{R_h} F(y) \, \Pi \, dy \simeq \frac{1}{R_h} \int_0^{\infty} F(y) \, dy. \tag{2.16}$$

Thus, the spatial average of Eq. (2.15) is

$$\langle u_1 \rangle = \frac{i}{\omega \rho_m} \left[1 - (1-i) \frac{\delta_\nu}{2R_h} \right] \frac{dp_1}{dx}. \tag{2.17}$$

In the previous section, the lossless momentum equation led to Eq. (2.5) and to the concept of inertance for a short channel with length Δx and area S. Now, including losses, Eq. (2.17) shows that the corresponding expression is

$$\Delta p_1 = -\frac{i\omega \rho_m \Delta x / A}{1 - (1-i)\delta_\nu / 2R_h} U_1 \tag{2.18}$$

$$= -Z U_1 \tag{2.19}$$

$$= -(i\omega L + R_\nu) U_1, \tag{2.20}$$

so viscosity adds viscous resistance R_ν in series with inertance L to comprise total series impedance $Z = R_\nu + i\omega L$ as shown in Fig. 2.7b. In this boundary-layer approximation, the inertance and resistance are

$$L \simeq \frac{\rho_m \Delta x}{A} \tag{2.21}$$

$$R_\nu \simeq \frac{\mu \Pi \Delta x}{A^2 \delta_\nu} = \frac{\mu \Delta S}{A^2 \delta_\nu} \tag{2.22}$$

to lowest order in δ_ν / R_h; Π is the perimeter of the channel and $\Delta S = \Pi \Delta x$ is its surface area. Note that R_ν and L are real; hence, the "i" in Eq. (2.20) implies that the inertial contribution to the pressure difference leads the resistive contribution by 90°, as shown in Fig. 2.7c.

So think of any length of channel as having resistance caused by viscosity and inertance caused by mass. A fat channel, with $R_h \gg \delta_\nu$, has $\omega L \gg R_\nu$. In fact, in that limit the ratio $\omega L / R_\nu$ is proportional to $A / \Pi \delta_\nu$, so it is useful to think of the core of the channel, with volume $A \Delta x$, as being responsible for the inertance, while the lossy inner skin of the channel, with volume of order $\Pi \delta_\nu \Delta x$ equal to the channel's surface area times the viscous penetration depth, as being responsible for the resistance.

Example: orifice pulse-tube refrigerator. Consider the lumped-element components at the top of the orifice pulse-tube refrigerator shown in Fig. 1.16: a compliance, an inertance, and two valves. The purpose of these components is to provide an adjustable acoustic impedance at the top of the pulse-tube refrigerator, with the adjustments made by the valve settings. To make a simple example, we will neglect resistances in the inertance and compliance, so that the network will be regarded as shown in Fig. 2.8a. We consider a 40-Hz, 3.1-MPa helium operating point, with the network at 300 K. The compliance has

a volume of 9.8 liters, so according to Eq. (2.3) $C = 1.9 \times 10^{-9}$ m^3/Pa and its impedance $1/\omega C = 2.1$ MPa-s/m^3. The inertance has a length of 2.5 m and a diameter of 2.4 cm, so according to Eq. (2.6) $L = 26\,800$ Pa-s^2/m^3 and its impedance $\omega L = 6.7$ MPa-s/m^3. To keep this example simple, regard the two valves as resistances R_s and R_p, adjustable from zero to infinity. Then the net impedance provided by the network is

$$Z = \frac{1}{1/(i\omega L + R_s) + 1/R_p} + \frac{1}{i\omega C}. \tag{2.23}$$

Plotting Eq. (2.23) for all values of R_s and R_p shows that adjustment of the two valves allows access to the entire region of complex Z that is shaded in Fig. 2.8b.

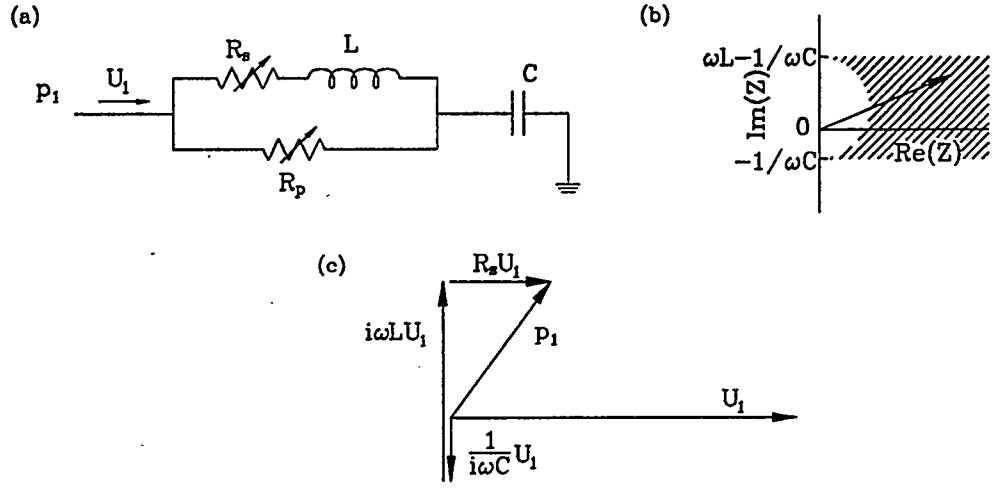

Figure 2.8: (a) Impedance diagram for the acoustic network at the top of the orifice pulse-tube refrigerator. (b) The shaded zone of the plot shows values of Z accessible by adjusting the two valves. (c) Phasor diagram for one case in which the valve labeled "R_p" is closed.

Suppose the valves were set so that $R_p = \infty$ (i.e. closed) and $R_s = 3.35$ MPa-s/m^3. Then Eq. (2.23) shows that $Z = (3.35 + i4.6)$ MPa-s/m^3, so the phase of Z is 54°. The phasor diagram for this case is shown in Fig. 2.8b, where we have arbitrarily chosen the phase of U_1 to be zero.

If we use DeltaE to model the inertance, we can account for its series resistance R_v. For one operating point, such a DeltaE model is

```
BEGIN       the setup
  3.1114E+06 a Mean P     Pa
    42.000   b Freq.      Hz
   305.20    c T-beg      K
  9.3205E+04 d |p|@0      Pa
     0.0000  e Ph(p)0     deg
  4.3536E-02 f |U|@0     m^3/s
  -98.944    g Ph(U)0     deg
 helium      Gas type
```

```
 ideal      Solid type
!---------------------------------  1 ---------------------------------
 ISODUCT    the inertance
  4.6400E-04 a Area       m^2            2.0075E+05 A |p|        Pa
  7.6360E-02 b Perim      m               159.47    B Ph(p)     deg
     2.4900  c Length     m              4.0435E-02 C |U|      m^3/s
  5.0000E-04 d Srough                    -96.129    D Ph(U)     deg
```

We compute $Z = \Delta p_1/U_1$, where $\Delta p_1 = (281 - i70)$ kPa is the pressure difference across the inertance and $U_1 = (0.0055 + i0.0416)$ m^3/s is the average of the volumetric velocities at the two ends of the inertance. The result is $Z = (0.78 + i6.86)$ MPa-s/m^3, so that $L = 27\,300$ Pa-s^2/m^3, $\omega L = 6.86$ MPa-s/m^3, and $R_\nu = 0.78$ MPa-s/m^3. Our neglect of R_ν with respect to ωL in the previous paragraph was reasonable but not excellent; this calculated R_ν is larger than we would guess from $\omega L \delta_\nu / R_h$ because DeltaE includes the effect of turbulence, which we will discuss in Chapter 5. Our estimate of L in the previous paragraph differed only 2% from the result of this numerical integration.

Example: standing-wave refrigerator. Consider one of the central tees in the standing-wave refrigerator of Fig. 1.11. These locations are pressure nodes, so compliance (though it could be calculated) is irrelevant here; these are locations of high velocity, so inertance and series resistance are important. Because of the way the black cones fit into the tees, the horizontal passage through each tee actually comprises three ducts in series: a 12.7-cm-long, 11.2-cm-diam duct between two 5.7-cm-long, 10.2-cm-diam ducts. We compute L and R_ν for each of these at a typical operating point: 300 K, 92 Hz, 8% argon and 92% helium at a mean pressure of 324 kPa. Since δ_ν is only 0.3 mm, the boundary-layer Eqs. (2.21) and (2.22) are appropriate. The results are $L = 24.1$ Pa-s/m^3, $\omega L = 13\,900$ Pa-s/m^3, and $R_\nu = 75$ Pa-s/m^3. Indeed, $\omega L \gg R_\nu$, as expected for a large-diameter component. These two tees, with parts of the cones nearby, contribute the inertance necessary for the full-wave resonance. Although the resonator is not really lumped-element, we could represent it crudely as such, as shown in Fig. 2.9.

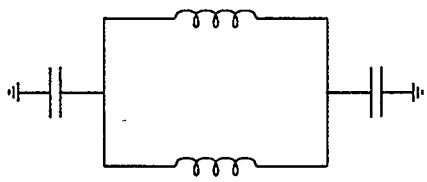

Figure 2.9: Crudest representation of the resonator of the standing-wave refrigerator.

2.2.2. Thermal-relaxation conductance

The viscous effects discussed thus far are only one component of acoustic attenuation at a solid boundary; thermal relaxation effects can be equally important wherever oscillating

pressure exists, as it causes an oscillating temperature. The general equation of heat transfer [26]

$$\rho c_p \left(\frac{\partial T}{\partial t} + \mathbf{v} \cdot \nabla T \right) - \left(\frac{\partial p}{\partial t} + \mathbf{v} \cdot \nabla p \right) = \nabla \cdot (k \nabla T) + (\text{terms quadratic in velocity}) \quad (2.24)$$

expresses the fact that the temperature changes with time because of the sum of three effects: pressure changes, thermal conduction, and some velocity terms that don't concern us in the acoustic approximation. An example of the pressure-induced temperature changes is shown in Ani. Thermal /w. The animation shows temperature, pressure, and gas motion in a half-wavelength resonance; the temperature oscillations are both proportional to and in temporal phase with the pressure oscillations. Such adiabatic temperature oscillations are present in all sound waves in free space, although for typical "audio" amplitudes they are too small to be readily noticed.

Adopting the usual complex notation for the relevant variables, as expressed above in Eqs. (2.10)–(2.13), we find that Eq. (2.24) reduces to

$$i\omega \rho_m c_p T_1 - i\omega p_1 = k \frac{\partial^2 T_1}{\partial y^2} \quad (2.25)$$

in the channel. Similar to the viscous derivation above, we have neglected the x derivatives of T_1 because they are of order $1/\lambda$, and hence are much smaller than the y derivatives, of order $1/\delta_\kappa$. The solid usually has sufficient heat capacity and thermal conductivity to enforce $T_1 = 0$ on the gas at the solid surface $y = 0$; the other necessary boundary condition is that $T_1(\infty)$ is finite. Equation (2.25) is an ordinary differential equation for $T_1(y)$, identical in form and boundary condition to Eq. (2.14) for $u_1(y)$. Exploiting the similarity, the solution can be written

$$T_1 = \frac{1}{\rho_m c_p} \left[1 - e^{-(1+i)y/\delta_\kappa} \right] p_1, \quad (2.26)$$

and its spatial average can be written

$$\langle T_1 \rangle = \frac{1}{\rho_m c_p} \left[1 - (1-i) \frac{\delta_\kappa}{2R_h} \right] p_1. \quad (2.27)$$

Equation (2.26) shows how thermal contact with the solid surface reduces the magnitude and shifts the phase of the oscillatory temperature, similar to the effect of viscosity on oscillatory velocity discussed above. Gas that is much farther than δ_κ from the nearest solid surface is essentially adiabatic, experiencing adiabatic temperature oscillations $T_1 = (1/\rho_m c_p) p_1$ in phase with the pressure oscillations (as shown in Ani. Thermal /w). The temperature of gas that is much closer than δ_κ to the nearest solid surface oscillates little; it is locked to the time-independent wall temperature T_m by the heat capacity of the solid wall. At approximately δ_κ from the nearest solid surface, these oscillations are reduced in magnitude and shifted in phase. In this boundary-layer limit, the functional dependence of Eq. (2.26) is shown in Ani. Thermal /y, in which the tics on the y axis are separated by δ_κ.

This animation shows the oscillating temperature as a function of time and distance y from the wall,

$$T(y,t) = T_m + \frac{1}{\rho_m c_p} \mathrm{Re}\left[\left(1 - e^{(1+i)y/\delta_\kappa}\right) p_1 e^{i\omega t}\right], \tag{2.28}$$

with the motion of the gas toward and away from the wall illustrated by the vertical straight lines moving left and right.

Using

$$d\rho = -\frac{\rho}{T} dT + \frac{\rho}{p} dp \tag{2.29}$$

we can express the spatially averaged density as

$$\langle \rho_1 \rangle = -\frac{\rho_m}{T_m} \langle T_1 \rangle + \frac{\rho_m}{p_m} p_1. \tag{2.30}$$

Now we are finally ready to work with the continuity equation. Averaging Eq. (1.9) over the cross-sectional area of the channel gives

$$i\omega \langle \rho_1 \rangle + \rho_m \frac{d\langle u_1 \rangle}{dx} = 0. \tag{2.31}$$

Using Eqs. (2.30) and (2.27), and eliminating c_p by using

$$c_p = \frac{\gamma}{\gamma - 1} \frac{p_m}{\rho_m T_m}, \tag{2.32}$$

yields

$$i\omega \left[1 + (\gamma - 1)(1 - i)\frac{\delta_\kappa}{2R_h}\right] \frac{p_1}{\gamma p_m} + \frac{d\langle u_1 \rangle}{dx} = 0 \tag{2.33}$$

as an acoustic expression of the continuity equation in the presence of thermal relaxation effects.

In the previous section, the lossless continuity equation led to Eq. (2.2) and the concept of compliance. Here, the continuity equation leads to Eq. (2.33), which includes both compliance and thermal relaxation. Equation (2.33) can be rewritten for a short channel shown in Fig. 2.10a with volume $V = A\,\Delta x$ as

$$p_1 = -Z\,\Delta U_1, \tag{2.34}$$

where Z is the parallel combination of a compliance and a resistance,

$$\frac{1}{Z} = i\omega C + \frac{1}{R_\kappa}, \tag{2.35}$$

as shown in Fig. 2.10b. The effective compliance is given by

$$C \simeq \frac{V}{\gamma p_m} \tag{2.36}$$

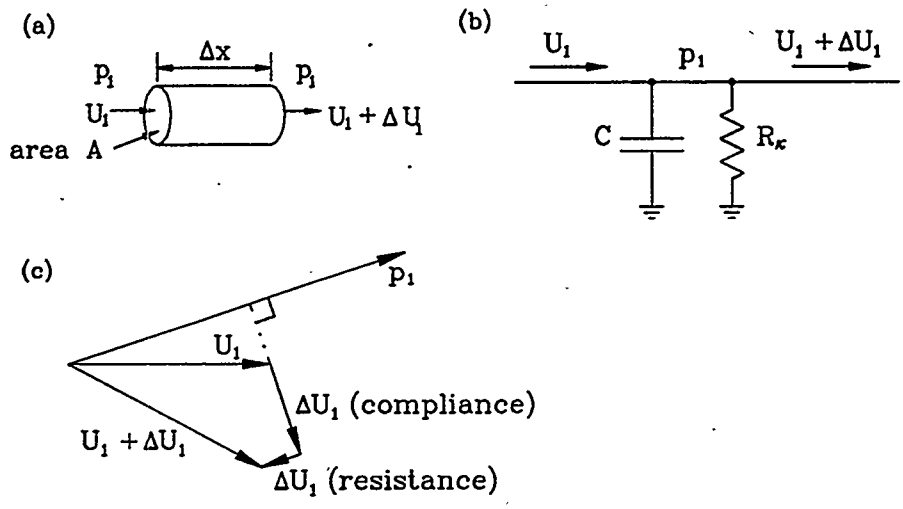

Figure 2.10: The continuity equation describes compliant and resistive effects in a channel. (a) A short channel, of length Δx and cross-sectional area A. (b) Impedance diagram showing compliance C and parallel resistance R_κ. (c) A typical phasor diagram for this situation, showing that the volumetric velocity change ΔU_1 is the sum of compliant and resistive components.

to lowest order in δ_κ/R_h. The effective resistance R_κ that is in parallel with the compliance is

$$R_\kappa \simeq \frac{2\gamma p_m}{\omega(\gamma-1)\delta_\kappa S}, \tag{2.37}$$

inversely proportional to the volume $S\delta_\kappa$ which experiences thermal relaxation.

So think of any channel as having compliance and thermal-relaxation resistance, which cause ΔU_1 to change from one end of the channel to the other. A wide open volume, with $V \gg S\delta_\kappa$, has $\omega C \gg 1/R_\kappa$, so the compliance dominates the net impedance. It is useful to think of the core of the volume V, with adiabatic compressibility, as being responsible for the compliance, while the vicinity of the inner surface, with effective volume $S\delta_\kappa$ equal to the channel's surface area times the thermal penetration depth, has a compressibility intermediate between the adiabatic and isothermal compressibilities and is responsible for the thermal-relaxation resistance.

Example: standing-wave engine. Consider one of the outer "hot ducts" (outboard of the hot heat exchangers) in the standing-wave engine of Fig. 1.10. This location is near a velocity node, so inertance and series resistance are unimportant. We will compute the compliance and its parallel thermal-relaxation resistance at a typical operating point: 3 MPa helium, 390 Hz, 800 K. Each hot duct has a volume of 120 cm^3 and a surface area of 130 cm^2 (accounting properly for the surface area and blocked volume due to electrical feedthroughs passing through this space). Since δ_κ is only 0.2 mm, we can use boundary-layer Eqs. (2.36) and (2.37), finding $C = 2.4 \times 10^{-11}$ m^3/Pa, $1/\omega C = 17$ MPa-s/m^3, and $R_\kappa = 2350$ MPa-s/m^3.

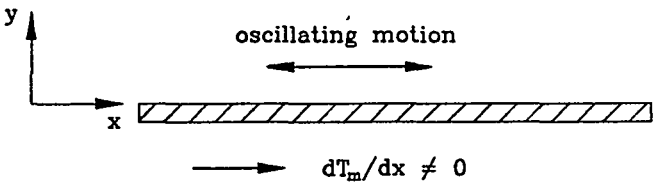

Figure 2.11: The coordinate system used in this section. In the boundary-layer approximation, the opposite wall of the channel is at such large $y >> \delta_\kappa$ that it doesn't apear in this figure.

Example: orifice pulse-tube refrigerator. The compliance at the top of the orifice pulse-tube refrigerator of Fig. 1.16 has a volume of 9.8 liters and a surface area of approximately 0.3 m^2. At 40 Hz with 3.1 MPa helium, we calculated a few pages ago that its compliance is $C = 1.9 \times 10^{-9}$ m^3/Pa and $1/\omega C = 2.1$ MPa-s/m^3. Equation (2.37) shows that $R_\kappa = 950$ MPa-s/m^3. Hence, $1/R_k$ can be safely neglected in comparison to ωC.

2.3. Inviscid boundary-layer thermoacoustics

Now we'll finally proceed to thermoacoustics problems in which a mean temperature gradient along the direction of acoustic oscillation is significant. The simplest such problem that I know of is not perfectly realistic, because viscosity is neglected. (However, viscosity can't really be neglected, because viscous and thermal penetration depths in gases are typically about the same size.) Nevertheless, to gain intuition about thermoacoustics, we'll begin with a brief consideration of this unrealistic inviscid problem.

Consider a nonzero temperature gradient dT_m/dx along the direction x of acoustic oscillations, with a plane solid boundary at $y = 0$, as shown in Fig. 2.11. Start from the general equation of heat transfer, Eq. (2.24), substitute the appropriate form of the acoustic approximation

$$p = p_m + \mathrm{Re}\left[p_1(x)e^{i\omega t}\right] + \dots , \tag{2.38}$$

$$u = \mathrm{Re}\left[u_1(x,y)e^{i\omega t}\right] + \dots , \tag{2.39}$$

$$T = T_m(x) + \mathrm{Re}\left[T_1(x,y)e^{i\omega t}\right] + \dots , \tag{2.40}$$

$$\rho,\ s,\ \text{etc.} = \text{similar to } T, \tag{2.41}$$

and keep first-order terms to obtain the appropriate acoustic equation of heat transfer,

$$\rho_m c_p \left(i\omega T_1 + u_1 \frac{dT_m}{dx}\right) - i\omega p_1 = k\frac{\partial^2 T_1}{\partial y^2} . \tag{2.42}$$

This differential equation for $T_1(y)$ is similar to Eq. (2.25) but with an additional nonzero dT_m/dx term. Remember we are assuming that the gas viscosity is zero, so u_1 is independent of y in this section. The necessary boundary conditions are $T_1(0) = 0$ and $T_1(\infty)$ is finite.

The solution is

$$T_1 = \left(\frac{p_1}{\rho_m c_p} - \frac{u_1}{i\omega} \frac{dT_m}{dx} \right) \left[1 - e^{-(1+i)y/\delta_\kappa} \right] \tag{2.43}$$

which resembles Eq. (2.26), but with more complexity arising from the $u_1\, dT_m/dx$ term. This solution is the product of two factors. The first factor gives the overall magnitude of the oscillating temperature at distances $y \gg \delta_\nu$ from the solid boundary, and the second factor describes the y dependence of that oscillating temperature close to the solid boundary.

The y-dependent factor is the same complex boundary-layer function that we've seen before, in Eqs. (2.15) and (2.26), and in Anis. Viscous /m and Thermal /y. View Ani. Thermal /y again, and consider Fig. 2.12, which shows the real and imaginary parts of the second factor in Eq. (2.43). You should be able to visualize the time evolution shown in the animation being a smooth progression in time between the real and imaginary parts shown in Fig. 2.12, from real part to minus imaginary part to minus real part to imaginary part and back to real part.

The magnitude factor in Eq. (2.43) is itself the sum of two terms, each of which is easy to understand. The first term is simply the adiabatic temperature oscillation: When the pressure goes up the temperature goes up, and when the pressure goes down the temperature goes down. The second term is due to gas motion along x, along the temperature gradient, and is due to the fact that the Eulerian, fixed-in-the-laboratory point of view used in the conventional formulation of the equations of fluid mechanics that we use. In all of our equations, such as Eqs. (2.38)–(2.43) in the present section, (x, y) refers to a fixed location in space, past which gas moves. The $u_1\, dT_m/dx$ term in Eq. (2.43) simply reflects this reference frame: When a gas with a temperature gradient moves adiabatically past that point in space, the temperature at that point in space changes. (The alternative, Lagragian point of view focuses greater attention on a particular parcel of gas as it moves, not on a fixed location in space. The Lagrangian viewpoint is often better for developing intuition, so we rely on it in most of the animations. In the Lagrangian viewpoint, a parcel of gas at $y \gg \delta_\kappa$ experiences $T_1 = p_1/\rho_m c_p$, quite independent of its velocity or whether a nonzero dT_m/dx exists.)

So the magnitude factor in Eq. (2.43) is simply the linear superposition of adiabatic pressure-induced temperature oscillations and adiabatic motion-induced temperature oscillations. The magnitude factor is complex: It can have any sign and phase, depending on the relative phases of p_1 and u_1 and the relative magnitude of the pressure term relative to the motion term.

For standing-wave phasing, the entire magnitude factor in Eq. (2.43) can be zero, if

$$\frac{|p_1|}{\rho_m c_p} = \frac{|u_1|}{\omega} \frac{dT_m}{dx}. \tag{2.44}$$

In this special circumstance, the gas properties, standing-wave impedance, and temperature gradient conspire so that the pressure-induced temperature oscillation and motion-induced temperature oscillation are equal in magnitude but opposite in sign. This circumstance is illustrated in Ani. Standing /c, where the upper part of the display shows a standing wave in a resonator with a stack near the left end, with blue marker lines showing the moving gas. One particular piece of gas is highlighted with a moving white dot in the stack. The yellow

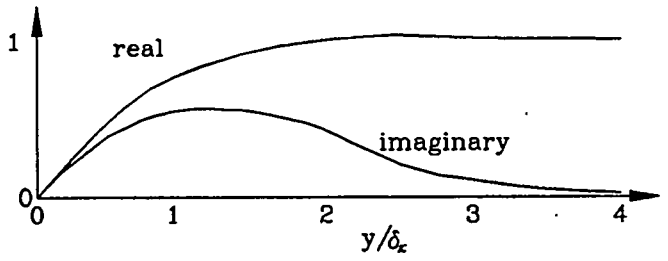

Figure 2.12: The real and imaginary part of the y-dependent factor in Eq.(2.43).

oval marks the region that is shown magnified at the left center of the display, which shows that same parcel of moving gas and short fragments of the two stack plates adjacent to it. The volume of that parcel of gas changes in response to pressure and temperature. At the bottom left of the display is a plot of temperature vs position, in which the temperature of the parcel is the blue trace, and that of the nearby plate in the stack is the white line. Here, $R_h \sim \delta_\kappa$, so the thermal contact is poor; the parcel's temperature oscillation is due entirely to adiabatic pressure oscillation, and its temperature oscillation and motion just happen to match the local temperature gradient dT_m/dx exactly, so that the temperature *at a fixed location* is independent of time.

This circumstance is sufficiently important for standing-wave engines and refrigerators that we give it a specific name, the critical temperature gradient:

$$\nabla T_{\text{crit}} = \frac{\omega A\,|p_1|}{\rho_m c_p\,|U_1|}. \tag{2.45}$$

[The notation $(\nabla T_m)_{\text{crit}}$, though more precise, is too awkward.] We will see later that inviscid standing-wave engines have $dT_m/dx > \nabla T_{\text{crit}}$, and inviscid standing-wave refrigerators have $dT_m/dx < \nabla T_{\text{crit}}$. Although the reality of nonzero viscosity blurs this boundary considerably, ∇T_{crit} as defined in Eq. (2.45) still provides a useful benchmark.

Equation (2.43) is complex enough—in the literal sense of "complex" with real and imaginary parts, and in the common English meaning of "complex"—that the combination of the complex y dependent factor with the complex magnitude factor can yield essentially any sign, phase, and overall magnitude that you might want. Much of the rich variety encountered in thermoacoustics—standing wave behavior, traveling wave behavior, small-pore behavior and well-spaced behavior—fundamentally arises from the complexity of Eq. (2.43), expressing the simple thermal contact between an acoustic wave and an adjacent solid boundary parallel to the wave propagation direction.

2.4. General thermoacoustics

Having gained some intuition with the inviscid, boundary-layer thermoacoustics problem in the previous section and the boundary-layer dissipation problem earlier, we now proceed with a fully general derivation of the dynamic equations of thermoacoustics, including viscosity and arbitrary shape and size of channels.

2.4.1. The math

Naturally, the equations are based on the acoustic approximation, with the relevant variables now written as

$$\begin{aligned} p &= p_m + \mathrm{Re}\left[p_1(x)e^{i\omega t}\right], && (2.46)\\ U &= \mathrm{Re}\left[U_1(x)e^{i\omega t}\right], && (2.47)\\ u &= \mathrm{Re}\left[u_1(x,y,z)e^{i\omega t}\right], && (2.48)\\ v,\, w &= \text{similar to } u, && (2.49)\\ T &= T_m(x) + \mathrm{Re}\left[T_1(x,y,z)e^{i\omega t}\right], && (2.50)\\ \rho,\, s &= \text{similar to } T\,, && (2.51)\\ \mu &= \mu(x)\,, && (2.52)\\ a,\, k,\, \text{etc.} &= \text{similar to } \mu && (2.53) \end{aligned}$$

In this section, we are most interested in p_1 and U_1, as described by the momentum and continuity equations.

For clarity, we continue to consider here only the case of large solid heat capacity, so that the temperature of the solid material in the stack is simply $T_m(x)$, independent of time, y, and z; and we continue to restrict our attention to ideal gases. (For finite solid heat capacity or non-ideal gas effects, see [25].)

The presence of nonzero dT_m/dx has no effect on the momentum equation in the acoustic approximation. Hence, we have for the x-component of the momentum equation

$$i\omega\rho_m u_1 = -\frac{dp_1}{dx} + \mu\left[\frac{\partial^2 u_1}{\partial y^2} + \frac{\partial^2 u_1}{\partial z^2}\right]. \qquad (2.54)$$

The x derivatives of u_1 have been neglected because they are of order $1/\lambda$, and hence are much smaller than the y or z derivatives, of order $1/\delta_\nu$. Regarding Eq. (2.54) as a differential equation for $u_1(y,z)$, with boundary condition $u_1 = 0$ at the solid surface, the solution is

$$u_1 = \frac{i}{\omega\rho_m}\left[1 - h_\nu(y,z)\right]\frac{dp_1}{dx}, \qquad (2.55)$$

where $h_\nu(y,z)$ depends on the specific geometry under consideration.

Integrating both sides of Eq. (2.55) with respect to y and z over the cross-sectional area A of the channel, we obtain the volumetric velocity U_1 on the left side and we convert h_ν on the right side into its spatial average f_ν. Solving for dp_1 yields

$$dp_1 = -\frac{i\omega\rho_m\, dx/A}{1 - f_\nu} U_1. \qquad (2.56)$$

In effect, we regard this approximation to the momentum equation as the origin of pressure gradient in thermoacoustics: The motion U_1 of the gas causes the pressure gradient. If $f_\nu = 0$, the pressure gradient is entirely "inertial", as indicated by the "i" in Eq. (2.56), but when $f_\nu \neq 0$ the presence of viscosity and the stationary boundaries adds a resistive component to the pressure gradient and also effectively changes the magnitude of the inertial contribution.

The function h_ν and its spatial average f_ν are known for many geometries. The complex function f_ν is plotted for some of these geometries in Fig. 2.13. As we saw above, for wide-open channels for which the boundary-layer approximation is appropriate,

$$h = e^{-(1+i)y/\delta}, \tag{2.57}$$

$$f = \frac{(1-i)\,\delta}{2R_h}. \tag{2.58}$$

If we take $y = 0$ to be the center between parallel plates of separation $2y_0 = 2R_h$,

$$h = \frac{\cosh\left[(1+i)\,y/\delta\right]}{\cosh\left[(1+i)\,y_0/\delta\right]}, \tag{2.59}$$

$$f = \frac{\tanh\left[(1+i)\,y_0/\delta\right]}{(1+i)\,y_0/\delta}. \tag{2.60}$$

For circular pores of radius $R = 2R_h$,

$$h = \frac{J_0\left[(i-1)\,r/\delta\right]}{J_0\left[(i-1)\,R/\delta\right]}, \tag{2.61}$$

$$f = \frac{2J_1\left[(i-1)\,R/\delta\right]}{J_0\left[(i-1)\,R/\delta\right]\,(i-1)\,R/\delta}, \tag{2.62}$$

where the coordinate $r = \sqrt{y^2+z^2}$. These functions are also known for rectangular channels [36] of dimensions $2y_0 \times 2z_0$:

$$h = 1 - \frac{16}{\pi^2}\sum_{m,n\,odd}\frac{\sin\left(m\pi y/2y_0\right)\sin\left(n\pi z/2z_0\right)}{mnY_{mn}}, \tag{2.63}$$

$$f = 1 - \frac{64}{\pi^4}\sum_{m,n\,odd}\frac{1}{m^2n^2Y_{mn}}, \tag{2.64}$$

where

$$Y_{mn} = 1 - i\frac{\pi^2\delta^2}{8y_0^2z_0^2}\left(m^2z_0^2 + n^2y_0^2\right), \tag{2.65}$$

and for the spaces between pins oriented along the direction of acoustic oscillations, each of radius r_i and arranged in a triangular array [37] with center-to-center spacing $\sqrt{2\pi}\,r_o/\sqrt[4]{3} \simeq 1.905r_o$:

$$h \simeq \frac{Y_1(\xi_o)\,J_0(\xi) - J_1(\xi_o)\,Y_0(\xi)}{Y_1(\xi_o)\,J_0(\xi_i) - J_1(\xi_o)\,Y_0(\xi_i)}, \tag{2.66}$$

$$f \simeq -\frac{2\xi_i}{\xi_o^2-\xi_i^2}\frac{Y_1(\xi_o)\,J_1(\xi_i) - J_1(\xi_o)\,Y_1(\xi_i)}{Y_1(\xi_o)\,J_0(\xi_i) - J_1(\xi_o)\,Y_0(\xi_i)}, \tag{2.67}$$

where $\xi = (i-1)\,r/\delta$.

In the continuity equation, an expression for the spatial average over y and z of the oscillatory temperature, $\langle T_1\rangle$, is required. As above, it is derived from the general equation of heat transfer, for which the acoustic approximation is

$$\rho_m c_p\left(i\omega T_1 + u_1\frac{dT_m}{dx}\right) - i\omega p_1 = \kappa\left[\frac{\partial^2 T_1}{\partial y^2} + \frac{\partial^2 T_1}{\partial z^2}\right]$$

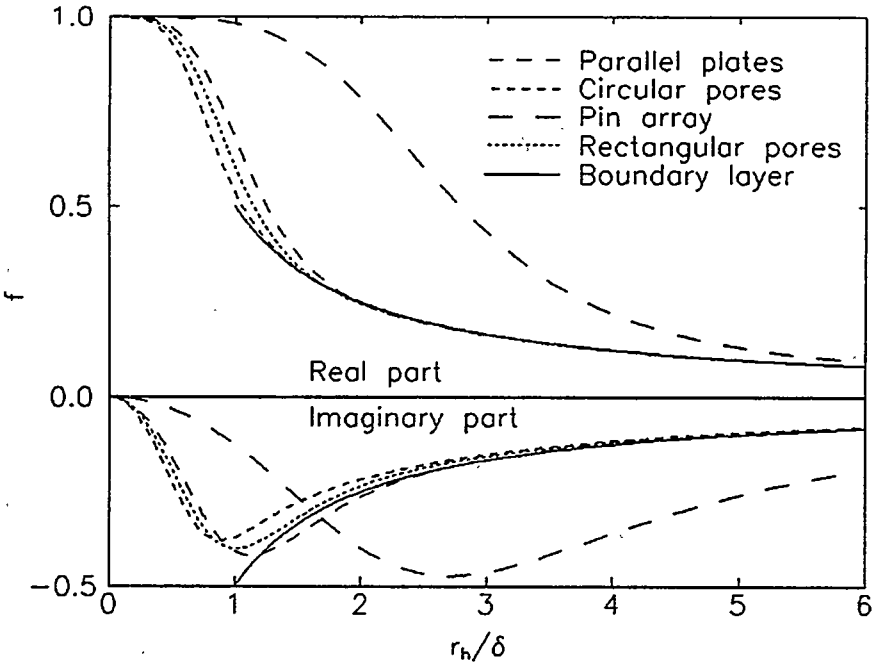

Figure 2.13: Spatial-average function f for several geometries. The rectangle here has 6:1 aspect ratio, and the pin array has $r_o/r_i = 6$. The boundary-layer limit is approached at large R_h in all geometries.

when $dT_m/dx \neq 0$. Regarding this as a differential equation for the y and z dependences of T_1, and following the same procedure as before but now including the y and z dependences of u_1 and allowing for arbitrary channel cross section, we find that

$$T_1 = \frac{1}{\rho_m c_p}(1 - h_\kappa)\, p_1 - \frac{1}{i\omega\,(1 - f_\nu)}\frac{dT_m}{dx}\left(1 - \frac{h_\kappa - \sigma h_\nu}{1 - \sigma}\right)\frac{U_1}{A} \tag{2.68}$$

and

$$\langle T_1 \rangle = \frac{1}{\rho_m c_p}(1 - f_\kappa)\, p_1 - \frac{1}{i\omega\,(1 - f_\nu)}\frac{dT_m}{dx}\left(1 - \frac{f_\kappa - \sigma f_\nu}{1 - \sigma}\right)\frac{U_1}{A}, \tag{2.69}$$

which are comparable to Eqs. (2.26), (2.27), and especially (2.43).

In the continuity equation, we must now include the x dependence of ρ_m :

$$i\omega \langle \rho_1 \rangle + \frac{d}{dx}\left(\rho_m \langle u_1 \rangle\right) = 0. \tag{2.70}$$

Substituting Eqs. (2.69) and (2.30) into this yields

$$dU_1 = -\frac{i\omega A\, dx}{\gamma p_m}[1 + (\gamma - 1) f_\kappa]\, p_1 + \frac{(f_\kappa - f_\nu)}{(1 - f_\nu)\,(1 - \sigma)}\frac{dT_m}{T_m} U_1. \tag{2.71}$$

This expression finds easy physical interpretation as a complete thermoacoustic approximation to the continuity equation. The two terms in Eq. (2.71) show that a gradient in U_1

can be caused either by pressure or by velocity along the temperature gradient. Consider the pressure term first. If $f_\kappa = 0$, there is no thermal contact between gas and solid, so the density oscillations are adiabatic; in this case, $1/\gamma p_m$ is the correct compressibility, and the compliance of the segment of channel of length dx must be $A\,dx/\gamma p_m = dV/\gamma p_m$, as we found in Eq. (2.3). At the other extreme, if $f_\kappa = 1$, the thermal contact between gas and solid is perfect, so the gas is anchored at the local solid temperature. In this case, the isothermal compressibility $1/p_m$ is appropriate. For intermediate thermal contact, an effective compressibility $[1 + (\gamma - 1)f_\kappa]/\gamma p_m$, intermediate in magnitude and with nontrivial phase, describes the spatial average of the density oscillations in response to pressure oscillations. Next consider the velocity term, in the easily interpreted inviscid limit (with $f_\nu = 0$ and $\sigma = 0$) so that it is simply $f_\kappa U_1\, dT_m/T_m$. If $f_\kappa = 0$, there is no thermal contact between gas and solid, the velocity term is zero, and the gas density does not change as it moves along x. In the other extreme, if $f_\kappa = 1$, the gas is always at the local solid temperature, so that as it flows toward higher T_m its density decreases and its velocity increases. In the more general, and more interesting, intermediate regime, oscillatory motion of the gas along the temperature gradient leads to complex density oscillations.

Equations (2.56) and (2.71) are applicable to a wide variety of thermoacoustic circumstances, and may be considered two of the principal tools of thermoacoustic analysis. Many earlier expressions in this chapter are simplified limits of these equations, and in the next subsection we will closely examine the effective compliance, inertance, and resistances indicated by these two equations.

[One more detail: The graphs and equations for f versus R_h/δ that we've seen so far have listed several different geometries of interest mostly for standing-wave thermoacoustics. It is possible to follow through the same kind of analysis for the stacked-screen regenerators that are usually used in Stirling systems. Here's an outline of the derivation [38]. Assuming a sinusoidal volumetric velocity through a stacked-screen regenerator, and assuming that published steady-flow data [39] for stacked-screen viscous pressure drop and heat transfer are valid at each instant of time during this oscillation, a Fourier transform of the appropriate continuity and momentum equations can be taken, with those very complicated published curves of pressure drop and heat transfer built in. The results can be rearranged to yield f_κ and f_ν as a function of R_h/δ_κ and R_h/δ_ν, the volumetric porosity of the screens, and the peak Reynolds number of the flow. The results are only valid for small R_h/δ_κ, which is the regime of interest for traveling-wave devices. The results look qualitatively like the low-R_h/δ parts of the curves in Fig. 2.13, with slightly different results for different porosities in the screen bed and for different Reynolds numbers (i.e., different acoustic amplitudes). Another minor detail that you can find in the Ref. [38]: the f_κ that shows up in the p_1 term of continuity equation is actually a little different than the f_κ that shows up in the U_1 term.]

Finally, at this point we could combine Eqs. (2.56) and (2.71), eliminating U_1, to obtain a second-order differential equation in p_1:

$$[1 + (\gamma - 1)f_\kappa]\,p_1 + \frac{\gamma p_m}{\omega^2}\frac{d}{dx}\left(\frac{1 - f_\nu}{\rho_m}\frac{dp_1}{dx}\right) - \frac{a^2}{\omega^2}\frac{f_\kappa - f_\nu}{1 - \sigma}\frac{1}{T_m}\frac{dT_m}{dx}\frac{dp_1}{dx} = 0\,. \qquad (2.72)$$

This is Rott's wave equation, a milestone in the development of thermoacoustics. (Strictly, we should call it a Helmholtz equation, because the time derivatives have been replaced by $i\omega$'s.) For numerical computations, it is easiest to use Eqs. (2.56) and (2.71) separately; and

I think that greater intuition can be gained by considering Eqs. (2.56) and (2.71) separately, as we shall do in the next subsection.

2.4.2. The ideas

The principal results of the last subsection were the thermoacoustic versions of the momentum and continuity equations, Eqs. (2.56) and (2.71):

$$\begin{aligned} dp_1 &= -\frac{i\omega\rho_m\,dx/A}{1-f_\nu}U_1, \\ dU_1 &= -\frac{i\omega A\,dx}{\gamma p_m}[1+(\gamma-1)f_\kappa]\,p_1 + \frac{(f_\kappa - f_\nu)}{(1-f_\nu)(1-\sigma)}\frac{dT_m}{T_m}U_1. \end{aligned}$$

In this subsection, we will try to gain a deep intuitive appreciation of these two equations, following the outline indicated in Fig. 2.14. In the figure, the channel of length Δx is considered in two ways: in terms of the momentum equation to obtain its inertance and viscous resistance, and in terms of the continuity equation to obtain its compliance, thermal-relaxation resistance, and thermally induced volumetric velocity source. Combining these two points of view yields a complete impedance picture for thermoacoustics, just as the momentum and continuity equations provide a complete description of the dynamics linking p_1 and U_1.

We begin with the momentum equation. If we rewrite Eq. (2.56) in the form

$$dp_1 = -\left(i\omega l\,dx + r_\nu\,dx\right)U_1, \tag{2.73}$$

as shown schematically in the left part of Fig. 2.14, then the inertance and viscous resistance per unit length of channel can be written

$$l = \frac{\rho_m}{A}\frac{1-\mathrm{Re}\,[f_\nu]}{|1-f_\nu|^2} \tag{2.74}$$

and

$$r_\nu = \frac{\omega\rho_m}{A}\frac{\mathrm{Im}\,[-f_\nu]}{|1-f_\nu|^2}. \tag{2.75}$$

The boundary-layer expressions earlier in this chapter, Eqs. (2.21) and (2.22), are simply limiting forms of Eqs. (2.74) and (2.75) for large R_h/δ_ν.

Study Eqs. (2.74) and (2.75) and Fig. 2.13 carefully, and think of any channel as having inertance and resistance, with the details depending on f_ν. Both l and r_ν are always positive (and real). Hence, the momentum equation can never give behavior that looks like negative inertial mass, nor can it give a negative flow resistance. From the limiting behavior of f_ν for large R_h shown in Fig. 2.13, it is clear that in that limit $l \longrightarrow \rho_m/A$ and $r_\nu \longrightarrow 0$. At less-than-infinite but still large R_h, r_ν rises above zero as the importance of viscous drag at the wall increase, and l rises above ρ_m/A as the viscous penetration depth at the wall effectively reduces the available flow area. This is the regime of interest in resonator components and in pulse tubes. Forming the ratio

$$\frac{r_\nu}{\omega l} = \frac{\mathrm{Im}\,[-f_\nu]}{1-\mathrm{Re}\,[f_\nu]}, \tag{2.76}$$

we can easily see that in the vicinity of $R_h \simeq \delta_\nu$ the resistive and inertial parts of the impedance are of comparable magnitude. This is the regime of interest in the stacks of standing-wave thermoacoustic devices. In the smallest passages, such as in the regenerators of traveling-wave devices, the inertial part of the impedance is negligible compared to the resistive part.

Now examine the continuity equation. We rewrite Eq. (2.71) in the form

$$dU_1 = -\left(i\omega c\,dx + \frac{1}{r_\kappa}dx\right) p_1 + e\,dx\,U_1, \tag{2.77}$$

as shown schematically in the right part of Fig. 2.14. The two familar symbols in the figure represent the compliance per unit length

$$c = \frac{A}{\gamma p_m}\left(1 + [\gamma - 1]\,\mathrm{Re}\,[f_\kappa]\right) \tag{2.78}$$

and the thermal-relaxation conductance per unit length, which is the inverse of a resistance

$$\frac{1}{r_\kappa} = \frac{\gamma - 1}{\gamma}\frac{\omega A\ \mathrm{Im}\,[-f_\kappa]}{p_m}. \tag{2.79}$$

The boundary-layer expressions earlier in this chapter, such as Eqs. (2.36) and (2.37), are simply limiting forms of Eqs. (2.78) and (2.79) for $R_h/\delta_\kappa \longrightarrow \infty$.

Study Eqs. (2.78) and (2.79) and Fig. 2.13 carefully. Both c and r_κ are always positive (and real). From the limiting behavior of f_κ for large channel size shown in Fig. 2.13, it is clear that in that limit $c \longrightarrow A/\gamma p_m$ and $r_\kappa \longrightarrow \infty$. At less-than-infinite but still large channel size, $1/r_\kappa$ rises above zero as the importance of thermal relaxation at the wall increase, and c rises above $A/\gamma p_m$ as the thermal penetration depth at the wall contributes a greater compressibility per unit volume than the compressibility far from the wall. This is the regime of interest in resonator components and in pulse tubes. Forming the ratio

$$\frac{1}{\omega r_\kappa c} = \frac{(\gamma - 1)\,\mathrm{Im}\,[-f_\kappa]}{1 + (\gamma - 1)\,\mathrm{Re}\,[f_\kappa]}, \tag{2.80}$$

we can easily see that in the vicinity of $R_h \simeq \delta_\kappa$ the thermal-relaxation resistance and the compliance parts of the impedance are of comparable magnitude. This is the regime of interest in the stacks of standing-wave thermoacoustic devices. In the smallest passages, such as in the regenerators of traveling-wave devices, the thermal-relaxation-resistance part of the impedance is negligible compared to the compliance part.

The third, new symbol in the impedance diagram represents a controlled source $e\,dx\,U_1$ (or sink, depending on sign) of volumetric velocity, proportional to the local volumetric velocity U_1 itself, with proportionality constant

$$e = \frac{(f_\kappa - f_\nu)}{(1 - f_\nu)\,(1 - \sigma)}\frac{1}{T_m}\frac{dT_m}{dx} \tag{2.81}$$

which represents a sort of complex gain/attenuation constant for volumetric velocity, and which arises only when the temperature gradient dT_m/dx along the channel is nonzero.

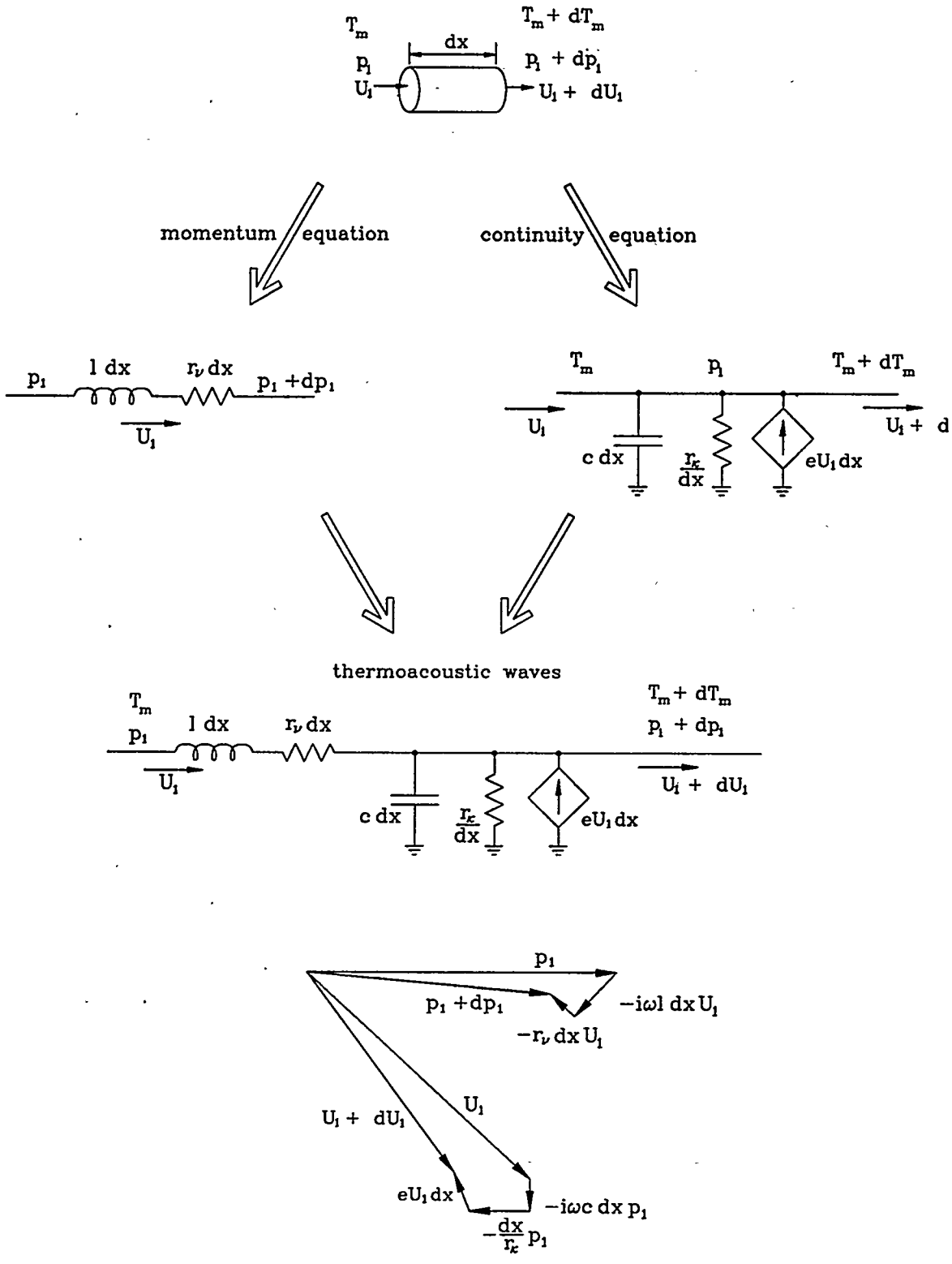

Figure 2.14: Summary of the most important concepts of this chapter.

The eU_1 term in the continuity equation has no dependence on p_1, so it must not represent any sort of compressibility. To understand this term, let $p_1 = 0$ so that c and r_κ don't confuse the issues in this paragraph. The dependence of the eU_1 term on dT_m/dx is key. In a pulse tube or other large-diameter thermal buffer column, f_κ and f_ν are very small, so that $e \simeq 0$ even though $dT_m/dx \neq 0$. In this case, the eU_1 term in the continuity equation simply says that whatever volumetric velocity goes in one end comes out the other end. The behavior is essentially the same as the displacement of a solid piston with a temperature gradient and mass-density gradient. At the opposite extreme, if a nonzero temperature gradient dT_m/dx exists along a channel with very small pore size, such as in a regenerator, the volumetric-velocity source term eU_1 is very important. The small-channel limit of Eq. (2.81) is most important and most easy to appreciate: For $R_h \ll \delta_\kappa$ and $R_h \ll \delta_\nu$,

$$eU_1 \simeq \frac{1}{T_m}\frac{dT_m}{dx}U_1. \tag{2.82}$$

In this case, the eU_1 term in the continuity equation says that $dU_1/U_1 = dT_m/T_m$: The volumetric velocity is amplified in proportion to the temperature rise (or attenuated in proportion to a temperature drop). This is easy to understand as constancy of first-order mass flux $\rho_m U_1$, which for an ideal gas is equivalent to constancy of U_1/T_m : Whatever mass flux goes in one end must come out the other. In this limit of good thermal contact, $T_1 = 0$ so there can be no oscillating mass density in the volume dV.

The even greater complications of the intermediate regime, $R_h/\delta_\kappa \sim 1$, encountered in the stacks of standing-wave systems, is suggested by the boundary-layer limit of Eq. (2.81):

$$eU_1 \simeq \frac{1-i}{2}\frac{1}{1+\sqrt{\sigma}}\frac{\delta_\kappa}{R_h}\frac{1}{T_m}\frac{dT_m}{dx}U_1. \tag{2.83}$$

In this case, the volumetric velocity source is proportional to the volumetric velocity itself, but with a phase shift of $-45°$.

If now we combine the momentum and continuity pictures as shown at the bottom of Fig. 2.14, we arrive at a complete, general impedance picture of thermoacoustics in any channel. We can think of p_1, U_1, T_m, dT_m, and the geometry as given, so that the impedance diagram serves as a reminder of how the continuity and momentum equations yield dp_1 and dU_1.

In most circumstances in a given location in a thermoacoustic system, many or most of the components in this general impedance picture can be neglected. Recalling that $\delta_\kappa \sim \delta_\nu$ for ideal gases, we can form a table that summarizes relative sizes and importance:

resonator	$R_h \gg \delta$	$\omega l \gg r_\nu$	$\omega c \gg 1/r_\kappa$	$e = 0$
pulse tube	$R_h \gg \delta$	$\omega l \gg r_\nu$	$\omega c \gg 1/r_\kappa$	$e \sim 0$
stack	$R_h \sim \delta$	$\omega l \sim r_\nu$	$\omega c \sim 1/r_\kappa$	e complex
regenerator	$R_h \ll \delta$	$\omega l \ll r_\nu$	$\omega c \gg 1/r_\kappa$	$e \simeq \nabla T_m/T_m$

Further simplification in understanding thermoacoustic devices can be achieved by considering the relative sizes of p_1 and U_1 in a given component, to determine whether either L or C can be neglected.

Example: Standing-wave engine. Each stack in the engine of Figs. 1.9 and 1.10 was of parallel-plate construction, with gaps between plates of 0.010 inch, so $R_h = 0.13$

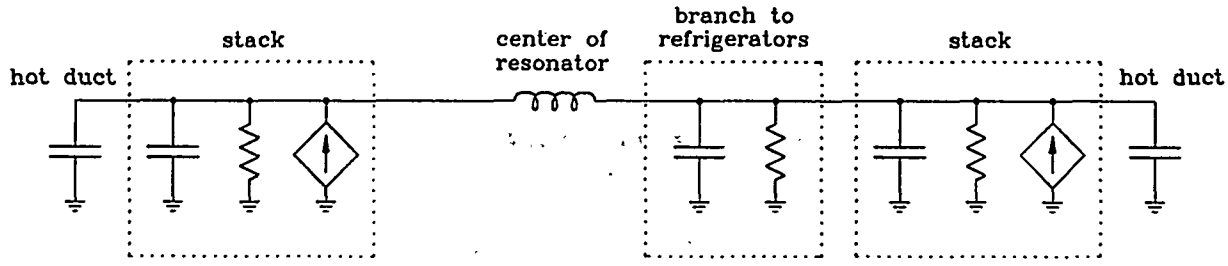

Figure 2.15: Schematic impedance diagram for the standing-wave engine example.

mm. At the stack center, where the temperature is about 550 K, the thermal and viscous penetration depths are $\delta_\kappa = 0.12$ mm and $\delta_\nu = 0.10$ mm at a typical operating point with 3 MPa helium at 390 Hz. Hence, with $R_h/\delta_\kappa = 1.1$ and $R_h/\delta_\nu = 1.3$, we know that all of the impedance components—inertance, viscous resistance, compliance, thermal-relaxation resistance, and volumetric-velocity source—could be important. However, the stacks are close to the velocity nodes of the standing wave, so it is likely that the inertance and viscous resistance will be less important than the other three components. The impedance diagram shown in Fig. 2.15 probably has adequate detail to convey the most important features of the apparatus. The overall resonance is portrayed as Helmholtz-like, with an inertance between two compliances. Although this level of detail does not show the wave nature of the x dependences of p_1 and U_1 in the apparatus, it does successfully show that the pressures on the left and right halves of the apparatus are 180° out of phase, with the pressure on the left half of the apparatus leading the volumetric velocity through the inertance by 90° and the pressure on the right half of the apparatus lagging the volumetric velocity through the inertance by 90°. Judging by eye in Fig. 1.10 that the volumes of gas in each stack and hot duct are comparable, we know that the stack compliance must be as important as the hot-duct compliance; the stack compliance causes ΔU_1 across the stack to be nearly as large as U_1 itself at the hot end of the stack. It turns out that the thermal-relaxation resistance and volume velocity source in the stack cause a smaller change in $|U_1|$ and only about a 5° phase shift between U_1 at the left and right ends of each stack; the effects of the branch to the refrigerators are comparable.

To obtain more detailed information about p_1 and U_1 in this system, I gave DeltaE all the geometry of half of the apparatus, the helium pressure, temperatures, etc., picked one particular operating amplitude, and asked DeltaE to tabulate p_1 and U_1 as a function of position in the apparatus. (See Appendix for details.) The result is shown in Fig. 2.16. (In anticipation of the next chapter, the figure is flipped left–to–right relative to previous figures of this apparatus.) I chose the phase of p_1 to be zero at $x = 0$. Then for a standing wave, we expect the pressure to remain real and to look largely like a cosine of x, and the volumetric velocity to be imaginary and look largely like a sine of x, as shown in the figure. The dependence of A on x, appararent in the scale drawing, causes $|p_1|$ and $|U_1|$ to deviate from perfect trigonometric functions, but these deviations are not visible to the naked eye in the figure. For the most part, dp_1/dx is due to inertance and U_1, and dU_1/dx is due to compliance and p_1.

However, there are small out-of-phase components to p_1 and U_1, which have been multi-

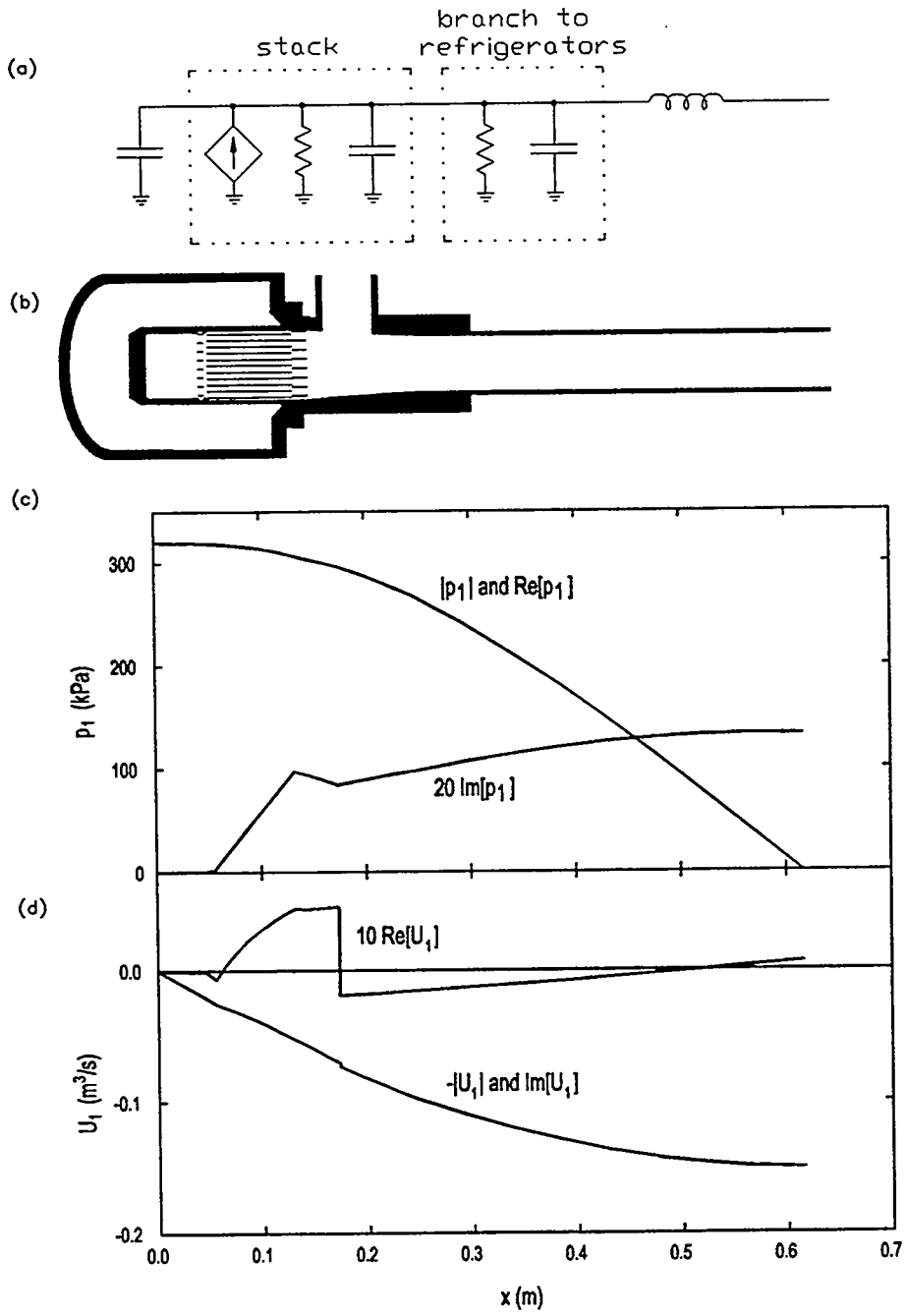

Figure 2.16: Results of numerical integration of the momentum and continuity equations for the standing-wave engine example. (a) Relevant portions of crude impedance diagram. (b) Scale drawing of apparatus. (c) p_1. (d) U_1.

plied by 20 and 10 respectively in Fig. 2.16 in order to display them clearly. As with most standing-wave systems, the phase difference between p_1 and U_1 remains so close to 90° that phasor diagrams are of limited usefulness. The step in $\mathrm{Re}[U_1]$ occurs at the branch to the refrigerators, and accounts for the U_1 flowing into the refrigerators. The upward slope of $\mathrm{Re}[U_1]$ through the stack is due to the volumetric-velocity source term throughout the stack, and the upward slope of $\mathrm{Im}[p_1]$ is due to r_ν in the stack. The weaker slopes of $\mathrm{Re}[U_1]$ and $\mathrm{Im}[p_1]$ elsewhere are partly due to r_κ and r_ν elsewhere, but also from c and l interacting with $\mathrm{Im}[p_1]$ and $\mathrm{Re}[U_1]$, respectively.

Example: Traveling-wave engine. The regenerator in the engine of Figs. 1.13 and 1.14 is a bed of stainless-steel screen with a hydraulic radius of 42 μm. At a typical operating point, 80 Hz and 3 MPa helium gas, and with the center of the regenerator at 650 K, the penetration depths are $\delta_\kappa = 300$ μm and $\delta_\nu = 250$ μm. Hence, we have $R_h \ll \delta$, so inertance and thermal-relaxation resistance are negligible, and the volumetric velocity source is well described by Eq. (2.82). The regenerator is adequately modeled with the three components labeled "regenerator" in Fig. 2.17. The thermal buffer column is 9 cm diam, so it has $R_h \gg \delta$, so its most important dynamic characteristic is its compliance, also shown in Fig. 2.17. The feedback path is most roughly modeled as an inertance (the straight section) in series with a compliance (the 180-degree U bend at the left end); we neglect the resistances associated with these two components for now. The resonator to the right of the junction is approximately an inertance (the uniform-diam section) in series with a compliance (the big volume on the end), with both of these components having associated resistances. Neither of these resonator components is really lumped, but we will neglect those details for now. The adjustable load on the system, comprising an adjustable valve in series with a tank, can be modeled as a resistance in series with a compliance. Hence, the impedance diagram of Fig. 2.17 shows the most important features of this system.

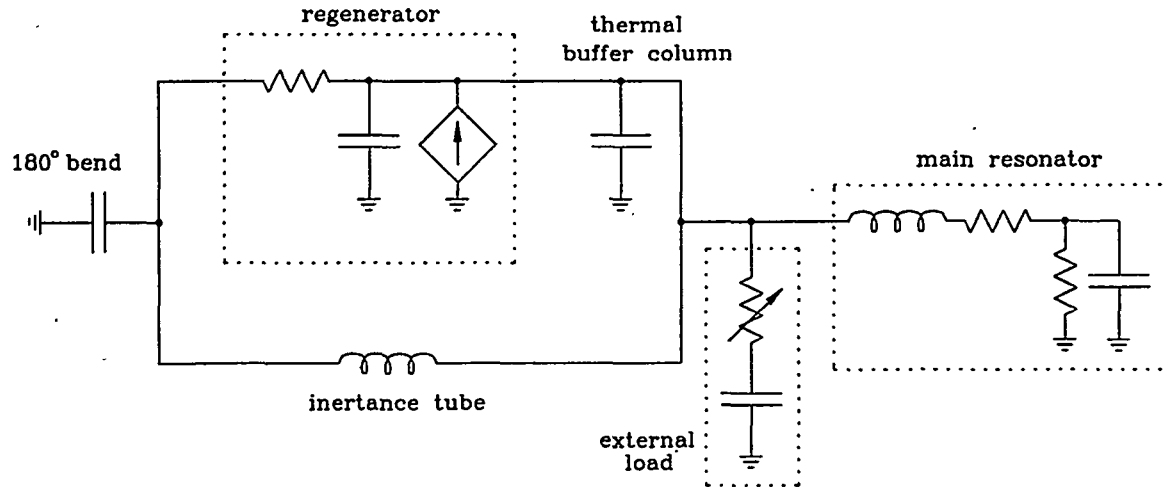

Figure 2.17: Impedance diagram for traveling-wave engine example.

Animation Tashe /t shows these same features for the traveling-wave engine, omitting the resonator and adjustable load. Study the animation and Fig. 2.17 together. In the

animation, you should be able to "see" many features that we have discussed in this chapter. The expected behavior of each of the two large compliances should be apparent, with U_1 "in" differing from U_1 "out"; close examination will show the 90° phase difference between ΔU_1 and p_1. The joining conditions—conservation of p_1 and U_1 at the transitions between components—should be apparent, such as at the ends of the inertance and at the three-way junction. It should be apparent that the velocity through the regenerator, which is resistive, is in phase with Δp_1, while the velocity through the inertance lags Δp_1 by 90°. I know that the compliance and volumetric-velocity source associated with the regenerator are correctly programmed in this animation too, but I confess they are too subtle for me to see here.

Example: Standing-wave refrigerator. Figure 2.18 shows a lumped-impedance diagram for the standing-wave refrigerator of Figs. 1.11 and 1.12. The stacks have $R_h/\delta \sim 1$, so all of the impedance components—inertance, viscous resistance, compliance, thermal-relaxation resistance, and volumetric-velocity source—could be important in them. In the standing-wave engine above, we argued that the stacks were close to the velocity nodes of the standing wave, so we neglected their inertance and viscous resistance. In this refrigerator, the stacks are not so close to the velocity nodes, so we cannot neglect these momentum-equation contributions. The loudspeakers contribute significantly to the dynamics, so we should at least include the mass and spring constant of each; I've made up new symbols for these—a rectangular brick for mass, and something that reminds me of automotive leaf springs for the spring constant.

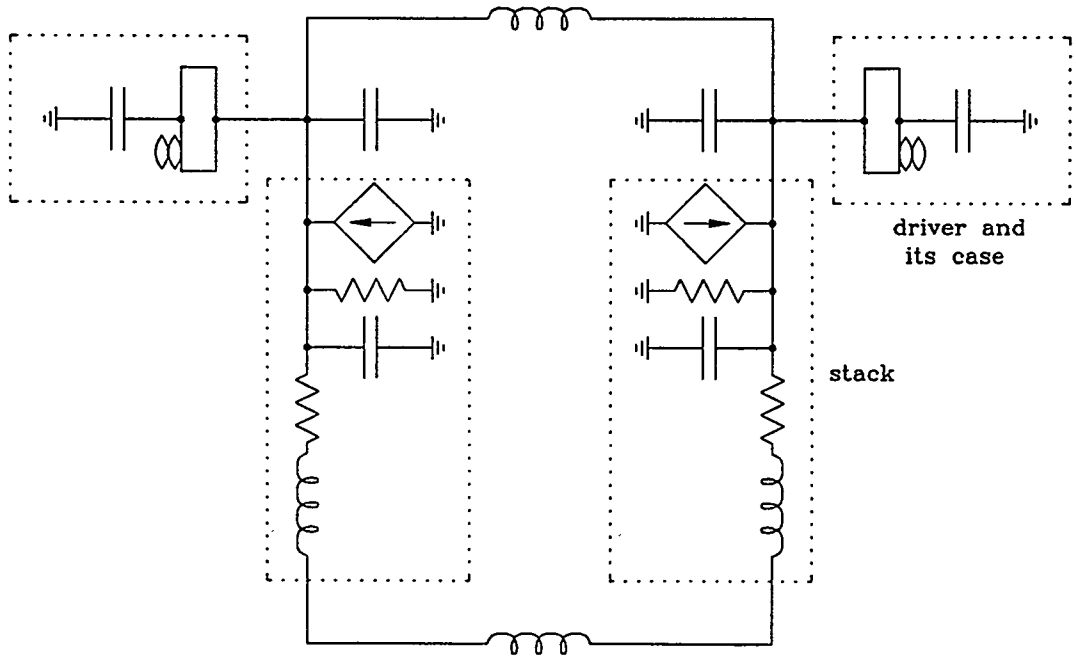

Figure 2.18: Schematic impedance diagram for the standing-wave refrigerator example.

Example: Traveling-wave refrigerator. The impedance diagram of Fig. 2.19a symbolically represents the most important dynamic features of the orifice pulse-tube refrigerator of Figs. 1.15 and 1.16. The rightmost compliance C is the so-called compliance itself. The adjacent inertance L and resistance R_s represent the refrigerator's inertance tube and two valves, with valve settings the same as in the related example near Fig. 2.8 above: The parallel valve R_p in Fig. 2.8 is closed, and the series valve R_s in Fig. 2.8 is adjusted so that $R_s = \omega L/2$. The compliance of the pulse tube is significant, and is shown as C_{pt}. With $R_h/\delta \sim 0.1$ in the regenerator, its compliance C_{reg}, viscous resistance R_{reg}, and volumetric velocity source $\Delta U_{1S} = -U_{1\text{in}}\,(T_{\text{in}} - T_{\text{cold}})\,/T_{\text{in}}$ represent the regenerator well.

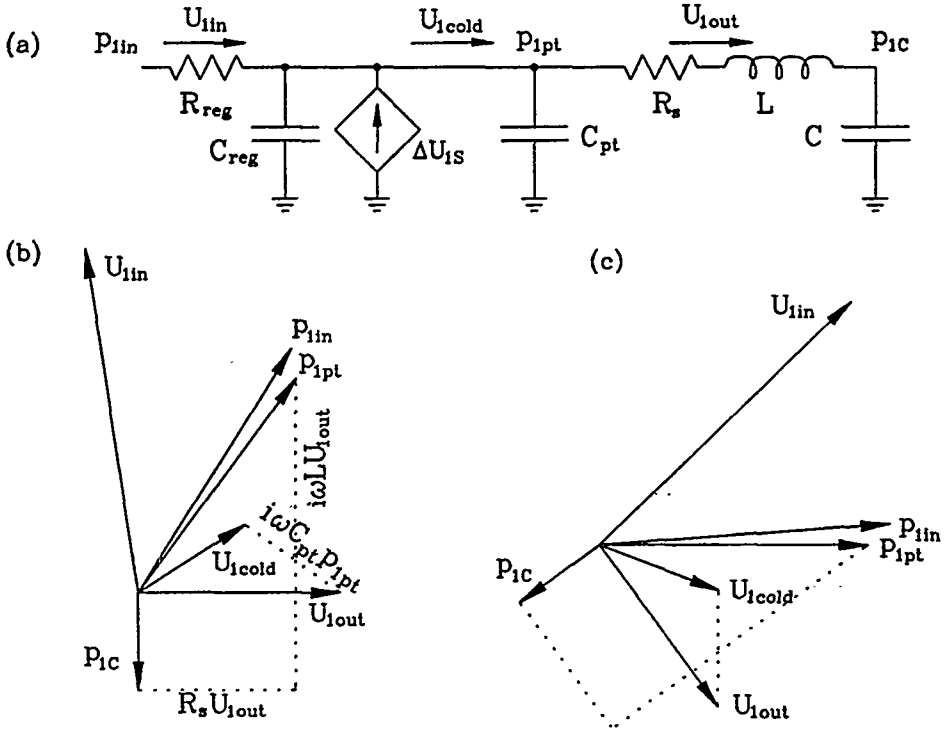

Figure 2.19: (a) Schematic impedance diagram of the orifice pulse-tube refrigerator. (b) Phasor diagram, with the phase of $U_{1\text{out}}$ set to zero. (c) Same phasor diagram, but rotated so that the phase of p_{1pt} is set to zero.

I used the impedance diagram of Fig. 2.19a and quantitative information about the hardware geometry to construct the phasor diagram of Fig. 2.19b, starting from the right end of the impedance network and working to the left. We already did part of the work in Fig. 2.8c above; p_{1C}, $U_{1\text{out}}$, and p_{1pt} are copied from that figure. The compliance of the pulse tube then determines $U_{1\text{cold}}$; next C_{reg} and ΔU_{1S} determine $U_{1\text{in}}$; finally R_{reg} determines $p_{1\text{in}}$.

Example: imperfect inertance. Sometimes it is impossible to provide a desired phase shift in $Z = p_1/U_1$ using an inertance, because the unavoidable compliance and viscous resistance can cause phase shifts of the opposite sign, as illustrated in Fig. 2.20.

These variables are not completely independent, because the cross-sectional area, volume, and surface area of a tube are not independent. Suppose that the viscous resistance r_ν and the compliance c per unit length of this inertance are not negligible, as shown in the figure, and suppose it is desired that Z_{In} should lead Z_{Out}. Figure 2.20b shows that, even though l works in the correct direction, causing p_{1In} to lead p_{1Out}, the compliance c works to shift U_{1In} ahead of U_{1Out}, so that the impact on the phase of Z could have either sign, depending on the quantitative details of l, r_ν, and c.

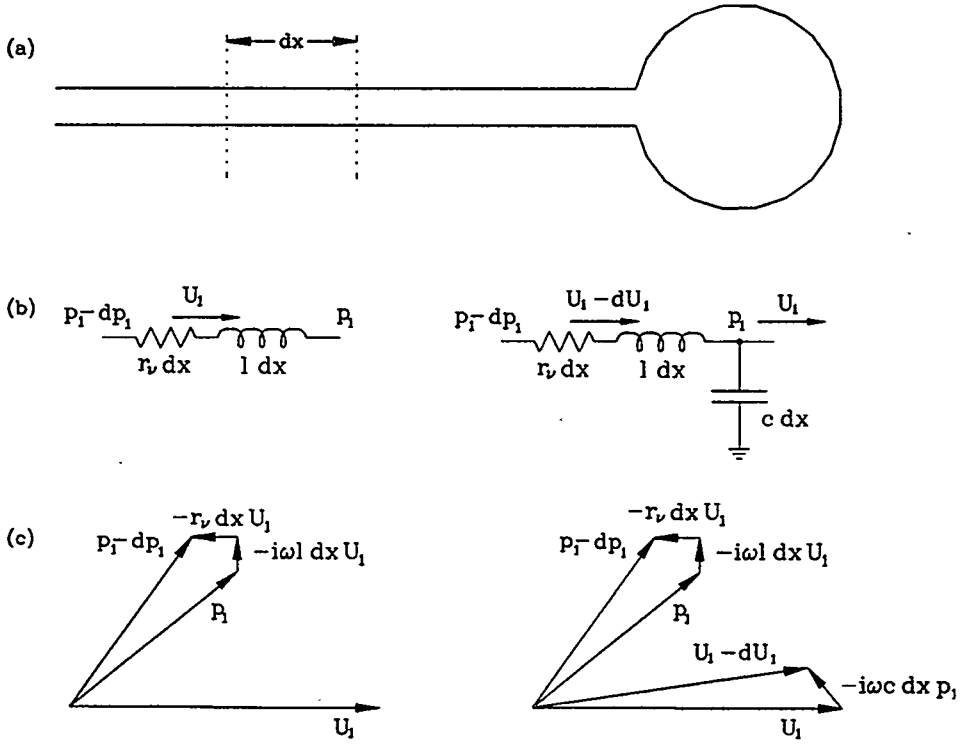

Figure 2.20: (a) A lossy inertance and a compliance, such as might be used at the end of a small pulse-tube refrigerator. A short length dx of the lossy inertance is highlighted. (b) Impedance diagrams for the short length dx of the lossy inertance; on the left, the compliance per unit length is negligible, while on the right it is not negligible. (c) Phasor diagrams for the short length dx of the lossy inertance; on the left, the compliance per unit length is negligible, while on the right it is not negligible.

2.5. Exercises

2.1 Review complex notation: show that $\overline{p(t)u(t)} = \mathrm{Re}[p_1\tilde{u_1}]/2 = |p_1|\,|u_1|\,(\cos\phi)\,/2$, where ϕ is the phase angle between p_1 and u_1.

2.2 More review: show that the phase of the ratio of two complex numbers is the difference between the phases of the numbers. Consider $Z = p_1/U_1$. What is the phase of the impedance

of a traveling wave? If pressure oscillations lead velocity oscillations in a more general wave, is the phase of the impedance positive or negative?

2.3 The sealed resonator shown in Fig. 2.21, consisting of a central duct of length $2\Delta x_1$ and area A_1 between two other ducts each of length Δx_2 and area A_2, is intermediate between a double Helmholtz resonator and a plane wave resonator. Show that the fundamental frequency is given by

$$\frac{A_2}{A_1} \tan \frac{\omega L_1}{a} \tan \frac{\omega L_2}{a} = 1. \tag{2.84}$$

Show that this reduces to something sensible when $A_2 = A_1$. Show that it reduces to the expression for a double Helmholtz resonator for $A_1 < A_2$, $\Delta x_1 \ll \lambda$, and $\Delta x_2 \ll \lambda$.

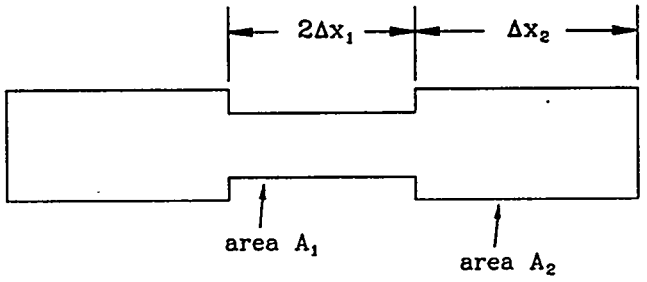

Figure 2.21: Geometry for exercise 2.3.

2.4 Does $p_1(x) = C \sin kx$ represent a standing wave or a traveling wave? Does $p_1(x) = Ce^{ikx}$ represent a standing wave or a traveling wave? Use the lossless first-order momentum equation to write down $u_1(x)$ in both cases. Use the lossless first-order continuity equation to check your expressions for $u_1(x)$. How would you write $p_1(x)$ for a standing wave with a temporal phase shift of 90° relative to this standing wave? What about a quarter-wavelength spatial shift in the node locations?

2.5 Consider a lossless duct of uniform cross-sectional area, sealed at both ends, of length Δx. The fundamental resonance frequency is $f = a/2\,\Delta x$, because that is the frequency for which a half-wavelength wave "fits" in the pipe, with velocity nodes at the sealed ends. If you knew nothing about waves, you might think this resonator was essentially like the double Helmholtz resonator, with an inertial mass of gas in the central third of the resonator bouncing against the compliances of gas in the outer thirds of the resonator. If you calculated the resonance frequency using this lumped-impedance picture, how different would your result be from the true resonance frequency $a/2\,\Delta x$? What if you used the central half and the outer quarters?

2.6 Verify that Eqs. (2.59) and (2.60) approach Eqs. (2.57) and (2.58) as $R_h/\delta \longrightarrow \infty$.

2.7 Combine Eqs. (2.56) and (2.71) to obtain Rott's wave equation.

2.8 Check the derivations of all equations in this chapter, except Eqs. (2.59)—(2.67).

2.9 Look closely at the computer animations Viscous and Oscwall. Use "pause" on your keyboard to study "viscous" very carefully. It looks like the gas motion about a penetration

depth away from the wall *leads* the motion farther from the wall. Does this make sense, or did the author make a minus-sign mistake when he made the animation?

2.10 The specific acoustic impedance of a wave is defined as

$$z = \frac{Ap_1}{U_1}. \tag{2.85}$$

Show that the specific acoustic impedance of a lossless plane traveling wave is $\pm\rho a$. Show that the specific acoustic impedance of a lossless plane standing wave is $\pm\rho a \tan\left[\omega\left(x - x_0\right)/a\right]$. As the wave crosses from a first duct of area A_f to a second duct of area A_s, which impedance is continuous—z or Z?

2.12 Show that $T_1/T_m = (\gamma - 1)p_1/\gamma p_m$ for an ideal gas experiencing adiabatic pressure oscillations. What is the value of $(\gamma - 1)/\gamma$ for your favorite gas? What is proportionality constant links T_1/T_m and p_1/p_m for an ideal gas experiencing isothermal pressure oscillations? How big is T_1 at a few locations in your favorite hardware? How big is T_1 for "audio" acoustics in air?

2.13 Sketch $|p_1|$ and either $|U_1|$ or $|\langle u_1\rangle|$ for your favorite piece of hardware.

2.14 Estimate the inertance, compliance, and resistances of some components in your favorite piece of thermoacoustics hardware. Compare R_ν, ωL, $1/\omega C$, and $1/G_\kappa$. Do the relative magnitudes make sense?

2.15 A Helmholtz resonator consists of a 4 liter spherical volume V and a cylindrical neck having a diameter of $2r = 2$ cm and a length $\Delta x = 5$ cm. It is filled with air at 300 Kelvin and 1 bar.

What is the inertance of the neck? How does it compare with the mass of gas in the neck? What is the compliance of the volume? What is the resonance frequency? At resonance, how does ωL compare with $1/\omega C$? How does λ compare with the various dimensions in the problem? How do δ_ν and δ_κ compare with the other dimensions?

2.16 Draw a reasonably detailed impedance diagram for your favorite piece of thermoacoustics hardware.

2.17 In this chapter, my choice of U_1 and p_1 as the variables of greatest interest led to the forms of the momentum and continuity equations that we used, and from there to the forms of the impedance diagrams that we used. However, other choices can be made, with equal success if employed self consistently. Your task: reconstruct some of the important results and figures of this chapter from a different point of view, with the variables of greatest interest being the average gas velocity $\langle u_1\rangle$ and the force $F_1 = Ap_1$ exerted by the gas at x on the gas at $x + dx$. To construct impedance diagrams, invent symbols for moving mass m, spring k, dashpots R_ν and G_κ, and thermally induced velocity source $d\langle u_{1S}\rangle$. Draw your version of the impedance diagram for the most general thermoacoustic element of length dx, thinking carefully which components should be drawn in parallel (sharing the same $\langle u_1\rangle$) and in series (sharing the same F_1). What are the joining conditions from one segment to the next, corresponding to our use of continuity of p_1 and U_1 in the text? Do you think your version is more intuitively understandable than the version used in the text? Why or why not?

2.18 Assign names to the pressures and volumetric velocities at key locations in Fig. 2.17. (Remember to define a positive direction for each velocity.) Construct a phasor diagram, by

examining the figure and Ani. Tashe /t. Don't worry about details; just try to get relative phase angles correct to within $\pm 45°$. Repeat this exercise for Fig. 2.18.

3. POWER

Products of first-order variables (such as p_1 and U_1) represent power, which is of paramount importance in thermoacoustic engines and refrigerators. Introductory acoustics textbooks teach that

$$\frac{\omega}{2\pi}\oint p(t)\mathrm{v}(t)\,dt = \frac{1}{2}\,\mathrm{Re}\left[p_1\tilde{\mathrm{v}}_1\right], \tag{3.1}$$

which is called the acoustic intensity, is the time-averaged "power per unit area" in a sound wave. It's not so simple in thermoacoustics. We must be very careful to identify which type of power we are talking about, because there are so many important types of energy and power in thermodynamics—enthalpy, heat, Gibbs free energy, etc., etc.

The concept of acoustic intensity is so familiar to acousticians that we are reluctant to abandon it. Hence, in this book we will make as much use as possible of the integral of the acoustic intensity across the cross-sectional area of the channel:

$$\begin{aligned}
\dot{E}_2(x) &= \frac{\omega}{2\pi}\oint \mathrm{Re}\left[p_1(x)e^{i\omega t}\right]\mathrm{Re}\left[U_1(x)e^{i\omega t}\right]\,dt && (3.2)\\
&= \frac{1}{2}\,\mathrm{Re}\left[p_1\widetilde{U_1}\right] = \frac{1}{2}\,\mathrm{Re}\left[\widetilde{p_1}U_1\right] && (3.3)\\
&= \frac{1}{2}\,|p_1|\,|U_1|\cos\phi_{pU}\,, && (3.4)
\end{aligned}$$

where ϕ_{pU} is the phase angle between p_1 and U_1. We call this the *acoustic power* flowing in the x direction, giving it the subscript 2 to remind us that it is second order—the product of two first-order quantities. Note also that it is a time average; we're not interested in instantaneous power delivered along x, only the power averaged over an integer number of cycles of the sound wave.

Similarly, enthalpy is very familiar to mechanical and chemical engineers, because it is the key energy of fluid dynamics, of great use when considering the first law of thermodynamics. We will see below that

$$\dot{H}_2(x) = \frac{1}{2}\rho_m\,\mathrm{Re}\left[h_1\widetilde{U_1}\right] - (Ak + A_{\mathrm{solid}}k_{\mathrm{solid}})\,\frac{dT_m}{dx}, \tag{3.5}$$

where h is the enthalpy per unit mass, is the acoustic approximation to the time-averaged *total power* flowing in the positive x direction.

In this chapter and Chapter 4 our understanding of the use and meaning of $\dot{E}_2$ and $\dot{H}_2$ will grow.

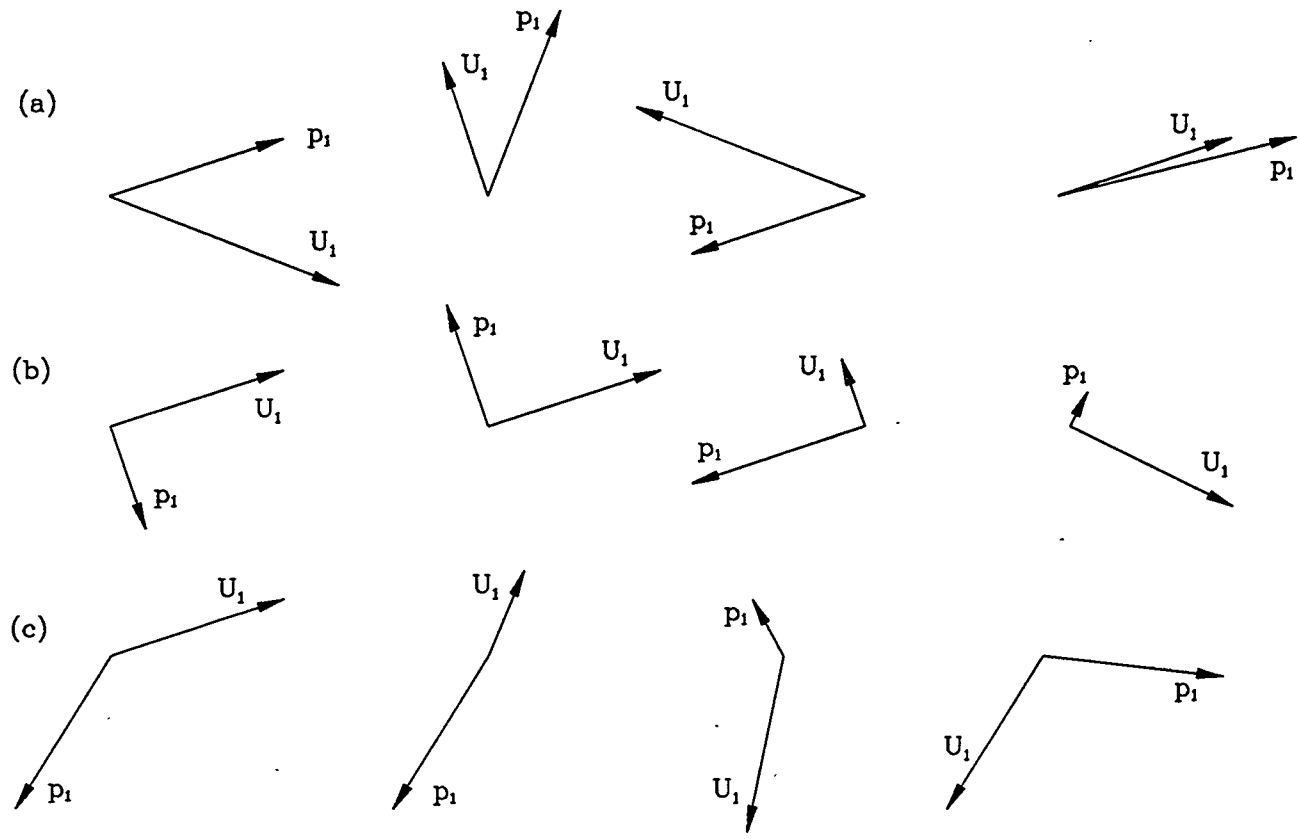

Figure 3.1: (a) Typical phasor diagrams for positive acoustic power flow in the positive x direction. The angle between p_1 and U_1 is acute. (b) Typical phasor diagrams for zero acoustic power flow. The angle between p_1 and U_1 is 90°. (c) Typical phasor diagrams for acoustic power flow in the negative x direction. The angle between p_1 and U_1 is obtuse.

3.1. Acoustic power

Acoustic power depends strongly on the phase angle between p_1 and U_1. Whether using Eq. (3.2), (3.3), or (3.4) for acoustic power $\dot{E}_2$, it is immediately apparent that $\dot{E}_2 = 0$ when the phase between pressure and volumetric velocity is 90°, i.e. for standing-wave phasing. For a pure rightward traveling wave, $\dot{E}_2 > 0$. For a pure leftward traveling wave, $\dot{E}_2 < 0$. Whenever $|\phi_{pU}| < 90°$, acoustic power flows in the positive x direction; when this angle is between 90° and 180°, acoustic power flows in the negative x direction, as illustrated in Fig. 3.1.

The utility of $\dot{E}_2(x)$ in acoustics is due largely to its intuitive appeal as describing a sort of flux of mechanical power past the location x. This interpretation is possible because the volumetric velocity $U_1(x)$ is equal (to first order only!) to the volumetric velocity of the particular slab of gas whose average position is at x. Letting V be the oscillating part of the volume of gas to the left of this slab of gas, so $U = dV/dt$,

$$\dot{E}_2(x) = \frac{\omega}{2\pi} \oint pU\, dt = \frac{\omega}{2\pi} \oint p\, dV, \tag{3.6}$$

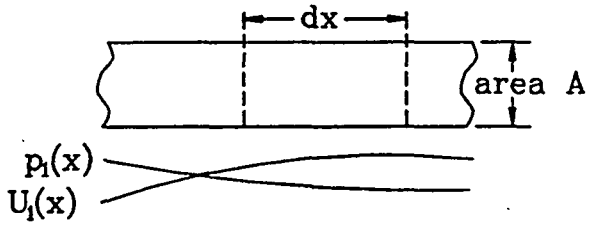

Figure 3.2: Acoustic power flows down a channel of area A. The absorption of acoustic power within the length dx is of interest.

which we recognize as the standard thermodynamic expression for the time-averaged rate at which work is done by a piston. Hence, $\dot{E}_2(x)$ can be interpreted as giving the work done by a slab of gas, whose average position is x, on the gas in front of it, as if the slab of gas whose average position is x were a solid piston.

These points are illustrated in Anis. Wave /v and Wave /u. Animation Wave /v is the same rightward-traveling wave we examined in Chapter 1, but with additional purple ellipses representing $\dot{E}_2$ at two typical locations. The horizontal coordinate of the small white dot tracing the ellipse is equal to the location of the slab of gas in question; the vertical coordinate is p. Hence, the purple area of the ellipse is proportional to $\oint p\,dV$, and so this area can be taken as a representation of $\dot{E}_2$. The clockwise rotation of the small white dot tracing the ellipse indicates that $\dot{E}_2 > 0$. Recalling from Fig. 1.19 that p_1 and U_1 are exactly in phase for this animation, i.e. p_1 and V_1 are 90° out of phase, we see that this case gives the fattest ellipse possible for these amplitudes $|p_1|$ and $|U_1|$.

Similarly, Ani. Wave /u is the same standing-wave animation we examined in Chapter 1, but with the addition of pV traces at two typical locations. Recalling from Fig. 1.19 that p_1 and U_1 are exactly 90° out of phase for this animation, i.e. p_1 and V_1 are exactly in phase, we see why the pV "ellipses" are nothing but reciprocating lines. Since these lines enclose no area, they show that $\dot{E}_2 = 0$. Pure standing waves carry no acoustic power.

Typical waves of interest in thermoacoustic engines and refrigerators are neither pure standing wave nor pure traveling wave. In the typical so-called standing wave engine or refrigerator, the phase between pressure and volumetric velocity is typically in the range of 85° to 95° in the stack. Such a wave is illustrated in Ani. Wave /k. At first glance this wave is barely distinguishable from a pure standing wave, but close examination shows nonzero area in the pV ellipses, i.e. nonzero acoustic power transmitted to the right by the wave. Also note that there are no longer true nodes of pressure or velocity; the locations that at first appear to be nodes are actually regions of small amplitude having a slight nonzero oscillation everywhere.

Animation Wave, with any of its /options, assumes that $\dot{E}_2$ is constant; $d\dot{E}_2/dx = 0$. However, the interaction of a sound wave in a channel with the channel walls leads to $d\dot{E}_2/dx \neq 0$. As in Chapter 2, we consider sound propagating in the x direction in an ideal gas within a channel with constant cross sectional area A, as shown in Fig. 3.2. We adopt the usual complex notation for time-oscillatory quantities, namely Eqs. (2.10)–(2.13). To

find the time-averaged acoustic power $d\dot{E}$ produced in a length dx of the channel, we write

$$\frac{d\dot{E}}{dx} = \int \frac{d\left(\overline{pu}\right)}{dx}\, dy\, dz \tag{3.7}$$

where the overbar denotes time averaging and the integral is over the cross-sectional area A of the channel. Rewriting Eq. (3.7) in complex notation and expanding the x derivative gives

$$\frac{d\dot{E}_2}{dx} = \frac{1}{2}\,\mathrm{Re}\left[\widetilde{U_1}\frac{dp_1}{dx} + \widetilde{p_1}\frac{dU_1}{dx}\right], \tag{3.8}$$

where the tilde denotes complex conjugation. We can obtain dp_1/dx and dU_1/dx from the momentum and continuity equations in Chapter 2; Equations. (2.73) and (2.77) provide a convenient form. Making these substitutions, we obtain

$$\frac{d\dot{E}_2}{dx} = -\frac{r_\nu}{2}\left|U_1\right|^2 - \frac{1}{2r_\kappa}\left|p_1\right|^2 + \frac{1}{2}\,\mathrm{Re}\left[e\widetilde{p_1}U_1\right]. \tag{3.9}$$

When you look at an impedance diagram for a thermoacoustic component, such as the general impedance diagram of Fig. 2.14, realize that Eq. (3.9) shows that only three of the five impedance components affect acoustic power; inertance and compliance have no direct effect on acoustic power; they only cause $p_1(x)$ and $U_1(x)$ to evolve in ways that keep $\frac{1}{2}\,\mathrm{Re}[\widetilde{p_1}U_1]$ independent of x.

The first two terms in Eq. (3.9) are always negative; the first term gives the viscous dissipation of sound and the second term gives the less intuitively obvious thermal-relaxation dissipation. The third term, which can have either sign, is of the greatest interest in thermoacoustic engines and refrigerators. We will spend the rest of this section interpreting these three terms.

3.1.1. Acoustic power dissipation with $dT_m/dx = 0$

With $dT_m/dx = 0$, Eq. (3.9) reduces to

$$\frac{d\dot{E}_2}{dx} = -\frac{r_\nu}{2}\left|U_1\right|^2 - \frac{1}{2r_\kappa}\left|p_1\right|^2. \tag{3.10}$$

This expression gives the ordinary dissipation of acoustic power per unit length in a channel. Fortunately, this expression is easy to interpret because it is so simple. Both terms are negative, so both always represent dissipation: If power flows in the positive x direction, then $|\dot{E}_2(x+dx)| < |\dot{E}_2(x)|$, while if power flows in the negative x direction, then $|\dot{E}_2(x)| < |\dot{E}_2(x+dx)|$. Both terms in $d\dot{E}_2/dx$ are independent of $\dot{E}_2 \sim p_1\widetilde{U_1}$ itself; i.e., the local dissipation of acoustic power is independent of the transmission of acoustic power. There is a clean separation between viscous and thermal-relaxation effects: The first term, describing viscous dissipation, is proportional to $|U_1|^2$ and is independent of thermal conductivity, while the second term, describing thermal-relaxation dissipation, is proportional to $|p_1|^2$ and is independent of viscosity.

In the boundary-layer approximation, in which all dimensions of the channel are much larger than the penetration depths, Eq. (3.10) can be written

$$\frac{d\dot{E}_2}{dS} = -\frac{1}{4}\rho_m \left|\frac{U_1}{A}\right|^2 \delta_\nu \omega - \frac{1}{4}\frac{|p_1|^2}{\gamma p_m}(\gamma - 1)\,\delta_\kappa \omega, \tag{3.11}$$

where S is the surface area of the channel. This expression gives the ordinary dissipation of acoustic power in a large channel, and is easily remembered in terms of the energy density. The mean kinetic energy per unit volume $\rho_m |U_1/A|^2/4$ times δ_ν is roughly the kinetic energy in the gas within a viscous penetration depth of the solid surface, per unit area of the surface; the viscous dissipation term shows that this energy is dissipated by viscous shear at an average rate ω. Similarly, the thermal-relaxation term shows that the mean adiabatic compressive energy density $|p_1|^2/4\gamma p_m$ stored in unit volume of the gas is dissipated at an average rate $(\gamma - 1)\,\omega$ within a region of thickness δ_κ near the solid surface. The extra factor $(\gamma - 1)$ appears because this thermal dissipation is proportional to the difference between the isothermal and adiabatic compressibilities, which is proportional to $(\gamma - 1)$.

The viscous term arose from the

$$\mathrm{Re}\left[\widetilde{U_1}\frac{dp_1}{dx}\right]$$

term in Eq. (3.8), and can be better appreciated by considering Ani. Viscous /m. Close examination of the animation shows that the gas motion far from the solid boundary is in phase with dp_1/dx, so the velocity $u_1(\infty)$ far from the solid boundary is 90° out of phase from dp_1/dx. Hence, the gas far from the solid boundary, where the dynamics is purely inertial, has $\mathrm{Re}[\widetilde{u_1}\,dp_1/dx] = 0$ and contributes nothing to $d\dot{E}_2/dx$. The dissipation arises close to the solid boundary, where the phase of u_1 is shifted by viscous interaction with the wall. Naively, when I watch Ani. Viscous I see layers of gas sliding relative to one another, with viscous "friction" between the layers turning mechanical energy into heat.

Example: Standing-wave refrigerator. In Chapter 2, we calculated the viscous resistance of the lower central tee of the standing-wave refrigerator to be $R_\nu = 75$ Pa-s/m^3. At a typical operating point, $|U_1| = 0.16$ m^3/s. Hence this component dissipates 1.0 Watt of acoustic power, due to viscosity. (There is negligible p_1 in this component, and hence negligible thermal-relaxation dissipation.) This is less than 2% of the total acoustic power supplied to the resonator by the loudspeakers. The center of this component is a center of symmetry of the apparatus, so it must be that $\dot{E}_2 = 0$ at the center. Hence, 0.5 W must flow into the tee from each side. Taking the positive x direction toward the right, we would say that $\dot{E}_2 = +0.5$ W at the left end of the tee, and $\dot{E}_2 = -0.5$ W at the right end of the tee.

Example: Traveling-wave refrigerator. Near Fig. 2.8, we introduced the impedance network at the end of the traveling-wave refrigerator, with an example in which $R_s = 3.35$ MPa-s/m^3. At a typical operating point, with $|U_1| = 0.04$ m^3/s, the flow resistance R_s

dissipates 2700 W of acoustic power. This impedance network consumes a significant fraction of the 9000 W of acoustic power supplied to the entire refrigerator.

Compared to viscous dissipation, the dissipation of acoustic power by thermal relaxation is more difficult to appreciate. Since thermal-relaxation dissipation is independent of U_1, we can clarify the issues by considering a location in the wave where $u_1 = 0$. Consider Ani. Thermal /e, showing a such a wave near a wall in boundary-layer approximation. (Note that we have made the wave-propagation direction x vertical in this animation, so everything fits on the display.) As we saw in Chapter 2, the temperature oscillates in phase with p_1 far from the wall; close to the wall, the wall's heat capacity provides a thermal anchor that reduces the amplitude of the temperature oscillation and shifts its phase.

To consider dissipation of acoustic power in this region, imagine a piston moving with the gas, and compute the work done by that piston on the gas to the left of it. The work done by a piston is $\oint p\,dV$. In the animation, the small dot traces out the intersection of the pressure line and the volume between the wall and the imaginary piston (whose average position is $4\delta_\kappa$ from the wall), so the area of the little ellipse drawn by the moving dot is proportional to $\oint p\,dV$. That slim elliptical area represents the work that the imaginary piston does on the gas between it and the wall. It's not zero, because of thermal relaxation of the gas to the wall. Gas immediately adjacent to the surface experiences isothermal density and pressure oscillations, which are perfectly springy; gas far from the surface experiences adiabatic density and pressure oscillations, which are also perfectly springy. In between, the gas approximately δ_κ from the surface experiences a complex, hysteretic cycle of density changes in response to the pressure oscillations: first an increase in density due to quasi-adiabatic compression by the sound wave, then a further increase in density as thermal relaxation to the surface removes heat from the gas, then a decrease in density due to quasi-adiabatic expansion by the sound wave, and finally a further decrease in density as thermal relaxation to the surface delivers heat to the gas. Since this gas experiences thermal expansion at low pressure and thermal contraction at high pressure, it absorbs work from the sound wave. This gas, approximately δ_κ *from the surface*, is the most effective at absorbing work from the sound wave, whereas in the case of viscous dissipation the gas *at the surface* is most effective.

The lowest plot in Ani. Thermal /e shows the area of such a work ellipse as a function of the distance of the imaginary piston from the wall. This curve is steepest at $y/\delta_\kappa \simeq 1$, which indicates that the gas approximately δ_κ from the surface dissipates the most acoustic power.

Example: Standing-wave engine. In Chapter 2 we calculated that the thermal-relaxation resistance of one of the hot ducts in the standing-wave engine is $R_\kappa = 2350$ MPa-s/m^3. At a typical operating point of $|p_1| = 300$ kPa, the thermal relaxation dissipation is $|p_1|^2/2R_\kappa = 20$ W. Hence, if this loss could be eliminated in both hot ducts, the 1 kW of acoustic power delivered to the refrigerator could rise by 4%.

Example: Orifice pulse-tube refrigerator. The compliance at the top of the orifice

pulse-tube refrigerator has only $|p_1| = 90$ kPa. Hence, even though it has 0.3 m^2 of surface area, the thermal-relaxation dissipation of acoustic power, obtained from the second term of Eq. (3.11), is only 5 W.

3.1.2. Acoustic power—general thermoacoustics, with $\mu = 0$

Equation (3.9), two sections above, was

$$\frac{d\dot{E}_2}{dx} = -\frac{r_\nu}{2}|U_1|^2 - \frac{1}{2r_\kappa}|p_1|^2 + \frac{1}{2}\mathrm{Re}\left[e\widetilde{p}_1 U_1\right].$$

We have just examined the first two terms, which always consume acoustic power, exist independent of any temperature gradient along x, and represent viscous and thermal-relaxation dissipation, respectively. Next we will examine the third term, which we will call the source/sink term because it can either produce or consume acoustic power and which exists only if $dT_m/dx \neq 0$. This term is difficult to fully understand, especially because dU_{1S} involves both f_κ and f_ν. To build understanding, our qualitative discussion in this subsection will neglect viscosity in dU_{1S}, setting $f_\nu \doteq 0$. In this limit, the third term of Eq. (3.9) can be written

$$\frac{1}{2}\mathrm{Re}\left[e\widetilde{p}_1 U_1\right] = \frac{1}{2}\frac{1}{T_m}\frac{dT_m}{dx}\mathrm{Re}\left[\widetilde{p}_1 U_1\right]\mathrm{Re}\left[f_\kappa\right] + \frac{1}{2}\frac{1}{T_m}\frac{dT_m}{dx}\mathrm{Im}\left[\widetilde{p}_1 U_1\right]\mathrm{Im}\left[-f_\kappa\right] \quad (3.12)$$

$$= \frac{1}{T_m}\frac{dT_m}{dx}\dot{E}_2\,\mathrm{Re}\left[f_\kappa\right] + \frac{1}{2}\frac{1}{T_m}\frac{dT_m}{dx}\mathrm{Im}\left[\widetilde{p}_1 U_1\right]\mathrm{Im}\left[-f_\kappa\right]. \quad (3.13)$$

Expressing it this way shows that $\mathrm{Re}\left[f_\kappa\right]$ is important for acoustic power in traveling-wave engines and refrigerators, in which $\mathrm{Re}\left[\widetilde{p}_1 U_1\right]$ is large, while $\mathrm{Im}\left[-f_\kappa\right]$ is important for acoustic power in standing-wave engines and refrigerators, in which $\mathrm{Im}\left[\widetilde{p}_1 U_1\right]$ is large.

Traveling waves

Begin by considering the regenerator of a traveling-wave engine. To make the most of the first term on the right side of Eq. (3.12) or (3.13), we should make $\mathrm{Re}\left[f_\kappa\right]$ as large as possible; examination of Fig. 2.13 shows that this is accomplished at $R_h \ll \delta_\kappa$, where $\mathrm{Re}\left[f_\kappa\right] \simeq 1$. Under these circumstances, thermal-relaxation resistance r_κ is negligible, as shown by Eq. (2.79). To generate (not dissipate) acoustic power requires that dT_m/dx and $\dot{E}_2$ share the same sign; i.e. the temperature must increase through the regenerator in the direction of acoustic power flow. This situation is illustrated in Anis. Tashe /s and Tashe /r. Animation Tashe /s shows an overview of a traveling-wave engine, namely a traditional Stirling engine. The sign of the circulation of the pV ellipses indicates that acoustic power flows from left to right. The temperature rises in the direction of this acoustic power flow, so the first term in Eq. (3.12) or (3.13) shows that the acoustic power should increase from left to right; indeed, the right pV ellipse has greater area than the left pV ellipse, showing this increase in acoustic power. If these two pistons were connected to a common crankshaft, that crankshaft would supply acoustic power to the gas at the left and remove it from the gas at the right. The extra acoustic power, represented by the difference between the right and left ellipse areas,

is the net acoustic power generated by the engine, available to do external work such as generating electricity.

Animation Tashe /r shows a close-up view inside the regenerator of Ani. Tashe /s. One small piece of gas is highlighted, oscillating left and right while experiencing oscillating pressure. The phasing between pressure and motion is predominantly traveling wave: The gas moves to the right while the pressure is high, and moves to the left while the pressure is low, so the acoustic power flows from left to right. Temperatures are shown in the lower-left plot, where the temperature of the highlighted piece of gas, shown as the blue trace, is always locked to the local solid temperature, represented by the white line. This indicates that $R_h \ll \delta_\kappa$; equivalently, $f_\kappa = 1$. The volume of the highlighted piece of gas is shown on the horizontal axis of the lower-right plot, with the pressure plotted vertically. The gas expands while it moves to the right, because its temperature rises; it contracts while it moves to the left, because its temperature falls. This is the physical effect responsible for the volume source eU_1 in a traveling-wave engine. The net effect—clockwise circulation on the pV diagram—is the production of acoustic power, because the expansion takes place while the gas is at high pressure and the contraction takes place while the gas is at low pressure. The difference between the right piston's work and the left piston's work in Ani. Tashe /s is the total acoustic power produced by all the pieces of gas in the regenerator, each behaving as shown in Ani. Tashe /r.

Example: Traveling-wave engine. The traveling-wave engine of Figs. 1.13 and 1.14 follows the same thermodynamic cycle as discussed in the previous two paragraphs, but without pistons. The acoustic network that serves the function of the two pistons and their crankshaft is shown schematically in Ani. Tashe /u. The acoustic power at several key locations is shown as purple ellipses. The size and signs of these pV ellipses show how acoustic power is produced in the regenerator, with some of the produced power flowing out of the display to the right and the remainder fed back to the left end of the regenerator through the inertance. In this animation, we assume that the regenerator is the only location where acoustic power is produced or dissipated. Hence, the areas of the lower two pV ellipses and the pV ellipse to the left of the regenerator are equal; the shape change at equal areas is due to C and L. Similarly, the areas of the two pV ellipses at the ends of the thermal buffer column are equal, but with a shape change due to the intervening C. Continuity of p_1 and U_1 at the three-way junction on the right ensures that the area of the pV ellipse representing power flowing out of the display to the right is the difference between the areas of the pV ellipses at the right end of the thermal buffer column and the right end of the inertance.

For a typical operating point of the actual engine of Figs. 1.13 and 1.14, 1250 W of acoustic power flows into the ambient end of the regenerator and 3150 W of acoustic power flows out of the hot end of the regenerator. The dT_m/T_m factor in Eq. (3.12) shows that, ideally, the ratio of these two powers, 2.5, could be the ratio of the engine's hot and ambient temperatures, (1000 K)/(300 K) = 3.3. The other two terms in Eq. (3.9), especially the viscous term, account for this missing acoustic power in the regenerator. In addition, some 400 W of acoustic power is dissipated in viscous and thermal-relaxation effects in the inertance and compliance that form the acoustic network at the bottom of the display in Ani. Tashe; these losses are not shown in the ideal case shown in the animation.

The regenerator of a traveling-wave refrigerator is very similar to that of a traveling-wave engine; the primary difference is that T_m decreases in the direction of positive acoustic power in the refrigerator, so the third term in Eq. (3.9) is negative, so this term consumes acoustic power. As with the engine, Re $[f_\kappa]$ should be as large as possible, so we want $R_h \ll \delta_\kappa$. This situation is illustrated in Anis. Ptr /s and Ptr /r. Animation Ptr /s shows an overview of a Stirling refrigerator. The sign of the circulation of the pV ellipses indicates that acoustic power flows from left to right. The temperature decreases in the direction of this power flow, so the first term in Eq. (3.12) shows that the acoustic power should decrease from left to right; indeed, the right pV ellipse has smaller area than the left pV ellipse, showing this decrease in acoustic power. If these two pistons were connected to a common crankshaft, that crankshaft would supply acoustic power to the gas at the left and remove it from the gas at the right. The difference between these two powers, represented by the difference between the left and right ellipse areas, is the net power required by the refrigerator, supplied by external means such as an electric motor.

Animation Ptr /r shows a close-up view inside the regenerator of Ani. Ptr /s. One small piece of gas is highlighted, oscillating left and right while experiencing oscillating pressure. The phasing between pressure and motion is predominantly traveling wave: The gas moves to the right while the pressure is high, and moves to the left while the pressure is low, so the acoustic power flows from left to right. Temperatures are shown in the lower-left plot, where the temperature of the highlighted piece of gas, shown as the blue trace, is always locked to the local solid temperature, represented by the white line. This indicates that $R_h \ll \delta_\kappa$; equivalently, $f_\kappa = 1$. The volume of the highlighted piece of gas is shown on the horizontal axis of the lower-right plot, with the pressure plotted vertically. The gas expands while it moves to the left, because its temperature rises; it contracts while it moves to the right, because its temperature falls. The net effect—counterclockwise circulation on the pV diagram—is the consumption of acoustic power, because the expansion takes place while the gas is at low pressure and the contraction takes place while the gas is at high pressure. The difference between the right piston's work and the left piston's work in Ani. Ptr /s is the total acoustic power consumed by all the pieces of gas in the regenerator, each behaving as shown in Ani. Ptr /r.

Example: Orifice pulse-tube refrigerator. The orifice pulse-tube refrigerator of Figs. 1.15 and 1.16 follows the same thermodynamic cycle as discussed in the previous two paragraphs, but without pistons. The acoustic network that allows the apparatus to follow this cycle is shown schematically in Ani. Ptr /p. The acoustic power at several key locations is indicated by purple ellipses. The size and signs of these pV ellipses show how acoustic power flows into the system from the left (supplied by external means, such as a motored piston or a thermoacoustic engine) and is absorbed in the regenerator and the LRC impedance network at the right end of the display. The areas of the two pV ellipses at the ends of the thermal buffer column (a.k.a. pulse tube) are equal.

For a typical operating point of the actual refrigerator of Figs. 1.15 and 1.16, 8800 W of acoustic power flows into the ambient end of the regenerator and 3000 W of acoustic power flows out of the cold end of the regenerator. The dT_m/T_m factor in Eq. (3.12) shows

that, ideally, the ratio of these two powers, 2.9, could be the ratio of the engine's hot and ambient temperatures, (300 K)/(120 K) = 2.5. The other two terms in Eq. (3.9), especially the viscous term, account for the additional absorption of acoustic power in the regenerator.

Standing waves

Next we will consider the stacks of standing-wave engines and refrigerators, continuing to imagine zero viscosity so that the source/sink term in $d\dot{E}_2/dx$ is tractable. The first term in Eq. (3.12) or (3.13) is zero for standing-wave phasing. To make the most of the second term in Eq. (3.12) or (3.13), we should make $\mathrm{Im}\left[-f_\kappa\right]$ as large as possible; examination of Fig. 2.13 shows that this is accomplished at $R_h \sim \delta_\kappa$, where $\mathrm{Im}\left[-f_\kappa\right] \simeq 0.4$. Equation (2.79) shows that G_κ cannot be neglected in this situation, so we should consider the source/sink term and the thermal-relaxation term in Eq. (3.9) together. Neglecting viscosity, we have from Eqs. (3.12), (3.9), and (2.79)

$$\frac{d\dot{E}_2}{dx} = \frac{1}{2}\left|p_1\right|^2 \frac{(\gamma-1)\omega A\,\mathrm{Im}\left[-f_\kappa\right]}{\gamma p_m} + \frac{1}{2}\mathrm{Im}\left[p_1 \widetilde{U_1}\right] \frac{1}{T_m}\frac{dT_m}{dx}\mathrm{Im}\left[-f_\kappa\right] \tag{3.14}$$

Using Eqs. (2.45) and (2.32) to rearrange this expression, and assuming standing-wave phasing, leads to

$$\frac{d\dot{E}_2}{dx} = \frac{1}{2}\left|p_1\right|^2 \omega A \frac{\gamma-1}{\gamma p_m}\mathrm{Im}\left[-f_\kappa\right]\left(\frac{dT_m/dx}{\nabla T_{\mathrm{crit}}} - 1\right), \tag{3.15}$$

where

$$\nabla T_{\mathrm{crit}} = \frac{\left|p_1\right|/\rho_m c_p}{\left|U_1\right|/A\omega}$$

is the critical temperature gradient we first encountered in Chapter 2, Eq. (2.45).

The situation where $dT_m/dx = \nabla T_{\mathrm{crit}}$, for which Eq. (3.15) shows that acoustic power is neither produced nor absorbed, is illustrated in Ani. Standing /c. In the upper left of the display is a stack, with blue marker lines showing the moving gas. One particular piece of gas is highlighted in white in the stack. The yellow oval marks the region that is shown magnified at the left center of the display, which shows that same piece of moving gas and short fragments of the two stack plates adjacent to it. The volume of that parcel of gas changes in response to pressure and temperature. At the bottom of the display are plots of pressure vs volume of the parcel of gas, and temperature vs position. In the temperature plot, the temperature of the parcel is the blue trace, and that of the nearby plate in the stack is the white line. In the previous, traveling-wave, animations, the blue trace and white line were superimposed because small R_h ensured good thermal contact between gas and solid. Here, $R_h \sim \delta_\kappa$, so the thermal contact is not so good; the alignment of the gas and solid temperatures is due only to the fact that we chose $dT_m/dx = \nabla T_{crit}$ for this animation. The parcel's temperature oscillation is due entirely to adiabatic pressure oscillation, and its temperature oscillation and motion just happen to match the local temperature gradient

dT_m/dx exactly. Since the gas oscillations are merely adiabatic, the pV trace for this parcel is simply a reciprocating adiabat, so this parcel of gas neither produces nor absorbs acoustic power. This operating condition does not appear in useful thermoacoustic engines and refrigerators; $dT_m/dx = \nabla T_{crit}$ is only of academic interest, as it separates the regimes of standing-wave engine and standing-wave refrigerator.

Animation Standing /e shows an overview of a standing-wave engine. The display is basically the same as for Ani. Standing /c discussed above, but now the temperature gradient is steeper, with $dT_m/dx > \nabla T_{crit}$, so that Eq. (3.15) indicates that acoustic power is produced. The steep temperature gradient means that the gas parcel's adiabatic temperature oscillation and motion do not match the local solid temperature gradient, so oscillatory heat transfer between the gas and the solid occurs, as indicated by the time-dependent red arrows in the magnified view of the stack. The phasing is such that thermal expansion occurs at high pressure and thermal contraction at low pressure, so the result is that the pV ellipse circulates clockwise, indicating that the parcel produces acoustic power. The acoustic power thus generated by all the parcels of gas in the stack is the power generated by the engine, available to do external work.

Similarly, Ani. Standing /r shows an overview of a standing-wave refrigerator. The display is basically the same as for Anis. Standing /c and Standing /e discussed above, but now the temperature gradient is less steep, with $dT_m/dx < \nabla T_{crit}$, so that Eq. (3.15) indicates that acoustic power is absorbed. The shallow temperature gradient means that the gas parcel's adiabatic temperature oscillation and motion do not match the local solid temperature gradient, so oscillatory heat transfer between the gas and the solid occurs, as indicated by the time-dependent red arrows in the magnified view of the stack. The phasing is such that thermal expansion occurs at low pressure and thermal contraction at high pressure, so the result is that the pV ellipse circulates counterclockwise, indicating that the parcel produces acoustic power. The acoustic power thus absorbed by all the parcels of gas in the stack must be supplied by and external agent, such as a loudspeaker.

Example: Standing-wave engine. The standing-wave engine of Figs. 1.9 and 1.10 operates just as Ani. Standing /e discussed above, but at 350 Hz instead of the 0.1 Hz frequency of the animation. For a typical operating point, almost 700 W of acoustic power flow is produced in each stack. Under these conditions, the temperature gradient in the stack is x dependent, but it is approximately equal to $(T_H - T_0)/\Delta x = 60$ K/cm. This is indeed larger than the critical temperature gradient, which we estimate to be 35 K/cm at the stack midpoint using Eq. (2.45).

3.2. Total power

Acoustic power is not the only power that is important in thermoacoustics; total power is perhaps of greater importance. Hence, we have to consider exactly what we mean by energy in thermoacoustics.

Engineers have long employed the concept of "control volume" for careful thought about energy balance issues in thermodynamic systems. A control volume is a space of interest, surrounded by a well-defined imaginary boundary, to which we can apply the first law of

thermodynamics and similar principles.

(Apologies for the English language: We do not have short, distinct terms for "rate at which work is done" or "rate at which heat is transferred." Most thermodynamics texts avoid this issue by sticking as much as possible with the variables having units of Joules, not Watts, but I prefer to focus attention on power. So, in the interest of brevity and readability, some of my vocabulary will be a little awkward or ambiguous. When in doubt, look at the variables: Those with overdots, $\dot{W}$, $\dot{Q}$, $\dot{E}_2$, $\dot{H}_2$, and Chapter 4's $\dot{X}_2$, are powers. However, for brevity I will refer to $\dot{W}$ simply as work, and to $\dot{Q}$ simply as heat.)

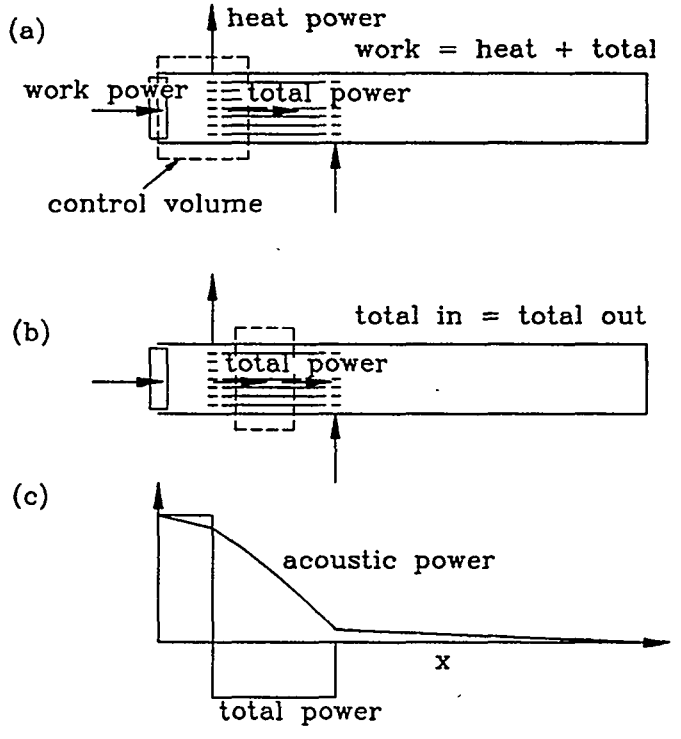

Figure 3.3: A standing-wave refrigerator, insulated everywhere except at the heat exchangers. (a) A useful control volume for thermoacoustics, enclosing the left end. (b) Another useful control volume, enclosing part of the stack. (c) Graph of $\dot{E}_2$ and $\dot{H}_2$ in the refrigerator. The discontinuities in $\dot{H}_2$ are the heats transferred at the heat exchangers.

Figure 3.3 introduces the topic of total power, showing two typical control volumes of interest in thermoacoustics. Consider the thermoacoustic refrigerator shown in Figs. 3.3a and 3.3b, driven by a piston or loudspeaker at the left and having thermal insulation around everything except the heat exchangers, so that heat can be exchanged with the outside world only at the two heat exchangers, and work can be exchanged with the outside world only at the piston. We can apply the principle of energy conservation to the control volume shown by the dotted line in Fig. 3.3a. In steady state, time-averaged over an integer number of acoustic cycles, the energy inside the control volume cannot change, so the rate at which energy flows into that control volume must equal the rate at which energy flows out. What flows in is clearly the time-averaged pV piston work power (which is exactly equal to the acoustic power flowing from the face of the piston into the gas). That must equal the sum

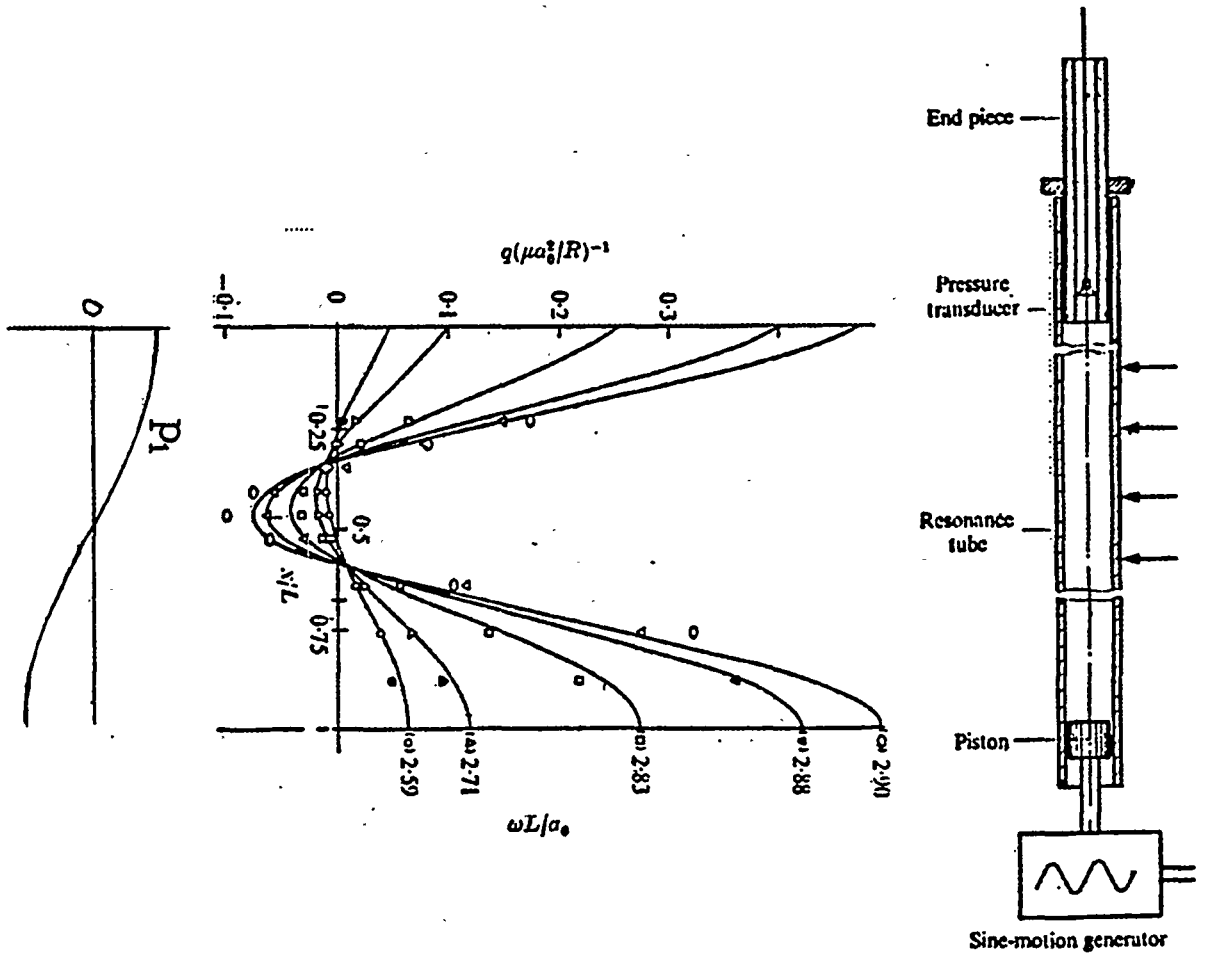

Figure 3.4: Merkli and Thomann's experiment, which detected cooling at the velocity antinode of a standing wave. Thermometers along the wall of the resonator detected temperature; these were used to infer local heat flux q to or from the wall. The negative values of q near the center of the resonance tube represent cooling.

of the two outflowing powers, labeled heat power and total power. The heat is easy to think about—it's simply heat. It's always easiest to discuss such heat flowing via conduction through a solid, so I like to imagine the control-volume boundary being within the metal case that separates the thermoacoustic gas from the outside world. The power flowing down the stack is much more subtle: It's not acoustic power, and it's not heat, and it's not work—but we'd better understand it, because it's what counts in conservation of energy. Another typical important control volume is shown in Fig. 3.3b, intersecting a stack or regenerator in two places, with insulation around the side walls. Here the only powers flowing are the total powers in and out of the two end surfaces of the control volume. Applying the principle of energy conservation (again, steady state; time-averaged) to this control volume shows that total power in equals total power out. So total power can't depend on x within a stack or regenerator—it has to be constant, independent of x, even while acoustic power depends strongly with x, as we saw in the previous section.

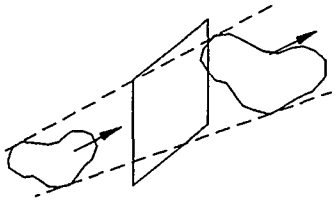

Figure 3.5: An irregular parcel of gas passing through an imaginary rectangular opening fixed in space. As the parcel of gas passes through the imaginary opening, the energy that passes through that opening has several parts. The kinetic and internal energies are convected along with the gas. The pressure does work on the gas ahead as the parcel pushes other gas out of its way in order to pass through the opening. If a temperature gradient in the correct direction exists, heat is conducted through the opening. If the directions of the velocity and its gradients are suitable, viscous shear forces do work on the gas on the other side of the opening.

The 1975 experiment of Merkli and Thomann [40] also helps motivate this discussion of total power. As shown in Fig. 3.4, an acoustic resonator was driven at the half-wavelength resonance, using an oscillating piston and employing sensitive thermometers all along the resonator side wall. Merkli and Thomann were surprised to find that the central thermometers cooled, at the location of greatest dissipation of acoustic power per unit length, $\frac{1}{2}|U_1|^2\, dR_v/dx$. That won't seem so surprising when we understand the important difference between total power and acoustic power.

So, what do we mean by total power? In moving gases (and liquids), the enthalpy is the correct energy to consider [26]. This is because the energy flux density in fluid mechanics is

$$\mathbf{v}\left(\rho v^2/2 + \rho h\right) - k\nabla T - \mathbf{v}\cdot\Sigma, \tag{3.16}$$

where h is the enthalpy per unit mass, $\rho v^2/2$ is the kinetic-energy density, and Σ is the viscous shear tensor. The enthalpy itself is the sum of other energies:

$$h = \epsilon + p/\rho, \tag{3.17}$$

where ϵ is internal energy per unit mass, so the energy flux density can be thought of as the superposition of three flux densities: kinetic energy, internal energy, and "p/ρ." Looking at Fig. 3.5, you can imagine the first two of these as being attached to the gas and hence being convected along with the gas at velocity $\mathbf{v}$, and you can imagine the pressure term to represent the rate at which the pressure of the gas "does work" on the gas it is pushing ahead of it. You can imagine the thermal conduction term as giving the rate at which heat is conducted across the cross section, and you might vaguely imagine the final term as representing work that viscous shear does across the cross section. Any thermodynamic/fluid mechanics text should explain this more carefully.

To simplify this to a usable form, we take the x component of Eq. (3.16), substitute our usual acoustic approximations, Eqs. (2.46)–(2.53), for all variables, keep terms through second order, take the time average, and integrate over the cross-sectional area of the channel. The viscous-shear term is generally much smaller than the other surviving terms. We will

call the result $\dot{H}_2$, the acoustic approximation to the total power flowing in the positive x direction in the channel—"total power" for short. This result is

$$\dot{H}_2(x) = \frac{1}{2}\rho_m \int \mathrm{Re}\left[h_1 \widetilde{u_1}\right] dA - \left(Ak + A_{\mathrm{solid}} k_{\mathrm{solid}}\right) \frac{dT_m}{dx}. \tag{3.18}$$

This acoustic approximation to the total power flowing in the x direction will suffice until we encounter streaming in Chapter 5.

The final term is simple conduction of heat, in which we've included conduction both in the gas and in whatever solid (e.g. stack or regenerator) is present. The first term is more interesting. Professor Thomann (of Merkli and Thomann) said that the energy equation is like a kaleidoscope: Every time you shake it, it looks completely different. There are many good ways to look at $\dot{H}_2$:

First, if we know $\dot{H}_2$ and work, we can deduce the heat transferred at heat exchangers in thermoacoustic engines and refrigerators, as illustrated in Fig. 3.3a. Alternatively, if we know both work and heat, we can deduce $\dot{H}_2$.

Second, if we think of enthalpy as a function of temperature and pressure,

$$dh = \rho_m c_p \, dT + (1 - T\beta) \, dp \tag{3.19}$$

$$= \rho_m c_p \, dT \tag{3.20}$$

and use the second version, which is true for an ideal gas, we find that Eq. (3.18) becomes

$$\dot{H}_2(x) = \frac{1}{2}\rho_m c_p \int \mathrm{Re}\left[T_1 \widetilde{u_1}\right] dA - \left(Ak + A_{\mathrm{solid}} k_{\mathrm{solid}}\right) \frac{dT_m}{dx}. \tag{3.21}$$

This point of view is useful for calculations of $\dot{H}_2$, and is especially useful for thinking about nearly ideal regenerators, in which $T_1 \simeq 0$. For example, consider the control volume shown by the dotted yellow box in the Stirling refrigerator shown in Ani. Ptr /c. For an ideal regenerator, the heat capacity of the regenerator solid and the good thermal contact in the small pores there maintain temporally isothermal conditions at every location, so $T_1 = 0$. If we can neglect the conduction of heat through the regenerator, Eq. (3.21) shows that $\dot{H}_2 = 0$. Hence, the time-averaged cooling power of the refrigerator must equal the time-averaged mechanical power extracted by the cold piston. That is, in suitable units, the area of the pV ellipse for the cold piston must equal the time-averaged width of the red heat arrow at the cold heat exchanger.

Using Eqs. (2.68) and (2.55) for T_1 and u_1, we can perform the integration in Eq. (3.21) to obtain

$$\dot{H}_2 = \frac{1}{2}\mathrm{Re}\left[\widetilde{p_1 U_1}\left(1 - \frac{\left(f_\kappa - \widetilde{f_\nu}\right)}{(1+\sigma)\left(1 - \widetilde{f_\nu}\right)}\right)\right]$$

$$+ \frac{\rho_m c_p \left|U_1\right|^2}{2A\omega(1-\sigma^2)\left|1 - f_\nu\right|^2} \mathrm{Im}\left(f_\kappa + \sigma \widetilde{f_\nu}\right) \frac{dT_m}{dx} - \left(Ak + A_{\mathrm{solid}} k_{\mathrm{solid}}\right) \frac{dT_m}{dx}, \tag{3.22}$$

first obtained by Rott [41].

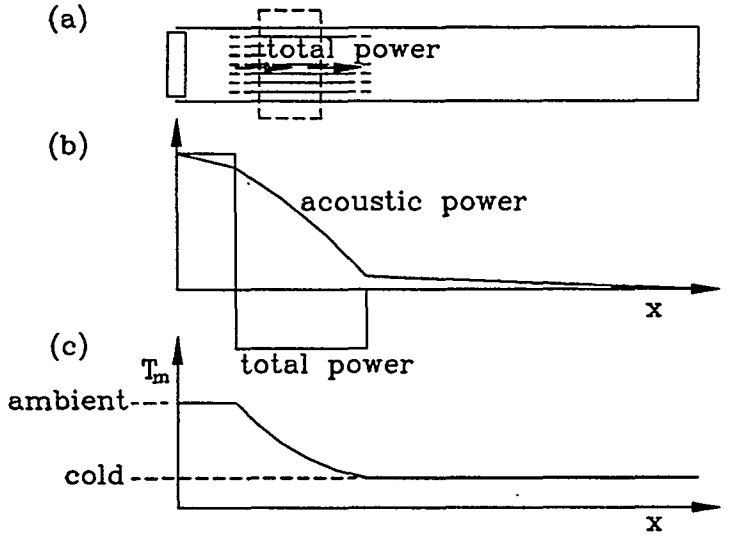

Figure 3.6: The fact that $\dot{H}_2$ is independent of x within an insulated stack or regenerator determines the temperature distribution $T_m(x)$ within the stack or regenerator.

If $dT_m/dx = 0$, such as in a water-jacketed resonator component, Eq. (3.22) gives $\dot{H}_2(x)$; in that case, $d\dot{H}_2/dx$ tells how much energy per unit length is deposited in (or removed from) the water jacket.

Third, if we think of enthalpy as a function of entropy and pressure,

$$dh = T\,ds + dp/\rho, \tag{3.23}$$

we find that the total power can be written

$$\dot{H}_2 = \frac{1}{2}\mathrm{Re}\left[p_1\widetilde{U_1}\right] + \frac{1}{2}\rho_m T_m \int \mathrm{Re}\left[s_1\widetilde{u_1}\right] dA - \left(Ak + A_{\mathrm{solid}}k_{\mathrm{solid}}\right)\frac{dT_m}{dx} \tag{3.24}$$

$$= \dot{E}_2 + \frac{1}{2}\rho_m T_m \int \mathrm{Re}\left[s_1\widetilde{u_1}\right] dA - \left(Ak + A_{\mathrm{solid}}k_{\mathrm{solid}}\right)\frac{dT_m}{dx}. \tag{3.25}$$

The first term is clearly nothing but acoustic power. The second term is T_m times the second-order hydrodynamic entropy flux, and the final term is simply conduction of heat. Many of us have found it helpful to our intuition to identify the sum of the last two terms

$$\dot{H}_2 - \dot{E}_2 = \frac{1}{2}\rho_m T_m \int \mathrm{Re}\left[s_1\widetilde{u_1}\right] dA - \left(Ak + A_{\mathrm{solid}}k_{\mathrm{solid}}\right)\frac{dT_m}{dx}. \tag{3.26}$$

as a sort of thermoacoustic heat-pumping power, with the s_1u_1 term generally by far the largest contributor. Many of us who have worked in standing-wave thermoacoustics for a decade loosely refer to this as "thermoacoustic heat flux," and we have been criticized for this practice by careful people who know thermodynamics. Such careful people correctly point out that multiplying a hydrodynamic entropy flux by T does not make a heat flux. The usual description of "bucket-brigade" standing-wave thermoacoustic "heat transport" as shown in Ani. Standing indeed shows heat flowing from plate to gas at one part of

the cycle and heat flowing from gas to a different part of the plate 180° later in time, but careful people correctly point out that it is not accurate to say that the gas carries heat from the first location to the second, because there is more to gas thermodynamics than simply heat capacity. I no longer use such careless vocabulary when talking with experts, both to avoid controversy and to avoid a false sense of simple understanding. On the other hand, I continue to use this careless vocabulary often [25], mostly because it allows thermoacoustics novices to understand the phenomena without bogging them down in details.

In wide-open isothermal channels, like most resonator components, most of the gas should experience adiabatic oscillations and s_1 should be near zero over most of the area A. Hence, Eq. (3.24) suggests that in this situation the total power and the acoustic power are nearly equal. This contributes to our ability to deduce a heat-exchanger's heat, from knowledge of the adjacent stack's total power and adjacent duct's acoustic power.

3.2.1. Traveling waves

Like a kaleidoscope: Shake the energy equation a little, and you see a new picture. If the total power through a good regenerator is approximately zero, then $\frac{1}{2}\rho_m T_m \int \mathrm{Re}\,[s_1 \widetilde{u_1}]\,dA$ must be approximately equal and opposite to the acoustic power $\frac{1}{2}\,\mathrm{Re}[p_1 \widetilde{U_1}]$ at each location x. This is another way of imagining the "cause" of the Stirling refrigerator's cooling power—as due to the large acoustic power flowing through the regenerator plus the fact that the total power flowing through the regenerator is nearly zero. In Ani. Ptr /r, which shows a close-up view inside the regenerator of an orifice pulse-tube refrigerator, the red arrows show heat flow into and out of the parcel of gas; these heat flows cause the oscillating entropy s_1, and its phasing relative to u_1, and hence cause $\mathrm{Re}\,[s_1 \widetilde{u_1}]$ to be nonzero.

In a pulse tube or thermal buffer column, s_1 is due almost entirely to $(u_1/i\omega)\,ds_m/dx$, so $\mathrm{Re}\,[s_1 \widetilde{u_1}] \simeq 0$. Hence $\dot{H}_2 \simeq \dot{E}_2$ in a pulse tube or thermal buffer column.

In the regenerators of traveling-wave systems, $T_1 \simeq 0$, and hence $\dot{H}_2 \simeq 0$. Hence, if a heat exchanger is sandwiched between a regenerator and a pulse tube or thermal buffer column, or between a regenerator and a resonator component, the heat-exchanger heat and the acoustic power flowing through it must be nearly equal. (In contrast, standing-wave systems have no such constraint on $\dot{H}_2$ and so the heat-exchanger heat can be significantly larger than the acoustic power.)

3.2.2. Standing waves

For standing-wave phasing, the inviscid limit of Eq. (3.22),

$$\dot{H}_2 \simeq \frac{1}{2}\,|p_1|\,|U_1|\,\mathrm{Im}\,[-f_\kappa] \left(\frac{dT_m/dx}{\nabla T_{\mathrm{crit}}} - 1 \right) - (Ak + A_{\mathrm{solid}} k_{\mathrm{solid}}) \frac{dT_m}{dx}, \tag{3.27}$$

is simple and interesting, especially when considered in concert with the standing-wave version of Eq. (3.24):

$$\dot{H}_2 = \frac{1}{2}\rho_m T_m \int \mathrm{Re}\,[s_1 \widetilde{u_1}]\,dA - (Ak + A_{\mathrm{solid}} k_{\mathrm{solid}}) \frac{dT_m}{dx} \tag{3.28}$$

The first term of Eq. (3.27) resembles Eq. (3.15) for $d\dot{E}_2/dx$ derived above: It has the same dependence on f_κ and on dT_m/dx. Hence, aside from the less interesting thermal-conduction

term, the total power and the *rate of change of* acoustic power have the same dependences on channel geometry in standing waves; and both are zero when $dT_m/dx = \nabla T_{\text{crit}}$, positive when $dT_m/dx > \nabla T_{\text{crit}}$, and negative when $dT_m/dx < \nabla T_{\text{crit}}$.

Furthermore, this term must be identified with the hydrodynamic entropy transport represented by the $\text{Re}\,[s_1\widetilde{u}_1]$ term in Eq. (3.28). Animation Standing /r illustrates this $\text{Re}\,[s_1\widetilde{u}_1]$ contribution to the total power in a standing-wave refrigerator. The parcel of gas absorbs a little heat from the solid walls at the right extreme of its motion, as shown by the red arrows, carries entropy to the left, and gives heat to the solid walls at the left extreme of its motion, and returns to the right with less entropy. In this case, $\dot{H}_2$ is negative. In moving left, the gas has moved up the temperature gradient, so it deposits its heat to the walls at a location of higher temperature than that at which it absorbed heat from the walls. Loosely speaking, the gas moves heat from right to left, up the temperature gradient. So this is a refrigerator, moving heat from right to left, up the temperature gradient. Overall, every parcel of gas in the entire stack, each cycle of the wave, picks up a little heat from solid, moves it a little to the left and deposits it again at a slightly higher temperature. The parcels in mid stack are like the middle members of a bucket brigade, passing heat along. At either end are parcels that oscillate between the stack and one of the heat exchangers. At the right end, such parcels absorb heat from the cold heat exchanger and deposit heat in the stack; at the left end, such parcels absorb heat from the stack and deposit heat in the ambient heat exchanger. So the net effect is to absorb heat from the cold heat exchanger, and reject waste heat at the ambient heat exchanger.

The process illustrated in Ani. Standing /r occurs in standing-wave refrigerators, for which $dT_m/dx < \nabla T_{crit}$. If the temperature gradient in the stack is steeper, the signs of all the heat transfers change, as shown for the standing-wave engine of Ani. Standing /e. In this case, even though the gas is heated adiabatically as it moves left, it's not hot enough at the left extreme of its motion to match the local solid temperature when it gets there. So at the left extreme of its motion, at high pressure, it's still cooler than the solid, so heat flows into it, which increases its entropy. Similarly, at the right extreme of its motion, heat flows out of the gas into the solid, decreasing the entropy of the gas. The gas effectively shuttles heat from hot to cold, left to right, down the temperature gradient; $\dot{H}_2$ is positive.

3.3. A point of view for computations

In Chapter 2, we developed the momentum equation to relate U_1 and dp_1/dx, as in Eq. (2.56) or (2.73). The momentum equation can be interpreted in two ways, either as an expression of how flow causes a pressure gradient or as an expression of how a pressure gradient causes flow, and both points of view are useful. In steady-flow hydrodynamics, it is usually obvious which point of view is preferable in a given circumstance—the flow of water down a dam's spillway is caused by the gravitational pressure gradient, while the pressure gradients in the oil pumped through the passages of an automobile engine are caused by the volumetric velocity coming from the positive-displacement oil pump. In acoustics, the "correct" point of view is more subtle, as the momentum equation relates U_1 and dp_1/dx while simultaneously the continuity equation relates p_1 and dU_1/dx.

Similarly, two interpretations of the thermoacoustic total-power equation are possible and useful, whether Eq. (3.18), (3.21), (3.22), or (3.24). In one interpretation, the temperature

gradient dT_m/dx (and all the other relevant variables, such as channel geometry, p_1, and U_1) cause total power $\dot{H}_2$ to flow through a stack or regenerator. In another interpretation, $\dot{H}_2$ (and all the other variables) cause the temperature gradient in the stack or regenerator. Both points of view are useful. For example, if you put a fixed heater power into the hot heat exchanger of the standing-wave engine of Fig. 1.10, that power has nowhere else to go but through the stack, so it determines the temperature gradient in the stack, in concert with many other variables such as those of the acoustic wave. On the other hand, if you power that heater using a thermostat set at a fixed T_H, the temperature difference across the stack determines the power flowing through the stack and hence determines the heater power that must be supplied.

The first interpretation of the total-power equation is particularly important because it shows that the total-power equation can be regarded as a first-order differential equation for $T_m(x)$ in a stack or regenerator, if p_1 and U_1 and the geometry are known. This is evident in the control-volume picture of Fig. 3.3b, which shows that the total power $\dot{H}_2$ must be a constant, independent of x, throughout the stack or regenerator whenever the side walls of the stack or regenerator are insulated. The other variables in Eq. (3.22) are presumably known from the considerations of Chapter 2. Although the temperatures at the ends of a stack or regenerator are often known, there is no better way than Eq. (3.22) to calculate the distribution of temperature at intermediate x.

Our numerical integrations in DeltaE rely on the first interpretation of the total-power, momentum, and continuity equations. DeltaE performs simultaneous integrations along x of the momentum, continuity, and total-power equations, in the form

$$dp_1 = F_{\text{mom}}(T_m, U_1; \omega, \text{gas properties, geometry})\, dx \tag{3.29}$$

$$dU_1 = F_{\text{cont}}(T_m, p_1, U_1; \omega, \text{gas properties, geometry})\, dx \tag{3.30}$$

$$dT_m = F_{\text{pow}}(T_m, p_1, U_1; \dot{H}_2, \omega, \text{gas properties, geometry})\, dx. \tag{3.31}$$

to find $p_1(x)$, $U_1(x)$, and $T_m(x)$. These complicated functions F_{mom}, F_{cont}, and F_{pow} are appropriate functional forms of the momentum, continuity, and total-power equations. In Eq. (3.31), $\dot{H}_2$ is taken to be independent of x within each stack or regenerator; its value may assigned based on nearby heat-exchanger heats, or may be found self-consistently. Once $p_1(x)$, $U_1(x)$, and $T_m(x)$ are found, other results such as $\dot{E}_2(x)$ are straightforward.

3.4. Examples

Example: Standing-wave engine. While producing the curves of p_1 and U_1 shown in Fig. 2.16 for the standing-wave engine, DeltaE also computed $T_m(x)$ and the powers. The results are shown in Fig. 3.7. Within the stack, total power $\dot{H}_2$ is constant at 2380 W, because of the sidewall insulation and the first law of thermodynamics. Its magnitude is the same as the heater power supplied at the hot heat exchanger. DeltaE used this value of $\dot{H}_2$ and the total-power equation to determine $T_m(x)$ in the stack; it deviates noticeably from a straight line.

The calculated values of acoustic power $\dot{E}_2(x)$ follow directly from the values of $p_1(x)$ and $U_1(x)$ plotted in Fig. 2.16. Note that $\text{Re}[p_1]\,\text{Im}[U_1]$ contributes nothing to $\dot{E}_2$; nonzero acoustic power arises from $\text{Re}[p_1]$ times the small $\text{Re}[U_1]$ and from $\text{Re}[U_1]$ times the small

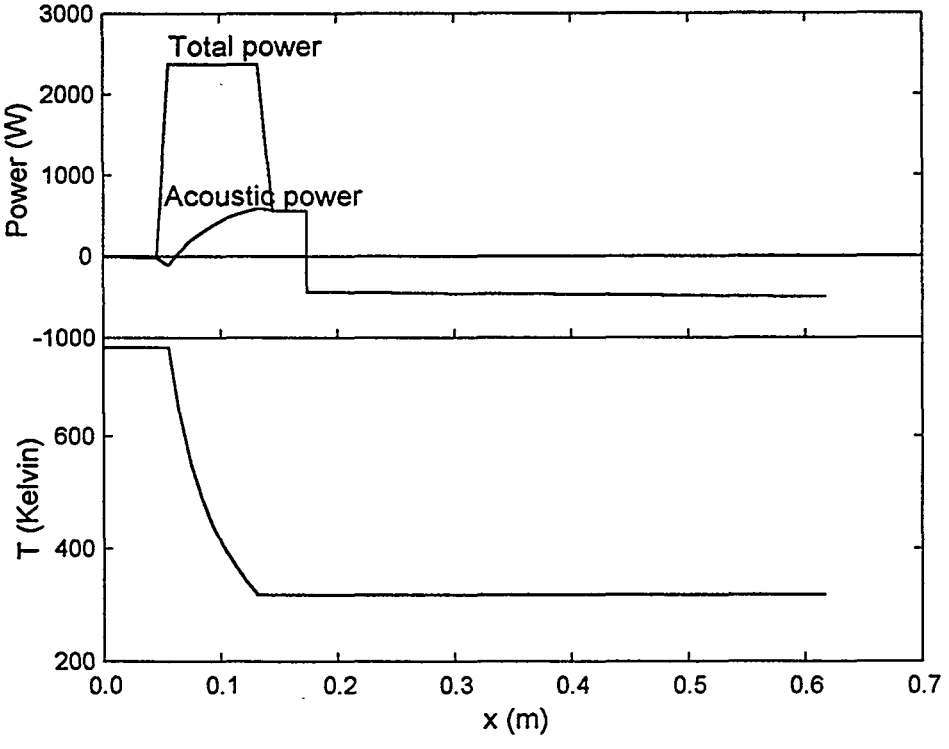

Figure 3.7: Acoustic power $\dot{E}_2$, total power $\dot{H}_2$, and mean temperature T_m as functions of position x for the standing-wave engine, under the same conditions as Fig. 2.16.

$\mathrm{Im}[p_1]$. A total of 670 W of acoustic power is generated throughout the stack, but especially near the hot end, and 500 W of acoustic power is assumed to flow from right to left at the right end of the figure, from the other acoustic engine shown in Fig. 1.10. This total of 1170 W of acoustic power is consumed elsewhere, most dramatically at the side branch to the refrigerators, where 1000 W is delivered. Acoustic power dissipation elsewhere is more subtle, as evidenced by the small negative slope of $\dot{E}_2(x)$ throughout the resonator; this negative slope is somewhat larger in the two heat exchangers. The small negative slope of $\dot{E}_2(x)$ in the hot duct, to the left of the stack and hot heat exchanger, which is almost invisible in the figure except as a slight change in line width between $x = 0$ and $x = 0.05$ m, shows the dissipation of 20 W estimated at the end of Section 3.1.1 above.

Example: Orifice pulse-tube refrigerator. A similar plot of results of DeltaE's numerical integration is shown in Fig. 3.8 for the orifice pulse-tube refrigerator, under conditions similar to those shown in the phasor diagram of Fig. 2.19.

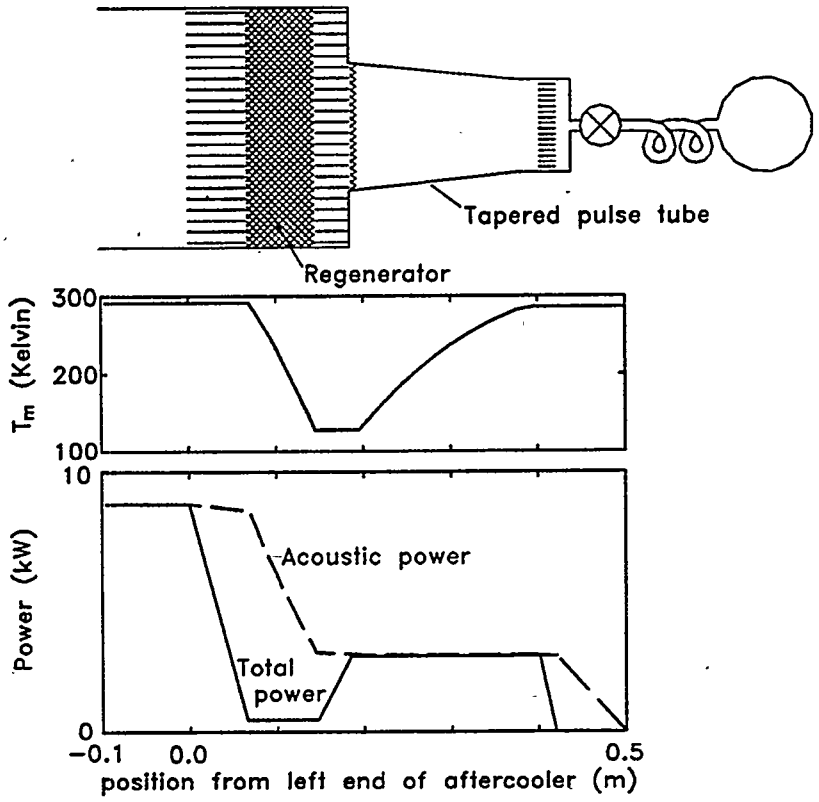

Figure 3.8: Temperature T_m, total power $\dot{H}_2$, and acoustic power $\dot{E}_2$ throughout the orifice pulse-tube refrigerator of Fig. 1.16. Horizontal dimensions in the sketch above are aligned with corresponding locations in the graphs.

In the regenerator and the pulse tube, $T_m(x)$ is obtained by integration of the total-power equation, for a total power $\dot{H}_2 = 0.48$ kW in the regenerator and of 2.92 kW in the pulse tube. In the regenerator, this results in only slight deviation of $T_m(x)$ from a straight line.

The value of 0.48 kW is obtained self-consistently by the calculation, in order to allow the regenerator to reach from its ambient temperature of 292 K to its cold temperature of 128 K. Both terms in Eq. (3.21) contribute to $\dot{H}_2$ in the regenerator; the sum is small compared with other powers in the problem. The pulse tube radius is much greater than δ_κ, so we expect $\dot{H}_2 \simeq \dot{E}_2$ as shown in the figure. The small difference between these two is due primarily to $A_{\text{solid}} k_{\text{solid}}\, dT_m/dx$ in Eq. (3.24). The large changes in $\dot{H}_2$ at each of the three heat exchangers represent the heats exchanged at these heat exchangers. The cooling power at 128 K is $2.92 - 0.48 = 2.44$ kW.

About 2/3 of the 8.77 kW of acoustic power is consumed in the regenerator, and about 1/3 is consumed in the flow resistance of the LRC network at the end of the refrigerator. These powers are calculated from the calculated values of $p_1(x)$ and $U_1(x)$ throughout, and are consistent with the phasors in Fig. 2.19 showing p_1 and U_1 at a few locations. Small amounts of acoustic power are also consumed in the two largest heat exchangers, and a negligible amount of acoustic power is consumed in the pulse tube and in the large duct to the left of all the heat-exchange components.

3.5. Exercises

3.1 In the spirit of Fig. 1.19, draw phasor diagrams for several locations of the wave shown in Ani. Wave /k. Discuss how your diagrams are consistent with positive acoustic power flow in the positive x direction, and with $d\dot{E}_2/dx = 0$.

3.2 In a double Helmholtz resonator, how much kinetic energy is in the gas in the neck when it is moving with velocity $|u_1|$? Express your answer in terms of L and U_1. A quarter cycle later, all that kinetic energy is converted to potential energy stored in the compliances. Express that energy in terms of p_1 and C.

Using Eq. (3.11), write down expressions for the time-averaged viscous absorption of acoustic power in the neck, and the time-averaged thermal-relaxation absorption of acoustic power the bulbs. Which is typically bigger?

The quality factor of a resonance is given by $Q = 2\pi(\text{Stored energy})/(\text{Energy dissipated per cycle})$. Write down an expression for the Q of this double Helmholtz resonator.

Acoustics experts only: In a simple acoustics textbook, look up the radiation impedance from a circular orifice whose diameter is much smaller than λ. There is an imaginary part, which adds to the inertance of the neck, and a real part, which adds to the dissipation. Estimate how much this "end effect" shifts the resonance frequency of the Helmholtz resonator. How much does it change the Q?

3.3 If your favorite piece of thermoacoustics hardware has a stack or regenerator, estimate the heat deposited and removed from the solid during each half cycle of the oscillation. If you don't have a favorite, estimate the heat deposited and removed during each half cycle of an audio-amplitude sound wave in air per square meter of a solid boundary.

3.4 Estimate the critical temperature gradient in the stack or regenerator of your favorite piece of hardware. If you don't have a favorite, estimate the critical temperature gradient halfway between the pressure node and adjacent velocity node in a 240 Hz standing wave in air at atmospheric pressure. How much of the information given in the preceding sentence was unnecessary to find the answer?

3.5 If your favorite acoustic hardware has a power transducer such as a loudspeaker, estimate the acoustic power it transduces, using its $|x_1|$, area, frequency, etc.

3.6 Draw a few control volumes for your favorite thermoacoustics hardware. Discuss thermal insulation, and where energy can cross the boundaries of the control volumes.

3.7 Estimate $\dot{H}_2$ for the stack or regenerator in your favorite piece of thermoacoustics hardware. Black-body radiation is another contributor to total power, which was not included in our discussion. Estimate it for the same component.

3.8 Sketch $\dot{H}_2$ and $\dot{E}_2$ vs x for your favorite thermoacoustics hardware. Don't worry about the actual magnitudes of things; just try to get the overall qualitative picture right: the signs of the powers, the signs and locations of discontinuities, the signs of slopes. Also sketch $|p_1|$ and $|U_1|$.

3.9 Look closely at Ani. Thermal /e. It looks like the power curve shows negative slope at about $y/\delta_\kappa = 4$. This suggests that thermal relaxation in gas at that distance from a solid wall does not dissipate acoustic power—it generates acoustic power!—because the imaginary piston at a distance $5\delta_\kappa$ from the wall has to supply *less* power to the gas between it and the wall than does the imaginary piston at a distance $4\delta_\kappa$ from the wall. Was the author was sloppy in programming the animation, or does the math confirm this surprising observation? Does something similar occur in boundary-layer viscous dissipation as illustrated in Ani. Viscous?

3.10 Can nonzero acoustic power pass a true pressure node in a standing wave? Can it pass a velocity node? Can nonzero total energy pass either a pressure node or a velocity node?

3.11 Consider a large-diameter channel with a nonzero temperature gradient, such as the thermal isolation tube or pulse tube of Figs. 1.14 or 1.16. Show that $\dot{H}_2 \simeq \dot{E}_2$ if you can neglect boundary-layer effects at the walls and ordinary thermal conduction along x (and if streaming, to be discussed in Chapter 6, is negligible). Discuss this result from several points of view: Eq. (3.21), Eq. (3.24), and a Lagrangian picture of moving parcels of gas. With respect to Eq. (3.24), be sure to notice that $s_1 \neq 0$.

3.12 Consider a channel large enough that the boundary-layer approximation is valid. The channel has a spatially uniform T_m, maintained by water flowing in a jacket around the channel. Suppose p_1 and U_1 are known. Use Eq. (3.22) for $\dot{H}_2$ and the principle of energy conservation to derive an expression for the heat dQ delivered to (or removed from?) the water in a length dx of the channel. In your answer, use results from Chapter 2 to express dp_1/dx in terms of U_1 and to express dU_1/dx in terms of p_1. Interpret the Merkli-Thomann experiment, Fig. 3.4, from this perspective—are their experimental results consistent with your answer?

3.13 Show that $\dot{H}_2 = \dot{E}_2$ when $dT_m/dx = 0$, $\mu = 0$, and $k = 0$, independent of the size of the channel.

3.14 Simplify Eq. (3.22) using boundary-layer expressions for f_κ and f_ν and assuming standing-wave phasing.

3.15 Evaluate $\int \mathrm{Re}\,[s_1 \widetilde{u_1}]\, dA$ in boundary-layer approximation. Make a graph, with the vertical axis $A\,|p_1|\,/\rho_m a\,|U_1|$ running from 0 to 10, and the horizontal axis $(dT_m/dx)/\nabla T_{crit}$ running from 0 to 4. On the graph, for p_1 and U_1 in phase, draw a line indicating where

$\int \mathrm{Re}\,[s_1\widetilde{u}_1]\,dA = 0$. Show which side of this line has $\int \mathrm{Re}\,[s_1\widetilde{u}_1]\,dA > 0$ and which side has $\int \mathrm{Re}\,[s_1\widetilde{u}_1]\,dA < 0$. Repeat for phase differences between p_1 and U_1 of 45°, 90°, 135°, ... Interpret some of these graphs in terms of Ani. standing.

4. EFFICIENCY

Both the raw efficiency and the "fraction of Carnot" serves as a useful measure of efficiency for the simplest thermodynamic systems, such as the simple heat engine or the simple refrigerator [2] shown in Fig. 1.1 at the beginning of the book and reproduced here in Fig. 4.1a. The raw efficiency is what you want divided by what you must spend, and in Chapter 1 we reviewed the well known bounds on raw efficiency given by Carnot's ratio of temperatures, which we quickly derived from the first and second laws of thermodynamics. So it is natural to also cite the fraction of Carnot, which is the ratio of the actual raw efficiency to the maximum raw efficiency allowed by the laws of thermodynamics. The physicists' ideal is 100%, but reality reduces this significantly. Typically, thermoacoustic engines and refrigerators that were designed for high efficiency have operated at or above 20% of Carnot; we expect to increase this to 40% of Carnot in the future.

Fraction of Carnot is fine for such simple systems. However, more complex systems need a more sophisticated measure of merit. For instance, consider the machine shown in Fig. 4.1b, which takes air at atmospheric temperature and pressure, and separates and cools it to produce liquid oxygen, liquid nitrogen, liquid argon, solid carbon dioxide, and liquid water. The machine is driven with some work power, and it dumps waste heat power to ambient temperature. How should we measure the efficiency of a complicated system like this? What we want to do and what we must spend in order to do it don't even have the same units. How can we understand what limit on the performance of such a system is imposed by the two laws of thermodynamics? This chapter introduces some advanced concepts in thermodynamics that can be used to answer these questions.

4.1. Lost work and entropy generation

In one common and powerful method of accounting for efficiency in complex thermodynamic systems [28, 42], all losses are measured in terms of equivalent lost work, and one temperature T_0 is identified as a special temperature, the environment temperature at which arbitrary amounts of heat of no value can be freely exchanged. (If *two* different environmental temperatures existed, with which heat of no value could be freely exchanged, then it would be possible to run a heat engine between them, producing unlimited work—of great value—from heat of no value. Hence, identification of a single "ambient" temperature T_0 is not at all artificial.) We begin this section with several examples illustrating the use of this method of accounting.

First consider a simple a heat engine as shown in Fig. 4.2a. The engine's cold temperature is labeled with the subscript 0, to specify it as the environment temperature where waste heat of no value is rejected. We can write the engine's work as the hot heat times the

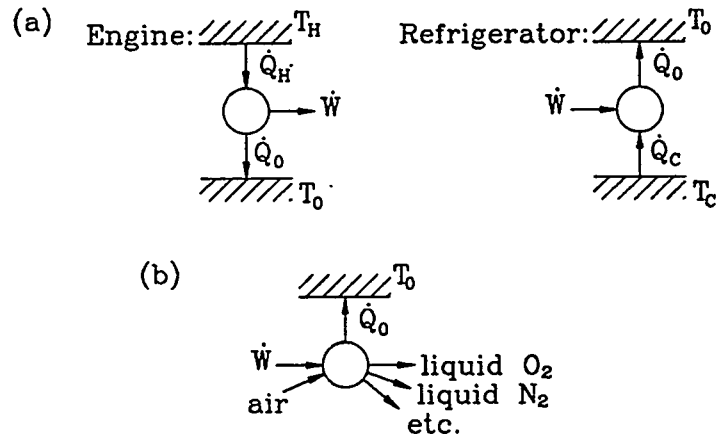

Figure 4.1: (a) The simplest engine and refrigerator, for which simple measures of efficiency suffice. (b) An air separator-liquefier, requiring a more sophisticated approach to efficiency.

Carnot efficiency minus something we'll call lost work:

$$\dot{W} = \dot{Q}_H \left(1 - \frac{T_0}{T_H}\right) - \dot{W}_{\text{lost}}. \tag{4.1}$$

The first term is the maximum work that an ideal engine could produce, according to the bounds imposed by the first and second laws of thermodynamics, as we reviewed at the beginning of Chapter 1. If the engine is not so ideal, the work it actually produces must be lower; we'll call the difference the lost work $\dot{W}_{\text{lost}}$. Similarly, for the simple refrigerator shown in Fig. 4.2b, the work required is the sum of the minimum work that an ideal refrigerator would require plus extra work we call $\dot{W}_{\text{lost}}$:

$$\dot{W} = \dot{Q}_C \frac{T_0 - T_C}{T_C} + \dot{W}_{\text{lost}}. \tag{4.2}$$

A third example, a very simple example of lost work, is illustrated in Fig. 4.2c: Friction in machinery at ambient temperature dissipates work, all of which is clearly lost, so

$$\dot{W}_{\text{lost}} = \dot{W}_{\text{fric}}\,. \tag{4.3}$$

The fourth example, illustrated in Fig. 4.2d, is more subtle, and begins to show how challenging and how powerful this point of view can be. Figure 4.2d shows a refrigerator, within which some frictional dissipation occurs at a temperature less than the environment temperature T_0. (Such dissipation could be due to drag on a piston in the cold part of the refrigerator.) How much lost work must be assigned to that frictional dissipation? Suppose that this friction is the only non-ideal feature in the system, so the system can be treated like an ideal refrigerator with Carnot's COP, powered by a drive mechanism with friction, with the drive mechanism thermally anchored to the cold temperature T_C, as shown in Fig. 4.2d. Some of the drive power $\dot{W}$ is dissipated into heat at T_C by friction; the remaining power drives an ideal refrigerator, which must pump the heat generated by friction plus the

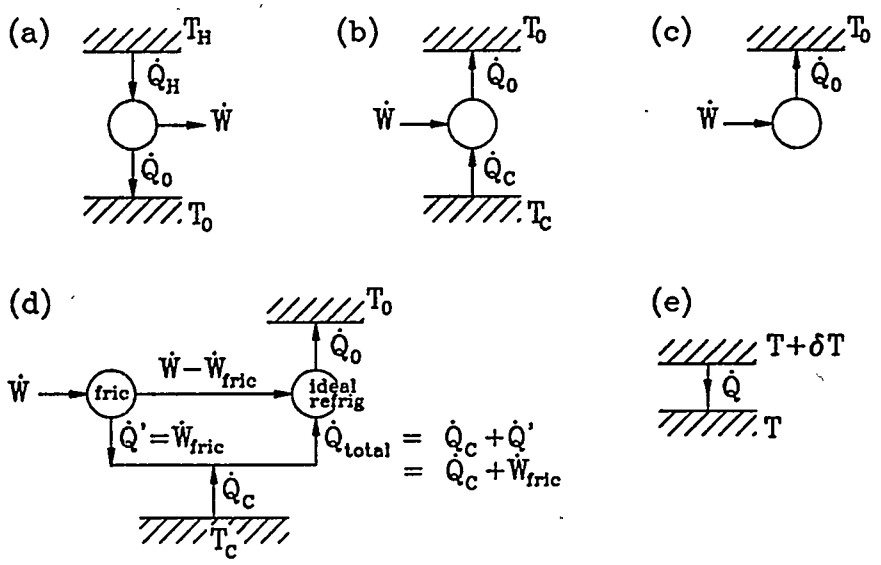

Figure 4.2: Several examples to illustrate the concept of lost work. (a) A simple engine. (b) A simple refrigerator. (c) Friction at temperature T_0. (d) Friction at a temperature $T < T_0$. (e) Heat transfer across a small thermal resistance.

external cooling load $\dot{Q}_C$ from the low temperature to the environment temperature. Since the ideal refrigerator has Carnot's COP, we have

$$\dot{W} - \dot{W}_{\text{fric}} = \left(\dot{Q}_C + \dot{W}_{\text{fric}}\right) \frac{T_0 - T_C}{T_C}, \tag{4.4}$$

which can be rewritten as

$$\dot{W} = \dot{Q}_C \frac{T_0 - T_C}{T_C} + \dot{W}_{\text{fric}} \frac{T_0}{T_C}. \tag{4.5}$$

Hence, the lost work in this system is

$$\dot{W}_{\text{lost}} = \dot{W}_{\text{fric}} \frac{T_0}{T_C}. \tag{4.6}$$

Indeed, it seems reasonable that the lost work should be greater than the frictional dissipation, by a factor depending on the temperatures, because intuitively we expect that dissipating work at low temperature should be worse than dissipating it at room temperature: If work is "lost" at low temperature, pumping the resulting heat up to room temperature costs even more work.

A fifth example—imperfect heat transfer—is shown in Fig. 4.2e. Two thermal reservoirs, at nearly equal temperatures $T + \delta T$ and T, are connected by a thermal resistance through which heat $\dot{Q}$ flows. The work lost in this process is the excess work that could have been produced by an ideal engine driving an ideal heat pump, with the engine operating between $T + \delta T$ and T_0 and the heat pump operating between T and T_0, with the same heat $\dot{Q}$

exchanged with both reservoirs:

$$\dot{W}_{\text{lost}} = \dot{W}_{\text{engine}} - \dot{W}_{\text{pump}} \tag{4.7}$$

$$= \dot{Q}\left(1 - \frac{T_0}{T+\delta T}\right) - \dot{Q}\left(1 - \frac{T_0}{T}\right) \tag{4.8}$$

$$\simeq \dot{Q}\frac{T_0\,\delta T}{T^2}, \tag{4.9}$$

which is small if the temperature difference δT is small. (For illustration here, we assumed $T > T_0$, but the same conclusion follows from assuming $T < T_0$.) Imperfect thermal contact in heat exchangers is responsible for this type of lost work.

These ideas are important because the lost work can be expressed as the product of the environment temperature T_0 and the sum of all the entropy generated in the system,

$$\dot{W}_{\text{lost}} = T_0 \sum \dot{S}_{\text{gen}}\,, \tag{4.10}$$

a result known as the Guoy–Stodola theorem [29]. This theorem is presented clearly in the physics literature [42], but without reference to the decades-earlier work of Guoy and Stodola. We won't prove this theorem here, but we use some of the examples of Fig. 4.2 to illustrate it. First: The entropy generated by imperfect thermal contact in Fig. 4.2e must be the difference between the entropy $\dot{Q}/T$ gained by the lower reservoir and the entropy $\dot{Q}/(T+\delta T)$ lost by the upper reservoir. The difference is $\dot{Q}\,\delta T/T^2$ to lowest order in δT; multiplying by T_0 indeed yields the lost work given in Eq. (4.9). Second: For friction at a temperature T as illustrated in Fig. 4.2c, the entropy generation must be the heat generated, which is exactly $\dot{W}_{\text{fric}}$, divided by T. Multiplying by T_0 as prescribed by Eq. (4.10), yields

$$\dot{W}_{\text{lost}} = \dot{W}_{\text{fric}}\frac{T_0}{T}, \tag{4.11}$$

in agreement with both Eq. (4.3) and Eq. (4.6).

This method and theorem are important because entropy is an extensive quantity. The sum Σ in Eq. (4.10) can be performed any of a number of ways. The sum can be performed component by component throughout a piece of experimental hardware, tabulating how much entropy is generated in each heat exchanger, stack, resonator, etc. It can even be performed by location within a component, e.g. to determine whether the hot end of the stack, the middle of the stack, or the cold end of the stack is the lossiest. This sum can be performed process by process, tabulating how much entropy is generated by viscous processes, thermal processes, frictional processes, etc., either within each component or system-wide. There seems to be no limit to how finely this sum can be subdivided; one could even ask how much of the thermal entropy generation at a given location is due to heat diffusing in the x direction, and how much is due to heat diffusing perpendicular to x. The sum can be performed with respect to time instead of location or process, e.g. to learn whether the entropy generated by thermal relaxation in a regenerator occurs mostly during the compression and expansion phases of the cycle or during the gas-motion phases of the cycle.

Taken to extreme, this point of view would let us write

$$\dot{S}_{\text{gen}} = \frac{\omega}{2\pi}\int_0^{2\pi/\omega}\int_V \rho\dot{s}_{\text{gen}}\,dV\,dt \tag{4.12}$$

where the instantaneous rate of entropy generation per unit volume is

$$\rho \dot{s}_{\text{gen}} = \frac{\mu}{T}\Phi + \frac{k\left(\nabla T\right)^2}{T^2} + \frac{j^2/\sigma}{T} + \text{friction} + \text{chemistry} + \ldots. \tag{4.13}$$

This displays the time-averaged rate of entropy generation as an integral, over time and over the whole volume of an apparatus, of the instantaneous rate of entropy generation, which is itself the sum effects coming from different processes: viscous, thermal, electrical, frictional, chemical, etc. Having this in mind will let you think about where and how the inefficiencies arise in a system. Quoting from a clear review [42] of this method: "In accordance with the circumstance that entropy is a quantity having extensive magnitude, it is evident that $[T_0 \dot{S}_{\text{gen}}]$ can be calculated by adding together separate terms of the form $[T_0 \dot{S}_{\text{gen}}]$ for each of the irreversible processes that accompany a total operation. This then allows us to take each of these separate terms ... as a measure of the loss in potential work that results from the corresponding particular irreversible processes in the total operation. This is an important principle, since it allows us to determine the reduction in efficiency resulting from any particular cause without making an analysis of the whole operation."

Source	$\dot{W}_{\text{lost}}$ (macroscopic)	$\rho \dot{s}_{\text{gen}}$ (microscopic)
Electrical	$I^2 R T_0/T$	$j^2/\sigma T$
Friction	$\dot{W}_{\text{fric}} T_0/T$	$v\sigma/T$ (per unit area)
Viscosity	$U\,\Delta p\, T_0/T$	$\mu\Phi/T + \zeta\left(\nabla\cdot\mathbf{v}\right)^2/T$ where $\Phi = \frac{1}{2}\left(\frac{\partial v_i}{\partial x_k} + \frac{\partial v_k}{\partial x_i} - \frac{2}{3}\delta_{ik}\frac{\partial v_l}{\partial x_l}\right)^2$
Imperfect heat transfer ($\delta T \ll T$)	$\dot{Q} T_0\, \delta T/T^2$	$k\left(\nabla T\right)^2/T^2$
Heat leak	$\dot{Q} T_0\, \left(T_H - T_C\right)/T_H T_C$	$k\left(\nabla T\right)^2/T^2$
Thermal mixing	$\dot{m} c_p T_0 \log\left[\left(x + \tau(1-x)\right)/\tau^{1-x}\right]$	where $m = m_1 + m_2$, $x = m_1/m_2$, and $\tau = T_1/T_2$
Free expansion	$\dot{m} c_p T_0 \log\left[p_{\text{final}}/p_{\text{initial}}\right]$	
Mass mixing		
Mass diffusion		
Chemical reaction		
... Etc.!		

The table above gives expressions for lost work and entropy generation for some dissipative processes encountered in thermoacoustics. (Watch out for factors of two if you use the macroscopic column for time-averaged acoustic situations.) For example, if dc electrical power is dissipated by resistance, the dissipated electrical power is I^2R, and the lost work is T_0/T times the dissipated power. Microscopically, the entropy generation is given by the heat generation rate j^2/σ per unit volume, divided by the temperature at which the heat is generated. Integrating that entropy generation over the whole volume of a resistor, and multiplying by T_0 to convert from entropy generation to lost work, yields the macroscopic expression for lost work. As a second example, viscous flow down a pipe, if we are not concerned about microscopic details such as whether the flow is turbulent or laminar, we can compute the lost work with the macroscopic expression. If instead we are concerned with microscopic details, perhaps to understand the spatial distribution of dissipation within a channel of a stack, then we can use the microscopic expression. This list of entropy-generating processes

could be extended greatly—it's amazing how many mechanisms contribute to the increase of the entropy of the universe!

Imperfect heat transfer is one of the most important loss mechanisms in engines and refrigerators, so consider the $k(\nabla T)^2/T^2$ term in more detail. If $k = 0$ —perfect insulation— there is no entropy generation. In the other extreme, $k = \infty$, there is also no loss, because in that case ∇T is zero. Only the in-between case is lossy. Unfortunately, all real gases and materials have nonzero, finite thermal conductivity, so all are lossy! In standing-wave systems, the situation is severe, because we depend on such imperfect thermal contact to get useful thermodynamic behavior, with heat being transferred irreversibly across a thermal penetration depth, throughout the stack, every cycle of the wave. For this reason, standing-wave systems have sometimes been called "intrinsically irreversible" [43].

In our experience at Los Alamos, the important types of processes that are responsible for irreversibility in thermoacoustic engines and refrigerators are:

(1) Thermal relaxation occurs within the stack in any standing-wave system, because imperfect thermal contact characterized by $\mathrm{Im}[f_\kappa] \neq 0$ in the stack is necessary for nonzero power in standing-wave systems. In traveling-wave systems, those losses are in principle and in practice smaller, giving traveling-wave systems an inherent efficiency advantage over standing-wave systems.

(2) Viscous drag in stacks and regenerators is important in both standing- and traveling-wave systems. Some viscous loss is unavoidable, because for anything except liquid metals [44] the Prandtl number is of order one so the viscous penetration depth is of the same order as the thermal penetration depth.

(3) Ordinary conduction of heat in the x direction from hot to cold along stacks and regenerators is conceptually a very simple loss. However, it is unavoidable, especially in the wall of the pressure vessel.

(4) Thermal-relaxation loss and viscous loss occurs not only in stacks and regenerators but also on resonator walls and in heat exchangers.

(5) Serious thermal bottlenecks can occur elsewhere in heat exchangers, in the solid metal parts and in the fluids such as water flowing through them to carry heat to or from the system.

(6) When used, electroacoustic transducers contribute significantly to system loss, through electrical dissipation and sometimes through piston friction.

(7) Finally, there are things that we don't yet understand; our systems never perform as well as we think they should. And effects beyond the acoustic approximation add to the severity of many of the items in this list; for example, turbulence in resonators adds to the viscous losses there.

4.2. Exergy

Consider the system shown in Fig. 4.3, processing a mass flow $\dot{m}$ of fluid from one temperature and pressure to another temperature and pressure. Liquefaction of nitrogen or methane is typical of such a process. The system consumes work $\dot{W}$, and waste heat $\dot{Q}_0$ is rejected at temperature T_0. The first law of thermodynamics indicates that the sum of the powers

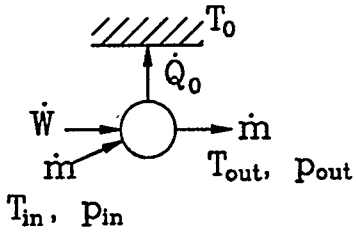

Figure 4.3: A thermodynamic device using work to process a flowing stream of material $\dot{m}$ from an input condition to an output condition. The device rejects waste heat at T_0.

going in must equal the sum of the powers going out:

$$\dot{W} + \dot{m}h_{\text{in}} = \dot{Q}_0 + \dot{m}h_{\text{out}}. \tag{4.14}$$

Note the use of enthalpy here; it is the correct energy to use in the first law for open systems, as discussed briefly in Chapter 3 and extensively in most thermodynamics texts [29]. The second law of thermodynamics indicates that the entropy leaving the system must equal the sum of the entropy entering the system plus entropy generation within the system:

$$\frac{\dot{Q}_0}{T_0} + \dot{m}s_{\text{out}} = \dot{m}s_{\text{in}} + T_0 \sum \dot{S}_{\text{gen}}. \tag{4.15}$$

The sources $\dot{S}_{\text{gen}}$ inside the system are viscous, frictional, and other dissipative processes as discussed in the previous section.

Combining these two equations by eliminating the uninteresting quantity $\dot{Q}_0$ yields

$$\dot{W} = \dot{m}\left[(h - T_0 s)_{\text{out}} - (h - T_0 s)_{\text{in}}\right] + T_0 \sum \dot{S}_{\text{gen}}. \tag{4.16}$$

This shows that $h - T_0 s$ is another important, special energy in thermodynamics problems. If the system is ideal—if there are no entropy-generating processes in the system, so $\Sigma \dot{S}_{\text{gen}} = 0$ —then the work needed to process unit mass of the fluid is given by the difference between the outgoing and incoming $h - T_0 s$. Any real system must use at least that much work to perform this process. Physicists note: This is *not* the Gibbs energy $h - Ts$. This energy per unit mass $b \equiv h - T_0 s$ is called the flow availability, well known to mechanical engineers and especially to chemical engineers. It is invaluable in evaluating the minimum work required to perform a complex process, such as that shown in Fig. 4.1b.

We can follow a similar philosophy [29] to derive an acoustic approximation to the Guoy–Stodola theorem, and to introduce the important concept of exergy X, an important energy that keeps track of the ability to do useful work when a thermal reservoir at temperature T_0 is freely accessible. Consider the schematic of a generalized portion of thermoacoustic system shown in Fig. 4.4. If the portion shown is in steady-state operation, the first law of thermodynamics shows that the difference between energy fluxes going out and going in must be zero:

$$0 = \dot{H}_{2\text{Out}} + \dot{W} - \dot{H}_{2\text{In}} - \dot{Q}_0 - \sum_i \dot{Q}_i. \tag{4.17}$$

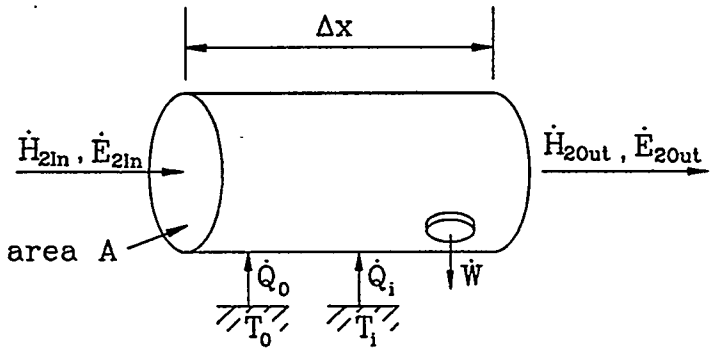

Figure 4.4: A generalized portion of thermoacoustic apparatus. The x direction is horizontal, and the portion, with length Δx, has acoustic power $\dot{E}_{2In}$ and total power $\dot{H}_{2In}$ flowing into the left open end and acoustic power $\dot{E}_{2Out}$ and total power $\dot{H}_{2Out}$ flowing out of the right open end. In between, the portion produces (or receives) time-averaged work power $\dot{W}$, absorbs (or rejects) heat power $\dot{Q}_0$ to ambient at T_0, and absorbs (or rejects) one or more other heat powers $\dot{Q}_i$ to other temperature(s) T_i. The sign conventions are indicated by the arrows.

The second law of thermodynamics says that the difference between the entropy fluxes going out and going in must equal the entropy generated within the portion:

$$\dot{S}_{\rm gen} = \frac{\dot{H}_{2\rm Out} - \dot{E}_{2\rm Out}}{T_{m\rm Out}} - \frac{\dot{H}_{2\rm In} - \dot{E}_{2\rm In}}{T_{m\rm In}} - \frac{\dot{Q}_0}{T_0} - \sum_i \frac{\dot{Q}_i}{T_i}. \tag{4.18}$$

In Eq. (4.18), we use $(\dot{H}_2 - \dot{E}_2)/T_m$ as the second-order entropy flux, as shown in Eq. (3.26) where the first term is T_m times the second-order hydrodynamic entropy flux and the second term is the conduction of heat along x through the gas and solid parts. Combining Eqs. (4.17) and (4.18) by eliminating the uninteresting heat $\dot{Q}_0$ easily yields

$$\begin{aligned} T_0\dot{S}_{\rm gen} \;=\; & \frac{T_0}{T_{m\rm In}}\dot{E}_{2\rm In} + \left(1 - \frac{T_0}{T_{m\rm In}}\right)\dot{H}_{2\rm In} - \frac{T_0}{T_{m\rm Out}}\dot{E}_{2\rm Out} + \left(1 - \frac{T_0}{T_{m\rm Out}}\right)\dot{H}_{2\rm Out} \\ & -\dot{W} + \sum_i \dot{Q}_i\left(1 - \frac{T_0}{T_i}\right). \end{aligned} \tag{4.19}$$

This is written in terms of exergy as

$$T_0\dot{S}_{\rm gen} = \dot{X}_{2\rm In} - \dot{X}_{2\rm Out} - \dot{X}_W + \sum_i \dot{X}_{Q_i}, \tag{4.20}$$

where the acoustic approximation to the time-averaged exergy flux $\dot{X}_2(x)$ in the x direction in a channel is

$$\dot{X}_2 = \frac{T_0}{T_m}\dot{E}_2 + \left(1 - \frac{T_0}{T_m}\right)\dot{H}_2. \tag{4.21}$$

Similarly, the exergy flux $\dot{X}_W$ associated with work power is the work power $\dot{W}$ itself,

$$\dot{X}_W = \dot{W}, \tag{4.22}$$

and the exergy flux $\dot{X}_Q$ associated with a heat power $\dot{Q}$ flowing from temperature T is

$$\dot{X}_Q = \dot{Q}(1 - T_0/T). \tag{4.23}$$

Each of these three expressions for exergy flux gives the ability of the associated power to do work, in the presence of a thermal reservoir at T_0. If $\dot{S}_{\text{gen}} = 0$, these expressions prescribe how work power, heat power, and oscillatory thermohydrodynamic power could be freely interchanged within the bounds of the first and second laws of thermodynamics.

Reminiscent of the total-power equation discussed in Chapter 3, the acoustic-approximation exergy-flux equation (4.21) is like a kaleidoscope, giving many different views depending on how it is shaken. We will look at a few:

In a stack, regenerator, or thermal buffer column, laterally insulated and bounded so that no exergy can flow out perpendicular to x, we have a thermoacoustic approximation to the Guoy-Stodola theorem:

$$T_0 \frac{d\sum \dot{S}_{\text{gen}}}{dx} = -\frac{d\dot{X}_2}{dx}. \tag{4.24}$$

This equation expresses the combined first and second laws of thermodynamics in thermoacoustics, showing that

$$\frac{d\dot{X}_2}{dx} \leq 0 \tag{4.25}$$

always, just like $0 = d\dot{H}_2/dx$ expresses the first law in a stack, regenerator, or thermal buffer column. Exergy is conserved if and only if no entropy is generated.

If $T_m = T_0$, then Eq. (4.21) shows that $\dot{X}_2 = \dot{E}_2$. In words, acoustic power at T_0 represents the ability to do work, in the thermodynamic sense. Thus far in this book, we may have tacitly assumed that this is true, but we have not proven it until this point! In this simplest situation, lost work and entropy generation are related in the most straightforward manner,

$$-\frac{d\dot{X}_2}{dx} = T_0 \frac{d\sum \dot{S}_{\text{gen}}}{dx} = -\frac{d\dot{E}_2}{dx}. \tag{4.26}$$

Now suppose that $T_m \neq T_0$, and consider an ideal regenerator with $\dot{H}_2 = 0$. Then $\dot{X}_2 = \dot{E}_2 T_0/T_m$. Hence, acoustic power in a temporally isothermal space, such as a regenerator, at temperature $T_m < T_0$ has an ability to do work that is greater than $\dot{E}_2$ itself. (This may make acousticians uneasy, but it is true, because a limitless source of heat at temperature T_0 is presumed to be available. The first law shows that some such source of heat *must* be utilized if work is to be extracted from an ideal regenerator, in which $\dot{H}_2 = 0$.) Similarly, acoustic power in a temporally isothermal space at temperature $T_m > T_0$ represents a reduced ability to do work; the full $\dot{E}_2$ cannot be converted to $\dot{W}$ without adding exergy from another source, such as heat at temperature $T_m > T_0$.

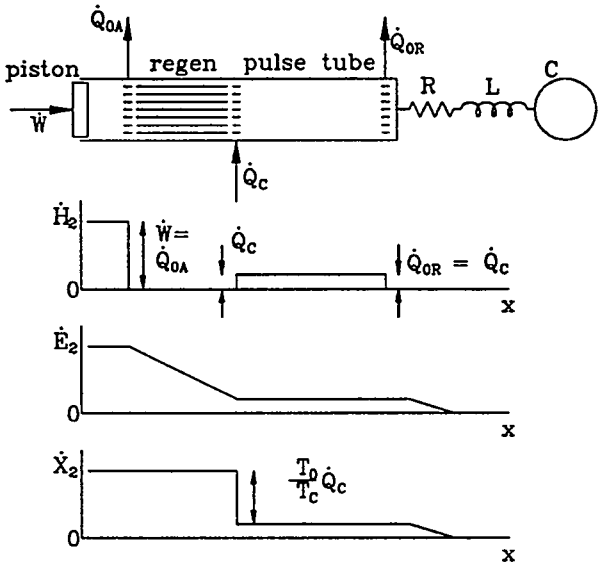

Figure 4.5: Schematic of an ideal orifice pulse tube refrigerator, showing the total power, acoustic power, and exergy flux as functions of position. The apparatus is insulated except at the heat exchangers, so the piston work $\dot{W}$, aftercooler heat $\dot{Q}_{0A}$, refrigeration load $\dot{Q}_C$, and final waste heat $\dot{Q}_{0R}$ are the only energies entering or leaving the apparatus.

Continuing to suppose that $T_m \neq T_0$, consider an ideal thermal buffer column or pulse tube, for which $\dot{E}_2 = \dot{H}_2$. Then $\dot{X}_2 = \dot{E}_2$, independent of T_m. In this case, Eq. (4.26) holds, with $d\dot{E}_2/dx = 0$ only if $\dot{S}_{\text{gen}} = 0$. Again, $\dot{E}_2$ represents the ability to do work.

These points are illustrated in Fig. 4.5 for an ideal orifice pulse-tube refrigerator, assumed to be thermally insulated except at the three heat exchangers. The total power must be piecewise constant, with discontinuities at the heat exchangers equal to the heats transferred there. The acoustic power must be continuous, decreasing through the regenerator not because of viscosity but rather because U_1 decreases as T_m decreases, and decreasing again in the flow resistance R due to viscosity. The exergy flux is constant throughout the regenerator. It decreases at the cold heat exchanger by $\dot{Q}_C(1-T_0/T_C)$, which is the amount of exergy carried out of the system by the heat load $\dot{Q}_C$. It is constant again along the pulse tube, finally dropping to zero smoothly in the flow resistance R, which is the only location with nonzero $\dot{S}_{\text{gen}}$.

Using Eq. (4.21) to write an explicit expression for $d\dot{X}_2/dx$ in a stack, regenerator, or thermal buffer column, in which $d\dot{H}_2/dx = 0$, yields

$$\frac{d\dot{X}_2}{dx} = \frac{T_0}{T_m}\left[\frac{d\dot{E}_2}{dx} + \left(\dot{H}_2 - \dot{E}_2\right)\frac{1}{T_m}\frac{dT_m}{dx}\right]. \tag{4.27}$$

In the inviscid limit, $\mu = 0$, and using appropriate expressions from Chapters 2 and 3, Eq.

(4.27) becomes

$$\frac{d\dot{X}_2}{dx} = -\frac{1}{2r_\kappa}|p_1|^2\left[1+2\frac{dT_m/dx}{\nabla T_{\text{crit}}}\sin\phi_{pU}+\left(\frac{dT_m/dx}{\nabla T_{\text{crit}}}\right)^2\right] -(Ak+A_{\text{solid}}k_{\text{solid}})\frac{(dT_m/dx)^2}{T_m} \tag{4.28}$$

which is always ≤ 0, for any values of dT_m/dx and ϕ_{pU}, as expected. The angle ϕ_{pU} is the phase difference by which p_1 leads U_1. The interpretation of the second term (i.e., second line) of Eq. (4.28) is trivial based on our discussion of heat-transfer irreversibility in the previous section. The first term (i.e., first line) is more interesting. It can be reduced to zero by making $r_\kappa = \infty$, as is approximately the case for traveling-wave systems. However, the intrinsic irreversibility of standing-wave systems is apparent here, as $1/r_\kappa \propto \text{Im}[-f_\kappa]$ must be nonnegligible for standing-wave systems; otherwise they develop no power, as shown by the discussion near Eq. (3.27). In this case, the only way to make the first term in Eq. (4.28) zero is by setting $\sin\phi_{pU} = 1$ (i.e., pure standing waves) and $dT_m/dx = \nabla T_{\text{crit}}$, exactly the situation for which standing-wave systems have zero power.

Thus far I have been unable to grind through the algebra to find a pretty version of $d\dot{X}_2/dx$ for $\mu \neq 0$. I had hoped it would depend cleanly on r_κ, r_ν, and $(dT_m/dx)/\nabla T_{\text{crit}}$, because the only sources of irreversibility are viscous shear, imperfect thermal contact, and the trivial term arising from ordinary conduction of heat along x.

4.3. Examples

Example: orifice pulse-tube refrigerator: The orifice pulse-tube refrigerator of Figs. 1.15 and 1.16 provides a realistic example similar to the ideal orifice pulse-tube refrigerator considered above. The flows of exergy, acoustic power, and total power are shown in Fig. 4.6, for the same operating point as that used to generate the power plots in Fig. 3.8 and the phasors in Fig. 2.19. The exergy curve was calculated using Eq. (4.21), using DeltaE's values for $\dot{H}_2$, $\dot{E}_2$, and T_m. Incoming from the left, the acoustic power, total power, and exergy flux are all nearly equal at 8.8 kW in the large-diameter entrance duct. The ambient-temperature aftercooler removes 8.3 kW of heat at T_0, which reduces the total power by that amount but has no effect on the exergy because heat at T_0 carries no ability to do work. There is a small reduction in acoustic power in the aftercooler, and the exergy decreases in step with this acoustic power, as required in a channel at temperature T_0. Next, in the regenerator the acoustic power drops considerably, but only part of this drop represents a loss in exergy (mostly due to viscosity); much of this decrease in acoustic power would occur even for $\mu = 0$, as a result of the mean temperature gradient. The exergy flux drops through the cold heat exchanger, but this represents no loss—only the flow of exergy out of the thermoacoustic part of the system and into the refrigeration load. Through the pulse tube, exergy decreases only a little, due largely to the heat leak down the walls of the pulse tube. At the end of the apparatus, exergy is destroyed in viscous flow in the orifice, although thermal insulation around the orifice, inertance, and compliance ensure that the energy associated with that exergy destruction shows up at the adjacent heat exchanger. Overall, the exergy losses in the orifice and in the regenerator are comparable, and are larger than

that in the aftercooler. The fact that almost half the exergy loss in this system occurs in the orifice motivated our research [45] into methods of feeding acoustic power from the hot end of the pulse tube back to the left of the heat exchange components instead of dissipating it in the orifice.

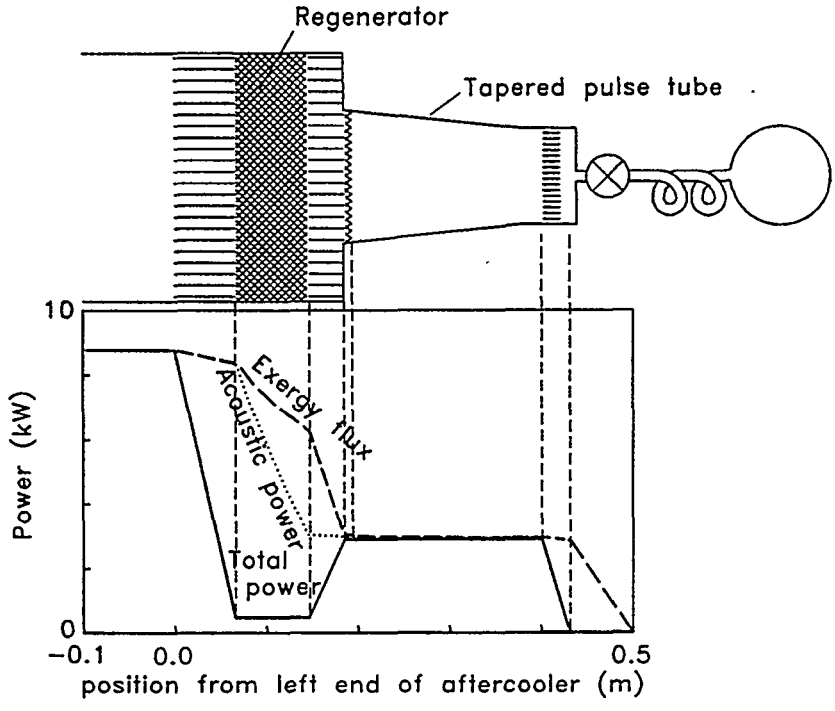

Figure 4.6: Schematic of Cryenco pulse-tube refrigerator, with lengths along x to scale, and diagram showing acoustic power, total power, and exergy flux at a representative operating point.

Example: standing-wave engine: The engine of Figs. 1.9 and 1.10 serves as an additional illustration of the use of exergy. In Fig. 4.7, we have added an exergy curve calculated using Eq. (4.21) to the energy plot of Fig. 3.7. At the hot heat exchanger, 2380 W of heat was added, causing 2380 W of total power to flow down the stack. This heat, at a temperature of 760 K, carried only 1440 W of exergy into the system. Some 720 W of this exergy is lost in the stack, due to viscosity, imperfect thermal contact, and conduction of heat along x, in the process of generating 670 W of acoustic power. A full 1000 W of exergy flows into the refrigerator at the side branch, in the form of 1000 W of acoustic power at T_0.

At another operating point for the standing-wave engine, one which received both experimental and calculational attention, a total of 3000 W of electric power was supplied to the heaters of the two engines, and 490 W of acoustic power was delivered to the pulse-tube refrigerator. The lost work is the difference between these: 2510 W. Although we didn't measure it, we would infer that 2510 W of heat was showing up in the room-temperature cooling-water streams at T_0.

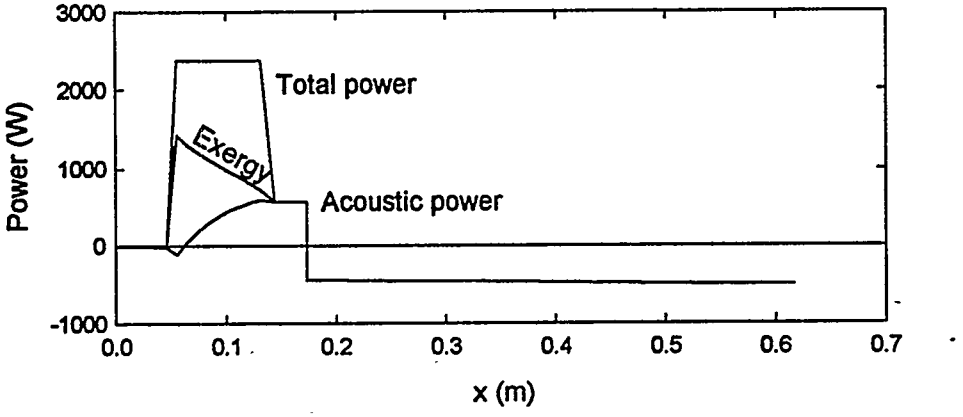

Figure 4.7: Powers for the standing-wave engine, at the same operating point as in Fig. 3.7, with an exergy curve added.

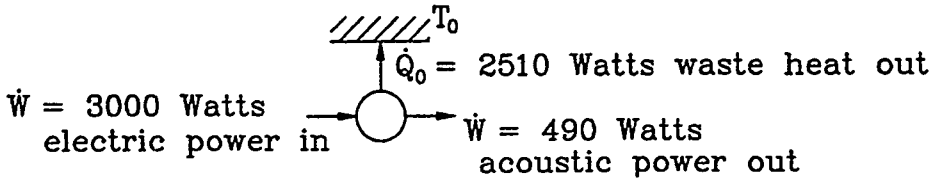

Figure 4.8: At one experimental operating point, the standing wave engine accepted 3000 W of input electrical power and rejected 2510 W of waste heat at T_0. Hence, 2510 W of work was lost.

To gain understanding of the sources of irreversibility in the system at this operating point, I made an arbitrary choice of how to break up this lost work: mostly by component, but with some subdividing according to process. Making intelligent estimates based partly on measurement and partly on a corresponding DeltaE model of this system generated this table.

Source	$\dot{W}_{\text{lost}}$
I^2R	730 W
room heat leak	300 W
hot heat exchgs acoustics	20 W
hot heat exchgs δT	10 W
stacks	950 W
stacks pressure vessel heat leak	150 W
cold heat exchgs acoustics	10 W
cold heat exchgs δT	70 W
resonator	35 W
unknown	235 W
Total:	2510 W

Such a table can serve as one guide when contemplating improvements to a thermoacoustic system, to help decide which components are responsible for losses, and maybe to help decide how to spend time and money most effectively to improve the overall system efficiency. In this case, consider the sources of lost work starting with the largest: The stacks contribute 950 W. I believe I optimized the gaps, lengths, and positions of these parallel-plate stacks well during the design of this system, so I doubt that rebuilding the stacks with different gaps or lengths would improve performance much. However, most of that 950 W is thermal-relaxation loss, not viscous losses. The thermal-relaxation loss is large in this system because of the size constraint imposed by the project's sponsor; if we were free to make the system bigger, we could operate closer to the critical temperature gradient and thus have a more efficient thermoacoustic engine. Hence, this table strongly suggests that we should re-negotiate the size constraint with the sponsor. We might consider trying to build a pin-array stack, because computer calculations usually show that a pin-array stack should perform about 20% better than a parallel-plate stack. However, building such an intricate pin array, with supports for the pins that don't block the sound wave badly, seems daunting (i.e. expensive). The second-largest loss in the table is the I^2R loss in the NiCr heaters in the two thermoacoustic engines. What does this mean, that 730 W is lost to I^2R, when 3000 W is converted from electricity to heat in the heaters? We're turning 3000 W of electrical power into 3000 W of heat at temperature T_H. The formula in the previous table shows that the lost work in that process is I^2RT_0/T_H. "Work is lost" in this process because the first and second laws allow for a more efficient way to deliver 3000 W of heat to T_H, in principle: This 3000 W of heat could be delivered to the engine at $T_H = 1230$ Kelvin by spending only 2270 W of electric power, driving a heat pump with Carnot's COP operating between T_0 and T_H. The difference, 3000 W − 2270 W, is the lost work. Reducing lost work from this source also sounds expensive. The next largest sources seem more promising. Heat leak from T_H to the room contributes 300 W, which might be reduced simply by more insulation, if the sponsor's size constraint is not compromised. Unknown sources contribute 235 W, which might serve as justification for asking the sponsor for more funds for funda-

mental research in thermoacoustics. The heat leaks along the two pressure vessels enclosing the two stacks contribute 150 W, which suggests that we might look for a reasonable-cost alloy with greater strength or lower thermal conductivity than the Incolloy 800H used here.

4.4. Exercises

4.1 A simple heat engine operates between temperatures T_H and T_0. Its work output is used to drive a simple refrigerator, which pumps heat from a load at temperature T_C ; it rejects waste heat at temperature T_0. The efficiency of this composite system is the ratio of heat pumped from T_C to heat consumed from T_H. What is the limit on efficiency imposed by the first and second laws of thermodynamics?

4.2 An ideal gas, with temperature-independent specific heat c_p, flowing with mass flow rate $\dot{m}$, must be cooled from T_0 to T_C. In case 1, the cooling is provided by a Carnot refrigerator removing heat from T_C and rejecting waste heat to T_0. In case 2; the cooling power is provided by two Carnot refrigerators rejecting waste heat to T_0; the gas stream first encounters the first refrigerator, whose cold end is at $(T_0+T_C)/2$, and then encounters the second refrigerator, whose cold end is at T_C. Case 3 is similar to case 2, except that the colder refrigerator rejects its waste heat at $(T_0+T_C)/2$ and the first refrigerator must absorb that heat in addition to the heat from the gas stream. Calculate the work required in all three cases, and compare it to the minimum work given by Eq. (4.16). How might you design cooling hardware that would approach the minimum work more closely?

4.3 Demonstrate the Guoy–Stodola theorem for the system of Fig. 4.2d, by showing that the difference between the entropy increase of the reservoir at T_0 and the entropy decrease of the reservoir at T_C equals the lost work given by Eq. (4.6) divided by T_0.

4.4 Investigate $\rho \dot{s}_{\text{gen}}$ for the simplest thermal-penetration-depth problem, with $u_1 = 0$ and boundary-layer approximation. Make a plot of the time-average of the entropy generation per unit volume, as a function of distance from the wall. How does this plot compare with the plot of power dissipated per unit volume shown in Ani. Thermal? Does this make sense? Compare $\int \rho \dot{s}_{\text{gen}}\, dy$ with the results of exercise 4.8, to verify the Guoy-Stodola theorem in this context.

4.5 Pick one process, one component, or one process within one component of your favorite thermoacoustic system, and estimate (order of magnitude) the lost work. What fraction of the total lost work for the whole system does this represent?

4.6 In Chapter 3, we demonstrated the "intrinsic irreversibility" of standing-wave engines and refrigerators, even in the inviscid limit $\mu = 0$, by showing that both the useful eU_1 term and the harmful r_κ term in $d\dot{E}_2$ are proportional to $\text{Im}[f_\kappa]$. With $\mu = 0$ and ignoring thermal conduction along x, re-examine the question of intrinsic irreversibility from the point of view of the exergy flux $\dot{X}_2$, showing that within a stack (where $\dot{H}_2$ is independent of x) exergy is destroyed unless the temperature gradient equals ∇T_{crit}.

4.7 On a trans-Pacific airplane flight, you are surprised to see your rich uncle, a banker, whom you haven't seen in 10 years. He tells you that he is about to invest heavily in a natural-gas recovery project that will make him unimaginably wealthy.

The project involves a huge, high-pressure natural-gas reservoir under the Arctic Ocean. The gas will arrive at the floating platform on the ocean surface in a pipe, at a pressure of

100 bar and a temperature of zero degrees Centigrade, which is the temperature of the ocean. He says that the brilliant scientist he will be investing in has invented two special machines. One machine will use the gas pressure to drive a special turbine, to generate power from the 100 bar gas. As it does work on the turbine, the gas will expand to atmospheric pressure, and cool. He doesn't remember how much it will cool. The second machine will use some of the power from the turbine to further cool the gas and liquefy it. There will be power left over, to run the lights, water pumps, radios, computers, heaters, etc. for the workers on the platform. The liquefied gas will be carried in cryogenic tankers to Tokyo.

He is certain that the planned platform will require no external source of power, nor will it need to burn any of the gas. It will be completely powered by the expansion of the gas from 100 bar. He remembers that one or both of the two machines will have a large heat exchanger connected to the ocean water.

You remember that methane liquefies at 112 Kelvin at atmospheric pressure, and that the latent heat is approximately equal to the total heat that must be removed to cool gaseous methane from zero degrees Centigrade to 112 Kelvin. You assume that the gaseous methane, CH_4, can be treated as an ideal gas. You remember that changes in enthalpy of an ideal gas are given by $dh = c_p\,dT$, and that changes in entropy of an ideal gas are given by $ds = (c_p/T)\,dT - (1/\rho T)\,dp$.

Evaluate the feasibility of this scheme using the first and second laws of thermodynamics. Convince your uncle that the first and second laws of thermodynamics are applicable to this scheme, and that you can decide that his investment plan is unwise without understanding any of the details of the two machines.

4.8 Derive the boundary-layer expression for $d\dot{X}_2/dx$ in a stack. Express your answer using the same variables as in Eq. (4.28) plus r_ν and σ. Then assume standing-wave phasing to simplify your result, showing that it is ≤ 0.

4.9 Resolve this paradox: For an ideal gas, $\oint pu\,dt = \oint (p/\rho)\rho u\,dt = R\oint T\rho u\,dt$. In a perfect regenerator, T is independent of time, so it can be pulled outside the integral, leaving $RT\oint \rho u\,dt$. But $\oint \rho u\,dt = 0$ because there is no net time-averaged mass flux through a perfect regenerator. Hence, $\oint pu\,dt = 0$. So acoustic power cannot flow through a perfect regenerator. (If you get stuck, wait until Chapter 5.)

4.10 NASA probes to the outer planets require electric power generators that operate for a decade with extremely high reliability. Currently, this electricity is generated with the thermoelectric effect in a solid. The high-temperature heat is supplied to the thermoelectric component by radioactive decay of a plutonium isotope, and waste heat carried away from the thermoelectric component by a heat pipe and finally rejected by means of black-body radiation to space. The efficiency, i.e. the ratio of electric power to plutonium heat, is 7%.

Consider a thermoacoustic engine as an alternative to the thermoelectric component, perhaps with piezoelectric or electrodynamic transduction of acoustic to electric power. Your assignment: Decide whether this idea might be worth pursuing. Make some plausible assumptions, and make a few rough estimates using various approximate relations throughout the book, to see if a thermoacoustic system might have an efficiency greater than 7%, while maintaining extremely high reliability. If you decide this idea might be worth pursuing, write a letter to your friend the program manager at NASA, explaining why you think it's worth pursuing—try to convince her that her office should provide you with financial support to attempt a meaningful design. If you decide the idea is *not* worth pursuing, write a letter to

her explaining why she should reject any half-baked thermoacoustics proposals she receives.

4.11 A simple thermoacoustic refrigerator, with COP equal to 0.3 times Carnot's COP, lifts heat from 276 K and rejects waste heat at $T_0 = 300$ K. The refrigerator is used to cool a stream of 10 grams/sec of water from 300 K to 276 K; this cooling load is the only load on the refrigerator.

In addition to the obvious irreversibility within the thermoacoustic refrigerator, the heat transfer in the cold heat exchanger must be irreversible, because this heat exchanger is at 276 K but the water enters it at 300 K. (Assume water's heat capacity is 4.2 Joule/gm-K, independent of temperature.)

How much heat must be removed from the water stream? How much work power is used to run this refrigerator? Calculate the lost work in the refrigerator and the lost work in the irreversible heat transfer. Compare the appropriate sum/difference of these three numbers with the minimum work required to cool this stream, using Eq. (4.16). How much exergy is added to the water stream? (Comment on the sign of this exergy term, regarding the ability of the cold water stream to do work.)

To reduce the irreversibility in the heat exchanger, it is proposed to use two refrigerators instead of one; the first will operate at 288 K and remove half the heat load from the water stream and the second will operate at 276 K and remove the other half of the heat load from the water stream. (Hence, each refrigerator will have half the cooling power of the original refrigerator.) Assume that both refrigerators reject heat to 300 K, and both have $COP/COP_{\text{Carnot}} = 0.3$. What is the total work power required by this system? Tabulate the lost work in four locations: the two refrigerators, and the two cold heat exchangers.

Now suppose the colder of the two refrigerators rejects its waste heat at 288 K instead of 300 K, so that the warmer of the two refrigerators must pump this heat load in addition to the heat load due to the water stream. Again calculate the total work required, and tabulate the lost work in the four locations. Discuss some of this in terms of exergy; for example, where is exergy destroyed, where does it flow into and out of the apparatus, etc.

4.12 Show that heat exergy $Q(1 - T_0/T)$ indeed represents the maximum ability to do work, by considering a Carnot engine operating between T and T_0 when $T > T_0$.

4.13 A machine absorbs heat at a rate $\dot{Q}_C$ at temperature T_C. Show that a Carnot engine attached to this machine could produce work at a rate $\dot{W} = (T_0/T_C - 1)\dot{Q}_C$. Interpret this result in terms of the heat exergy associated with $\dot{Q}_C$.

5. BEYOND ROTT'S THERMOACOUSTICS

We have now completed our review of the well-established foundations of thermoacoustics, as based mostly on the work of Nikolaus Rott. In Chapter 2, as summarized in Fig. 2.14, we came to regard any thermoacoustic apparatus as a series of short channels (possibly with internal structure, such as in a stack), each of which can be analyzed using the momentum and continuity equations. This allows us to view a short length of arbitrary thermoacoustic component as a combination of only five impedance elements: series inertance, series viscous resistance, parallel compliance, parallel thermal-relaxation resistance, and the parallel current-controlled current source that appears when a nonzero temperature gradient exists along the channel. In this representation, each dynamical variable, such as pressure p, is assumed to have a sinusoidally oscillating part, with the amplitude and phase of the oscillation the only variables of interest. Once oscillating pressure and oscillating velocity are understood in this context, other oscillating variables such as temperature and density follow easily. The acoustic power $\dot{E}_2$, the second-order total power $\dot{H}_2$, the time-averaged heats $\dot{Q}$ transferred at heat exchangers, and the second-order exergy flux $\dot{X}_2$ can be calculated without controversy from these oscillating variables, when the first and second laws of thermodynamics are brought into consideration.

If an engine or refrigerator is built according to these principles, and no mistakes are made (see Chapter 8), it will work as designed—but only in the limit of low amplitudes. Figure 5.1 illustrates this typical behavior, showing data obtained during early debugging of the standing-wave engine of Figs. 1.9 and 1.10, using only one engine and no load on the resonator. Heater power, displayed on the horizontal axis, was applied, resulting in measured pressure oscillations and hot temperatures as shown by the circles. The lines are calculations using DeltaE, based on the acoustic approximation and hence consistent with the discussion in Chapters 2 and 3. At low power, measurements and calculations agree, but at the highest powers the measured and calculated temperatures differ by almost 200°C and the measured and calculated pressure amplitudes differ by almost 25%. Thermoacoustic engines and refrigerators with practical levels of power per unit volume and per unit mass must operate at high amplitudes such as these, where actual behavior deviates significantly from the acoustic approximation. In the early days of thermoacoustic research, we were impressed that the acoustic approximation came so close to the truth at high amplitudes, but our standards are higher now: We hope to understand such deviations quantitatively.

In this chapter, we will examine some of the gas-dynamics phenomena leading to high-amplitude deviations from the acoustic approximation. We know all the fundamental physics involved. Most of the relevant gas dynamics and thermodynamics are believed to be included in the general momentum, continuity, and energy equations

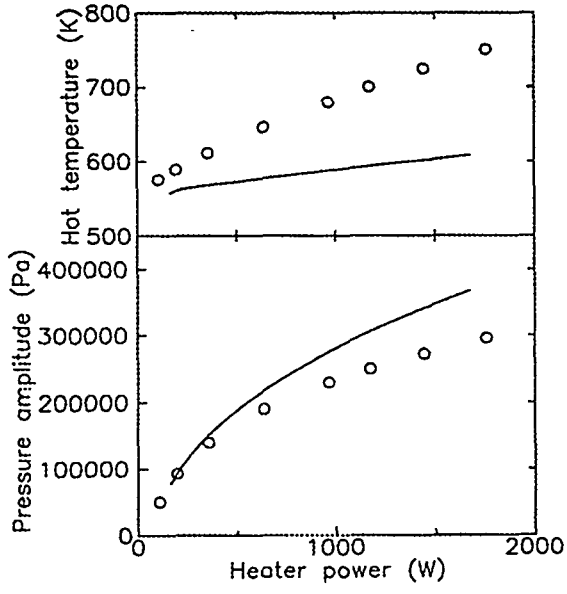

Figure 5.1: Pressure amplitude and hot temperature as functions of heater power, during early debugging of the standing-wave engine of Figs. 1.9 and 1.10, with the side branch to the refrigerators blocked, and using one spiral stack with its heat exchangers in one end of the resonator but no stack or hot heat exchanger in the other end of the resonator. Helium, 3 MPa, 370 Hz. The points are measurements; the lines are calculations using DeltaE, assuming laminar flow in the resonator.

$$\frac{\partial \rho}{\partial t} + \nabla \cdot (\rho \mathbf{v}) = 0, \tag{5.1}$$

$$\rho \left[\frac{\partial \mathbf{v}}{\partial t} + (\mathbf{v} \cdot \nabla) \mathbf{v} \right] = -\nabla p + \nabla_i \mu \nabla_j v_k + \nabla \zeta (\nabla \cdot \mathbf{v}), \tag{5.2}$$

$$\frac{\partial}{\partial t} \left(\frac{1}{2} \rho v^2 + \rho \varepsilon \right) = -\nabla \cdot \left[\frac{1}{2} \rho v^2 \mathbf{v} + \rho h \mathbf{v} - \mathbf{v} \cdot \Sigma - k \nabla T \right], \tag{5.3}$$

with appropriate boundary conditions, and in the properties of the gas

$$p = \rho R T, \tag{5.4}$$

$$\mu = \mu(p, T), \tag{5.5}$$

$$k = k(p, T), \tag{5.6}$$

$$\gamma = \text{constant}. \tag{5.7}$$

The time-averaged total power [26] flowing in the x direction

$$\dot{H} = \int \left[\overline{\rho u (v^2/2 + h)} - \overline{k \frac{dT}{dx}} - \overline{(\mathbf{v} \cdot \Sigma)_x} \right] dA \tag{5.8}$$

and the time-averaged exergy flux [29] in the x direction

$$\dot{X} = \int \left[\overline{\rho u [v^2/2 + (h - h_0)]} - T_0 \overline{\rho u (s - s_0)} - \overline{k \left(1 - \frac{T_0}{T} \right) \frac{dT}{dx}} - \overline{(\mathbf{v} \cdot \Sigma)_x} \right] dA, \tag{5.9}$$

where h_0 and s_0 are the enthalpy and entropy per unit mass in the so-called dead state [29], are also unambiguous. However, knowing that all the fundamental physics involved is captured in these deceptively simple equations is of little use in the day-to-day practice of high-amplitude thermoacoustics, because personal computers and human brains are incapable of processing such complicated equations and truths quickly. The challenge is to find the relevant aspects of the truths expressed in Eqs. (5.1)–(5.9) and to distill them into comprehensible, compact forms and into usable design procedures and analysis procedures. Our "acoustic approximation" of Chapters 2–4 is one such distillation, represented in the computer code DeltaE, but data like those displayed in Fig. 5.1 demonstrate that this approximation omits some important phenomena. Other computer codes include more physics and hence work better at high amplitudes, but sacrifice speed to do so.

While the first four chapters of the book are built on a well-established foundation, the topics discussed in this chapter are at the frontiers of current understanding. If this chapter seems inelegant or confused, it may be due to the fact that these issues are indeed complicated, and are not well understood. I will not be surprised if some of this chapter turns out to be wrong.

Our approach here will be to build upon and extend our acoustic approximation, adding (you might say kludging) various phenomena onto it. One strength of this approach is that it builds on a firm foundation. One danger of this approach is that it will never find dramatically new phenomena, no matter how interesting or important they might be.

This chapter is still under construction. I have not yet incorporated examples tied to the "example" hardware of Chapter 1. I have not done sections on porous media, harmonics, or similitude.

5.1. Tortuous porous media

In preparation. Screens [38], steel wool, sandstone?, power-law correlations.

5.2. Turbulence

Figure 5.2 is the well-known friction-factor diagram [27] for steady flow in a circular pipe. [Here "steady" means that U is independent of time, although $u(x, y, z, t)$ may fluctuate rapidly.] The figure summarizes all practical knowledge about pressure drops in such flows. Although Eq. (5.2) includes all the physics displayed in Fig. 5.2, Eq. (5.2) is too far removed from the engineering reality of turbulent steady flow to be useful in daily engineering work.

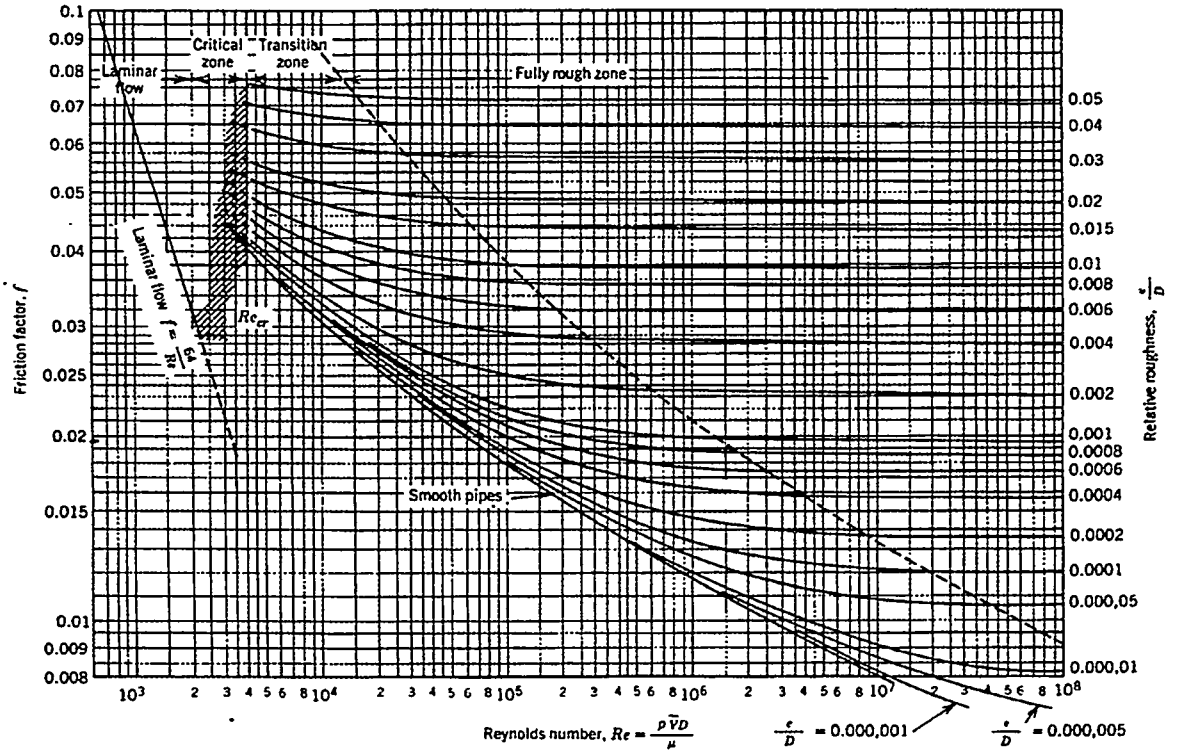

Figure 5.2: Friction factor vs Reynolds number in steady flow in a circular pipe. Reproduced from Fox and McDonald [27]. The different curves in the turbulent regime are for different surface roughnesses in the pipe. This figure (and everything else in Ref. [27]) uses Re to signify the Reynolds number on the horizontal axis, but we will use N_R to avoid confusion with the real part of a variable.

Note the use of dimensionless groups of variables in Fig. 5.2. Engineers have long realized that correlating data using such dimensionless groups provides the only practical, compact approach for sharing data. The Reynolds number $N_R = \rho \langle u \rangle D/\mu$ is a dimensionless measure of the average velocity, where D is the diameter of the pipe. The vertical axis is the dimensionless Moody friction factor f_M, which is the ratio of pressure drop Δp to

$\frac{1}{2}\rho\langle u\rangle^2 L/D$, where L is the pipe length. The dimensionless relative roughness ε is the roughness height on the pipe's inner surface divided by the pipe diameter. We will often use such dimensionless groups in this chapter, and in the last section we will outline a formal approach to the selection of dimensionless groups for thermoacoustic phenomena.

Figure 5.2 shows that steady flow in a *smooth* circular pipe has two regimes. Below $N_R \sim 2000$, the flow is laminar. In this regime, the second term on the left side of Eq. 5.2 can be neglected, and the equation is simple enough for analysis leading to a closed-form solution for the friction factor,

$$f_M = 64/N_R, \tag{5.10}$$

which is the straight line in the left part of Fig. 5.2. Above $N_R \sim 2000$ the flow is turbulent. Roughness $\varepsilon > 0$ gives higher friction factors in the turbulent regime.

For such steady flow in a circular pipe, two dimensionless parameters—N_R and ε—are sufficient to span the space of all possible flows, so the friction factor of *any* steady flow can be obtained from Fig. 5.2 by specifying these two parameters. In oscillating flow, however, one additional parameter is needed, which must be related to the frequency of oscillations. The viscous penetration depth is a familiar frequency-dependent variable, so R/δ_ν (where R is pipe radius) provides a convenient dimensionless form for this third parameter. [The Womersley number $D/\sqrt{2}\delta_\nu$ is also commonly used [46] for this third parameter.) One slice through the three-dimensional parameter space of oscillating flow is shown in Fig. 5.3 for a circular pipe; this slice is for $\varepsilon = 0$, and shows the regimes of behavior as a function of *peak* Reynolds number $N_{R,\text{peak}} = |U_1|\, D\rho/A\mu$ and R/δ_ν.

Figure 5.3 represents more complicated behavior than Fig. 5.2 represents. The laminar regime of Fig. 5.3 was the subject of chapter 2, and is well understood. We believe that the weakly turbulent regime shares the laminar regime's mathematically simple behavior in the boundary layers, with the turbulence essentially confined to the center of the tube, not in the boundary layers. A transitional zone exists between the weakly turbulent and conditionally turbulent regimes. In the conditionally turbulent regime, hot-wire anemometer measurements [48] show that the flow alternates between weakly turbulent and violently turbulent behavior, with the transition to turbulence occurring at the peak velocity and the return to weak turbulent flow occurring at the zero crossings of velocity. At higher Reynolds numbers, the flow is fully turbulent, essentially resembling the steady turbulent flow at high Reynolds number in Fig. 5.2. The mathematics we developed in Chapters 2 and 3 is probably inapplicable in the transitional, conditionally turbulent, and fully turbulent regimes, because in these regimes the turbulence disturbs the boundary layer deeply and violently.

At the high amplitudes necessary to achieve high power density, various components in thermoacoustic engines and refrigerators operate in all regimes shown in Fig. 5.3, and it is important to calculate peak Reynolds numbers at typical locations in each component to get a rough idea whether deviations from the acoustic approximation might be expected. Pulse tubes and thermal buffer tubes typically operate in the weakly turbulent regime. Resonator components are often fully turbulent, conditionally turbulent, or in the transition regime. Inertances in pulse-tube refrigerators are usually fully turbulent. For other components having non-circular cross sections but with parallel walls, we can only hope that Fig. 5.3 gives reasonable guidance, using $R \sim 2r_h$; with this criterion, we often find that standing-

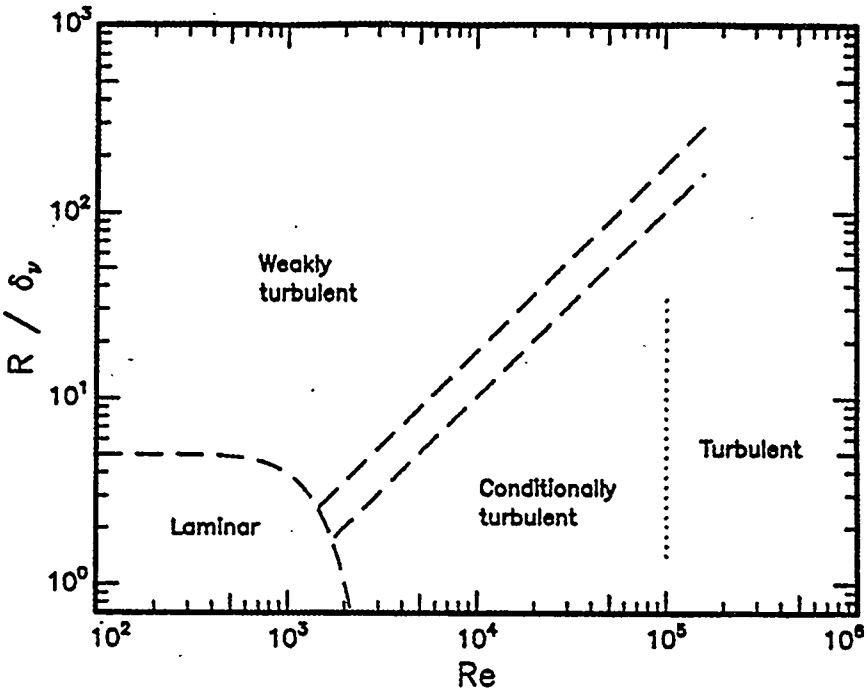

Figure 5.3: Regimes of oscillating flow, in a smooth circular pipe, as a function of peak Reynolds number Re (= $N_{R,\text{peak}}$ in text) and the ratio of pipe radius R to viscous penetration depth δ_ν. Adapted from [47].

wave stacks are in the high-Reynolds part of the laminar regime, sometimes with their cold ends extending into the conditionally turbulent regime, and heat exchangers may fall in any regime except fully turbulent. (As discussed in the previous section, the screen beds of regenerators typically have $r_h/\delta_\nu \ll 1$ and $N_{R,\text{peak}} \sim 500$, but Fig. 5.3 offers no guidance for the microscopically tortured geometry of screen beds.)

In Chapters 2 through 4, we learned how useful it is to have expressions for dp_1/dx, dU_1/dx, $d\dot{E}_2/dx$, and $\dot{H}_2$ everywhere. Reality today is not satisfactory in this regard. We're only certain of these expressions in the laminar regime in Fig. 5.3 (and even there entrance effects, to be discussed later this chapter, confuse the issue). We believe that the mathematical expressions developed in Chapter 2 are applicable in the distorted laminar regime, because we believe that the weak turbulence doesn't penetrate significantly into the boundary layer, and because we have some experimental evidence [49, 50] that laminar boundary-layer mathematics predicts phenomena accurately. Everywhere else in Fig. 5.3, our present understanding is too incomplete to give complete, quantitatively accurate predictions.

However, in the fully turbulent regime, Iguchi's hypothesis gives partial, quantitatively accurate guidance. In this regime, the displacement amplitude $|x_1|$ of the gas is much larger than both δ_ν and R, so Iguchi [47] suggested that the flow at any instant of time should have little memory of its past history: The flow at each instant of time should be identical to that of fully developed steady flow with that same velocity, represented by Fig. 5.2. This hypothesis must be excellent in the low frequency limit, in which $R/\delta_\nu \longrightarrow 0$, a limit that is approached in the inertances of many pulse-tube refrigerators. We do not know how good the assumption is for large R/δ_ν, which is of interest in many resonators.

To incorporate Iguchi's hypothesis into the impedance framework of Chapter 2, we can derive an expression for dp_1/dx, modified to account for the turbulence. If the volumetric velocity and hence Reynolds number N_R vary sinusoidally in time, then the instantaneous friction factor $f_M(t)$ obtained from Fig. 5.2 has a complicated time dependence. We can simplify this time dependence by using a Taylor-series expansion around the peak Reynolds number:

$$f_M(t) \simeq f_M + \frac{df_M}{dN_R} N_{R,\text{peak}} \left(\frac{|\text{Re}\,[U_1 e^{i\omega t}]|}{|U_1|} - 1 \right), \tag{5.11}$$

where f_M and the derivative on the right-hand side are evaluated at the peak Reynolds number. It is then straightforward to integrate the instantaneous power dissipation over a full cycle, obtaining for the time-averaged dissipation of acoustic power per unit length

$$\frac{d\dot{E}_2}{dx} = \frac{\rho |U_1|^3}{3\pi^3 R^5} \left[f_M - \left(1 - \frac{9\pi}{32} \right) N_{R,\text{peak}} \frac{df_M}{dN_R} \right], \tag{5.12}$$

where, again, f_M and df_M/dN_R are evaluated at the peak Reynolds number.

When this is compared to the equivalent result for laminar flow

$$\frac{d\dot{E}_2}{dx} = \frac{\rho |U_1|^2 \omega}{2\pi R^2} \text{Re} \left[\frac{i}{1 - f_\nu} \right], \tag{5.13}$$

it is apparent that turbulence multiplies the power dissipation and the effective viscous resistance per unit length, r_ν, by a factor m given by the ratio of the two expressions above:

$$m = \frac{\delta_\nu^2 N_R \left[f_M - (1 - 9\pi/32)\, N_{R,\text{peak}}\, df_M/dN_R \right]}{6\pi R^2 \qquad \text{Re}\left[i/(1 - f_\nu) \right]}. \tag{5.14}$$

We can evaluate f_M and df_M/dN_R as a function of N_R and ε directly from Fig. 5.2, or by using the iterative expression

$$\frac{1}{\sqrt{f_M}} = 1.74 - 2\log_{10}\left(2\varepsilon + \frac{18.7}{N_R\sqrt{f_M}} \right), \tag{5.15}$$

which is a remarkably good approximation to the friction factor [51].

At low enough velocities, $m \longrightarrow 1$ and the flow is laminar. According to Eq. (5.14), the $m = 1$ boundary between laminar and turbulent zones occurs roughly at

$$N_{R,\text{peak}} \simeq 2000 \text{ for } R/\delta_\nu < 2, \tag{5.16}$$

$$\frac{N_{R,\text{peak}}}{R/\delta_\nu} \simeq 1000 \text{ for } R/\delta_\nu > 2, \tag{5.17}$$

which is in general agreement with the transitions from laminar or weakly laminar to transitional or conditionally turbulent in Fig. 5.3.

Turbulence must also affect the other parts of the impedance picture of Chapter 2: the inertance per unit length l, the compliance per unit length c, the thermal-relaxation resistance r_κ, and the source/sink factor e. As turbulence increases r_ν, it probably changes the average velocity gradient at the wall, so the boundary-layer thickness probably changes, changing the effective area in the center of the duct that is available to carry the plug flow responsible for most of the inertance. Turbulence must also allow the influence of the isothermal boundary condition at the wall to reach farther into the gas, making more of the channel appear isothermal and hence increasing c. With more volume affected by thermal relaxation, r_κ probably decreases, and e may increase.

This analysis does not inspire confidence. Experimental confirmation exists only for r_ν [47], and only in a limited regime. Even in the fully turbulent regime, where Iguchi's hypothesis is most credible, we have no expression for $\dot{H}_2$ and only qualitative ideas of the corrections to inertance, compliance, and thermal-relaxation resistance. Experiments and more careful analysis are clearly needed to improve the situation. Accurate estimates or experiments are needed for $u_1(y)$ and $T_1(y)$ in and near the boundary layer.

5.2.1. Minor losses

In flow at high Reynolds number, additional pressure drops are associated with the transitions between channels, and with changes in direction of channels. These effects are known as "minor losses" because in long piping systems such transitions are indeed minor contributors to overall pressure drop. However, in thermoacoustic engines and refrigerators operating at high amplitudes, these so-called minor losses can be major, as in the traveling-wave engine of Figs. 1.13 and 1.14, where minor losses are severe in the tee and in the 180° and 90° bends.

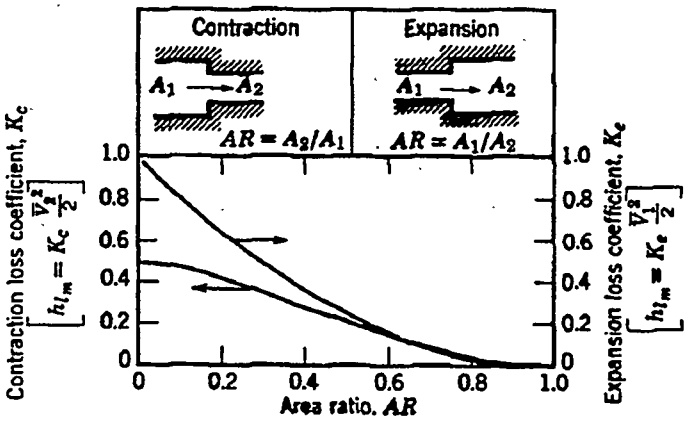

Figure 5.4: Typical chart giving minor loss coefficient K. Reproduced from Fox and McDonald [27].

For steady flow, the pressure drop arising from minor losses is characterized by the dimensionless minor-loss coefficient K,

$$\Delta p = K\frac{1}{2}\rho u^2 = K\frac{\rho U^2}{2A^2}, \tag{5.18}$$

with K tabulated for a wide variety of geometries [51, 52], as illustrated in Fig. 5.4. These losses arise from turbulence and other types of "secondary" flow, as illustrated in Figs. 5.5 and 5.6.

For flow of such high amplitude that the displacement amplitude $|x_1|$ is far larger than all other dimensions in the vicinity, Iguchi's hypothesis should be applicable: We can assume that Eq. (5.18) holds at each instance of time-dependent flow, so that

$$\Delta p(t) = \frac{K}{2A^2}\rho(t)\left[U(t)\right]^2. \tag{5.19}$$

Using sinusoidal velocity

$$U(t) = |U_1|\sin\omega t \tag{5.20}$$

and constant ρ, we can quickly calculate the fundamental Fourier component of $\Delta p(t)$,

$$|\Delta p_1| = \frac{4}{3\pi}\frac{K\rho_m}{A^2}|U_1|^2 \tag{5.21}$$

and the acoustic power dissipated by minor loss in the gas,

$$\Delta\dot{E}_2 = \overline{\Delta p(t)\,U(t)} = \frac{2}{3\pi}\frac{K\rho_m}{A^2}|U_1|^3. \tag{5.22}$$

Hence, in the impedance viewpoint of Chapter 2 we can assign a viscous flow resistance

$$R_v = \frac{4}{3\pi}\frac{K\rho_m}{A^2}|U_1| \tag{5.23}$$

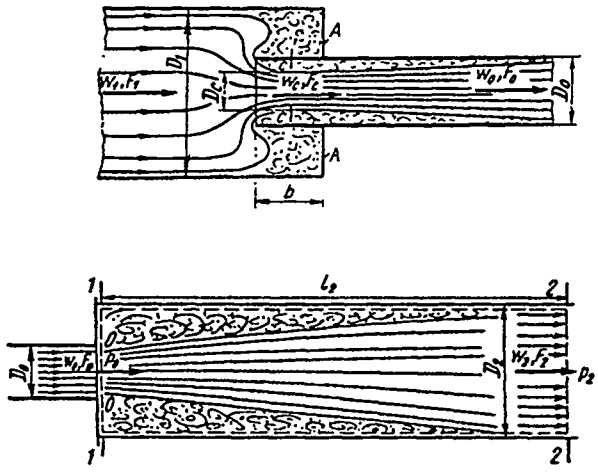

Figure 5.5: Illustrations of turbulent eddies at abrupt expansions and contractions. Reproduced from Idelchik [52].

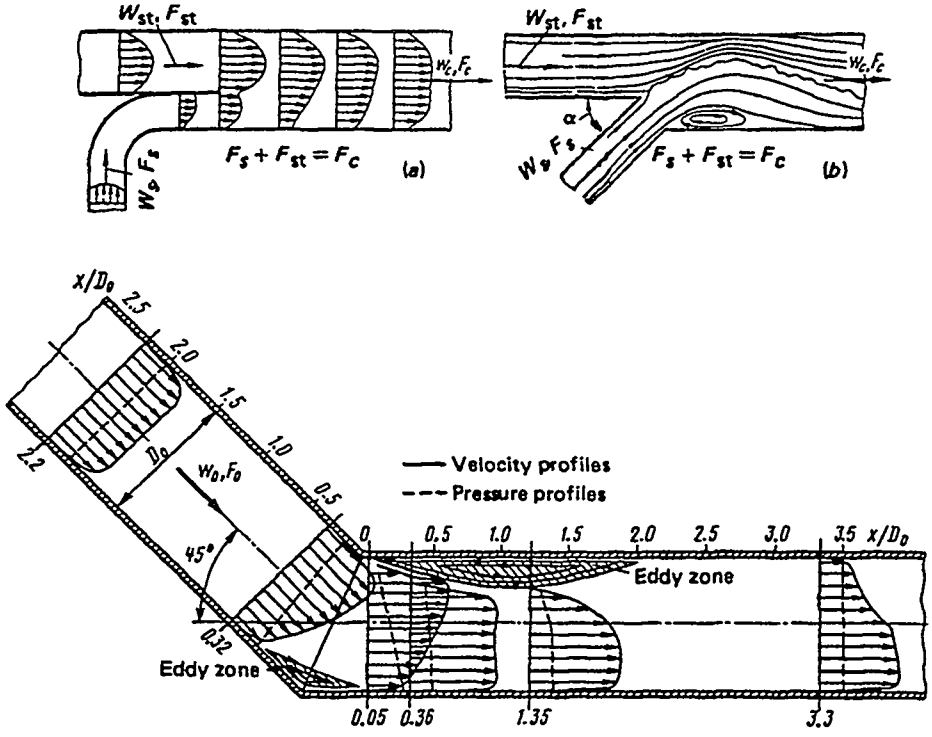

Figure 5.6: Illustrations of turbulent losses and dissipation at unions and in an elbow. Reproduced from Idelchik [52].

to each minor-loss location, if we can take K to be independent of velocity. In the DeltaE file for the traveling-wave engine included in the Appendix, many such minor-loss resistances are included, using Idelchik's extensive tabulations [52] of K.

This type of nonlinear flow, with an amplitude-dependent resistance, is also present in the orifice (typically an adjustable valve) of an orifice pulse-tube refrigerator. Handbooks give typical values for the dimensionless head-loss coefficient K for valves and fittings, but American valve manufacturers usually specify a valve's flow impedance by C_V. Although catalogs give values for C_V without units, it is not a dimensionless number: C_V is defined by the equation

$$\Delta p = \rho U^2 / C_V^2 \tag{5.24}$$

for steady flow, using gallons per minute, pounds per square inch, and gm/cm^3 for U, Δp, and ρ respectively, so C_V has units of

$$\frac{\text{gal}}{\text{min}} \sqrt{\frac{\text{gm/cm}^3}{\text{psi}}}, \tag{5.25}$$

which is a unit of area equal to 24×10^{-6} m^2. The use of C_V instead of K in valve catalogs eliminates ambiguity about whether the area A appearing in Eq. (5.18) is the inside diameter of the pipes entering the valve, the smallest cross section inside the valve itself, or the "nominal" pipe size of the valve. To convert between K, C_V, and R_ν for *steady* flow, use any of

$$K = \frac{2A^2}{\left[(24 \times 10^{-6}\,\text{m}^2) C_V\right]^2}, \tag{5.26}$$

$$R_\nu = \frac{\rho U}{\left[(24 \times 10^{-6}\,\text{m}^2) C_V\right]^2} = \frac{\sqrt{\rho\,\Delta p}}{\left[(24 \times 10^{-6}\,\text{m}^2) C_V\right]}, \tag{5.27}$$

$$R_\nu = \frac{K \rho U}{2A^2} = \sqrt{\frac{K \rho\,\Delta p}{2A^2}}; \tag{5.28}$$

for sinusoidal flow, use any of

$$K = \frac{2A^2}{\left[(24 \times 10^{-6}\,\text{m}^2) C_V\right]^2}, \tag{5.29}$$

$$R_\nu = \frac{8\rho_m |U_1|}{3\pi \left[(24 \times 10^{-6}\,\text{m}^2) C_V\right]^2} = \frac{\sqrt{8\rho_m\,|\Delta p_1|\,/3\pi}}{\left[(24 \times 10^{-6}\,\text{m}^2) C_V\right]}, \tag{5.30}$$

$$R_\nu = \frac{4K\rho_m |U_1|}{3\pi A^2} = \sqrt{\frac{4K\rho_m\,|\Delta p_1|}{3\pi A^2}}. \tag{5.31}$$

We hope that Eq. (5.23) and its variants incorporate the most important features of minor losses for thermoacoustics, but our understanding is very incomplete. When minor-loss locations are close together, such as the tee and elbow of Fig. 1.13, we do not know how their minor-loss phenomena interact, so we do not know what effective R_ν to assign. Sometimes we know that minor losses are large even when $|x_1|$ is small enough that Iguchi's

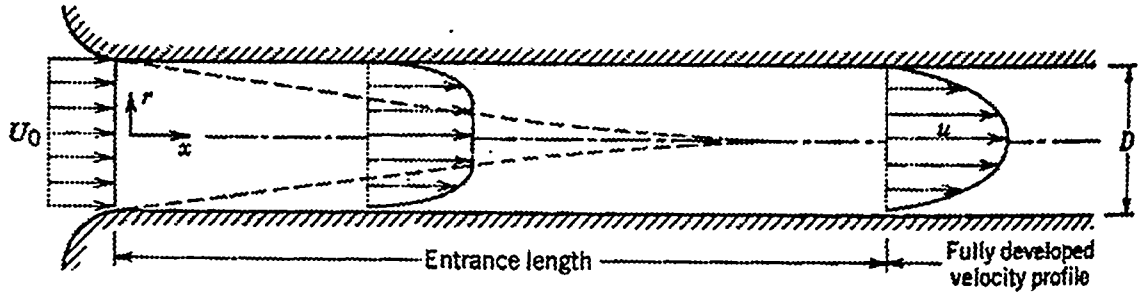

Figure 5.7: Illustration of entrance effects for steady laminar flow, from [27]. The flow has its "fully developed" parabolic profile only at distances greater than L_{entr} downstream of the entrance to the channel; at shorter distances, the flow retains memory of its condition upstream of the entrance.

hypothesis may not be applicable and hence Eq. (5.23) is questionable. We do not know whether to assign to each minor-loss location some correction for inertance, compliance, or thermal-relaxation resistance in addition to the correction to viscous resistance given by Eq. (5.23). When both $U(t)$ and $\Delta p(t)$ contain harmonics, Eq. (5.23) is much too simple.

5.3. Entrance effects and joining conditions

One of the unspoken assumptions of our acoustic approximation is that the gas displacement amplitude $|x_1|$ is much smaller than all other relevant dimensions in the x direction. This assumption is violated in thermoacoustic engines and refrigerators operating high amplitudes, where the displacement amplitude is typically comparable to the entire length of heat exchangers and may be one-tenth of the length of the stack.

5.3.1. Entrance effects

Figure 5.7 illustrates one aspect of this situation for steady flow. Flow enters a channel from wide open space to the left with a flat velocity profile. It takes time for viscosity to diffuse the influence of the zero-velocity boundary condition at the wall into the flow, and time is equivalent to distance along the flow. For laminar flow, the entrance length [27] is given by

$$L_{entr} \simeq 0.06\, N_R\, D. \tag{5.32}$$

To our knowledge, this phenomenon has not been carefully investigated for oscillating flow. However, a rough estimate is very illuminating. Let us assume that the entrance length for oscillating laminar flow is comparable to that for steady laminar flow. Then with

$$D = 4r_h, \tag{5.33}$$

$$N_{R,\mathrm{peak}} = \frac{\rho\,|u_1|\,D}{\mu} = \frac{8r_h\,|x_1|}{\delta_\nu^2}, \tag{5.34}$$

$$|x_1| = |U_1|/\omega A, \tag{5.35}$$

we have

$$L_{entr} \simeq 2\left(\frac{r_h}{\delta_\nu}\right)^2 |x_1|. \tag{5.36}$$

Hence, in a stack where typically $r_h \sim \delta_\nu$, the entrance length is of the order of the displacement amplitude. At the 10% pressure amplitudes typical of the standing-wave engine of Figs. 1.9 and 1.10, roughly 10% of the length of the stack may be affected. In this region, the assumptions underlying all the derivations of Chapter 2 and 3 are violated.

5.3.2. Joining conditions

Some thermoacoustic computation algorithms have used continuity of complex pressure amplitude p_1, complex volumetric velocity amplitude U_1, and mean gas temperature T_m as "joining conditions," i.e., boundary conditions to match solutions across the interface between two adjacent thermoacoustic components. For example, DeltaE [20] has used these joining conditions to pass from the end of one segment to the beginning of the next. There are many situations for which we already know that these traditional acoustic joining conditions may be inadequate. We saw above that continuity of p_1 is inappropriate if minor losses are important. Storch *et al.* [53] observed a distorted temperature profile near the ends of a pulse tube, as shown in Fig. 5.8, which we will attribute to an effective mismatch in T_m between the end of the pulse tube and the adjacent heat exchanger. Swift [54] observed a similar discontinuity in T_m between a hot heat exchanger and the adjacent duct in a standing-wave engine; the discontinuity in T_m was proportional to $|p_1|$. As a hypothetical example, consider two adjacent heat exchangers, with separation (along the direction of oscillatory gas motion) much less than the gas displacement amplitude, and each having plate spacing much smaller than the thermal penetration depth δ_κ. If the two heat exchangers are at equal temperatures, then U_1 is continuous across the interface between them. However, if the temperatures of the two heat exchangers differ by δT_m, continuity of first-order mass flux $\rho_m U_1$ (with ρ_m the mean gas density) more accurately describes flow across the interface. Hence, U_1 is discontinuous, with $\delta|U_1| \sim |U_1|\,\delta T_m/T_m$.

As an alternative to continuity of U_1, Rott [55, 14] proposed continuity of

$$\psi_1 = \frac{\omega}{i}\exp\left[-\int \frac{(f_\kappa - f_\nu)\,dT_m}{(1-\sigma)(1-f_\nu)T_m}\right] U_1. \tag{5.37}$$

The plausibility of ψ_1 as a joining variable is easily examined for some simple cases. For example, Eq. (5.37) becomes

$$\psi_1 = \frac{\omega}{i}\left[1 - \int \frac{f_\kappa\, dT_m}{T_m}\right] U_1 \tag{5.38}$$

for an inviscid ideal gas, if the integral is much smaller than unity. Then, in the adiabatic limit ($f_\kappa \longrightarrow 0$) of traditional acoustics, continuity of ψ_1 and of U_1 are identical, so the ψ_1

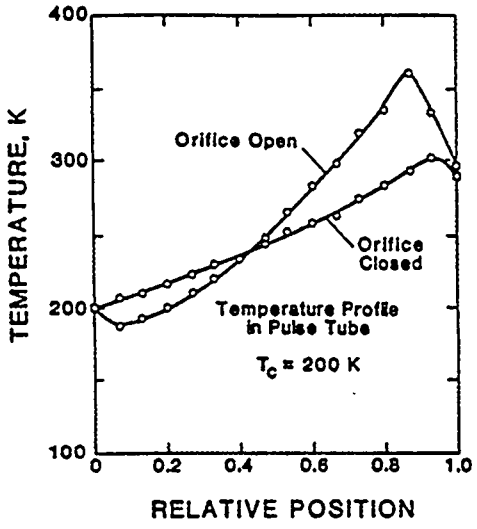

Figure 5.8: Temperature profile in the pulse tube of a pulse tube refrigerator, reproduced from Storch *et al.* [53]. Naively one might expect a smooth profile, without the overshoots at the ends, whose magnitude is of the order of the adiabatic temperature oscillation amplitude.

joining condition reduces to the traditional acoustic U_1 joining condition. In contrast, in the isothermal limit ($f_\kappa \longrightarrow 1$), Eq. (5.38) becomes

$$\psi_1 = \frac{\omega}{i}\left[1 + \frac{\delta\rho_m}{\rho_m}\right] U_1, \tag{5.39}$$

so that in this case continuity of ψ_1 and of first-order mass flux $\rho_m U_1$ are identical. As we argued in the preceding paragraph, this is the correct joining condition between two heat exchangers at different temperatures, with plate spacing $\ll \delta_\kappa$.

Although continuity of ψ_1 appears plausible in these two limiting situations, we do not believe that it is generally correct. To demonstrate this, we will derive joining conditions for the interface between an isothermal space ($f_\kappa = 1$, such as a good heat exchanger) and an adiabatic space ($f_\kappa = 0$, such as a pulse tube, thermal buffer tube, or resonator duct), as shown in Fig. 5.9. We seek expressions for the discontinuities to lowest order, hence we seek a first-order expression for δT_m and second-order expressions for δU_1 and δp_1. We will assume that flow in the adiabatic space is stratified, as it would be for a pulse tube or buffer tube with adequate flow straightening (see "Jet-driven streaming" below).

Mean temperature

Following Smith and Romm [56] (see also Kittel [57]), consider the interface, illustrated in Fig. 5.9, between an isothermal heat exchanger at temperature T_0 and an open space in which the gas is stratified (such an ideal pulse tube). Neglect viscosity, and let the frequency be low so that the acoustic wavelength is much larger than any other distance of interest. Suppose that pistons or other external means cause the mass flux (positive to the right) across the interface at $x = 0$ to be exactly $\omega M_a \sin\omega t$ and the pressure to be exactly $p_m + |p_1| \sin(\omega t - \theta)$. Assume that the gas displacement amplitude is much greater than δ_κ.

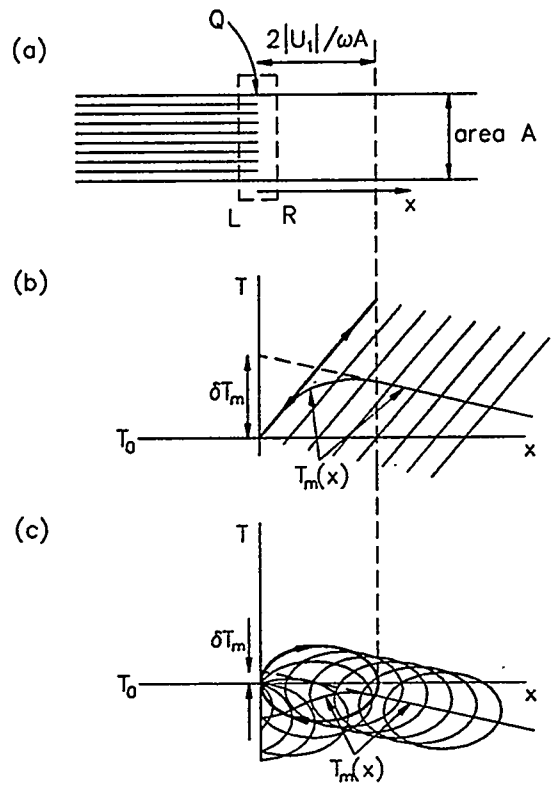

Figure 5.9: A guide to the discussion of joining conditions. (a) The geometry under consideration. The interface between an isothermal heat exchanger (left) and an adiabatic duct (right) of area A is at $x = 0$, with x increasing to the right. In the duct, the peak-to-peak gas displacement is $2|U_1|/\omega A$. Locations "L" and "R" are just to the left and right, respectively, of the interface. (b) For $\theta = 90°$, the gas motion is essentially that of a standing wave, with pressure and displacement in phase. The "particular" slice of gas has both $x(t)$ and $T(t) - T_0$ proportional to $1 - \cos\omega t$. The heavy line shows $T(t)$ vs $x(t)$ for this slice. Slices to the right of the "particular" slice have similar $T(t)$ vs $x(t)$ traces, shown as parallel lines. Slices to the left follow a portion of the "particular" slice's line while $x(t) > 0$, and have $T \equiv T_0$ while $x(t) < 0$. (c) For $\theta = 0$, the gas motion is essentially that of a traveling wave, with pressure and velocity in phase. The "particular" slice of gas has $x(t) \propto 1 - \cos\omega t$ and $T(t) - T_0 \propto \sin\omega t$. The heavy ellipse shows $T(t)$ vs $x(t)$ for this slice. Slices to the right of the "particular" slice follow similar $T(t)$ vs $x(t)$ ellipses; slices to the left follow truncated ellipses while $x(t) > 0$ and $T \equiv T_0$ while $x(t) < 0$. In both (b) and (c), the resulting Eulerian $T_m(x)$ is shown as the solid curve; extrapolating it from large x to $x = 0$ gives the effective discontinuity δT_m in mean temperature.

Because the gas in the open cylinder is stratified, we can (in principle) follow each differential slice of gas dM as it moves, considering its temperature, position, etc. as functions of time t. We begin by considering $T(t)$ for the slice of gas that is at $x = 0$ at $t = 0$. This particular slice touches the heat exchanger only at $t = 0$; slices to the right of it never touch the heat exchanger; slices to the left of it spend a nonzero fraction of their time inside the heat exchanger. At $t = 0$, this particular slice has temperature T_0, because at that moment it is in thermal contact with the heat exchanger. Thereafter, its temperature evolves adiabatically in response to the changing pressure:

$$T(t) = T_0 \left[\frac{p_m + |p_1| \sin(\omega t - \theta)}{p_m - |p_1| \sin\theta} \right]^{(\gamma-1)/\gamma}. \tag{5.40}$$

To first order in p_1, Eq. (5.40) becomes

$$T(t) = T_0 \left\{ 1 + \frac{\gamma - 1}{\gamma} \frac{|p_1|}{p_m} [\sin(\omega t - \theta) + \sin\theta] \right\}. \tag{5.41}$$

Meanwhile, the position of that slice of gas is

$$x(t) = \frac{M_a}{\rho_m A} (1 - \cos\omega t) = \frac{|U_1|}{\omega A} (1 - \cos\omega t) \tag{5.42}$$

to first order, where A is the cross-sectional area of the open space. The path $T(x)$ traced out by this particular slice of gas is shown as the heavy solid line with attached arrowheads in Figs. 5.9(b) and 5.9(c) for two choices of θ. Its average temperature is $T_0 + [(\gamma - 1)|p_1|/\gamma p_m] T_0 \sin\theta$, and its average location is $|U_1|/\omega A$.

Slices of gas to the right of the particular slice essentially share its oscillating motion and oscillating temperature, but with different average values. For $x > 2|U_1|/\omega A$, the slope of their average temperatures dT_m/dx is determined by phenomena outside the scope of this paper (such as heat conduction in the gas). Slices of gas to the left of the particular slice we have considered have complicated temperature histories, with constant temperatures for times when $x(t) < 0$, and temperatures evolving according to trigonometric functions of t (to first order) when $x(t) > 0$. The net effect of all such slices is to produce an average temperature profile $T_m(x)$, shown in Figs. 5.9(b) and 5.9(c), which is unremarkable for $x > 2|U_1|/\omega A$ but which is rather complicated for $0 < x < 2|U_1|/\omega A$. Experimental evidence of such complicated $T_m(x)$ in a pulse tube is shown in Fig. 5.8.

A suitable joining condition for T_m would allow convenient matching of the $x < 0$ and $x > 2|U_1|/\omega A$ solutions, each extrapolated to $x = 0$. Examination of Figs. 1(b) and 1(c) shows that this occurs if T_m is given a discontinuity δT_m at $x = 0$:

$$T_{m,R} - T_{m,L} = \delta T_m = T_m \frac{\gamma - 1}{\gamma} \frac{|p_1|}{p_m} \sin\theta - \frac{|U_1|}{\omega A} \frac{dT_m}{dx}. \tag{5.43}$$

The discontinuity is first order in the acoustic amplitudes, and it can have either sign. Equation (5.43) is in reasonable agreement with the measurements of Storch [53] (as far as I can tell) and Swift [54].

It turns out that Eq. (5.43) works whether the open cylinder is on the right [as in Fig. 1(a)] or on the left, as long as these conventions are followed: θ is the angle by which U_1 leads p_1, U_1 is positive in the $+x$ direction, and dT_m/dx is positive if T_m increases with x.

Oscillating volumetric velocity

To deduce a suitable joining condition for volumetric velocity, we must consider in more detail the slices to the left of the "particular" slice of the previous section. We label each such slice by t^*, the time at which it crosses $x = 0$ from right to left; thus $\pi \leq \omega t^* \leq 2\pi$ includes all slices, and the "particular" slice of the previous section has $\omega t^* = 2\pi$. Each slice crosses $x = 0$ from left to right at time t^{**} given by $\omega t^{**} = 2\pi - \omega t^*$. While each slice enjoys adiabatic conditions at $x > 0$, its pressure changes from $p_m + |p_1| \sin(2\pi - \omega t^* - \theta)$ to $p_m + |p_1| \sin(\omega t^* - \theta)$, a net pressure change of $2|p_1| \cos\theta \sin\omega t^*$. Hence, just before that slice enters the heat exchanger, its temperature is $T_0 \{1 + 2[(\gamma - 1)|p_1|/\gamma p_m] \cos\theta \sin\omega t^*\}$. As it enters the heat exchanger, returning to temperature T_0, its volume dM/ρ_m changes abruptly by $-2[(\gamma - 1)|p_1|/\gamma p_m] \cos\theta \sin\omega t^* \, dM/\rho_m$. The discontinuity in volumetric velocity is obtained by dividing by dt^*:

$$\begin{aligned} \delta U(t^*) &= 2\frac{\gamma - 1}{\gamma p_m}\frac{\omega M_a}{\rho_m}|p_1| \cos\theta \sin^2\omega t^*, \qquad \pi \leq \omega t^* \leq 2\pi \\ \delta U(t^*) &= 0, \qquad 0 \leq \omega t^* \leq \pi \end{aligned} \tag{5.44}$$

The fundamental Fourier component of this function of t^* is

$$\begin{aligned} \delta U(t) &\cong -\frac{8}{3\pi}\frac{(\gamma - 1)}{\gamma p_m}\frac{\omega M_a}{\rho_m}|p_1| \cos\theta \sin\omega t \\ &= -\frac{8}{3\pi}\frac{(\gamma - 1)}{\gamma p_m}|p_1|\,|U_1| \cos\theta \sin\omega t. \end{aligned} \tag{5.45}$$

Hence, the discontinuity of volumetric velocity contains a Fourier component at frequency ω; we may correctly refer to it as δU_1. This discontinuity is in phase with the volumetric velocity itself, so there is no discontinuity in the phase of U_1. The discontinuity in $|U_1|$ is

$$|U_1|_R - |U_1|_L = \delta|U_1| = -\frac{8}{3\pi}\frac{\gamma - 1}{\gamma}\frac{|p_1|\,|U_1|}{p_m}\cos\theta \tag{5.46}$$

$$= -\frac{16}{3\pi}\frac{\gamma - 1}{\gamma}\frac{\dot{E}_2}{p_m} \tag{5.47}$$

where $\dot{E}_2 = \frac{1}{2}|p_1|\,|U_1| \cos\theta$ is the acoustic power. This expression may be used whether the open cylinder is on the right or on the left, as long as $\dot{E}_2$ is taken to be positive when power flows in the $+x$ direction. Note that $\delta|U_1|$ is second order in the acoustic amplitudes, and it is zero for standing-wave phasing. Hence, it larger for pulse-tube and Stirling refrigerators than for low-amplitude standing-wave thermoacoustic engines and refrigerators.

The overall form of Eq. (5.46) is not surprising. In the geometry under consideration, there is a volume of order $|U_1|/\omega$ in the open cylinder, adjacent to the heat exchanger, that might naively be considered adiabatic; in fact, the gas occupying this volume behaves as near to isothermally as to adiabatically. Hence, its response to changing pressure must be corrected in rough proportion to the difference between the adiabatic and isothermal compressibilities:

$$\delta V \sim \frac{|U_1|}{\omega}|p_1|\left(\frac{1}{\gamma p_m} - \frac{1}{p_m}\right). \tag{5.48}$$

With multiplication by ω to convert from δV to $\delta |U_1|$, and by $\cos\theta$ to eliminate the effect for standing-wave phasing, we recover the form of Eq. (5.46).

Note that $\theta = 0$ and $dT_m/dx = 0$ makes $\delta T_m = 0$ in Eq. (5.43). In that case, examination of Eq. (5.37) or (5.38) shows that continuity of ψ_1 implies continuity of U_1, yet Eq. (5.45) or (5.46) shows a maximum (with respect to θ) discontinuity in $|U_1|$. Hence, the joining condition derived here is fundamentally different from continuity of ψ_1. We suspect these two joining conditions are applicable in different circumstances.

Oscillating pressure

Consistent with the previous section, we might expect a pressure discontinuity

$$\delta p \sim U_1 \, \delta U_1 \tag{5.49}$$

at the interface, due to the $(\mathbf{v} \cdot \nabla)\,\mathbf{v}$ term in the momentum equation. Since this pressure discontinuity would apparently be third order in the acoustic amplitude, we will neglect it.

Acoustic power dissipation and entropy generation

With spatially uniform oscillatory pressure, the discontinuity in volumetric velocity causes a third-order dissipation of acoustic power

$$\begin{aligned} \delta \dot{E}_2 &= \dot{E}_{2,L} - \dot{E}_{2,R} = \frac{1}{2\pi} \int_0^{2\pi} p(t)\, \delta |U_1| \sin\omega t \, d(\omega t) \\ &= \frac{4}{3\pi} \frac{\gamma - 1}{\gamma p_m} |p_1|^2 |U_1| \cos^2\theta. \end{aligned} \tag{5.50}$$

Naturally, this expression is never negative. It represents an inherent irreversibility at such an interface due to irreversible heat transfer in slices of gas approaching $x = 0$ from the right with temperatures different from T_0. This irreversibility was discussed by Smith and Romm [56] from the point of view of entropy generation. Combining our notation and their results, the interface dissipation per cycle $2\pi\, \delta \dot{E}_3/\omega = T_0 S_{gen}$, where S_{gen} is the entropy generation per cycle, obtained from the second law of thermodynamics

$$S_{gen} = \int S_R \, dM - \int S_L \, dM - \frac{1}{T_0} \int dQ \tag{5.51}$$

where S_R and S_L are the entropies per unit mass just right and left of the interface, and $dQ = c_p(T_R - T_L)\, dM$ is the heat absorbed by mass dM crossing the interface. Smith and Romm numerically integrated Eq. (5.51) for a monatomic ideal gas ($\gamma = 5/3$), without making the acoustic approximation, and they display a graph of their results as a function of θ and $|p_1|/p_m$. Our Eq. (5.50) is indistinguishable from their results at $|p_1|/p_m \sim 0.1$, and disagrees with their more accurate results by at most 10% at $|p_1|/p_m \sim 0.3$.

[An expression similar to Eq. (5.50), but with $\theta = 0$, was derived incorrectly by Swift [58]. The error in that derivation arises on page 4162, where the equation in the second line should be $\delta S = \delta Q\, \delta T/2T^2$. This error propagated through that analysis, to Eqs. (27) and (28), which should have been divided by two.]

Summary

This rather intricate derivation provides higher-order joining conditions between an isothermal channel and a stratified adiabatic channel. It lacks careful experimental confirmation, and it provides no guidance for higher-order joining conditions between other types of channels encountered throughout thermoacoustic engines and refrigerators.

5.4. Streaming

In acoustics, the term "streaming" refers to steady velocity that is superimposed on the larger oscillating acoustic velocity [59]. When streaming exists, it is useful to think of the motion of a parcel of gas during each cycle as something like 102 steps forward and 98 steps backward, equivalent to the superposition of a steady drift forward of 4 steps and an oscillating motion with a peak–to–peak amplitude of 100 steps. In thermoacoustic engines and refrigerators, streaming is important because it is a mechanism for convective heat transfer. Carrying heat, streaming can be either an undesirable loss mechanism or an essential heat-transfer method.

Pulse tubes and thermal buffer tubes are usually oriented vertically to avoid gravity-driven convection, which is one form of time-independent velocity superimposed on the oscillating velocity. In this section, we will consider four other undesirable steady flows, which can be called streaming because they are driven by the first-order acoustic phenomena. I will refer to the first two of these as Gedeon streaming and Olson streaming, because David Gedeon [60] and Jeff Olson [49] wrote clear papers on these subjects in the context of engines and refrigerators. Gedeon streaming is a time-averaged mass flux along x through a regenerator, pulse tube, etc. that accompanies $\dot{E}_2$. Olson streaming is a time-averaged toroidal circulation within a pulse tube or thermal buffer tube, driven by boundary-layer effects at the side walls. Jet-driven streaming is a third type, which is also a toroidal circulation within a pulse tube or buffer tube, but which is driven by inadequate flow straightening at an end of the tube. A fourth type, toroidal streaming within a regenerator or stack, presumably might also occur under some circumstances. These generally undesirable types of streaming are illustrated in Fig. 5.10.

On the other hand, we can deliberately use superimposed steady flow to advantage in some circumstances, to deliberately transfer heat. This steady flow can be either parallel or perpendicular to x, as illustrated in Fig. 5.11. The purpose of such flow is to carry heat, which is a second-order quantity in thermoacoustics, so we will think of these flows as second order, refer to them as streaming, and treat them in this section.

To discuss streaming, we extend the perturbation-series expansion of relevant variables one step beyond the acoustic approximation:

$$\xi(t) = \xi_m + \mathrm{Re}\left[\xi_1 e^{i\omega t}\right] + \xi_{2,0} + \mathrm{Re}\left[\xi_{2,2} e^{2i\omega t}\right]. \tag{5.52}$$

The subscript "2,0" identifies the streaming term, which is independent of time. (The second-order oscillating term, which oscillates at 2ω, is of no interest in this section, but will be considered in "Harmonics" below.) The second-order time-averaged mass flux density $\dot{m}_{2,0}(x,y,z)$ is of primary interest, because it convects a time-averaged heat flux density $\dot{m}_{2,0} c_p T$. As illustrated in Figs. 5.10 and 5.11, the second-order time-averaged mass flow

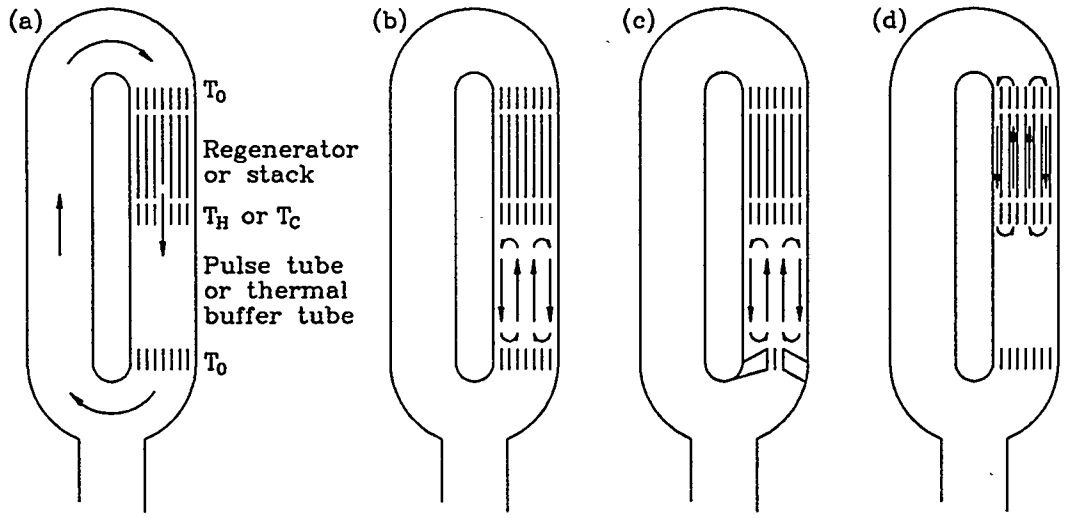

Figure 5.10: Illustration of some types of streaming, generally harmful to thermoacoustic engines and refrigerators. Arrows indicate the time-averaged velocity, which is superimposed on the much larger oscillating velocity discussed in Chapter 2. (a) Gedeon streaming. (b) Olson streaming. (c) Jet-driven streaming. (d) Streaming within a regenerator or stack.

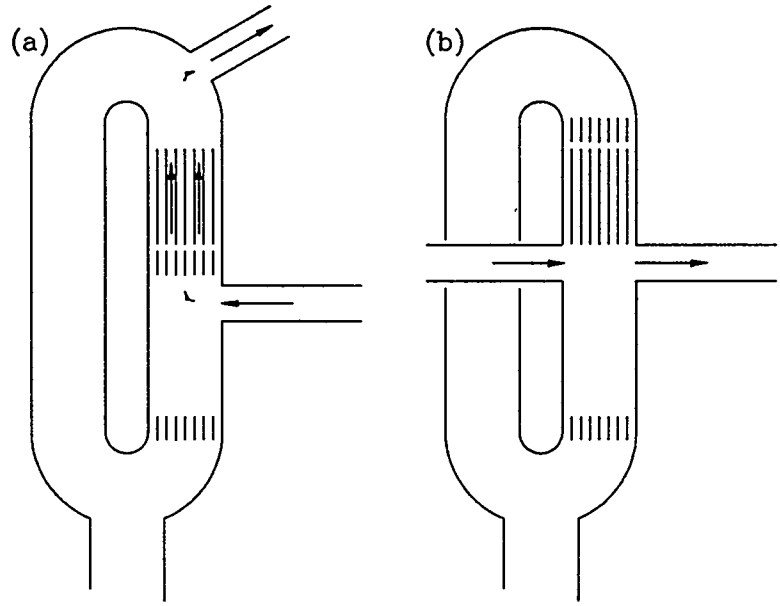

Figure 5.11: Illustration of streaming that might be beneficial. Note the elimination of a heat exchanger in each case. (a) Flow parallel to x, through a stack or regenerator. (b) Flow perpendicular to x, across one end of a stack or regenerator.

$\dot{M}_2 = \int \dot{m}_{2,0}\, dA$ in the x direction may be either zero or nonzero, depending on the circumstances. Gradients in the second-order time-averaged pressure $p_{2,0}$ are also important, and can be either large or small, depending on the impedance of the space through which $\dot{m}_{2,0}$ flows.

5.4.1. Gedeon streaming

It is important that the time-averaged mass flow $\dot{M}$ in the x direction through a regenerator, pulse tube, stack, etc. should be near zero, to prevent a large time-averaged convective heat flux $\dot{M}c_p(T_H - T_0)$ or $\dot{M}c_p(T_0 - T_C)$ from flowing from hot to cold. In a refrigerator, such a steady energy flux would add an unwanted thermal load to the cold heat exchanger; in an engine, it would wastefully remove high-temperature heat from the hot heat exchanger without creating acoustic power. This type of streaming is illustrated in Fig. 5.10a.

In a traditional orifice pulse-tube refrigerator such as shown in Fig. 1.16 or in something like the standing-wave engine shown in Fig. 1.10, $\dot{M}$ is exactly zero in steady state operation: Otherwise, mass would steadily accumulate (or deplete, depending on sign) in the dead-end components. This means that every time-averaged term in the perturbation expansion of $\dot{M}$ must be zero; in particular, $\dot{M}_2 = 0$ in Eq. (5.52). In terms of density and volumetric velocity,

$$\dot{M}_2 = \frac{1}{2}\mathrm{Re}\left[\rho_1 \widetilde{U_1}\right] + \rho_m U_{2,0}. \tag{5.53}$$

Hence, in a traditional orifice pulse-tube refrigerator or standing-wave thermoacoustic engine or refrigerator, the two terms on the right hand side *must* turn out to be equal and opposite. The two first-order factors ρ_1 and U_1 are "known" from the considerations of Chapter 2, so setting $\dot{M}_2 = 0$ in Eq. (5.53) determines what $U_{2,0}$ must be. The second-order time average of the momentum equation,

$$\omega\rho_1 \mathbf{v}_1 \text{ term } + \rho_m \mathbf{v}_1 \nabla \mathbf{v}_1 \text{ term } = -\frac{dp_{2,0}}{dx} + r_\nu U_{2,0} \tag{5.54}$$

must also be true, so a nonzero $dp_{2,0}/dx$ will generally also exist in a regenerator or stack whenever $\dot{M}_2 = 0$ through it. It is helpful to think of the $\Delta p_{2,0}$ that exists across the regenerator as causing the viscous flow of $U_{2,0}$ through the regenerator. In a traditional orifice pulse-tube refrigerator, this small time-averaged pressure difference appears automatically, because the topology imposes $\dot{M}_2 = 0$.

However, as shown in Fig. 5.10, any system with the topology of a torus, such as the traveling-wave engine of Fig. 1.14, can have $\dot{M}_2 \neq 0$ if the two terms on the right side of Eq. (5.53) are not in balance. To estimate how severe the time-averaged convective heat flux carried by such streaming might be in a cryogenic refrigerator if this requirement is ignored, Gedeon [60] showed that

$$\frac{1}{2}\,\mathrm{Re}\left[\rho_1 \widetilde{U_1}\right] = \rho_m \dot{E}_2 / p_m \tag{5.55}$$

in a regenerator, where $\dot{E}_2 = \frac{1}{2}\,\mathrm{Re}[p_1 \widetilde{U_1}]$ is the acoustic power passing through the regenerator. Hence, $\frac{1}{2}\,\mathrm{Re}[\rho_1 \widetilde{U_1}]$ *must* be nonzero in traveling-wave engines and refrigerators. Setting

Eq. (5.53) equal to zero shows that efficient regenerator operation requires

$$U_{2,0} = -\frac{1}{2}\,\mathrm{Re}\left[\rho_1 \widetilde{U_1}\right]/\rho_m = -\dot{E}_2/p_m. \tag{5.56}$$

The consequences of ignoring this requirement can be severe indeed. If $\dot{M}_2 > 0$, an undesired, streaming-induced heat load

$$\dot{Q}_{\mathrm{loss}} \sim \dot{M}_2 c_p \left(T_0 - T_C\right) \tag{5.57}$$

flows from ambient to cold through the regenerator. (If $\dot{M}_2 < 0$, such heat flows from hot to cold through the pulse tube, with equally harmful effect.) For $U_{2,0} = 0$, the ratio of $\dot{Q}_{\mathrm{loss}}$ to the ordinary regenerator loss $\dot{H}_{2,\mathrm{reg}}$ is of the order of

$$\frac{\dot{Q}_{\mathrm{loss}}}{\dot{H}_{2,\mathrm{reg}}} \sim \frac{\gamma}{\gamma-1}\frac{(T_0 - T_C)}{T_0}\frac{\dot{E}_2}{\dot{H}_{2,\mathrm{reg}}} \sim \frac{\gamma}{\gamma-1}\frac{(T_0 - T_C)}{T_C}\frac{\dot{Q}_{C,\mathrm{gross}}}{\dot{H}_{2,\mathrm{reg}}}, \tag{5.58}$$

where $\dot{Q}_{C,\mathrm{gross}}$ is the gross cooling power, equal to $\dot{E}_2$ in the cold heat exchanger [see Chapter 3]. In the final expression in Eq. (5.58), each of the three fractions is > 1 for cryocoolers; hence their product is $\gg 1$, and the unmitigated streaming-induced heat load would be much greater than the ordinary regenerator loss.

A toroidal topology, such as shown in Fig. 5.10a, ensures that the path integral of ∇p around the torus must be zero, in order that the pressure p at any location will be uniquely defined. At second order, this means that $\oint (dp_{2,0}/dx)\,dx = 0$ around the torus. Equation (5.54) shows what $\Delta p_{2,0}$ must exist across the regenerator to obtain the desired $U_{2,0}$ in the regenerator. Hence, we must design the other components of the loop so that their aggregate $\Delta p_{2,0}$ is equal and opposite to the $\Delta p_{2,0}$ desired across the regenerator.

The desired $\Delta p_{2,0}$ can be estimated using the low-Reynolds-number limit of Fig. 7-9 of Kays and London[39]

$$\frac{dp}{dx} \simeq -\frac{6U\mu}{A r_h^2} \tag{5.59}$$

for the pressure gradient in a screen bed of cross-sectional area A and hydraulic radius r_h, where U is the volumetric velocity and μ is the viscosity. (The numerical factor depends weakly on the volumetric porosity of the bed.) With Eq. (5.56) for U, this yields

$$\Delta p_{2,0} \simeq \frac{6}{A r_h^2 p_m}\int_{reg} \mu_m(x)\dot{E}_2(x)\,dx \tag{5.60}$$

for the pressure difference across the regenerator when $\dot{M}_2 \equiv 0$. (The x dependence of the viscosity is due to the temperature gradient.) For the apparatus of Figs. 1.14 and 1.16 and for other traveling-wave systems having p_m of tens of bar and $|p_1|/p_m \sim 0.1$, $\Delta p_{2,0}$ is typically of the order of a few hundred Pa.

In the limit of low viscosity or large tube diameters and in the absence of turbulence, $p_{2,0}$ would be described by some acoustic version of the Bernoulli equation. This suggests that an acoustically ideal path through the torus from one end of the regenerator to the other

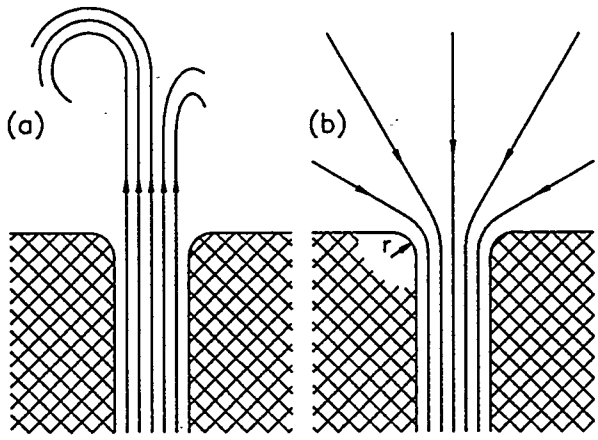

Figure 5.12: Asymmetry of high-Reynolds-number flow at a transistion between a small tube and wide-open space. (a) For outflow, a jet extends far into the open space, and downstream turbulence dissipates kinetic energy. (b) For inflow with a well-rounded entrance lip, there is little dissipation.

would impose across the regenerator a pressure difference of the order of $\Delta\left[\rho_m u_1 \widetilde{u_1}\right]$. (Such an ideal loop might include a pulse tube or thermal buffer tube, inertance or transmission line, and compliance, without heat exchangers or other components with small passages.) This pressure difference is typically much smaller than the $\Delta p_{2,0}$ given in Eq. (5.60) that is required for $\dot{M}_2 = 0$. Hence, to produce the required $\Delta p_{2,0}$, we need an additional physical effect or structure in the torus, relying on turbulence, viscosity, or some other physical phenomenon not included in the Bernoulli equation.

Asymmetry in hydrodynamic end effects can produce this required $\Delta p_{2,0}$. In a tapered transition between a small-diameter tube, where $|u_1|$ is large, and a large-diameter tube, where $|u_1|$ is small, turbulence would be avoided and Bernoulli's equation would hold if the taper were sufficiently gentle. At the opposite extreme, for an abrupt transition, we expect large $|u_1|$ to generate significant turbulence, and further we expect the oscillatory pressure drop across the transition to exhibit minor losses. Hence, the minor-loss coefficient K depends strongly on the direction of flow through the transition. In the example shown in Fig. 5.12, a small tube is connected to an essentially infinite open space. When the gas (at velocity u inside the tube) flows out of the tube, a jet occurs, and kinetic energy is lost to turbulence downstream of the jet; $K_{out} = 1$. In contrast, when gas flows into the tube, the streamlines in the open space are widely and smoothly dispersed; K_{in} varies from 0.5 to 0.04, with smaller values for larger radius r of rounding of the edge of the entrance. For such asymmetric transitions, we must allow K to have time dependence in Eq. (5.19), which becomes

$$\Delta p(t) = \frac{1}{2A^2} K(t) \rho(t) \left[U(t)\right]^2 . \tag{5.61}$$

If $U = |U_1| \sin \omega t$, we can calculate the time-averaged pressure drop by integrating Eq.

(5.61) in time:

$$\begin{aligned}\overline{\Delta p_{ml}} &= \frac{\omega}{2\pi A^2}\left(\int_0^{\pi/\omega} K_{out}\frac{1}{2}\rho\,|U_1|^2\sin^2\omega t\,dt - \int_{\pi/\omega}^{2\pi/\omega} K_{in}\frac{1}{2}\rho\,|U_1|^2\sin^2\omega t\,dt\right)\\ &= \frac{1}{8A^2}\rho\,|U_1|^2\,(K_{out}-K_{in})\,. \qquad (5.62)\end{aligned}$$

This is the source of $\Delta p_{2,0}$ that we will use. Such simple control of $\dot{M}_2$ is not without penalty, however; acoustic power is dissipated at a rate

$$\begin{aligned}\Delta\dot{E}_2 &= \frac{\omega}{2\pi}\int_0^{2\pi/\omega}\Delta p_{ml}\,U\,dt\\ &= \frac{\omega}{2\pi A^2}\left(\int_0^{\pi/\omega} K_{out}\frac{1}{2}\rho\,|U_1|^3\sin^3\omega t\,dt - \int_{\pi/\omega}^{2\pi/\omega} K_{in}\frac{1}{2}\rho\,|U_1|^3\sin^3\omega t\,dt\right)\\ &= \frac{1}{3\pi A^2}\rho\,|U_1|^2\,|U_1|\,(K_{out}+K_{in}) \qquad (5.63)\\ &= \frac{8}{3\pi}\overline{\Delta p_{ml}}\,|U_1|\,\frac{K_{out}+K_{in}}{K_{out}-K_{in}}, \qquad (5.64)\end{aligned}$$

where A is the area of the small tube. Equation (5.64) shows that the best way to produce a desired $\overline{\Delta p_{ml}}$ is to insert the device at a location where $|U_1|$ is small, and to shape it so that $K_{out}-K_{in}$ is as large as possible. Even though the acoustic power dissipation given in Eqs. (5.63) and (5.64) is formally of third order, it is large if u_1 is large enough to generate a substantial Δp_{ml}.

Our measurements at Los Alamos provide qualitative support of most of the features discussed here, but quantitative agreement between Eqs. (5.62) and (5.60) is poor. Once again, there is something important that we do not understand well.

5.4.2. Olson streaming

Ideally, the gas in a pulse tube or thermal buffer tube acts as a long (and slightly compressible) piston, transmitting pressure and velocity oscillations from one end to the other. The gas must also thermally insulate the ends of the tube from each other. Unfortunately, convective heat transfer *within* the tube can carry heat from one end to the other, adding a heat load to the cold heat exchanger in a refrigerator or consuming heat at the hot heat exchanger of an engine. If Gedeon streaming is eliminated, there can be no net mass flux $\dot{M}_2$ through the tube, but the possibility remains that mass flux density $\dot{m}_{2,0}(r)$ can stream upward near the side walls of the tube and downward in the central portion of the tube. Such streaming can be caused by jetting due to inadequate flow straightening at either end of the tube, as described in the next subsection, but here we review Olson streaming, which is convection confined within the tube and driven by viscous and thermal boundary-layer phenomena at the side walls of the tube, as illustrated in Fig. 5.10c. The boundary-layer calculation [49] of streaming in such a geometry, based on the earlier work of Rott [61] and incorporating variable cross-sectional area $A(x)=\pi[R(x)]^2$, yields a prediction for the

side-wall taper angle that suppresses streaming:

$$\tan\frac{\phi}{2} = \frac{\pi R^3\omega\,|p_1|}{2\gamma p_m\,|U_1|}\left[\left(1+\frac{2\,(\gamma-1)\,(1-b\sigma^2)}{3\sigma\,(1+\sigma)}\right)\cos\theta + \left(1+\frac{2\,(\gamma-1)\,(1-b)\,\sqrt{\sigma}}{3\,(1+\sigma)}\right)\sin\theta\right] + \frac{(1-b)\,(1-\sqrt{\sigma})}{6\,(1+\sigma)\,(1+\sqrt{\sigma})}\frac{R}{T_m}\frac{dT_m}{dx} \quad (5.65)$$

$$\simeq (7.4\cos\theta + 6.3\sin\theta)\frac{R^3 f\,|p_1|}{p_m\,|U_1|} + 0.0029\frac{R}{T_m}\frac{dT_m}{dx}. \quad (5.66)$$

In Eq. (5.66), f is frequency and numerical values for helium gas are used: $\gamma = 5/3$, $\sigma = 0.69$, and $b = (T/\mu)\,d\mu/dT = 0.68$.

When Eq. (5.65) or (5.66) is satisfied, a large number of side-wall boundary-layer effects are in delicate balance, with some trying to cause streaming up along the side walls and down through the center, while others try to cause streaming down along the side walls and up through the center. One such effect is easily imagined and is illustrated in Fig. 5.13c. Consider a small parcel of gas oscillating up and down along the wall, at a distance from the wall of the order of the relevant boundary layer: the viscous penetration depth δ_ν. On average, the gas between the parcel and wall will have a different temperature during the parcel's upward motion than during its downward motion, due to imperfect thermal contact with the wall's temperature gradient and due to the adiabatic temperature oscillations with time phasing between oscillatory motion and oscillatory pressure. The moving parcel will experience a different amount of viscous drag during its upward motion than during its downward motion because the viscosity depends on temperature, so it will undergo a different displacement during its upward motion than during its downward motion. After a full cycle, the parcel does not return to its starting point; it experiences a small net drift which contributes to $u_{2,0}$ at its location. This process is represented by terms proportional to the product of b, T_1, and u_1 in the nonlinear equations of the derivation, and is responsible for the presence of b in Eq. (5.65).

The effect of a taper on streaming can also be imagined, with reference to Fig. 5.13d. In general, a gas parcel close to the wall will be farther from the wall during, say, its upward motion than during its downward motion, due to, for example, the compressibility of the gas in the boundary layer and the phasing between oscillatory motion and pressure. Hence, again the moving parcel will experience a different amount of viscous drag during its upward motion than during its downward motion, and so the parcel will again fail to return to its starting point after a full cycle. This effect is represented in the starting equations of the derivation by terms proportional to the product of u_1 and v_1. However, the boundary-layer continuity equation couples v_1 and du_1/dx, while the y-averaged continuity equation $i\omega A\,\langle\rho_1\rangle + \rho_m d\,\langle Au_1\rangle\,/dx = 0$ couples du_1/dx to dA/dx. Hence, the process shown in Fig. 5.13d is controlled in part by the taper dA/dx, and is responsible for the presence of ϕ in Eq. (5.65).

Including all such second-order streaming effects in the calculations allow determination of the conditions under which they all add to zero, represented by Eq. (5.65). Note that all the variables in the right hand side of Eq. (5.65) or (5.66) should be known during the design of a pulse tube refrigerator and are experimentally accessible.

The effort necessary to obtain expressions for p or u at second order, describing streaming,

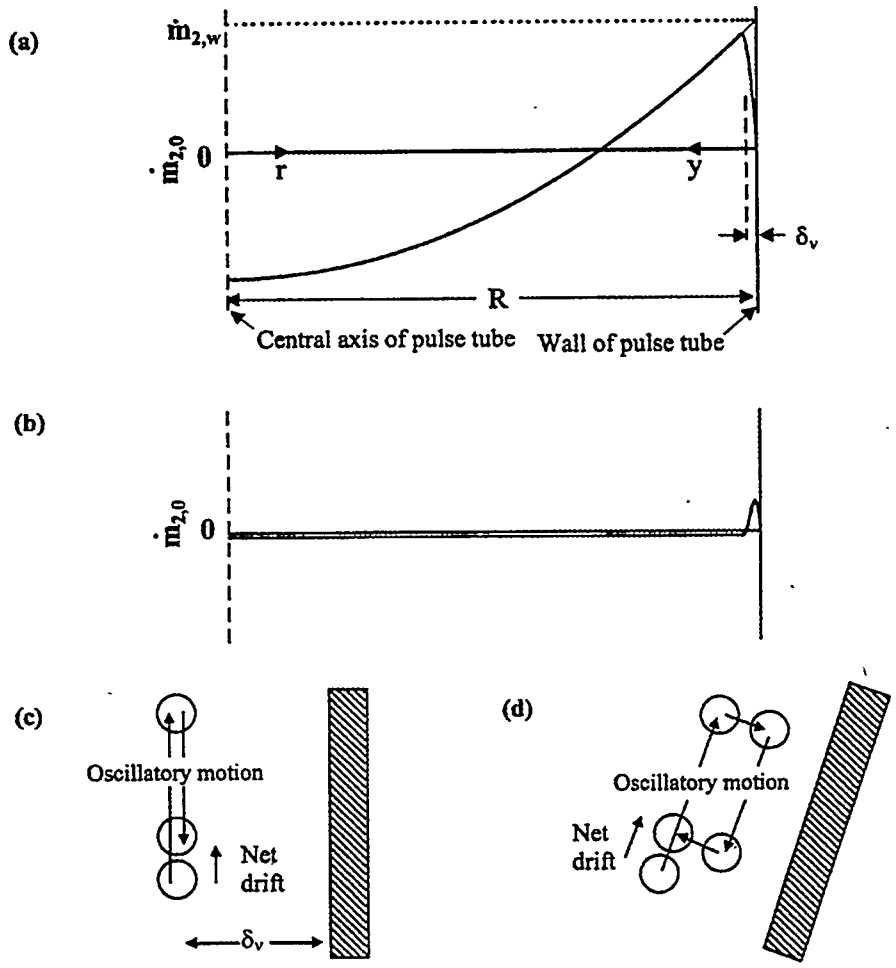

Figure 5.13: (a) The net drift near the wall, illustrated in (c) and (d), affects the entire tube, causing an offset parabolic velocity profile which contributes to a second-order mass flux density $\dot{m}_{2,0}(r)$. For the signs chosen here for illustration, the gas moving downward in the center of the tube is hotter than the gas moving upward around it, so that heat is carried downward. The coordinate r measures the distance from the center of the tube, of radius R. The calculations are for $R \gg \delta_\nu$, but, for clarity, δ_ν is exaggerated in the figure. (b) Mass flux density for the case where the streaming is suppressed by tapering the tube. Although there is still some streaming near the wall and a correspondingly small offset mass flux in the rest of the tube, they carry negligible heat. (c) Illustration of net drift caused by one process within δ_ν of the tube wall. A parcel of gas is shown in three consecutive positions. Here we imagine that the temperature dependence of the viscosity is the only important effect, and assume that the temperature is lower during upward motion than during downward motion. (d) Illustration of net drift caused by a different process, as discussed in the text.

is far greater than the effort of Chapter 2 to obtain first-order expressions for these variables. For example, Olson's calculation begins with the x component of the general momentum equation [26]

$$\rho\left[\frac{\partial u}{\partial t}+(\mathbf{v}\cdot\nabla)\,u\right]=-\frac{\partial p}{\partial x}+\frac{\partial}{\partial x}\left[\mu\left(\frac{4}{3}\frac{\partial u}{\partial x}+\frac{\partial v}{\partial y}\right)+\frac{\partial}{\partial y}\left(\frac{\partial u}{\partial y}+\frac{\partial v}{\partial x}\right)\right], \tag{5.67}$$

which becomes, to second order,

$$\begin{aligned}\frac{1}{2}\,\mathrm{Re}\left[-i\omega\rho_1\widetilde{u_1}+\rho_m\widetilde{u_1}\frac{\partial u_1}{\partial x}+\rho_m\widetilde{v_1}\frac{\partial u_1}{\partial y}\right]\\ =\ -\frac{dp_{2,0}}{dx}+\rho_m\frac{\partial^2 u_{2,0}}{\partial y^2}+\frac{1}{2}\,\mathrm{Re}\left[\frac{\partial}{\partial y}\left(\mu_1\frac{\partial\widetilde{u_1}}{\partial y}\right)\right].\end{aligned} \tag{5.68}$$

This is far more complicated than the first-order x component of the momentum equation, Eq. (2.54). In particular, to obtain correct answers at second order, viscosity must be kept inside the derivative on the right-hand side; this aspect of the present problem differs from most problems in acoustics and fluid dynamics.

The fact that Olson streaming in a pulse tube or thermal buffer tube can be suppressed so simply and conveniently is the result of a remarkable series of fortunate coincidences. First, there is no a priori guarantee that tapering the tube would have a large enough effect on streaming to cancel streaming's other causes. Second, it might have turned out that rather large taper angles (say, greater than 10° or 20°) were required; in this case, jet-like flow separation of the high-Reynolds-number first-order velocity from the tube wall would have invalidated the entire laminar, boundary-layer approach. Third, it is fortunate that most tubes operate in the "weakly turbulent" regime of oscillatory flow, and with tube surface roughness much smaller than the boundary-layer thickness, so that laminar analysis is adequate in the boundary layer.

Fourth, the perturbation expansion upon which this calculation is based is only valid for zero or extremely weak streaming—the very situation we are most interested in. This point is subtle. Strong streaming (but nevertheless with streaming velocity small compared to the oscillatory velocity) distorts the axial temperature profile of the pulse tube significantly, contradicting the fundamental assumption that the time-averaged temperature, density, etc. in the boundary layer are well approximated by their zero-oscillation values $T_m(x)$, $\rho_m(x)$, etc. This fundamental assumption requires that the streaming be so weak that the temperature profile in the pulse tube is unperturbed by the streaming—or, equivalently, that the streaming is so weak that it carries negligible heat! Hence, the calculation self-consistently predicts the conditions of zero streaming, but it cannot be relied on to accurately predict the magnitude of strong streaming.

Fifth, there are numerous other fourth-order energy flux terms in addition to $\dot{m}_{2,0}c_pT_{2,0}$ which would in principle have to be considered to obtain a formally correct fourth-order result. Fortunately, the only other large term, $\rho_{2,0}c_p\,\mathrm{Re}[T_1\widetilde{U}_1]$, is zero at the same taper angle that makes $\dot{m}_{2,0}c_pT_{2,0}$ zero, while the remaining terms, such as those involving products of first and third order quantities, are small for all angles. Hence, the suppression of $\dot{m}_{2,0}$ is sufficient to suppress all fourth-order heat transport.

Finally, as a practical matter, it is extremely convenient that the streaming-suppression taper is independent of oscillation amplitude and is only weakly dependent on temperature gradient.

5.4.3. Jet-driven tube streaming

Ideally, the gas in a pulse tube or thermal buffer tube would do nothing more than oscillate in plug flow, transmitting $\dot{E}_2 \equiv \dot{H}_2$ from one end to the other. In reality, several nonidealities can cause $\dot{E}_2 \neq \dot{H}_2$, carrying heat down the temperature gradient: ordinary conduction along x (discussed in Chapter 3), ordinary thermoacoustic boundary-layer phenomena carrying entropy along x near the wall, bucket-brigade fashion (discussed in Chapter 3), Gedeon streaming (discussed in this chapter), Olson streaming (discussed in this chapter), gravity-driven convection, and jet-driven convection (discussed here). Simultaneous suppression of all these heat-transport mechanisms is not trivial.

A rough estimate indicates how easily Olson streaming or other convection internal to a pulse tube or thermal buffer tube can ruin $\dot{E}_2 \equiv \dot{H}_2$. In a tube with reasonably large diameter, such as $100\delta_\kappa$, there is little radial thermal contact in the gas, so any time-averaged flow $u_{2,0}$ from end to end carries a full ΔT load of heat the length of the tube. If we desire a 98% effective pulse tube, this heat must be only 2% of $\dot{E}_2$:

$$\rho c_p u_{2,0} \Delta T \sim (0.02) \frac{1}{2} |p_1| |u_1| . \tag{5.69}$$

Using $\rho c_p = \gamma p/(\gamma - 1)T$ and solving for $u_{2,0}$ yields

$$u_{2,0} \sim 10^{-2} \frac{\gamma - 1}{\gamma} \frac{T}{\Delta T} \frac{|p_1|}{p_m} |u_1| . \tag{5.70}$$

Hence, in a typical case we might need $u_{2,0} \lesssim 10^{-3}$ m/s in the presence of $|u_1| = 10$ m/s. In terms of displacements, this means that we need gas displacements in the $+x$ and $-x$ directions be matched to within 10^{-4}.

We want this "imaginary piston" of gas in the tube to execute plug flow, but it is a very fragile object. Working to *mix up* this plug flow are the various streaming mechanisms listed in the first paragraph of this subsection. Working to *maintain* the plug flow are only a few subtle effects. First, gravity and the mean density gradient tend to keep this fragile imaginary piston stratified. With a typical mean-density difference of only a few kg/m^3, only $\Delta p \sim \Delta\rho\, g\, \Delta x \sim 1$ Pa is available, in the presence of oscillations typically at least 10^4 times larger. Viscous shear forces caused by gradients in $u_{2,0}$ also tend to reduce $u_{2,0}$, but the pressure differences available from this source are only of order $\mu \Delta x\, u_{2,0}/R^2$, which is typically much smaller than 1 Pa.

Good radial thermal contact in the tube could prevent $u_{2,0}$ from carrying the full ΔT from end to end, essentially allowing the upflowing and downflowing streams of Olson streaming or jet-driven streaming to experience counterflow heat exchange, so that the tube would enjoy $\dot{E}_2 \sim \dot{H}_2$ even in the presence of a $u_{2,0}$ greater than the value estimated above. If $u_{2,0} \sim 0.1$ m/s and $\Delta x \sim 0.1$ m, then 1 second is available while the stream traverses the length of the tube. If the oscillation frequency is of order 100 Hz, then 100 acoustic periods are available; during this time, heat can diffuse roughly $10\delta_\kappa$. Only the pulse tubes of the smallest cryocoolers are this small; most tubes are too large to enjoy substantial benefit from this mechanism. [However, note that the weak turbulence of most pulse tubes and buffer tubes may enhance such radial heat transport slightly.]

If either end of the tube has a small-diameter entrance, a jet may blow into the tube when gas enters, driving streaming within the tube, as illustrated in Fig. 5.10d. The spreading

angle [51] of a high-Reynolds-number jet in free space is roughly 10°, so such a jet can extend a large distance, and even the array of small jets formed by flow out of a heat exchanger or similar periodic structure requires some distance to heal into plug flow. Hence, flow straighteners are typically employed to break up such jets. A nonlinear impedance, such as that of a short stack of screens in which $N_{R,\text{peak}} \gtrsim 10^3$, is most effective at straightening jets. We typically employ such a flow straightener whenever a jet, spreading at an angle of 10°, would reach more than about $2\,|x_1|$ into the tube; we choose the flow straightener's resistance $R_{\text{straightener}}$ by simply making the peak pressure drop across the straightener (assuming well-straightened U_1) equal to about a fifth of the Bernoulli pressure of the strongest jet in the vicinity:

$$|U_1|\,R_{\text{straightener}} \sim \frac{1}{10}\rho\left[\frac{|U_1|}{A_{\text{jet}}}\right]^2. \tag{5.71}$$

Because flow straighteners dissipate acoustic power, research leading to more quantitative design methods for flow straighteners will help improve the efficiency of thermoacoustic engines and refrigerators.

5.4.4. Streaming within a regenerator or stack

We know little about streaming within a regenerator or stack, except that it should be avoided for the same reasons that Olson streaming should be avoided. We know it can occur, because we once suffered from harmful toroidal streaming within a regenerator when a narrow jet blew strongly on the heat exchanger at one end of the regenerator, due to an abrupt transition from a small duct to the diameter of the regenerator and heat exchanger. We fear that such toroidal time-averaged flows might also occur spontaneously, as has been observed when two or more regenerators are operated in parallel.

5.4.5. Deliberate streaming

Thermoacoustic systems suffer from a practical difficulty: They need heat exchangers to transfer heat between the thermodynamic working gas and the process fluid (usually air, combustion products, or water). Heat exchangers are expensive, and contribute to system inefficiency via temperature differences and viscous effects in the working fluid, in the process fluid, and often in an intermediate heat-exchange fluid. This difficulty is serious. For example, the decline of the Stirling engine and the rise of the Diesel and other internal combustion engines occurred in large part because the internal combustion engine needs no combustion-temperature heat exchanger (and also rejects most of its waste heat in its exhaust instead of through heat exchangers).

For some applications, we hope that some or all of the heat exchangers can be eliminated from thermoacoustic systems, by superposing the steady flow needed to deliver the process gas with the oscillatory flow needed for the thermodynamic cycle in the gas. We hope this idea will lead ultimately to thermoacoustic equipment for purposes such as drying of compressed air, combustion-powered air conditioning, combustion-powered dehumidification drying (such as for lumber), gas purification, or cryogen liquefaction.

To introduce some of the expected features that thermoacoustic systems with deliberate steady flow might have, we will focus attention on one specific case: a thermoacoustic air

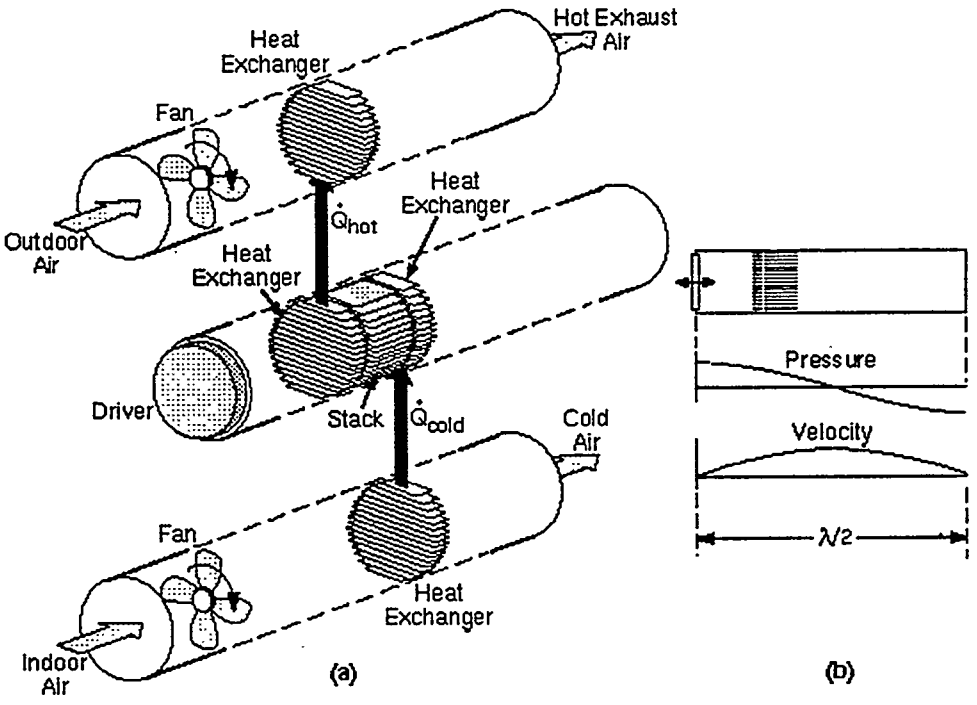

Figure 5.14: A half-wavelength standing-wave thermoacoustic refrigerator, thermally coupled to two air ducts to form an air conditioner.

conditioning system. The ideas we illustrate using this example are equally applicable to other thermoacoustic engines and refrigerators and to Stirling engines and refrigerators.

Parallel flow

As a point of departure, Fig. 5.14 shows the main parts of an air conditioning system using conventional thermoacoustic refrigeration. Four heat exchangers are required: two in the thermoacoustic working gas and one in each of the two air streams. Heat transfer between working-gas heat exchangers and air heat exchangers, indicated by heavy black arrows, is accomplished via pumped water loops (or heat pipes, thermosyphons, etc.). The four heat exchangers and two water loops account for most of the capital cost of the system.

The air conditioning system in Fig. 5.15 illustrates a simplification that is possible by using the indoor air itself as the thermoacoustic gas. A midwall in the indoor-air duct separates two acoustic resonators, driven 180° out of phase from each other by an oscillating piston in the center of the midwall. The drive frequency is chosen to make the acoustic wavelength equal to twice the midwall length, so there will be pressure nodes at the ends of the midwall and, hence, negligible acoustic power radiated to distant parts of the duct. The position of the stack relative to the nodal pattern of the standing wave is chosen so that conventional standing-wave thermoacoustic processes pump heat from right to left. Superimposed on that thermoacoustic process, the gas drifts slowly through the stack from ambient to cold, so that it leaves the right end of the apparatus at the cold temperature.

This superposition can give the system of Fig. 5.15 a higher efficiency than that of the

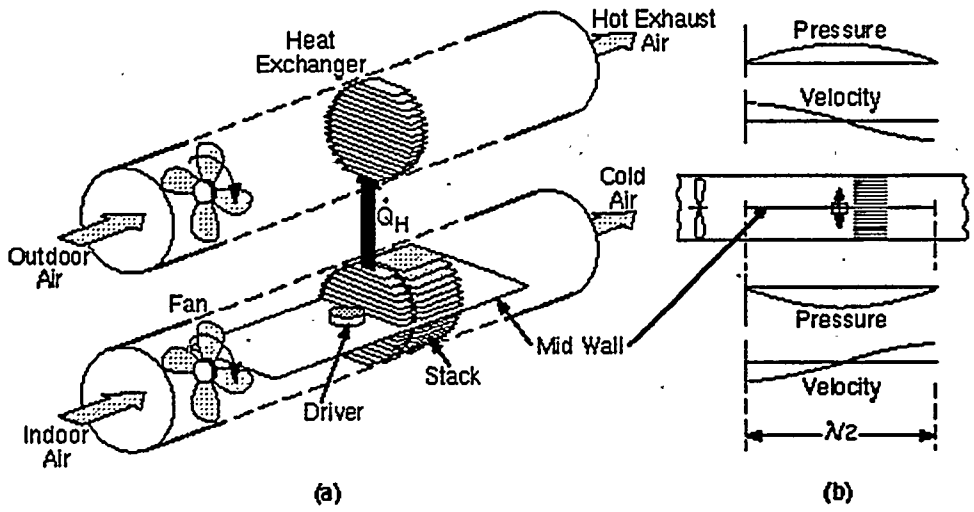

Figure 5.15: Two side–by–side half-wavelength thermoacoustic refrigerators in an air duct allow direct thermoacoustic cooling of the air. The standing-wave refrigerator of Figs. 1.11 and 1.12 has this topology, with the midwall in this figure equivalent to the large empty space in the center of the torus in Figs. 1.11 and 1.12.

system of Fig. 5.14, for two reasons. First, two heat exchangers, and their internal small temperature differences, are eliminated. Second, a much more subtle improvement in efficiency arises because the system of Fig. 5.15 essentially puts the air stream sequentially in thermal contact with a large number of refrigerators in series—a sort of continuum limit of staged refrigeration. To understand this point, first imagine that thermoacoustic refrigerators are ideal, having Carnot's $COP = T_C/(T_0 - T_C)$. Then, in the case of Fig. 5.14, removing heat $\dot{m}c_p(T_0 - T_C)$ at temperature T_C with the refrigerator requires work

$$\dot{W} = \dot{m}c_p(T_0 - T_C)^2/T_C. \tag{5.72}$$

This is more than twice the minimum work required by the first and second laws of thermodynamics for this process, which we saw in Chapter 4 is given by the difference between the outgoing and incoming flow availabilities:

$$\dot{W} = \dot{m}\left[(h_C - h_0) - T_0\,(s_C - s_0)\right] \tag{5.73}$$

$$= \dot{m}c_p[T_C - T_0 + T_0 \ln(T_0/T_C)]. \tag{5.74}$$

(The second expression results from using ideal-gas expressions for h and s.) The trouble with the simple, one-stage refrigerator is that it removes *all* the heat load at T_C, where every watt of cooling power requires the same amount of work. It is much more efficient to remove as much of the heat load as possible at higher temperatures T'_C, where each watt of cooling power requires less work because the Carnot $COP = T'_C/(T_0 - T'_C)$ is higher. The perfect embodiment of this idea would employ an infinite number of ideal refrigerators, each providing an infinitesimal cooling power $\dot{m}c_p\,dT'_C$ at T'_C and rejecting an infinitesimal amount of waste heat at T_0. The flow-through thermoacoustic refrigerator of Fig. 5.15 has some features of this perfect situation, if we imagine each length dx of the stack to be a

refrigerator unto itself, lifting heat from T'_C to $T'_C + dT'_C$. The flow-through system removes each watt of heat from the flowing stream at the highest possible temperature—but with an "infinite" number of less-than-ideal refrigerators, each of which must handle the waste heat of all its downstream neighbors in addition to the local heat load of the flowing stream.

With the addition of nonzero mean velocity along x, the gas moves through the system in a repetitive, "102 steps forward, 98 steps back" manner, in position, in temperature, and in density and entropy. This violates one assumption on which Chapters 2 and 3 are based, because there we assumed $u \doteq \mathrm{Re}[u_1 e^{i\omega t}]$, with no "$u_m$". The apparatus shown in Figs. 1.11 and 1.12 was built to study this type of deliberate steady flow [16].

To derive corresponding equations in the presence of nonzero parallel steady flow, we again begin with the momentum, continuity, and energy equations. We write

$$\begin{aligned} p &= p_m(x) + \mathrm{Re}\left[p_1(x)e^{i\omega t}\right], && (5.75)\\ u &= u_m(x,y,z) + \mathrm{Re}\left[u_1(x,y,z)e^{i\omega t}\right], && (5.76)\\ v &= \mathrm{Re}\left[v_1(x,y,z)e^{i\omega t}\right], && (5.77)\\ w &= \text{similar to } v, && (5.78)\\ T &= T_m(x) + T'_m(x,y,z) + \mathrm{Re}\left[T_1(x,y,z)e^{i\omega t}\right], && (5.79)\\ \rho &= \rho_m(x) + \rho'_m(x,y,z) + \mathrm{Re}\left[\rho_1(x,y,z)e^{i\omega t}\right], && (5.80)\\ \mu,\ k,\ \text{etc.} &= \text{similar to } \rho \text{ (but see below)}. && (5.81) \end{aligned}$$

We will consider p_1/p_m and v_1/a to be small, and will keep terms to first order in smallness in the momentum and continuity equations and to second order in smallness in the energy equation as usual. Note that we consider dT_m/dx to be of zeroth order. We will see below that the energy equation then requires us to consider u_m/a to be of second order; for the moment, we may imagine this to be an assumption.

Substituting Eqs. (5.75)–(5.81) into the momentum equation, and requiring that the time-independent terms and the terms proportional to $e^{i\omega t}$ must equate separately, yields the same first-order momentum equation as in Chapter 2, and a time-averaged equation:

$$0 = -dp_m/dx + \mu\nabla^2_{y,z} u_m\,. \tag{5.82}$$

This time-averaged equation simply expresses the fact that viscosity and steady flow cause a steady pressure gradient. It shows that dp_m/dx is of second order (the same order as u_m), so we will neglect it, regarding p_m as a x-independent constant.

In the continuity and energy equations below, we will require expressions for the oscillatory temperature T_1 and its spatial average $\langle T_1 \rangle$ over y and z. Starting from the general equation of heat transfer as we did in Chapter 2, we find the same first-order equation for T_1 as in Chapter 2, and a time-averaged equation

$$\rho_m c_p u_m\, dT_m/dx = k\nabla^2_{y,z} T'_m\,. \tag{5.83}$$

Our only use of Eq. (5.83) is to note that it implies T'_m is of second order. Hence T'_m, and similarly ρ'_m, μ'_m, k'_m, etc., can be neglected, because their contributions are of negligible order.

Next we consider the continuity equation

$$\partial\rho/\partial t + \boldsymbol{\nabla}\cdot(\rho\mathrm{v}) = 0, \tag{5.84}$$

which can be integrated with respect to y and z to obtain to lowest order

$$i\omega A \langle \rho_1 \rangle + \frac{d(\rho_m U_1)}{dx} = 0, \tag{5.85}$$

$$\frac{d(\rho_m U_m)}{dx} = 0. \tag{5.86}$$

Again, the first-order expression is the same as in Chapter 2. Using $d\rho = -(\rho/T)\, dT + (\gamma/a^2)\, dp$, we can express the mean density as

$$d\rho_m/dx = -(\rho_m/T_m)\, dT_m/dx. \tag{5.87}$$

to lowest order. Substituting this into Eq. (5.86) yields

$$\frac{dU_m}{dx} - \frac{1}{T_m}\frac{dT_m}{dx} U_m = 0\,, \tag{5.88}$$

which can be used to predict the x dependence of U_m during numerical integration along x.

Finally, we consider the energy equation, as we did in Chapter 3. There, we saw that the important terms in the time-averaged energy equation are

$$0 = \frac{d}{dx}\left[A\langle \overline{\rho u h}\rangle - A\left\langle \overline{k\,\partial T/\partial x}\right\rangle - A_{\text{solid}}\left\langle \overline{k_{\text{solid}}\,\partial T_{\text{solid}}/\partial x}\right\rangle_{\text{solid}}\right]. \tag{5.89}$$

In principle, we must consider each of these terms to second order, but in practice, for situations of interest to us, zeroth order suffices for the last two terms, as it did in Chapter 3. Hence, we begin with the first term. Its expansion to second order is

$$A\left\langle \rho_m u_m h_m + \overline{\rho_1 u_1} h_m + \rho_m \overline{u_2} h_m + \rho_m \overline{u_1 h_1}\right\rangle\,, \tag{5.90}$$

where we have already set five terms equal to zero because the time average of first order quantities (e.g., $\overline{\rho_1}$ or $\overline{u_1}$) is zero. We regard the steady mass flow as fixed at $\rho_m U_m = A\langle \rho_m u_m\rangle$, so that the second-order time-averaged mass flux $A\langle \overline{\rho_1 u_1} + \rho_m \overline{u_2}\rangle = 0$. Hence (5.90) reduces to

$$A\left\langle \rho_m u_m h_m + \rho_m \overline{u_1 h_1}\right\rangle\,. \tag{5.91}$$

Using $dh = c_p\, dT$, and combining this with the other significant terms from Eq. (5.89), we conclude that

$$\dot{H}_2 = \rho_m c_p (T_m - T_0) U_m + A\rho_m c_p \langle \overline{T_1 u_1}\rangle - (Ak + A_{\text{solid}} k_{\text{solid}})\, dT_m/dx\,. \tag{5.92}$$

The new term, $\rho_m c_p (T_m - T_0) U_m$, is of the same order (second) as the old $A\rho_m c_p \langle \overline{T_1 u_1}\rangle$ we obtained in Chapter 3. With $\dot{H}_2$ independent of x in a stack, regenerator, or other thermally insulated channel, this equation allows us to predict the x dependence of T_m during numerical integration along x when steady flow U_m is superimposed on thermoacoustic oscillations. Generally, the steady flow causes $T_m(x)$ to bend significantly, as steady flow from hot to cold pushes the center of the stack or regenerator to warmer temperatures, or steady flow from cold to hot pushes the center of the stack or regenerator to colder temperatures [16].

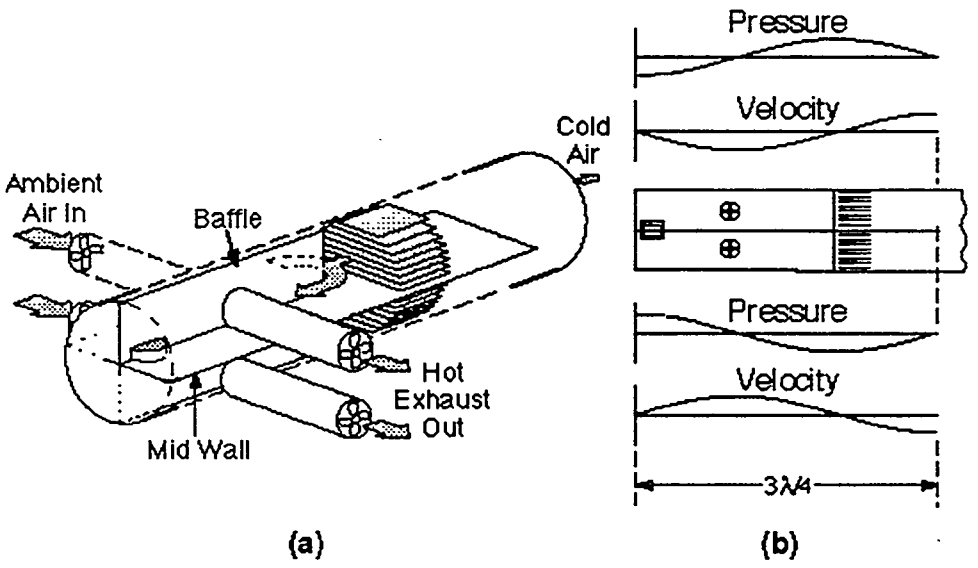

Figure 5.16: Two side–by–side three-quarter-wavelength thermoacoustic refrigerators, each with a baffle to direct the superimposed steady flow, in an air duct network. This arrangement allows direct thermoacoustic cooling of some of the steady air flow, rejecting waste heat to the remainder of the steady air flow, with no heat exchangers except the stack.

Perpendicular flow

Thus far, we have discussed steady flow superimposed *parallel* to the oscillating flow. To introduce the idea of steady flow superimposed *perpendicular* to the oscillating flow, we return to our air-conditioner motif, showing in Fig. 5.16 the elimination of *all* heat exchangers from a thermoacoustic system. As in Fig. 5.15, a midwall separates the duct into two regions that resonate 180° out of phase from each other. The drive frequency is chosen so that 3/4 of the acoustic wavelength equals the midwall length, thereby putting a pressure antinode at the hard duct closure at the left end of the midwall and a pressure node at the right, open end of the midwall. Deflector walls further divide each of these two resonators in order to direct the steady flow of the air. This steady flow is introduced into the resonator at the pressure node 1/4 of a wavelength from the hard closure, so that negligible acoustic power is radiated into the air inlet duct. A significant fraction of the steady flow passes through the stack, is thereby cooled and dehumidified, and leaves the right end of the duct. Most of the steady flow passes vigorously past the hot end of the stack, moving perpendicular to the oscillating flow, in order to remove the waste heat from the thermoacoustic system and exhaust it. The quantitative understanding of oscillating thermodynamics in the presence of such a perpendicular steady flow is a significant and exciting challenge.

The air conditioner described above will, incidentally, dehumidify the air, returning cold dry air. But for many important drying applications, it is desired to dehumidify air and return it *warm* and dry. Hence, we could also consider configurations comprising coolers and heat pumps in the same resonator, to put the waste heat from the hot end of the cooling stack back into the air stream. This is but one of many possibilities for open thermoacoustic systems in which multiple stacks, serving multiple functions, share a resonator. As another

example, industry has long dreamed of a combustion-powered heat pump hot water heater, which would have a (first-law) efficiency greater than 100%: It would use part of the heat of combustion to drive an engine, which would drive a heat pump to draw heat from ambient air and deliver it to the hot water. Such devices can (and have) been built with existing technology, but only at a cost that is prohibitive to today's consumer. We can imagine such a system using open flows through a thermoacoustic system, with a pulse combustor, thermoacoustic engine, and thermoacoustic heat pump in an air stream, all delivering heat to hot water passing through a heat exchanger.

5.5. Harmonics and shocks

In preparation.

5.6. Dimensionless groups

In preparation. Something like a summary of [62].

5.7. Exercises

5.1 Calculate the molecular mean free path for your favorite gas in your favorite thermoacoustic apparatus, by looking up the appropriate equations in something like an introductory statistical-mechanics textbook such as Reif's Statistical and Thermal Physics. Compare to dimensions in the apparatus and to δ_ν and δ_κ. Is the mean free path so negligible compared to δ_ν that the representation in Ani. viscous should be accurate? Are the crevices between screen wires in your regenerator large compared to the mean free path?

5.2 Calculate the peak Reynolds number and r_h/δ_ν at a few locations in your favorite thermoacoustic apparatus. Where are they, on Fig. 5.3?

5.3 In the section on minor losses, we assumed that $U(t)$ was sinusoidal. In some situations, it may be better to assume that $\Delta p(t)$ is sinusoidal. Repeat the derivation of Eq. (5.23) assuming that $\Delta p(t)$ is sinusoidal. Can you reconcile this answer with Eq. (5.23)?

5.4 To help assure yourself that the similitude-variable list is complete, express the Prandtl number at the reference temperature in terms of the variables listed: μ_{ref}, K_{ref}, a_{ref}, p_m, T_{ref}, and γ.

5.5 Express the Mach number u_1/a and the Reynolds number in terms of ratios of lengths, using $|\langle x_1 \rangle|$, r_h, λ, and δ_ν.

5.6 Your sponsor wants you to build a thermoacoustic engine to generate electricity on a satellite. The engine will operate from a plutonium heat source at 1800 K, and dump its waste heat to a tiny black-body radiator at 900 Kelvin. Helium will be the gas, at a pressure of 20 bar. You want to use similitude to do some preliminary tests in a model that operates between 600 Kelvin and 300 Kelvin—exactly 1/3 the ultimate temperatures—so you can experiment using stainless steel instead of iridium and platinum. You want the model to have the same dimensions as the ultimate hardware. What mean pressure of helium must you use in the model? How much higher or lower will all powers be in the model? If you

wanted to use a different monatomic gas instead of helium in the model, could you keep the mean pressure in the model lower/safer?

5.7 Figure 5.2 shows that the laminar friction factor is $f_M = 64/N_R$ for steady flow in a circular pipe. Derive this from Eq. (5.2). Begin this process by justifying the neglect of most terms in Eq. (5.2), leaving only $0 = -dp/dx + \mu\nabla^2 u$.

For a serious mathematical challenge, show that combining Eqs. (2.56) and (2.62) gives the same result, in the limit $\omega \rightarrow 0$.

5.8 Review Exercise 4.2. Repeat that exercise, assuming that all refrigerators operate at the same fraction η_{II} of Carnot's *COP*. In which direction does the comparison between Case 2 and Case 3 shift? Now extend Case 3 of the original exercise from two refrigerators to an infinite number of refrigerators, showing by comparison to Eq. (5.74) that the work required is the minimum allowed by the laws of thermodynamics. Can you repeat this continuum calculation assuming that all the refrigerators operate at the same fraction η_{II} of Carnot's *COP*?

6. HARDWARE

In preparation.
remember thermal stress in pressure vessels

7. Measurements

In preparation.

8. Common pitfalls

in preparation

9. APPENDIX

These are DeltaE files for parts of the example hardware shown in the Examples section in Chapter 1 and referred to throughout the book.

9.1. Standing-wave engine

This model of part of the standing-wave engine starts at the right end of Fig. 1.10 and integrates to the left, past the branch up to the refrigerators, ending at the pressure node at the center of the resonator. The point of view adopted in this particular file is this: In order to have the as-built hardware run with $|p_1| = 297$ kPa at the branch to the refrigerators and supply 1000 W of acoustic power to the refrigerators, what hot temperature and heater power are required at the hot heat exchanger at the hot end of the stack, and at what frequency will the system resonate? (In this simplified model, we assume that the left engine can supply 500 W of acoustic power, but at Los Alamos we would typically fully include the left engine in the model.)

```
TITLE     One engine, branch to OPTRs; stop calc at midplane. As-built dims.
!->staneng.out
!Created@13:50:34  2-Jan-99 with DeltaE Vers. 4.5b7 for the IBM/PC-Compatible
!---------------------------------- 0 ----------------------------------
 BEGIN      the setup
  2.9660E+06 a Mean P    Pa                390.27    A Freq.  G( 0b)      P
   390.27    b Freq.     Hz       G        758.28    B T-beg  G( 0c)      P
   758.28    c T-beg     K        G       3.1963E+05 C |p|@0  G( 0d)      P
  3.1963E+05 d |p|@0     Pa       G       2392.4     D HeatIn G( 3e)      P
     0.0000  e Ph(p)0    deg
     0.0000  f |U|@0     m^3/s
     0.0000  g Ph(U)0    deg
 helium     Gas type
 ideal      Solid type
!---------------------------------- 1 ----------------------------------
 ENDCAP     hot end
 sameas  2a  a Area      m^2             3.1963E+05 A |p|        Pa
                                            0.0000  B Ph(p)     deg
                                        2.3740E-05 C |U|      m^3/s
                                         180.00    D Ph(U)     deg
                                          -3.7940  E Hdot       W
 sameas  0  Gas type                      -3.7940  F Work       W
```

```
ideal      Solid type                          -3.7940  G HeatIn    W
!---------------------------------  2 ---------------------------------
ISODUCT    hot duct
 2.8580E-03 a Area      m^2              3.1885E+05 A |p|       Pa
    0.1900  b Perim     m                1.3951E-03 B Ph(p)     deg
 4.5900E-02 c Length    m                2.0855E-02 C |U|     m^3/s
                                          -90.264   D Ph(U)     deg
                                          -15.375   E Hdot      W
sameas  0  Gas type                       -15.375   F Work      W
ideal      Solid type                     -11.581   G HeatIn    W
!---------------------------------  3 ---------------------------------
HXFRST     hot heat exchanger
sameas  6a  a Area     m^2               3.1843E+05 A |p|       Pa
    0.8800  b GasA/A                     1.7874E-02 B Ph(p)     deg
 9.5000E-03 c Length    m                2.5615E-02 C |U|     m^3/s
 3.8000E-04 d y0        m                 -91.519   D Ph(U)     deg
 2392.4     e HeatIn    W       G        2377.0     E Hdot      W
  950.00    f Est-T     K       (t)      -109.41    F Work      W
sameas  0  Gas type                       2392.4    G Heat       W
copper     Solid type                     781.38    H MetalT     K
!---------------------------------  4 ---------------------------------
STKSLAB    stack
sameas  6a  a Area     m^2               3.0688E+05 A |p|       Pa
    0.8100  b GasA/A                       0.9075  B Ph(p)     deg
 7.6200E-02 c Length    m                5.3140E-02 C |U|     m^3/s
 1.3000E-04 d y0        m                 -84.938   D Ph(U)     deg
 2.5400E-05 e Lplate    m                2377.0     E Hdot      W
                                          590.70    F Work      W
                                          758.28    G T-beg      K
sameas  0  Gas type                       318.27    H T-end      K
stainless  Solid type                     700.11    I StkWrk     W
!---------------------------------  5 ---------------------------------
HXLAST     cold heat exchanger
sameas  6a  a Area     m^2               3.0349E+05 A |p|       Pa
    0.7500  b GasA/A                       0.8885  B Ph(p)     deg
 1.2700E-02 c Length    m                5.7824E-02 C |U|     m^3/s
 8.2600E-04 d y0        m                 -85.412   D Ph(U)     deg
    0.0000  e HeatIn    W       (t)       566.12    E Hdot      W
  295.00    f Est-T     K    = 5H?        566.12    F Work      W
sameas  0  Gas type                      -1810.9    G Heat       W
copper     Solid type                     295.00    H MetalT     K
!---------------------------------  6 ---------------------------------
ISOCONE    adapter
 3.1670E-03 a AreaI     m^2               2.9660E+05 A |p|       Pa
    0.1990  b PerimI    m                   0.8144  B Ph(p)     deg
```

```
 2.9000E-02 c Length      m              7.0745E-02 C |U|      m^3/s
sameas  8a  d AreaF      m^2              -86.112   D Ph(U)     deg
sameas  8b  e PerimF     m                562.55    E Hdot      W
sameas  0  Gas type                       562.55    F Work      W
ideal      Solid type                      -3.5678  G HeatIn    W
!--------------------------------- 7 ---------------------------------
BRANCH     branch to OPTRs, appearing partly resistive, partly complian
 3.9590E+07 a Re(Zb) Pa-s/m^3          2.9660E+05 A |p|        Pa
-1.3200E+07 b Im(Zb) Pa-s/m^3             0.8144  B Ph(p)     deg
                                       7.2951E-02 C |U|      m^3/s
                                        -91.502   D Ph(U)     deg
                                       -437.33    E Hdot      W
sameas  0  Gas type                    -437.33    F Work      W
ideal      Solid type                   999.88    G Work_B    W
!--------------------------------- 8 ---------------------------------
ISOCONE    a little more of the adapter
 2.8200E-03 a AreaI       m^2          2.6735E+05 A |p|        Pa
    0.1880  b PerimI      m               1.0419  B Ph(p)     deg
 7.3000E-02 c Length      m            9.7815E-02 C |U|      m^3/s
sameas  9a  d AreaF      m^2              -90.915   D Ph(U)     deg
sameas  9b  e PerimF     m               -446.54    E Hdot      W
sameas  0  Gas type                      -446.54    F Work      W
ideal      Solid type                     -9.2134  G HeatIn    W
!--------------------------------- 9 ---------------------------------
ISODUCT    long thin duct at ambient temperature
 2.0270E-03 a Area        m^2          6622.8     A |p|        Pa
    0.1600  b Perim       m              90.229   B Ph(p)     deg
    0.3700  c Length      m               0.1510  C |U|      m^3/s
                                        -89.771   D Ph(U)     deg
                                       -500.00    E Hdot      W
sameas  0  Gas type                    -500.00    F Work      W
ideal      Solid type                   -53.456   G HeatIn    W
!--------------------------------- 10 --------------------------------
SOFTEND    pressure "node", with 500 W coming from other engine
    0.0000  a Re(Z)              (t)   6622.8     A |p|        Pa
    0.0000  b Im(Z)            =10H?     90.229   B Ph(p)     deg
                                          0.1510  C |U|      m^3/s
                                        -89.771   D Ph(U)     deg
                                       -500.00    E Hdot      W
                                       -500.00    F Work      W
                                      -1.8879E-02 G Re(Z)
sameas  0  Gas type                    3.1658E-11 H Im(Z)
ideal      Solid type                   318.27    I   T        K
!--------------------------------- 11 --------------------------------
FREETARG   Ampl at branch to OPTRs
```

```
  2.9660E+05 a Target          =11A?     2.9660E+05 A FreeT
   7A b ResAdr
!-------------------------------- 12 --------------------------------
 FREETARG   acoustic power from other engine
  -500.00    a Target          =12A?     -500.00    A FreeT
  10F b ResAdr

! The restart information below was generated by a previous run
! You may wish to delete this information before starting a run
! where you will (interactively) specify a different iteration
! mode.  Edit this table only if you really know your model!
INVARS      4  0  2  0  3  0  4  3  5
TARGS       4  5  6 10  2 11  1 12  1
SPECIALS    0
```

9.2. Standing-wave refrigerator

This model of part of the standing-wave refrigerator starts near the drivers at one side of the refrigerator shown in Fig. 1.12 and integrates downward, through a stack and its neighboring heat exchangers, ending at the pressure node at the center of the bottom leg of the resonator. The point of view adopted in this particular file is this: In order to have the as-built hardware run with $|p_1| = 6467$ Pa near the drivers and to reach an experimentally observed cold temperature of 285.6 K, what U_1, f, and heat load on the cold heat exchanger should occur?

```
TITLE     segments 1-7 < Bob 9/97;  segs 8-14 < Hiller ntbk, pg one, 10/97
!->stanfrid.out
!Created@13:58:15  2-Jan-99 with DeltaE Vers. 4.5b7 for the IBM/PC-Compatible
!-------------------------------- 0 --------------------------------
 BEGIN      Initialize in main duct where drivers are attached
  3.2388E+05 a Mean P    Pa            -5.2625E-02 A |U|@0  G( 0f)      P
    91.650   b Freq.     Hz              187.09    B Ph(U)0 G( 0g)      P
   307.80    c T-beg     K               -32.862   C HeatIn G( 3e)      P
  6467.0     d |p|@0     Pa
    90.000   e Ph(p)0    deg
 -5.2625E-02 f |U|@0    m^3/s    G
   187.09    g Ph(U)0    deg      G
 0.920hear   Gas type
 ideal       Solid type
!-------------------------------- 1 --------------------------------
 MEANFlow   mean flow
     0.0000  a  U_m     m^3/s           6467.0     A |p|        Pa
                                          90.000   B Ph(p)      deg
```

```
                                        5.2625E-02 C |U|      m^3/s
                                          7.0926   D Ph(U)     deg
                                         21.011    E Hdot       W
                                         21.011    F Work       W
sameas  0  Gas type                       0.0000   G  U_m     m^3/s
ideal      Solid type                     0.0000   H  H_m       W
!--------------------------------  2 ---------------------------------
INSDUCT    Pre-stack Duct
 1.8430E-02 a Area       m^2           6215.5      A |p|        Pa
    0.4813  b Perim      m               89.766    B Ph(p)      deg
    0.1494  c Length     m             7.1223E-02  C |U|      m^3/s
                                          5.1494   D Ph(U)      deg
                                         21.011    E Hdot       W
sameas  0  Gas type                      20.765    F Work       W
ideal      Solid type                     0.0000   G HeatIn     W
!--------------------------------  3 ---------------------------------
HXFRST     Hot Heat exchanger
 1.7211E-02 a Area       m^2           6154.2      A |p|        Pa
    0.5227  b GasA/A                     89.884    B Ph(p)      deg
 1.2700E-02 c Length     m             7.2140E-02  C |U|      m^3/s
 6.3500E-04 d y0         m               4.9381    D Ph(U)      deg
  -32.862   e HeatIn     W      G       -11.851    E Hdot       W
  299.70    f Est-T      K      (t)      19.554    F Work       W
                                        -32.862    G Heat        W
                                        307.22     H MetalT      K
sameas  0  Gas type                       0.0000   I  U_m     m^3/s
copper     Solid type                     0.0000   J  H_m       W
!--------------------------------  4 ---------------------------------
STKREct    rectangular-pore stack
 1.8824E-02 a Area       m^2           5558.2      A |p|        Pa
    0.7050  b GasA/A                     93.242    B Ph(p)      deg
    0.1524  c Length     m             8.6737E-02  C |U|      m^3/s
 4.0640E-04 d     a      m               3.8486    D Ph(U)      deg
 1.1811E-04 e Lplate     m             -11.851     E Hdot       W
 6.3500E-03 f     b      m               2.5538    F Work       W
                                        307.80     G T-beg       K
                                        285.60     H T-end       K
                                        -17.000    I StkWrk      W
sameas  0  Gas type                       0.0000   J  U_m     m^3/s
kapton     Solid type                     0.0000   K  H_m       W
!--------------------------------  5 ---------------------------------
FREETarget first stack thermocouple location
  307.80    a Target           (t)      307.80     A FreeT
  4G b ResAdr
!--------------------------------  6 ---------------------------------
```

```
FREETarget last stack thermocouple location
  285.60    a Target          = 6A?      285.60    A FreeT
  4H b ResAdr
!--------------------------------- 7 ---------------------------------
HXLAST     Cold heat exchanger
 1.7211E-02 a Area      m^2              5537.1     A |p|       Pa
    0.9300  b GasA/A                      93.272   B Ph(p)     deg
 6.3500E-03 c Length     m              8.7412E-02  C |U|     m^3/s
 1.0414E-03 d y0         m                 3.7945   D Ph(U)     deg
    0.0000  e HeatIn     W       (t)        0.0000   E Hdot      W
    0.0000  f Est-T      K       (t)        2.2065   F Work      W
sameas  0   Gas type                       11.851   G Heat      W
copper      Solid type                     285.98   H MetalT    K
!--------------------------------- 8 ---------------------------------
INSDUCT    From cold hx to bolt flange, + a half inch
 2.0180E-02 a Area      m^2              5229.9     A |p|       Pa
    0.5036  b Perim      m                93.256   B Ph(p)     deg
    0.1210  c Length     m                 0.1015  C |U|     m^3/s
                                          3.6951   D Ph(U)     deg
                                          0.0000   E Hdot      W
sameas  0   Gas type                       2.0337   F Work      W
ideal       Solid type                     0.0000   G HeatIn    W
!--------------------------------- 9 ---------------------------------
INSDUCT    Duct, beginning 1/2 in below big bolt flange
 1.8485E-02 a Area      m^2              4698.8     A |p|       Pa
    0.4820  b Perim      m                93.235   B Ph(p)     deg
    0.1650  c Length     m                 0.1177  C |U|     m^3/s
                                          3.6063   D Ph(U)     deg
                                          0.0000   E Hdot      W
sameas  0   Gas type                       1.7925   F Work      W
ideal       Solid type                     0.0000   G HeatIn    W
!-------------------------------- 10 ---------------------------------
INSDUCT    Elbow, 6 inch diam, 5 inch radius of curvature on centerline
 1.8240E-02 a Area      m^2              3947.2     A |p|       Pa
    0.4788  b Perim      m                93.211   B Ph(p)     deg
    0.2000  c Length     m                 0.1346  C |U|     m^3/s
                                          3.5336   D Ph(U)     deg
                                          0.0000   E Hdot      W
sameas  0   Gas type                       1.4961   F Work      W
ideal       Solid type                     0.0000   G HeatIn    W
!-------------------------------- 11 ---------------------------------
INSDUCT    straight part of big black cone
 1.8240E-02 a Area      m^2              3582.2     A |p|       Pa
    0.4788  b Perim      m                93.200   B Ph(p)     deg
 8.9000E-02 c Length     m                 0.1412  C |U|     m^3/s
```

```
                                          3.5093  D Ph(U)      deg
                                          0.0000  E Hdot       W
sameas  0  Gas type                       1.3635  F Work       W
ideal      Solid type                     0.0000  G HeatIn     W
!-------------------------------- 12 ---------------------------------
INSCONE    The long black plastic cone
sameas 11a  a AreaI      m^2           1139.0     A |p|        Pa
sameas 11b  b PerimI      m              93.164   B Ph(p)      deg
    0.3635  c Length     m               0.1547  C |U|       m^3/s
sameas 13a  d AreaF      m^2             3.4614  D Ph(U)      deg
sameas 13b  e PerimF      m              0.0000  E Hdot       W
sameas  0  Gas type                       0.4570  F Work       W
ideal      Solid type                     0.0000  G HeatIn     W
!-------------------------------- 13 ---------------------------------
INSDUCT    little straight section of black cone
 8.1070E-03 a Area       m^2            545.42    A |p|        Pa
    0.3192  b Perim      m               93.178   B Ph(p)      deg
 5.7200E-02 c Length     m               0.1551  C |U|       m^3/s
                                          3.4598  D Ph(U)      deg
                                          0.0000  E Hdot       W
sameas  0  Gas type                       0.2078  F Work       W
ideal      Solid type                     0.0000  G HeatIn     W
!-------------------------------- 14 ---------------------------------
INSDUCT    half the white "tee", up to the symmetry midpoint
 9.8100E-03 a Area       m^2          6.4730E-12 A |p|        Pa
    0.3511  b Perim      m               90.016   B Ph(p)      deg
 6.3500E-02 c Length     m               0.1553  C |U|       m^3/s
 1.0000E-03 d Srough                     3.4592  D Ph(U)      deg
                                          0.0000  E Hdot       W
sameas  0  Gas type                    3.0183E-14 F Work       W
ideal      Solid type                     0.0000  G HeatIn     W
!-------------------------------- 15 ---------------------------------
SOFTEND    pressure node
    0.0000  a Re(Z)          =15G?     6.4730E-12 A |p|        Pa
    0.0000  b Im(Z)          =15H?       90.016   B Ph(p)      deg
                                          0.1553  C |U|       m^3/s
                                          3.4592  D Ph(U)      deg
                                          0.0000  E Hdot       W
                                       3.0183E-14 F Work       W
                                       3.4519E-17 G Re(Z)
sameas  0  Gas type                    5.7367E-16 H Im(Z)
ideal      Solid type                    285.60    I   T        K
!-------------------------------- 16 ---------------------------------
THERMO     properties
                                          1.6667  A  gamma
```

```
                                        758.53    B    a    m/s
                                          0.9382  C   rho   kg/m^3
                                       3021.9     D   c_p   J/kg/K
                                          0.1252  E   K0    W/m/K
                                       2.0110E-05 F   mu    kg/s/m
                                       3.5014E-03 G  beta    1/K
                                       3.9157E-04 H deltaK    m
                                       2.7285E-04 I deltaN    m
                                       1.0000E+08 J  rho_s kg/m^3
 sameas  0  Gas type                   1.0000E+08 K   c_s  J/kg/K
 ideal      Solid type                 1.0000E+08 L   Ks   W/m/K

! The restart information below was generated by a previous run
! You may wish to delete this information before starting a run
! where you will (interactively) specify a different iteration
! mode.  Edit this table only if you really know your model!
INVARS      3  0  6  0  7  3  5
TARGS       3  6  1 15  1 15  2
SPECIALS    0
```

9.3. Traveling-wave engine

This model of the entire traveling-wave engine seems dauntingly complicated, but it is in fact typical of how our models at Los Alamos evolve after many months of interaction between experiments and computations. The model starts near the top of of Fig. 1.14, just above the ambient heat exchanger. It integrates up, left, and down, through the compliance and inertance to the junction. It then starts again just above the ambient heat exchanger, going down through the regenerator and thermal buffer column to reach the junction a second time, where complex p_1 must match up. The integration then proceeds through the resonator.

```
TITLE     original, unpublished engine
!->scotstrp.out
!Created@14: 3:56  2-Jan-99 with DeltaE Vers. 4.5b7 for the IBM/PC-Compatible
!-------------------------------- 0 --------------------------------
 BEGIN      the setup
  3.1030E+06 a Mean P    Pa                80.762    A Freq.  G( 0b)      P
    80.762   b Freq.     Hz       G     -3.2035E+07 B Re(Zb) G( 1a)      P
   302.00    c T-beg     K              1.3860E+07 C Im(Zb) G( 1b)      P
  3.1000E+05 d |p|@0     Pa            -1620.9     D HeatIn G(24e)      P
     0.0000  e Ph(p)0    deg            3599.7     E HeatIn G(30e)      P
     0.0000  f |U|@0     m^3/s          2.4773E-08 F Target G(45a)      P
     0.0000  g Ph(U)0    deg
 helium     Gas type
```

```
ideal       Solid type
!---------------------------------- 1 ----------------------------------
TBRANCH     Split
-3.2035E+07 a Re(Zb) Pa-s/m^3   G       3.1000E+05 A |p|        Pa
 1.3860E+07 b Im(Zb) Pa-s/m^3   G          0.0000  B Ph(p)      deg
                                        8.8813E-03 C |U|      m^3/s
                                         -156.60    D Ph(U)      deg
                                        -1263.4     E Hdot       W
helium      Gas type                    -1263.4     F Work       W
ideal       Solid type                   1263.4     G Work_T     W
!---------------------------------- 2 ----------------------------------
ISODUCT     Jetting space (pg 25 book 4)
 6.8250E-03 a Area       m^2            3.0996E+05 A |p|        Pa
    0.2930  b Perim      m              1.0637E-02 B Ph(p)      deg
 1.9100E-02 c Length     m              1.1083E-02 C |U|      m^3/s
 3.0000E-04 d Srough                    -137.41    D Ph(U)      deg
                                        -1264.8     E Hdot       W
helium      Gas type                    -1264.8     F Work       W
stainless   Solid type                    -1.3376  G HeatIn     W
!---------------------------------- 3 ----------------------------------
RPNTARGET   Calculate jet pump minor loss resistor (pg 26 book 4)
    1.7000  a Target             (t)    1.5222E+06 A RPNval
1.05  2C *  5a /  5a /  3a *
!---------------------------------- 4 ----------------------------------
IMPEDANCE   Jet pump minor loss Res. (pg 26 book 4 + minor loss notes)
sameas  3A  a Re(Zs) Pa-s/m^3          3.2259E+05 A |p|        Pa
    0.0000  b Im(Zs) Pa-s/m^3             2.0384  B Ph(p)      deg
                                        1.1083E-02 C |U|      m^3/s
                                         -137.41    D Ph(U)      deg
                                        -1358.2     E Hdot       W
helium      Gas type                    -1358.2     F Work       W
ideal       Solid type                   -93.483    G HeatIn     W
!---------------------------------- 5 ----------------------------------
ISOCONE     Jet pump / estimated dimensions (pg 25 and 97 bk 4)
 1.1400E-04 a AreaI      m^2            3.2154E+05 A |p|        Pa
    0.1850  b PerimI     m                 2.4967  B Ph(p)      deg
 2.5400E-02 c Length     m              1.1294E-02 C |U|      m^3/s
 5.8880E-04 d AreaF      m^2            -136.37    D Ph(U)      deg
    0.4210  e PerimF     m             -1367.7     E Hdot       W
 3.0000E-04 f Srough                   -1367.7     F Work       W
helium      Gas type                      -9.4273  G HeatIn     W
stainless   Solid type
!---------------------------------- 6 ----------------------------------
ISODUCT     Paddle space above jet pump (pg 27 book 4)
 8.1500E-03 a Area       m^2            3.2152E+05 A |p|        Pa
```

```
    0.3200  b Perim      m                 2.4997  B Ph(p)     deg
 6.3500E-03 c Length     m              1.2434E-02 C |U|      m^3/s
 3.0000E-04 d Srough                    -130.70    D Ph(U)     deg
                                        -1368.2    E Hdot      W
 helium     Gas type                    -1368.2    F Work      W
 stainless  Solid type                    -0.5225  G HeatIn    W
!--------------------------------- 7 ---------------------------------
 ISODUCT    180 bend plus brass connecting flange (pg 27 book 4)
 8.1500E-03 a Area       m^2            3.1575E+05 A |p|        Pa
    0.3200  b Perim      m                 2.6691  B Ph(p)     deg
    0.3480  c Length     m              9.8509E-02 C |U|      m^3/s
 6.0000E-04 d Srough                    -92.484    D Ph(U)     deg
                                        -1396.9    E Hdot      W
 helium     Gas type                    -1396.9    F Work      W
 stainless  Solid type                    -28.728  G HeatIn    W
!--------------------------------- 8 ---------------------------------
 RPNTARGET  Calc minor loss resistor for 180 bend (pg 28,52 book 4)
    0.5000  a Target           (t)        778.61    A RPNval
 1.05  7C *  8a *  7a /  7a /
!--------------------------------- 9 ---------------------------------
 IMPEDANCE  Minor loss resistor for 180 bend (pg 28 book 4)
 sameas  8A  a Re(Zs) Pa-s/m^3          3.1576E+05 A |p|        Pa
    0.0000  b Im(Zs) Pa-s/m^3              2.6829  B Ph(p)     deg
                                        9.8509E-02 C |U|      m^3/s
                                         -92.484   D Ph(U)     deg
                                        -1400.7    E Hdot      W
 helium     Gas type                    -1400.7    F Work      W
 ideal      Solid type                    -3.7778  G HeatIn    W
!-------------------------------- 10 ---------------------------------
 ISOCONE    4" to 3" Concentric reducer (pg 36 book 4)
 8.1070E-03 a AreaI      m^2            3.1113E+05 A |p|        Pa
    0.3190  b PerimI     m                 2.7551  B Ph(p)     deg
    0.1020  c Length     m                 0.1181  C |U|      m^3/s
 sameas 13a d AreaF      m^2     S=-3     -91.644   D Ph(U)     deg
    0.2390  e PerimF     m    Fnc(10d) -1409.6     E Hdot      W
 6.0000E-04 f Srough                    -1409.6    F Work      W
 helium     Gas type                      -8.8766  G HeatIn    W
 stainless  Solid type
!-------------------------------- 11 ---------------------------------
 RPNTARGET  Calculate minor loss resistor for 4" to 3" exp (pg 37 book 4
    0.2600  a Target           (t)       1550.9     A RPNval
 1.05 10C * 10d / 10d / 11a *
!-------------------------------- 12 ---------------------------------
 IMPEDANCE  Minor loss resistor for 4" to 3" expansion (pg 37 book 4)
 sameas 11A  a Re(Zs) Pa-s/m^3          3.1114E+05 A |p|        Pa
```

```
    0.0000  b Im(Zs) Pa-s/m^3              2.7887  B Ph(p)      deg
                                           0.1181  C |U|      m^3/s
                                         -91.644   D Ph(U)      deg
                                       -1420.4     E Hdot       W
helium      Gas type                   -1420.4     F Work       W
ideal       Solid type                   -10.822   G HeatIn     W
!---------------------------------- 13 ----------------------------------
ISODUCT     3" FB Duct - Length given in concept.skf
 4.5600E-03 a Area       m^2    S=-2   2.9173E+05 A |p|        Pa
    0.2390  b Perim      m    Fnc(13a)    3.0672  B Ph(p)      deg
    0.2600  c Length     m                0.1533  C |U|      m^3/s
 3.0000E-04 d Srough                    -90.650   D Ph(U)      deg
                                       -1449.9     E Hdot       W
helium      Gas type                   -1449.9     F Work       W
stainless   Solid type                   -29.529   G HeatIn     W
!---------------------------------- 14 ----------------------------------
RPNTARGET   Calc minor loss resistor for 1/2 of elbow (pg 37,52 book 4)
    0.1700  a Target            (t)     1316.1     A RPNval
1.05 13C * 16a / 16a / 14a *
!---------------------------------- 15 ----------------------------------
IMPEDANCE   Minor loss resistor for 1/2 of elbow (pg 37 book 4)
sameas 14A  a Re(Zs) Pa-s/m^3          2.9174E+05 A |p|        Pa
    0.0000  b Im(Zs) Pa-s/m^3              3.1067  B Ph(p)      deg
                                           0.1533  C |U|      m^3/s
                                         -90.650   D Ph(U)      deg
                                       -1465.4     E Hdot       W
helium      Gas type                   -1465.4     F Work       W
ideal       Solid type                   -15.469   G HeatIn     W
!---------------------------------- 16 ----------------------------------
ISOCONE     3.5" to 3" Long radius reducing elbow (pg 36 book 4)
sameas 13a  a AreaI     m^2    S=-2    2.7526E+05 A |p|        Pa
    0.2390  b PerimI    m    Fnc(16a)    3.3339  B Ph(p)      deg
    0.2090  c Length    m                0.1845  C |U|      m^3/s
 6.2070E-03 d AreaF     m^2            -90.038   D Ph(U)      deg
    0.2790  e PerimF    m            -1493.7     E Hdot       W
 6.0000E-04 f Srough                 -1493.7     F Work       W
helium      Gas type                   -28.310   G HeatIn     W
stainless   Solid type
!---------------------------------- 17 ----------------------------------
RPNTARGET   Calc minor loss resistor for 2nd 1/2 of elbow (pg 37 book 4)
    0.1700  a Target            (t)      854.91    A RPNval
1.05 16C * 16d / 16d / 17a *
!---------------------------------- 18 ----------------------------------
IMPEDANCE   Minor loss resistor for 2nd 1/2 of elbow (pg 37 book 4)
sameas 17A  a Re(Zs) Pa-s/m^3          2.7527E+05 A |p|        Pa
```

```
    0.0000  b Im(Zs) Pa-s/m^3              3.3667  B Ph(p)      deg
                                           0.1845  C |U|      m^3/s
                                         -90.038   D Ph(U)      deg
                                        -1508.3     E Hdot       W
 helium     Gas type                    -1508.3     F Work       W
 ideal      Solid type                    -14.554   G HeatIn     W
!---------------------------------- 19 ----------------------------------
 ISODUCT    FB connector/part of tee (Pg 55 book 4 concept.skf)
 6.2070E-03 a Area      m^2             2.6989E+05 A |p|        Pa
    0.2790  b Perim     m                  3.4386  B Ph(p)      deg
 7.0000E-02 c Length    m                  0.1962  C |U|      m^3/s
 6.0000E-04 d Srough                     -89.848   D Ph(U)      deg
                                        -1517.5     E Hdot       W
 helium     Gas type                    -1517.5     F Work       W
 stainless  Solid type                    -9.2787  G HeatIn     W
!---------------------------------- 20 ----------------------------------
 RPNTARGET  Calc minor loss resistor for FB-Res (pg 53-55 book 4)
    0.3400  a Target            (t)     2053.6     A RPNval
 1.05 39C SQRD * 19C / 48a / 48a / 20a *
!---------------------------------- 21 ----------------------------------
 IMPEDANCE  Minor loss resistor for FB to resonator junction
 sameas 20A a Re(Zs) Pa-s/m^3           2.6992E+05 A |p|        Pa
    0.0000  b Im(Zs) Pa-s/m^3              3.5240  B Ph(p)      deg
                                           0.1962  C |U|      m^3/s
                                         -89.848   D Ph(U)      deg
                                        -1557.1     E Hdot       W
 helium     Gas type                    -1557.1     F Work       W
 ideal      Solid type                    -39.515   G HeatIn     W
!---------------------------------- 22 ----------------------------------
 SOFTEND    End of feedback branch
    0.0000  a Re(Z)              (t)     2.6992E+05 A |p|        Pa
    0.0000  b Im(Z)              (t)       3.5240  B Ph(p)      deg
                                           0.1962  C |U|      m^3/s
                                         -89.848   D Ph(U)      deg
                                        -1557.1     E Hdot       W
                                        -1557.1     F Work       W
                                        -9.9306E-02 G Re(Z)
 helium     Gas type                       1.6856  H Im(Z)
 ideal      Solid type                   302.00    I   T        K
!---------------------------------- 23 ----------------------------------
 ISODUCT    Dummy duct used to get input properties
    1.0000  a Area      m^2             3.1000E+05 A |p|        Pa
    1.0000  b Perim     m                  0.0000  B Ph(p)      deg
    0.0000  c Length    m               8.8813E-03 C |U|      m^3/s
    0.0000  d Srough                      23.395   D Ph(U)      deg
```

```
                                        1263.4      E Hdot       W
helium      Gas type                    1263.4      F Work       W
ideal       Solid type                    0.0000    G HeatIn     W
!---------------------------------- 24 ----------------------------------
TXFRST      Main room temp water HX (pg 90 book 3)
 6.6580E-03 a Area       m^2            3.1008E+05 A |p|        Pa
    0.2275  b GasA/A                   -5.7858E-02 B Ph(p)      deg
 2.0400E-02 c Length     m              8.4615E-03 C |U|      m^3/s
 1.2700E-03 d radius     m                17.266   D Ph(U)      deg
-1620.9     e HeatIn     W      G       -357.45    E Hdot       W
  300.00    f Est-T      K      (t)     1252.4     F Work       W
helium      Gas type                   -1620.9     G Heat       W
stainless   Solid type                  268.66     H MetalT     K
!---------------------------------- 25 ----------------------------------
STKDUCT     Regen cold end dead space due to ribs (pg 91 book 3)
 4.9700E-03 a Area       m^2            3.1008E+05 A |p|        Pa
    0.7400  b Perim      m             -6.0230E-02 B Ph(p)      deg
 3.1750E-03 c Length     m              8.3289E-03 C |U|      m^3/s
 2.7000E-02 d WallA      m^2              14.079   D Ph(U)      deg
                                       -357.45    E Hdot       W
                                       1252.2     F Work       W
                                        302.00    G T-beg      K
helium      Gas type                    314.90    H T-end      K
stainless   Solid type                   -0.1465  I StkWrk     W
!---------------------------------- 26 ----------------------------------
STKSCREEN   Regenerator (pg 92 book 3) (Ks frac est:pg 20 book 4)
 6.2070E-03 a Area       m^2            2.7522E+05 A |p|        Pa
    0.7190  b VolPor                      3.7737  B Ph(p)      deg
 7.3000E-02 c Length     m              3.2050E-02 C |U|      m^3/s
 4.2200E-05 d   r_H      m               -39.852   D Ph(U)      deg
    0.3000  e KsFrac                   -357.45    E Hdot       W
                                        3192.5     F Work       W
                                        314.90     G T-beg      K
helium      Gas type                   1000.0     H T-end      K
stainless   Solid type                 1940.3     I StkWrk     W
!---------------------------------- 27 ----------------------------------
RPNTARGET   Fix hot end gas temperature
 1000.0      a Target          =27A?    1000.0     A RPNval
26H
!---------------------------------- 28 ----------------------------------
RPNTARGET   Estimated heat leak through FiberFrax (pg 22 book 4)
    0.0000  a Target            (t)      282.63    A RPNval
26H 273 - 1.89 * 26H 273 - 1.11E-4 * 0.125 + *
!---------------------------------- 29 ----------------------------------
INSDUCT     All regen hot end dead space (pg 92 book 3)(area is avg)
```

```
 4.6200E-03 a Area       m^2              2.7518E+05 A |p|        Pa
    2.0000  b Perim      m                  3.7669  B Ph(p)     deg
 8.7000E-03 c Length     m                3.2811E-02 C |U|      m^3/s
 6.0000E-04 d Srough                       -41.385  D Ph(U)     deg
                                          -357.45   E Hdot       W
helium      Gas type                     3183.7    F Work       W
stainless   Solid type                     0.0000  G HeatIn     W
!-------------------------------- 30 --------------------------------
HXMIDL      HHX (pg 93 book 4) heat xfer area used/not acoustic area
 5.6970E-03 a Area       m^2              2.7515E+05 A |p|        Pa
    0.9867  b GasA/A                        3.7634  B Ph(p)     deg
 6.3500E-03 c Length     m                3.3501E-02 C |U|      m^3/s
 7.9400E-04 d y0         m                 -42.982  D Ph(U)     deg
 3599.7     e HeatIn     W       G        3242.3    E Hdot       W
  900.00    f Est-T      K       (t)      3158.2    F Work       W
helium      Gas type                     3599.7    G Heat       W
stainless   Solid type                   1095.0    H MetalT     K
!-------------------------------- 31 --------------------------------
STKDUCT     hhx dead space (pg 94 book 3) stainless used for Qdot
 5.4400E-03 a Area       m^2              2.7514E+05 A |p|        Pa
    0.2620  b Perim      m                  3.7610  B Ph(p)     deg
 3.6830E-03 c Length     m                3.3896E-02 C |U|      m^3/s
 4.0540E-03 d WallA      m^2               -43.616  D Ph(U)     deg
                                          3242.3    E Hdot       W
                                          3157.7    F Work       W
                                          1000.0    G T-beg      K
helium      Gas type                      995.76   H T-end      K
stainless   Solid type                    -0.5036  I StkWrk     W
!-------------------------------- 32 --------------------------------
STKDUCT     Straight section of pulse tube (pg 101 bk 4)
 6.2070E-03 a Area       m^2     S=-2     2.7477E+05 A |p|        Pa
    0.2790  b Perim      m    Fnc(32a)      3.7072  B Ph(p)     deg
 8.0000E-02 c Length     m                4.4652E-02 C |U|      m^3/s
 1.1600E-03 d WallA      m^2               -55.409  D Ph(U)     deg
                                          3242.3    E Hdot       W
                                          3148.9    F Work       W
                                           995.76   G T-beg      K
helium      Gas type                      748.68   H T-end      K
stainless   Solid type                    -8.8289  I StkWrk     W
!-------------------------------- 33 --------------------------------
STKCONE     Taperred section of pulse tube (pg 101 bk 4)
sameas 32a  a AreaI     m^2              2.7272E+05 A |p|        Pa
sameas 32b  b PerimI    m^2                3.5274  B Ph(p)     deg
    0.1600  c Length     m               7.1159E-02 C |U|      m^3/s
 7.3700E-03 d AreaF      m^2     S=-3      -67.560  D Ph(U)     deg
```

```
   0.3048  e PerimF      m     Fnc(33d)  3242.3      E Hdot       W
 1.1400E-02 f f_wall                    3145.1      F Work       W
                                         748.68     G T-beg      K
helium      Gas type                    296.41      H T-end      K
stainless   Solid type                   -3.7294    I StkWrk     W
!-------------------------------- 34 --------------------------------
TXLASt      Small water Xger
 6.6580E-03 a Area       m^2            2.7167E+05  A |p|        Pa
    0.2690  b GasA/A                      3.4652    B Ph(p)      deg
 1.0160E-02 c Length     m              7.1632E-02  C |U|        m^3/s
 2.2860E-03 d radius     m               -67.707    D Ph(U)      deg
 -250.00    e HeatIn     W       (t)    3140.1      E Hdot       W
  290.00    f Est-T      K     =34H?    3140.1      F Work       W
sameas  0   Gas type                   -102.14     G Heat       W
ideal       Solid type                  290.00     H MetalT     K
!-------------------------------- 35 --------------------------------
ISODUCT     PT connector (see pg 55 book 4 and concept.skf)
 6.2070E-03 a Area       m^2            2.7015E+05  A |p|        Pa
    0.2790  b Perim      m                3.3628    B Ph(p)      deg
 5.1000E-02 c Length     m              7.9654E-02  C |U|        m^3/s
 6.0000E-04 d Srough                     -69.683    D Ph(U)      deg
                                        3137.4      E Hdot       W
helium      Gas type                   3137.4      F Work       W
stainless   Solid type                   -2.7235    G HeatIn     W
!-------------------------------- 36 --------------------------------
RPNTARGET   Calc velocity in after union for minor loss
    0.0000  a Target           (t)        0.2723    A RPNval
35D 22D - COS 35C * 22C + SQRD 35D 22D - SIN 35C * SQRD + SQRT
!-------------------------------- 37 --------------------------------
RPNTARGET   Calc minor loss resistor for PT to resonantor (pg 45 book 4)
    0.6700  a Target           (t)     9966.4      A RPNval
1.05 36A SQRD * 35C / 48a / 48a / 37a *
!-------------------------------- 38 --------------------------------
IMPEDANCE   Minor loss resistor for PT-Res (pg 53-55 book 4)
sameas 37A  a Re(Zs) Pa-s/m^3          2.6992E+05  A |p|        Pa
    0.0000  b Im(Zs) Pa-s/m^3            3.5240    B Ph(p)      deg
                                       7.9654E-02  C |U|        m^3/s
                                        -69.683    D Ph(U)      deg
                                       3105.8      E Hdot       W
helium      Gas type                   3105.8      F Work       W
ideal       Solid type                  -31.617    G HeatIn     W
!-------------------------------- 39 --------------------------------
UNION       Rejoin
   22.000   a TendSg                   2.6992E+05  A |p|        Pa
 2.6992E+05 b |p|End     Pa    =39A?     3.5240    B Ph(p)      deg
```

```
    3.5240  c Ph(p)E    deg   =39B?        0.2723  C |U|      m^3/s
                                          -84.061   D Ph(U)     deg
                                         1548.7     E Hdot      W
 helium      Gas type                    1548.7     F Work      W
 ideal       Solid type                     0.0000  G HeatIn    W
!-------------------------------- 40 --------------------------------
 ISODUCT     Section of 3.5" tee
  6.2070E-03 a Area       m^2          2.5893E+05  A |p|        Pa
     0.2790  b Perim      m               3.4433  B Ph(p)     deg
  9.5300E-02 c Length     m               0.2878  C |U|      m^3/s
  6.0000E-04 d Srough                   -84.211   D Ph(U)     deg
                                         1524.8     E Hdot      W
 helium      Gas type                    1524.8     F Work      W
 stainless   Solid type                  -23.965   G HeatIn    W
!-------------------------------- 41 --------------------------------
 RPNTARGET   Calc minor loss resistor for 3.5" to 4" adapt (pg 93 bk 4)
  2.0000E-02 a Target           (t)       148.44    A RPNval
 1.05 39C * 43a / 43a / 41a *
!-------------------------------- 42 --------------------------------
 IMPEDANCE   Minor loss resistor for 3.5" to 4" adapter (pg 93 bk 4)
 sameas 41A  a Re(Zs) Pa-s/m^3         2.5893E+05  A |p|        Pa
     0.0000  b Im(Zs) Pa-s/m^3            3.4527  B Ph(p)     deg
                                          0.2878  C |U|      m^3/s
                                         -84.211   D Ph(U)     deg
                                         1518.6     E Hdot      W
 helium      Gas type                    1518.6     F Work      W
 ideal       Solid type                    -6.1459  G HeatIn    W
!-------------------------------- 43 --------------------------------
 ISOCONE     3.5" to 4" cone to adapt to resonator (pg 93 book 4)
  6.2070E-03 a AreaI      m^2          2.4783E+05  A |p|        Pa
     0.2790  b PerimI     m               3.3664  B Ph(p)     deg
     0.1040  c Length     m               0.3062  C |U|      m^3/s
  8.1070E-03 d AreaF      m^2           -84.371   D Ph(U)     deg
     0.3200  e PerimF     m            1498.3     E Hdot      W
  3.0000E-04 f Srough                  1498.3     F Work      W
 helium      Gas type                   -20.290   G HeatIn    W
 stainless   Solid type
!-------------------------------- 44 --------------------------------
 ISODUCT     Initial section of resonator
  8.1070E-03 a Area       m^2          2.4233E+05  A |p|        Pa
     0.3200  b Perim      m               3.3234  B Ph(p)     deg
  5.6000E-02 c Length     m               0.3172  C |U|      m^3/s
  6.0000E-04 d Srough                   -84.459   D Ph(U)     deg
                                         1487.4     E Hdot      W
 helium      Gas type                    1487.4     F Work      W
```

```
stainless  Solid type                    -10.941   G HeatIn    W
!---------------------------------- 45 ----------------------------------
RPNTARGET  Guess at 1/Re[Zbranch]
 2.4773E-08 a Target            G       2.4773E-08 A RPNval
45a
!---------------------------------- 46 ----------------------------------
RPNTARGET  Calculate Zbranch
    0.0000  a Target            (t)     4.0367E+07 A RPNval
1 45A /
!---------------------------------- 47 ----------------------------------
BRANCH     RC dissipator - Imaginary part is not set yet
sameas 46A  a Re(Zb) Pa-s/m^3           2.4233E+05 A |p|       Pa
    0.0000  b Im(Zb) Pa-s/m^3              3.3234  B Ph(p)     deg
                                           0.3170  C |U|     m^3/s
                                         -85.543   D Ph(U)     deg
                                         760.02    E Hdot      W
helium     Gas type                      760.02    F Work      W
ideal      Solid type                    727.38    G Work_B    W
!---------------------------------- 48 ----------------------------------
ISODUCT    Continuation of resonator
sameas 44a  a Area      m^2             1.4307E+04 A |p|       Pa
    0.3189  b Perim      m              -172.90    B Ph(p)     deg
    1.8500  c Length     m                0.4990  C |U|     m^3/s
sameas 44d  d Srough                    -86.201   D Ph(U)     deg
                                        205.31    E Hdot      W
helium     Gas type                     205.31    F Work      W
stainless  Solid type                   -554.71   G HeatIn    W
!---------------------------------- 49 ----------------------------------
RPNTARGET  Calc length of 7deg cone (pg 87 book 4)
    0.0000  a Target            (t)        1.2502  A RPNval
.2545 4 48a * 3.14159 / sqrt - .1223 /
!---------------------------------- 50 ----------------------------------
RPNTARGET  Calc minor loss coeff for 7 deg diffuser
    0.1200  a Target            (t)      956.71    A RPNval
1.05 48C * 48a / 48a / 50a *
!---------------------------------- 51 ----------------------------------
IMPEDANCE  Minor loss resistor for 7 deg diffuser
sameas 50A  a Re(Zs) Pa-s/m^3           1.4287E+04 A |p|       Pa
    0.0000  b Im(Zs) Pa-s/m^3          -174.82    B Ph(p)     deg
                                           0.4990  C |U|     m^3/s
                                         -86.201   D Ph(U)     deg
                                          86.188   E Hdot      W
helium     Gas type                      86.188    F Work      W
ideal      Solid type                   -119.13    G HeatIn    W
!---------------------------------- 52 ----------------------------------
```

```
ISOCONE    7 degree cone - 10.02" final diameter
sameas 48a  a AreaI     m^2     S=-2     8.6185E+04 A |p|       Pa
    0.3194  b PerimI     m     Fnc(52a)  -176.16    B Ph(p)     deg
sameas 49A  c Length     m                 0.2661   C |U|     m^3/s
 5.0870E-02 d AreaF      m^2              -86.205   D Ph(U)     deg
    0.8000  e PerimF     m                 9.6170   E Hdot      W
sameas 48d  f Srough                      9.6170   F Work      W
helium      Gas type                     -76.571   G HeatIn    W
stainless   Solid type
!---------------------------------- 53 ----------------------------------
ISODUCT    10" duct                          P8
 5.0870E-02 a Area       m^2               8.9816E+04 A |p|       Pa
    0.8000  b Perim      m                 -176.16    B Ph(p)     deg
    0.4088  c Length     m                 8.5729E-02 C |U|     m^3/s
sameas 48d  d Srough                      -86.206    D Ph(U)     deg
                                            3.0371   E Hdot      W
helium      Gas type                        3.0371   F Work      W
stainless   Solid type                     -6.5799   G HeatIn    W
!---------------------------------- 54 ----------------------------------
ISODUCT    10" duct
 5.0870E-02 a Area       m^2               9.0079E+04 A |p|       Pa
    0.8000  b Perim      m                 -176.16    B Ph(p)     deg
 7.6200E-02 c Length     m                 5.1487E-02 C |U|     m^3/s
sameas 48d  d Srough                      -86.206    D Ph(U)     deg
                                            1.8215   E Hdot      W
helium      Gas type                        1.8215   F Work      W
stainless   Solid type                     -1.2156   G HeatIn    W
!---------------------------------- 55 ----------------------------------
ISODUCT    ellipsoidal head
 5.0870E-02 a Area       m^2               9.0227E+04 A |p|       Pa
    0.8000  b Perim      m                 -176.16    B Ph(p)     deg
    0.1143  c Length     m                 5.1221E-07 C |U|     m^3/s
sameas 48d  d Srough                        94.624   D Ph(U)     deg
                                          3.1683E-04 E Hdot      W
helium      Gas type                      3.1683E-04 F Work      W
stainless   Solid type                     -1.8212   G HeatIn    W
!---------------------------------- 56 ----------------------------------
HARDEND    end of duct
    0.0000  a R(1/Z)          =56G?       9.0227E+04 A |p|       Pa
    0.0000  b I(1/Z)          =56H?       -176.16    B Ph(p)     deg
                                          5.1221E-07 C |U|     m^3/s
                                            94.624   D Ph(U)     deg
                                          3.1683E-04 E Hdot      W
                                          3.1683E-04 F Work      W
                                          7.8115E-09 G R(1/Z)
```

```
 helium     Gas type                    -5.6968E-07 H I(1/Z)
 stainless  Solid type                    296.41    I  T       K
!--------------------------------- 57 ---------------------------------
 RPNTARGET  Stirling figure of merit based on metal temperatures
     0.0000  a Target            (t)        0.5447  A RPNval
 39F 30G 28A + / 30H * 30H 293 - /
!--------------------------------- 58 ---------------------------------
 RPNTARGET  System figure of merit based on metal temperatures
     0.0000  a Target            (t)        0.2558  A RPNval
 47G 30G 28A + / 30H * 30H 293 - /

! The restart information below was generated by a previous run
! You may wish to delete this information before starting a run
! where you will (interactively) specify a different iteration
! mode.  Edit this table only if you really know your model!
INVARS      6  0  2  1  1  1  2 24  5 30  5 45  1
TARGS       6 27  1 34  6 39  2 39  3 56  1 56  2
SPECIALS    6 10 -3 13 -2 16 -2 32 -2 33 -3 52 -2
```

9.4. Traveling-wave refrigerator

Cryenco is presently unwilling to share construction details of the refrigerator of Fig. 1.15 publicly, so this model only covers the *LRC* network at the top of Fig. 1.16. The model starts in the compliance and ends just above the hot heat exchanger at the top of the pulse tube. The point of view adopted in this particular file is this: In order to achieve the values of p_1 (both magnitude and phase) in the compliance and at the top of the pulse tube that were observed in a certain experiment, what must the flow resistances of the two valves be? One of those resistances has turned out to be negative, indicating an error in the model—perhaps DeltaE's estimate of turbulent effects in the inertance is inaccurate.

```
TITLE     LRC network only
!->ptrstrp.out
!Created@14:10:27  2-Jan-99 with DeltaE Vers. 4.5b7 for the IBM/PC-Compatible
!--------------------------------  0 ---------------------------------
 BEGIN      at compliance!
  3.1114E+06 a Mean P     Pa              6.4274E+06 A Re(Zb) G( 2a)      P
    42.000   b Freq.      Hz              2.8415E+06 B Im(Zb) G( 2b)      P
   305.20    c T-beg      K               2.2699E+07 C Re(Zs) G( 4a)      P
  9.3205E+04 d |p|@0      Pa             -1.4258E+05 D Re(Zs) G( 9a)      P
  -153.30    e Ph(p)0     deg
     0.0000  f |U|@0      m^3/s
     0.0000  g Ph(U)0     deg
 helium     Gas type
 ideal      Solid type
```

```
!-------------------------------  1 -------------------------------
COMPLIANCE reserv. vol.
    0.3000  a SurfAr     m^2            9.3205E+04 A |p|        Pa
 9.8100E-03 b Volum      m^3            -153.30    B Ph(p)      deg
                                        4.6530E-02 C |U|      m^3/s
                                         116.57    D Ph(U)      deg
                                          -4.7356  E Hdot       W
sameas  0  Gas type                       -4.7356  F Work       W
ideal      Solid type                     -4.7356  G HeatIn     W
!-------------------------------  2 -------------------------------
TBRANCH    to bypass path
 6.4274E+06 a Re(Zb) Pa-s/m^3   G       9.3205E+04 A |p|        Pa
 2.8415E+06 b Im(Zb) Pa-s/m^3   G       -153.30    B Ph(p)      deg
                                        1.3263E-02 C |U|      m^3/s
                                        -177.15    D Ph(U)      deg
                                         565.31    E Hdot       W
sameas  0  Gas type                      565.31    F Work       W
ideal      Solid type                   -570.05    G Work_T     W
!-------------------------------  3 -------------------------------
ISODUCT    nuisance inertance
 3.4000E-04 a Area       m^2            8.0592E+04 A |p|        Pa
 6.5400E-02 b Perim       m              173.61    B Ph(p)      deg
    1.0000  c Length      m             1.3511E-02 C |U|      m^3/s
 3.0000E-04 d Srough                     176.46    D Ph(U)      deg
                                         543.77    E Hdot       W
sameas  0  Gas type                      543.77    F Work       W
ideal      Solid type                    -21.545   G HeatIn     W
!-------------------------------  4 -------------------------------
IMPED      bypass valve
 2.2699E+07 a Re(Zs) Pa-s/m^3   G       2.2623E+05 A |p|        Pa
    0.0000  b Im(Zs) Pa-s/m^3             -2.5287  B Ph(p)      deg
                                        1.3511E-02 C |U|      m^3/s
                                         176.46    D Ph(U)      deg
                                        -1528.1    E Hdot       W
sameas  0  Gas type                     -1528.1    F Work       W
ideal      Solid type                   -2071.9    G HeatIn     W
!-------------------------------  5 -------------------------------
COMPL      little header
 1.0000E-03 a SurfAr     m^2            2.2623E+05 A |p|        Pa
 3.0000E-05 b Volum      m^3              -2.5287  B Ph(p)      deg
                                        1.3510E-02 C |U|      m^3/s
                                         177.92    D Ph(U)      deg
                                        -1528.2    E Hdot       W
sameas  0  Gas type                     -1528.2    F Work       W
ideal      Solid type                   -9.3003E-02 G HeatIn    W
```

```
!---------------------------------- 6 ----------------------------------
 ISODUCT     short tube
 sameas  3a  a Area        m^2            2.2650E+05 A |p|         Pa
 sameas  3b  b Perim        m               -0.9736  B Ph(p)      deg
     0.1200  c Length       m            1.3536E-02 C |U|       m^3/s
 sameas  3d  d Srough                       180.00    D Ph(U)      deg
                                           -1532.7    E Hdot       W
 sameas  0   Gas type                      -1532.7    F Work       W
 ideal       Solid type                      -4.5318  G HeatIn     W
!---------------------------------- 7 ----------------------------------
 SOFTEND     connect bypass to tr
     0.0000  a Re(Z)               (t)     2.2650E+05 A |p|         Pa
     0.0000  b Im(Z)               (t)       -0.9736  B Ph(p)      deg
                                           1.3536E-02 C |U|       m^3/s
                                            180.00    D Ph(U)      deg
                                           -1532.7    E Hdot       W
                                           -1532.7    F Work       W
                                              -1.1276 G Re(Z)
 sameas  0   Gas type                       1.9123E-02 H Im(Z)
 ideal       Solid type                     305.20    I   T         K
!---------------------------------- 8 ----------------------------------
 ISODUCT     the inertance
  4.6400E-04 a Area        m^2            2.1066E+05 A |p|         Pa
  7.6360E-02 b Perim        m               -3.0564  B Ph(p)      deg
     2.4900  c Length       m            3.9429E-02 C |U|       m^3/s
 sameas  3d  d Srough                       104.14    D Ph(U)      deg
                                           -1227.9    E Hdot       W
 sameas  0   Gas type                      -1227.9    F Work       W
 ideal       Solid type                     -657.84   G HeatIn     W
!---------------------------------- 9 ----------------------------------
 IMPEDANCE   valve-inertance set
 -1.4258E+05 a Re(Zs) Pa-s/m^3   G      2.0907E+05 A |p|         Pa
     0.0000  b Im(Zs) Pa-s/m^3            -1.5845  B Ph(p)      deg
                                           3.9429E-02 C |U|       m^3/s
                                            104.14    D Ph(U)      deg
                                           -1117.1    E Hdot       W
 sameas  0   Gas type                      -1117.1    F Work       W
 ideal       Solid type                     110.83    G HeatIn     W
!---------------------------------- 10 ---------------------------------
 COMPL       little header
  2.0000E-03 a SurfAr      m^2            2.0907E+05 A |p|         Pa
  6.0000E-05 b Volum       m^3              -1.5845  B Ph(p)      deg
                                           3.8815E-02 C |U|       m^3/s
                                            104.40    D Ph(U)      deg
                                           -1117.2    E Hdot       W
```

```
sameas  0  Gas type                      -1117.2     F Work       W
ideal      Solid type                      -0.1588   G HeatIn     W
!--------------------------------- 11 ---------------------------------
ISODUCT    short tube
sameas  6a  a Area       m^2             2.2650E+05 A |p|        Pa
sameas  6b  b Perim       m                -0.9736  B Ph(p)      deg
sameas  6c  c Length      m              3.8344E-02 C |U|      m^3/s
sameas  6d  d Srough                       104.67    D Ph(U)      deg
                                          -1170.8    E Hdot       W
sameas  0  Gas type                       -1170.8    F Work       W
ideal      Solid type                      -53.541   G HeatIn     W
!--------------------------------- 12 ---------------------------------
UNION      connect bypass here
    7.0000  a TendSg                     2.2650E+05 A |p|        Pa
 2.2650E+05 b |p|End    Pa    =12A?       -0.9736  B Ph(p)      deg
   -0.9736  c Ph(p)E    deg   =12B?     4.3776E-02 C |U|      m^3/s
                                           122.07    D Ph(U)      deg
                                          -2703.5    E Hdot       W
sameas  0  Gas type                       -2703.5    F Work       W
ideal      Solid type                       0.0000   G HeatIn     W
!--------------------------------- 13 ---------------------------------
ISODUCT    short tube
sameas  8a  a Area       m^2             2.3837E+05 A |p|        Pa
sameas  8b  b Perim       m                0.5000   B Ph(p)      deg
    0.1100  c Length      m              4.3251E-02 C |U|      m^3/s
 3.0000E-04 d Srough                       122.58    D Ph(U)      deg
                                          -2738.1    E Hdot       W
sameas  0  Gas type                       -2738.1    F Work       W
ideal      Solid type                      -34.620   G HeatIn     W
!--------------------------------- 14 ---------------------------------
FREETARG   pulsetube magnitud
 2.3837E+05 a Target          =14A?      2.3837E+05 A FreeT
 13A b ResAdr
!--------------------------------- 15 ---------------------------------
FREETARG   pulsetube  phase
    0.5000  a Target          =15A?        0.5000   A FreeT
 13B b ResAdr
!--------------------------------- 16 ---------------------------------
COMPLIANCE volume under head
 1.0000E-02 a SurfAr    m^2              2.3837E+05 A |p|        Pa
 7.5000E-05 b Volum     m^3                 0.5000  B Ph(p)      deg
                                          4.2488E-02 C |U|      m^3/s
                                           123.25    D Ph(U)      deg
                                          -2739.1    E Hdot       W
sameas  0  Gas type                       -2739.1    F Work       W
```

```
 ideal      Solid type                    -1.0325  G HeatIn    W

! The restart information below was generated by a previous run
! You may wish to delete this information before starting a run
! where you will (interactively) specify a different iteration
! mode.  Edit this table only if you really know your model!
INVARS      4  2  1  2  2  4  1  9  1
TARGS       4 12  2 12  3 14  1 15  1
SPECIALS    0
```

10. List of Symbols

Roman

A	area, or amplitude, or a constant
a	sound speed
B	magnetic field, or flow availability
b	exponent for T dependence of μ or k, or flow availability per unit mass
C	compliance, or a constant
c	compliance per unit length
COP	coefficient of performance
c_p	isobaric heat capacity per unit mass
D	diameter
e	complex gain factor arising in continuity equation
E	energy
$\dot{E}$	acoustic power
F	a function
f	frequency, or spatially averaged thermoviscous function
G	conductance (inverse of resistance)
H	total energy
$\dot{H}$	rate at which total energy flows (total power)
h	thermoviscous function, or enthalpy per unit mass
I	electric current
i	$\sqrt{-1}$
j	electrical current density
K	minor-loss coefficient
k	thermal conductivity
L	inertance, or length
l	inertance per unit length
m	mass, or multiplier for turbulent viscous dissipation
N_R	Reynolds number
p	pressure
Q	heat, or quality factor of resonance
$\dot{Q}$	rate at which heat is transferred (thermal power)
R	resistance, or gas constant, or radius
r	resistance per unit length, or radius, or radial coordinate
S	entropy, or surface area
s	entropy per unit mass
T	temperature
t	time

U volumetric velocity
u x component on velocity
V volume
v y component of velocity
W work
$\dot{W}$ rate at which work is done (mechanical power)
w z component of velocity
x coordinate along sound-propagation direction
X exergy
$\dot{X}$ rate at which exergy flows (power)
y coordinate perpendicular to sound-propagation direction
z coordinate perpendicular to sound-propagation direction, or specific acoustic impedance
Z acoustic impedance

Greek

α attenuation constant
Γ normalized temperature gradient
γ ratio of isobaric to isochoric specific heats
Δ big difference
δ penetration depth, or small difference
ε surface roughness
ϵ internal energy per unit mass
η efficiency
κ thermal diffusivity
λ wavelength
μ dynamic viscosity
ν kinematic viscosity
π 3.14159...
ψ Rott's joining function
ρ density
σ Prantl number, or electrical conductivity
ϕ phase angle
Φ viscous dissipation function
θ phase angle
ω angular frequency
ζ bulk viscosity
ξ arbitrary variable

Subscripts

C	cold, or Carnot
H	hot
h	hydraulic (i.e., R_h is hydraulic radius)
m	mean (or mechanical)
R	Reynolds (in N_R)
κ	thermal
ν	viscous
0	"environment"
1	first-order (usually a complex amplitude)
2	second-order
gen	generated
ref	reference location or temperature
reg	regenerator
pt	pulse tube
crit	critical (i.e., ∇T_{crit})

Special symbols

Im[ ]	Imaginary part of
Re[ ]	Real part of
$\langle\rangle$	average in y, z plane
||	magnitude of complex number
overdot	time derivative
overbar	time average, time rate
tilde	complex conjugate

BIBLIOGRAPHY

[1] G. J. Van Wylen and R. E. Sonntag. *Fundamentals of Classical Thermodynamics.* Wiley, 1965.

[2] H. B. Callen. *Thermodynamics and an Introduction to Thermostatistics.* Wiley, 1985.

[3] P. M. Morse. *Thermal Physics.* Benjamin, 1969.

[4] G. Walker. *Stirling Engines.* Clarendon, Oxford, 1960.

[5] G. Walker. *Cryocoolers.* Plenum, New York, 1983.

[6] J. R. Senft. *Ringbom Stirling Engines.* Oxford University Press, 1993.

[7] I. Urieli and D. M. Berchowitz. *Stirling Cycle Engine Analysis.* Adam Hilger, Bristol UK, 1984.

[8] C. D. West. *Liquid Piston Stirling Engines.* Van Nostrand Reinhold, 1983.

[9] P. H. Ceperley. A pistonless stirling engine–the traveling wave heat engine. *J. Acoust. Soc. Am.*, 66:1508–1513, 1979.

[10] P. H. Ceperley. Gain and efficiency of a short traveling wave heat engine. *J. Acoust. Soc. Am.*, 77:1239–1244, 1985.

[11] C. D. West. *Liquid piston Stirling engines.* Van Nostrand Reinhold, 1983.

[12] L. E. Kinsler, A. R. Frey, A. B. Coppens, and J. V. Sanders. *Fundamentals of Acoustics.* John Wiley and Sons, 1982.

[13] A. D. Pierce. *Acoustics: An Introduction to Its Physical Principles and Applications.* Acoustical Society of America, Woodbury, New York, 1989.

[14] N. Rott. Damped and thermally driven acoustic oscillations in wide and narrow tubes. *Z. Angew. Math. Phys.*, 20:230–243, 1969.

[15] K. M. Godshalk, C. Jin, Y. K. Kwong, E. L. Hershberg, G. W. Swift, and R. Radebaugh. Characterization of 350 Hz thermoacoustic driven orifice pulse tube refrigerator with measurements of the phase of the mass flow and pressure. *Advances in Cryogenic Engineering*, 41:1411–1418, 1996.

[16] R. S. Reid, W. C. Ward, and G. W. Swift. Cyclic thermodynamics with open flow. *Phys. Rev. Lett.*, 80:4617–4620, 1998.

[17] S. Backhaus and G. W. Swift. A thermoacoustic-stirling engine. 1999. Submitted to Nature.

[18] Cryenco manufactures large-scale cryogenic hardware, such as liquid-nitrogen tank trucks, storage tanks, and the cryogenic vessels for General Electric's MRI systems. 3811 Joliet, Denver CO 80239.

[19] G. W. Swift. Thermoacoustic natural gas liquefier. 1997. In proceedings of the DOE Natural Gas Conference, Houston TX, March 1997. Also available at http://lib-www.lanl.gov/la-pubs/00412750.pdf.

[20] W. C. Ward and G. W. Swift. Design environment for low amplitude thermoacoustic engines (DeltaE). *J. Acoust. Soc. Am.*, 95:3671–3672, 1994. Fully tested software and users guide available from Energy Science and Technology Software Center, US Department of Energy, Oak Ridge, Tennessee. To review DeltaE's capabilities, visit the Los Alamos thermoacoustics web site at http://rott.esa.lanl.gov/. For a beta-test version, contact ww@lanl.gov (Bill Ward) via Internet.

[21] D. Gedeon. A globally implicit Stirling cycle simulation. In *Proceedings of the 21st Intersociety Energy Conversion Engineering Conference*, page 550. American Chemical Society, 1986.

[22] A. Tominaga, Institute of Physics, University of Tsukuba, Tsukuba 305, Japan.

[23] J. Gary, A. O'Gallagher, and R. Radebaugh. A numerical model for regenerator performance. Technical report, NIST-Boulder, 1994. Also known as REGEN 3.1 Users Guide.

[24] R. Radebaugh. A review of pulse tube refrigeration. *Adv. Cryogenic Eng.*, 35:1191–1205, 1990.

[25] G. W. Swift. Thermoacoustic engines. *J. Acoust. Soc. Am.*, 84:1145–1180, 1988.

[26] L. D. Landau and E. M. Lifshitz. *Fluid Mechanics.* Pergamon, 1982.

[27] R. W. Fox and A. T. McDonald. *Introduction to Fluid Mechanics.* Wiley, 1985.

[28] A. Bejan. *Entropy Generation Minimization: The Method of Thermodynamic Optimization of Finite-Size Systems and Finite-Time Processes.* CRC press, 1995.

[29] Adrian Bejan. *Advanced Engineering Thermodynamics.* Wiley, second edition, 1997.

[30] A. Tominaga. *Fundamental Thermoacoustics.* ISBN4-7536-5079-0, 1998. In Japanese.

[31] G. W. Swift. Thermoacoustic engines and refrigerators. *Physics Today*, pages 22–28, July 1995.

[32] G. W. Swift. *Encyclopedia of Applied Physics*, volume 21, chapter Thermoacoustic engines and refrigerators, pages 245–264. Wiley, for American Institute of Physics, 1997.

[33] N. Rott. Thermoacoustics. *Adv. Appl. Mech.*, 20:135–175, 1980. and references therein.

[34] A. J. Organ. *Thermodynamics and Gas Dynamics of the Stirling Cycle Machine.* Cambridge University Press, 1992.

[35] G. Walker, L. Bauwens, and E. Bingham. *Pulse-tube refrigerators: an introduction.* ??, 1996. Available through Stirling Machine World, stirmach@juno.com.

[36] W. P. Arnott, H. E. Bass, and R. Raspet. General formulation of thermoacoustics for stacks having arbitrarily shaped pore cross sections. *J. Acoust. Soc. Am.*, 90:3228–3237, 1991.

[37] G. W. Swift and R. M. Keolian. Thermoacoustics in pin-array stacks. *J. Acoust. Soc. Am.*, 94:941–943, 1993.

[38] G. W. Swift and W. C. Ward. Simple harmonic analysis of regenerators. *Journal of Thermophysics and Heat Transfer*, 10:652–662, 1996.

[39] W. M. Kays and A. L. London. *Compact Heat Exchangers.* McGraw-Hill, New York, 1964.

[40] P. Merkli and H. Thomann. Thermoacoustic effects in a resonance tube. *J. Fluid Mech.*, 70:161–177, 1975.

[41] N. Rott. Thermally driven acoustic oscillations, part iii: Second-order heat flux. *Z. Angew. Math. Phys.*, 26:43, 1975.

[42] R. C. Tolman and P. C. Fine. On the irreversible production of entropy. *Rev. Mod. Phys.*, 20:51–77, 1948.

[43] J. C. Wheatley, T. Hofler, G. W. Swift, and A. Migliori. An intrinsically irreversible thermoacoustic heat engine. *J. Acoust. Soc. Am.*, 74:153–170, 1983.

[44] A. Migliori and G. W. Swift. Liquid sodium thermoacoustic engine. *Appl. Phys. Lett.*, 53:355–357, 1988.

[45] G. W. Swift, D. L. Gardner, and S. Backhaus. Acoustic recovery of lost power in pulse tube refrigerators. *J. Acoust. Soc. Am.*, ??:??, 1999. To appear in February issue.

[46] J. R. Womersley. Method for the calculation of velocity, rate of flow, and viscous drag in arteries when the pressure gradient is known. *Journal of Physiology*, 127:553–563, 1955.

[47] M. Iguchi, M. Ohmi, and K. Maegawa. Analysis of free oscillating flow in a U-shaped tube. *Bull. JSME*, 25:1398, 1982.

[48] S. M. Hino, M. Sawamoto, and S. Takasu. Experiments on transition to turbulence in an oscillatory pipe flow. *J. Fluid Mech.*, 75:193–207, 1976.

[49] J. R. Olson and G. W. Swift. Acoustic streaming in pulse tube refrigerators: Tapered pulse tubes. *Cryogenics*, 37:769–776, 1997.

[50] G. W. Swift, M. S. Allen, and J. J. Wollan. Performance of a tapered pulse tube. 1998. To be submitted to the proceedings of the 10th International Cryocooler Conference, Monterey CA, May 1998.

[51] V. L. Streeter. *Handbook of Fluid Dynamics.* McGraw-Hill, 1961.

[52] I. E. Idelchik. *Handbook of Hydraulic Resistance.* CRC Press, 3rd edition, 1994.

[53] P. J. Storch, R. Radebaugh, and J. E. Zimmerman. Analytical model for the refrigeration power of the orifice pulse tube refrigerator. Technical note 1343, National Institute of Standards and Technology, 1990.

[54] G. W. Swift. Analysis and performance of a large thermoacoustic engine. *J. Acoust. Soc. Am.*, 92:1551–1563, 1992.

[55] N. Rott and G. Zouzoulas. Thermally driven acoustic oscillations, part IV: Tubes with variable cross section. *Z. Angew. Math. Phys.*, 27:197–224, 1976.

[56] J. L. Smith and M. Romm. Thermodynamic loss at component interfaces in Stirling cycles. In *Proceedings of the 27th Intersociety Energy Conversion Engineering Conference*, pages 5.529–5.532. Society of Automotive Engineers, 1992.

[57] P. Kittel. Temperature profile within pulse tubes. *Adv. Cryogenic Eng.*, 43:1927–1932, 1998.

[58] G. W. Swift. A Stirling engine with a liquid working substance. *J. Appl. Phys.*, 65:4157–4172, 1989.

[59] W. L. M. Nyborg. Acoustic streaming. In W. P. Mason, editor, *Physical Acoustics, Volume IIB*, page 265. Academic Press, 1965.

[60] David Gedeon. DC gas flows in Stirling and pulse-tube cryocoolers. In R. G. Ross, editor, *Cryocoolers 9*, pages 385–392. Plenum, New York, 1997.

[61] N. Rott. The influence of heat conduction on acoustic streaming. *Z. Angew. Math. Phys*, 25:417, 1974.

[62] J. R. Olson and G. W. Swift. Similitude in thermoacoustics. *J. Acoust. Soc. Am.*, 95:1405–1412, 1994.